The University of Nottingham

UNITED KINGDOM · CHINA · MALAYSIA

Exploring Sustainability in Fluorine Methodologies

Patrick J. Morgan

Thesis submitted to the University of Nottingham

for the degree of Doctor of Philosophy

September 2021

To my fiancé,
my rock during the hard times
and my wings in the good

"To the moon and back!"

Abstract

The fluorination of organic compounds is extremely important to the modern world, especially within the chemical sciences, however as we transition to a more sustainable future, current industrial fluorination methodologies grow increasingly unsuitable towards the preparation of these fluorinated molecules, especially from an energy and materials perspective. To address this new fluorination, defluorination and fluorine transfer methodologies have been developed with a focus on improved sustainability over traditional fluorination techniques.

This thesis explores new methodologies to control the reactivity of fluorine: from the enhancement of reactivity of metal fluoride salts, one of the more sustainable sources of fluorine available, through the treatment with organometallic complexes; to the activation of fluorine within perfluorinated organic moieties, enabling the selective transfer of fluorine between two organic substrates, providing the potential of utilising waste sources of fluorine as feedstocks in the future.

A series of group 9 organometallic complexes were targeted and synthesised, to investigate their catalytic fluorination potential upon treatment with metal fluoride salts. Treatment of these complexes bearing fluorinated ligands with silver oxide resulted in the formation of a new class of *cyclo*metallated and *ortho*metallated rhodium and iridium complexes, providing new catalytic targets for the fluorination of organic electrophiles.

The fluorination potential of transition metal fluoride complexes upon treatment with acyl chlorides was examined, providing first evidence of nucleophilic fluorination from $[RhF(CO)(PPh_3)_2]$. The catalytic fluorination of acyl chlorides with $[(\eta^5,\kappa_2C\text{-}C_5Me_4CH_2C_6F_5CH_2NC_3H_2NMe)\text{-}RhCl]$ was investigated, utilising metal fluoride salts as the fluorine source, affording the quantitative fluorination of a range of electron deficient and electron rich acyl chlorides under mild conditions. A procedure for catalyst recovery, regeneration and reuse was established. *In-situ* FTIR analysis and variable time normalised analysis of this catalytic fluorination procedure gave further insights into this catalytic reaction enabling a plausible mechanism to be proposed.

A transfer fluorination reaction was developed through the treatment of $[(\eta^5,\kappa_2C\text{-}C_5Me_4CH_2C_6F_5CH_2NC_3H_2NMe)\text{-}RhCl]$ **22**, and organic electrophiles in the absence of an external fluorine source, resulting in the formation of a bimetallic rhodacycle and a new fluorinated product. Multi-spectral analysis provided an understanding of the environment required to generate nucleophilic fluorine within the perfluorinated ligand, enabling the

transfer of fluorine to occur between the perfluorinated group and an organic electrophile *via* C−F bond activation. The transfer of fluorine was tracked in real time using *in-situ* IR analysis

The synthesis of functionalised partially fluorinated heteroarenes was investigated through the defluorination of pentafluoropyridine. A catalytic transfer fluorination protocol was adapted enabling fluorine transfer from pentafluoropyridine to benzoic anhydride. Additionally, the catalytic selective mono-defluorination and hydrodefluorination of pentafluoro-pyridine was achieved using commercially available group 8 and 9 catalysts.

Declaration

All work conducted as part of this thesis was conducted by myself, Patrick Morgan, unless otherwise noted, with the assistance of my supervisors Peter Licence, at the University of Nottingham, and Andrew C. Marr, at Queen's University Belfast. Collaborators: Graham Saunders assisted with initial research development, research assistance and editorial oversight; Stuart MacGregor carried out computational analysis and data interpretation for work conducted in Chapter 4; Magnus Hanson-Heine carried out computational calculations and data analysis for work conducted as part of Chapter 4; Hannah Brown carried out experimental work and data analysis as part of Chapter 5.

Publication

Publications contributing to this thesis

- Morgan, P.J.; Macgregor S.A.; Saunders, G.C.; Marr, A.C.; Licence. P.; Catalytic nucleophilic fluorination forming acyl fluorides using a recyclable cyclometallated rhodium complex. **2022** (Accepted)
- Morgan, P. J; Hanson-Heine M.W.D; Thomas, H. P.; Saunders, G. C.; Marr, A. C.; Licence, P.; C−F bond activation of a perfluorinated ligand leading to nucleophilic fluorination of an organic electrophile, *Organometallics*, **2020**, 38, 2116 – 2124.
- Thomas, H. P.; Marr, A. C.; Morgan, P. J.; Saunders, G. C.; Tethering of Pentamethylcyclopentadienyl and N-Heterocycle Stabilized Carbene Ligands by Intramolecular 1,4-Addition to a Polyfluorophenyl Substituent. *Organometallics,* **2018**, *37*, 1339–1341.

Additional Publications

- Clarke, C.; Morgan, P.J.; Hallett, J.; Licence, P.; Linking Molecular Structure to Thermal and Electronic Properties of Functional Dicationic Salts. ACS Sustainable Chemistry and Engineering. **2021**, *9*, 6224 - 6234.
- Morgan, P.J;* Licence, P; Okoye, J.C.;Savin, R.S; Beddoe, R.H.; Kitagawa, A.; Delorme, A.E; Sustainable development through academic-industrial partnerships: A perspective on the chemical sciences. Encyclopedia for the UN Sustainable Development Goals: Partnership for the Goals. Vol. 17 Springer, **2021**.
- Thomas, H. P.; Morgan, P. J; Marr, A. C.; Saunders G. C.; Conversion of haloform to carbonate by iridium N-heterocyclic carbene complexes and silver(I) oxide, *Dalton Transactions*, **2019**, *48*, 1947 – 1949.
- Ma, Y.; Wang Y. M.; Morgan, P. J.; Jackson, R. E.; Liu, X. H.; Saunders, G. C.; Lorenzini, F.; Marr, A. C.; Designing effective homogeneous catalysis for glycerol valorisation: selective synthesis of a value-added aldehyde from 1,3-propanediol *via* hydrogen transfer catalysed by a highly recyclable, fluorinated Cp*Ir(NHC) catalyst. *Catal. Today*, **2018**, *307*, 248–259.

Acknowledgements

"*Sometimes the best way to learn something is by doing it wrong and looking at what you did.*" Neil Gaiman

Abbreviations, acronyms and initialisms

|	
18-Crown-6	1,4,7,10,13,16-hexaoxacyclooctadecane
ACS GCIPR	American Chemical Society Green Chemical Institute Pharmaceutical Roundtable
AIM	Atoms in molecule
BCP	Bond critical point
CFCs	Chlorofluorocarbons
cm^{-1}	Wavenumber
Cp*	Pentamethylcyclopentadienyl ligand
DAST	(Diethylamino)sulfur trifluoride
DCM	Dichloromethane
DFT	Density functional theory
DME	Dimethoxyethane
DMF	Dimethylformamide
DMSO	Dimethyl sulfoxane
EA	Elemental analysis
EDG	Electron-donating group
Equiv.	Equivalents
ESI	Electro spray ionisation
EWG	Electron-withdrawing group
FDA	U.S. Food and Drug Administration
FTIR	Fourier transform infrared
HB-PTC	Hydrogen bonded phase transfer catalyst
HFCs	Hydrofluorocarbons
HOMO	Highest occupied molecular orbital
HP-ZSM-5	Hierarchical Porous-Zeolite Socony Mobil-5
IPr	1,3-bis(2,6-dipropylphenyl)imidazole-ylidene
LUMO	Lowest unoccupied molecular orbital
MS	Mass spectrometry
MTBE	tert-Butyl methyl ether

|	
NHC	N-heterocyclic carbene
NMR	Nuclear magnetic resonance
Ox. Add.	Oxidative addition
PFAS	Polyfluoroalkyl substance
PFP	Pentafluoropyridine
ppm	Parts per million
r.t.	Room temperature
Red. Elim.	Reductive Elimination
RMS	Root-mean-square deviations of atomic positions
rpm	revolutions per minute
SDGs	Sustainable development goals
S_NAr	Nucleophilic aromatic substitution
TBAF	Tetrabutylammonium fluoride
TBAT	Tetrabutylammonium difluorotriphenylsilicate
TCCA	Trichloroisocyanuric acid
TMAF	Tetramethylammonium fluoride
TMF	Transition metal fluorides
TOF	Turn over frequency
TON	Turn over number
TREAT.HF	Triethylamine trihydrogenfluoride
UV	Ultra violet
Vis	Visible
VTNA	Variable time normalised analysis
XRD	X-Ray Diffraction

Numbered Compounds
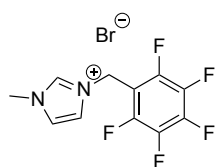
3-methyl-1-(2,3,4,5,6-
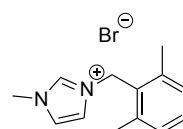pentafluorobenzyl)
imidazolium bromide

1
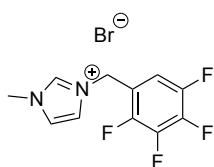
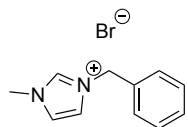3-methyl-1-(3,4,5,6-
tetrafluorobenzyl)
imidazolium bromide

2
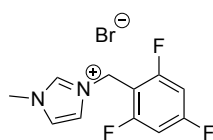
3-methyl-1-(2,4,6-
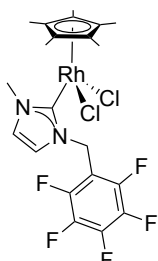trifluorobenzyl)
imidazolium bromide

3

3-methyl-1-(2,6-
dimethylbenzyl)
imidazolium bromide

4

3-methyl-1-benzyl
imidazolium bromide

5

Pentamethylcyclopentadienyl
rhodium-(-3-methyl-1-(2,3,4,5,6
-pentafluorobenzyl) imidazolium)
chloride

6
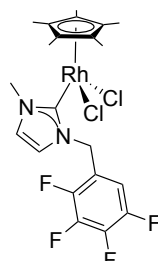
Pentamethylcyclopentadienyl
rhodium-(-3-methyl-1-(2,3,4,5
-tetrafluorobenzylimidazolium)
chloride

7

Pentamethylcyclopentadienyl
rhodium-(-3-methyl-1-(2,4,6)-
trifluorobenzylimidazolium)
chloride

8

Pentamethylcyclopentadieny
lrhodium-(-3-methyl-1-(2,6)-
dimethylbenzylimidazolium)
chloride

9

Pentamethylcyclopentadienyl
rhodium-(-3-methyl-1-benzyl
imidazolium)chloride

10

Pentamethylcyclopentadienyl
iridium-(-3-methyl-1-(2,3,4,5,6
-pentafluorobenzyl) imidazolium)
chloride

11
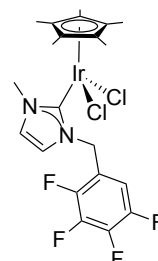
Pentamethylcyclopentadienyl
iridium-(-3-methyl-1-(2,3,4,5
-tetrafluorobenzylimidazolium)
chloride

12
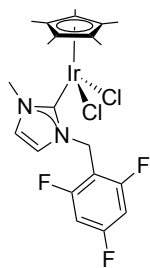
Pentamethylcyclopentadienyl rhodium-(-3-methyl-1-(2,4,6)-trifluorobenzyl imidazolium) chloride

13
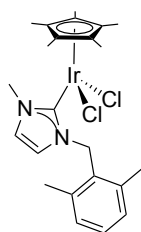
Pentamethylcyclopentadienyl rhodium-(-3-methyl-1-(2,6)-dimethylbenzylimidazolium) chloride

14
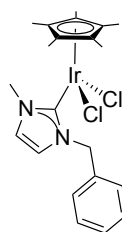
Pentamethylcyclopentadienyl rhodium-(-3-methyl-1-benzyl imidazolium) chloride
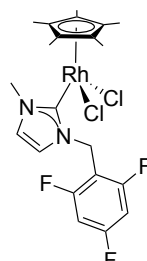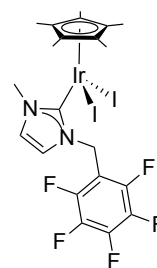
15

Pentamethylcyclopentadienyl iridium-(-3-methyl-1-(2,3,4,5,6-pentafluorobenzyl) imidazolium) iodide
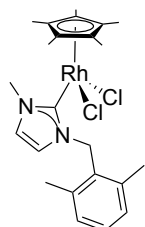
16
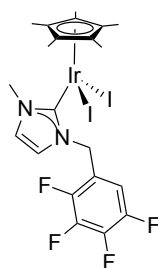
Pentamethylcyclopentadienyl iridium-(-3-methyl-1-(2,3,4,5-tetrafluorobenzylimidazolium) iodide
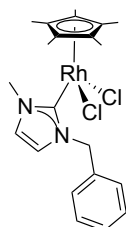
17
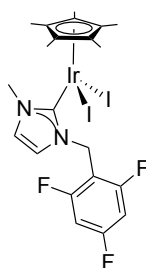
Pentamethylcyclopentadienyl rhodium-(-3-methyl-1-(2,4,6)-trifluorobenzyl imidazolium) iodide
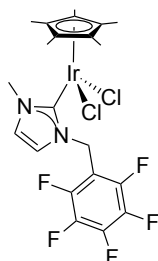
18
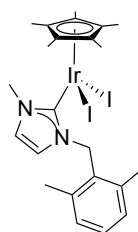
Pentamethylcyclopentadienyl rhodium-(-3-methyl-1-(2,6)-dimethylbenzylimidazolium) iodide

19
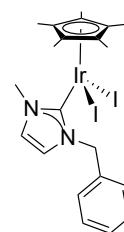
Pentamethylcyclopentadienyl rhodium-(-3-methyl-1-benzyl imidazolium) iodide

20

[Cp*IrCl(κC$_2$-MeNC$_3$H$_2$NCH$_2$C$_6$F$_4$)]

21
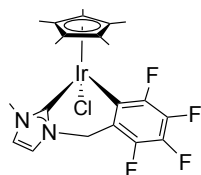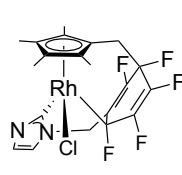
[(η^5,κ$_2$C-C$_5$Me$_4$CH$_2$C$_6$F$_5$CH$_2$NC$_3$H$_2$NMe)- RhCl]

22

[Cp*RhCl(κC$_2$-MeNC$_3$H$_2$NCH$_2$C$_6$F$_4$)]

23
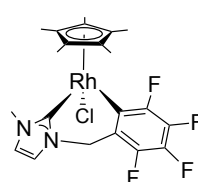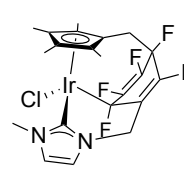
[(η^5,κ$_2$C-C$_5$Me$_4$CH$_2$C$_6$F$_5$CH$_2$NC$_3$H$_2$NMe)- IrCl]

24
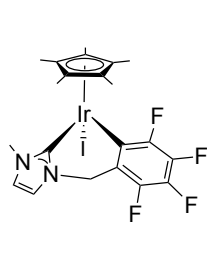
[Cp*IrI(κC₂-MeNC₃H₂NCH₂C₆F₄)]

25
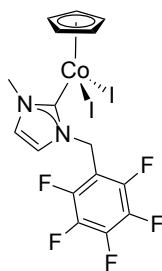
Cyclopentadienylcobalt-(-3-methyl-1-(2,3,4,5,6-pentafluorobenzyl)imidazolium) iodide

26
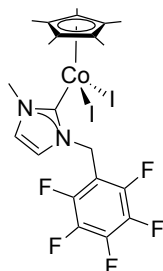
Pentamethylcyclopentadienylcobalt-(-3-methyl-1-(2,3,4,5,6-pentafluorobenzyl) imidazolium) iodide

27
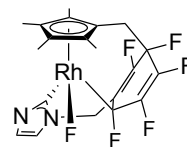
"[(η⁵,κ₂C-C₅Me₄CH₂C₆F₅CH₂NC₃H₂NMe)- RhF]"

'28'
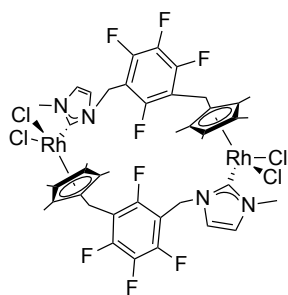
29
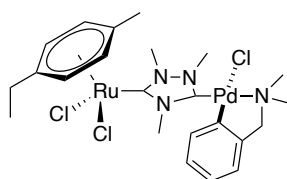
30
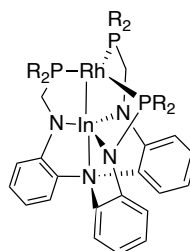
31
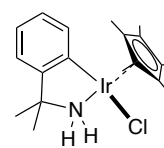
32
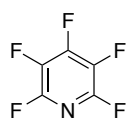
Pentafluoropyridine

33
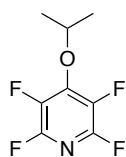
4-isopropoxy-2,3,5,6-tetrafluoropyridine

34
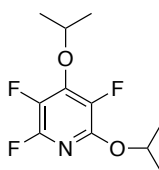
2,4-diisopropoxy-3,5,6-trifluoropyridine

35
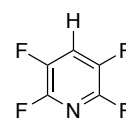
2,3,5,6-tetrafluoropyridine

36

See page at end for easy reference.

Table of Contents

1 Chapter 1: Introduction

1.1 Taming the dragon: The history of fluorine and traditional fluorination procedures

As the most reactive element on the periodic table, fluorine holds a special place in the annals of chemical science. With the ability to burn steel and react with every element bar helium and neon, the inherent reactivity of fluorine made discovery and isolation exceptionally difficult and dangerous, leading to injury and death.[1-4] It wasn't until 1886 that French chemist, Henri Moissan, first isolated this elusive and deadly element.[5, 6] The highly reactive nature of fluorine posed inherent issues to reactivity control, yet it is this reactivity and the ability to form very strong bonds with other elements that makes fluorine so useful and unique.

While a number of organofluorine compounds (an organic substrate that contains one or more C–F bond) were known prior to the isolation of fluorine,[7, 8] the industrial importance of fluorine and fluorine containing compounds only became established in the 1930s and 1940s. The introduction of chlorofluorocarbons (CFC's),[9, 10] the development of polymers, such as Teflon[11, 12] and the use of uranium hexafluoride for the manufacture of enriched uranium during the Manhattan project,[13] resulted in the rapid growth of the organofluorine industry, leading to health care,[14-16] electronics,[17] power generation and numerous safety and wellbeing applications.[18, 19]

However, the direct fluorination of organic substrates with fluorine gas in incompatible in most instance, leading to uncontrolled thermal decomposition. Therefore, alternative fluorine sources are required to synthesise these fluorinated compounds. Industrial techniques fluorination techniques require extremely energy and material intensive processes using forcing conditions to activate these fluorine sources towards fluorination resulting in uncontrollable over fluorination. This represents one of the major challenges associated with the industrial synthesis of organofluorine compounds. Some of the most industrially relevant fluorination procedures developed during the 20th century are highlighted below (Scheme 1-1). Alternative methodologies are required, not only to improve the overall sustainability of these systems, but also to access partially fluorinated molecules synthesised through selective fluorination and defluorination, which are incompatible with these traditional fluorination methodologies. There has been a major drive in the past 15 years to develop new fluorination techniques that combat the drawbacks in terms of safety, atom economy, toxicity, limited

substrate scope, extreme reaction conditions and the specialist equipment required for conventional fluorination techniques.

Halex Process:

Balz-Schiemann reaction:

$$ArN_2{}^+BF_4{}^- \xrightarrow[\Delta]{F^-} ArF \;+\; N_2 \;+\; BF_3$$

Swarts Reaction:

Fowler Process:

Simons Process:

$$R_3{-}H \;+\; HF \xrightarrow{\text{electrolysis}} R_3{-}F \;+\; H_2$$
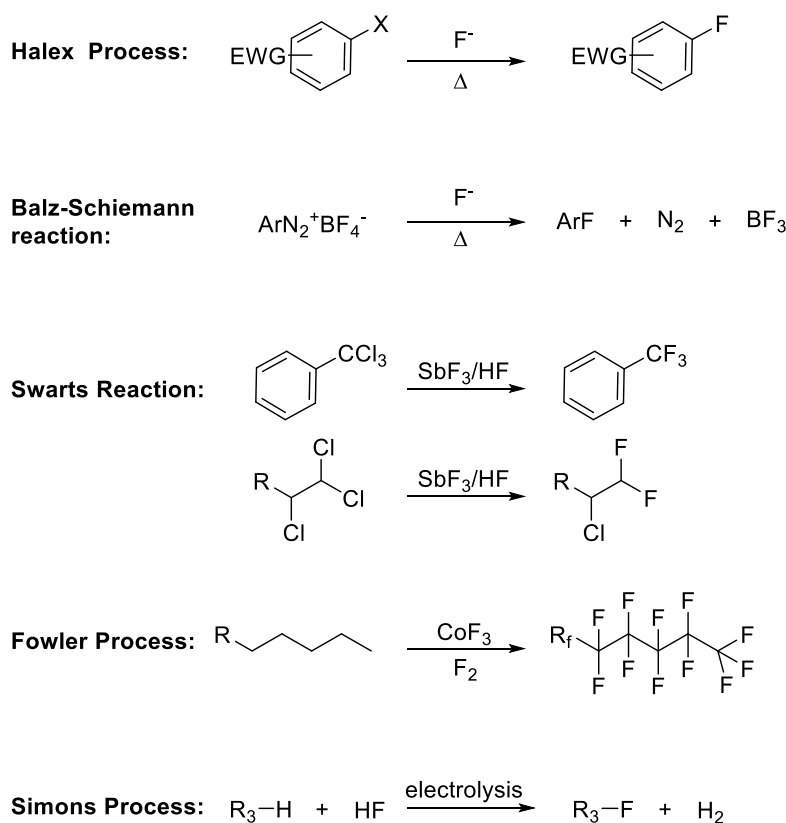
Scheme 1-1: Examples of industrial fluorination procedures developed during the 20th century, for the large scale synthesis of fluorinated compounds. [20-25] These procedures often require high temperatures, hazardous reagents and specialist equipment for the uncontrollable fluorination leading to mixtures of products in low yields. Adapted from *Recent Advances in Green Fluorine Chemistry.*[26]

1.2 The importance of fluorine

As outlined in the 2030 Agenda for Sustainable Development, 17 sustainable development goals (SDGs) were defined, describing measures to promote and tackle the challenges of sustainable development. Chemistry and the chemical sciences have a central role to play towards the success of the SDGs and the associated development targets, touching upon every aspect of the 17 SDGs. The development of more sustainable fluorination techniques has far reaching consequences towards the successful achievement of the 2030 agenda; from the development of fluorinated agrochemicals and pharmaceuticals (SDG 2 and 3); the responsible use of fluorinated feedstocks (SDG 9 and 12); next generation fluorinated batteries

and renewable energy generation (SDG 7, 11 and 13); and understanding the effects of anthropogenic fluorine on the biosphere (SDG 3, 6, 13, 14 and 15).

The fluorination of organic compounds is of significant interest, particularly within the pharmaceutical and agrochemical industry, contributing towards more than a third of all marketed pharmaceuticals and agrochemicals,[27] with revenues expected to exceed \$42 billion per year by 2030.[28] 37 % of all small molecule active pharmaceutical ingredients approved by the FDA in 2020 contained at least one fluorine moiety,[27] with fluorine-containing pharmaceuticals increasingly targeted in the last decade,[29] representing 26 % of all pharmaceuticals approved by the FDA between 2011 and 2020. In the past five years alone fluorinated pharmaceuticals represent 38 % of all small molecule pharmaceutical approvals within the US (Figure 1-1).
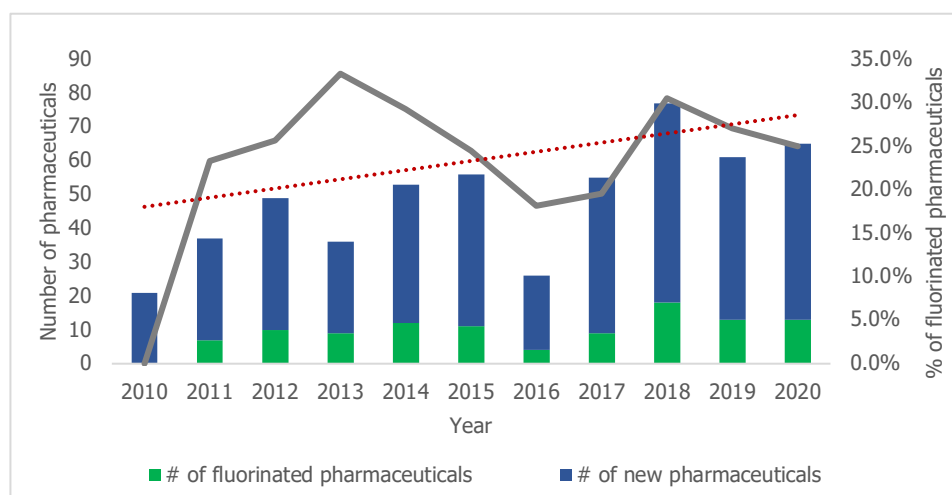
Figure 1-1: Proportion of fluorinated pharmaceuticals approved by the FDA over the past decade, showing the proportion of fluorinated pharmaceuticals approved trending upwards over the last decade (red trendline).

The American Chemical Society Green Chemical Institute Pharmaceutical Roundtable (ACS GCIPR) also outlined the need for new, greener fluorination methodologies, driven by the success of fluorinated pharmaceuticals. Within this first report,[30] it was identified that only a few reliable methods for the introduction of fluorine within a target molecule existed, the majority of which require harsh conditions that often use corrosive and hazardous reagents which were often incompatible with pharmaceutical targets. Over the past decade significant work has been conducted to expand the toolbox of fluorine chemists, with new synthetic pathways and strategies being proposed to prepare fluorinated building blocks.[31-42] The follow-up report, for the 10 year anniversary of the 2007 *Key Green Chemistry Research Areas* report,[43] highlighted that while the development of fluorination methodologies had seen

significant progress, especially towards the development of fluorination reagents (in particular nucleophilic deoxyfluorination reagents), little had been done to address the core requirements outlined in the 2007 report. Nonetheless, the growth in the proportion of fluorinated pharmaceuticals over the past decade can be partially attributed to the greater accessibility of methodologies available to incorporate a fluorine atom into their molecular structure.[44]

The incorporation of fluorine within pharmaceutical targets is of interest as the inclusion of fluorine can impart dramatic physiochemical or stereoelectronic changes, improving the bioavailability, molecular stability and lipophilicity of the molecule.[45-47] The enhancement of these properties within the biological environment are highly advantageous and are currently being exploited by the pharmaceutical and agrochemical industries, as demonstrated by the number of fluorinated molecules on the market. For example, three of the top twelve best-selling pharmaceuticals of all time contained a fluorine substituent. These include; GlaxoSmithKline's fluticasone propionate, AstraZeneca's Rosuvastatin, Gilead Science's Sofosbuvir and until it came off patent in 2011, the best-selling pharmaceutical drug was Pfizer's Lipitor (Figure 1-2), with new fluorinated pharmaceuticals dominating sales up to 2019.[48]

Flovent

Rosuvastatin

Sofosburvir

Lipitor
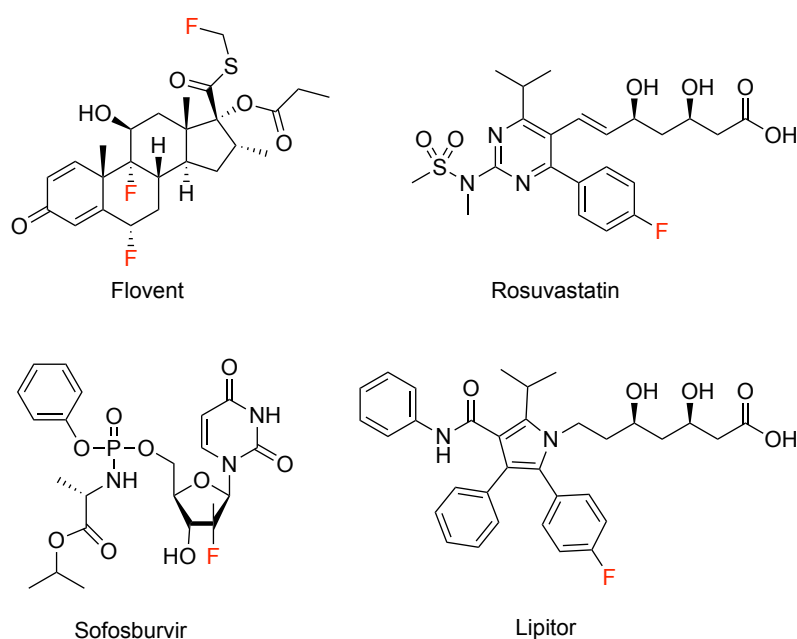
Figure 1-2: Exemplar blockbuster pharmaceuticals containing fluorine. Late stage fluorine functionalisation of Flovent and Sofosburvir achieved by Selectfluor[TM 49] and DAST[50] respectively. These fluorination reagents will be discussed in section 1.3. The aryl fluoride species present in Rosuvastatin and Lipitor are incorporated into the structure at an early stage using commercially available fluorinated compounds, synthesised using traditional fluorination techniques.

1.3   Fluorination reagents

The formation of C−F bonds industrially is well documented [8, 21-23, 51] and numerous extensive reviews on the subject of carbon-fluorine bond formation have been published over the past two decades, [26, 43, 47, 52-63] showing the growth of interest in the formation of these bonds and their importance towards many sectors of the chemical industry. Early work within this period primarily required the use of highly energetic fluorine carriers, such as xenon difluoride at elevated reaction temperatures to carry out the fluorination of activated substrates.[64-66] These compounds are highly toxic and although more moderate than the fluorine gas they replaced, their reactivity was difficult to control, with one publication stating "*reaction of XeF$_2$ compounds may lead to explosions*."[67] Further development, spurred by the need to find more accessible reagents for fine chemical fluorination, resulted in the discovery of new classes of fluorination reagent bearing the "N-SF$_3$" and "N-F" moiety.[68, 69] Of these N-Fluorobenzenesulfonimide (NFSI)[70] and Selectfluor[TM71] are the most well known, however a wide array of fluorination reagents are available (Figure 1-3).[68]

One of the issues initially associated with these substrates was the unselective nature of fluorination, which required the development of directing substrates.[72-76] However, these fluorine carriers have been further developed exhibiting greater thermal stability with improved selectivity. Fluorination reagents are now regularly used in drug discovery for the late-stage fluorination of pharmaceutical targets.[48, 77] With this came a better understanding of how these fluorination reagents work, resulting in the development of a scale of electrophilic power for the electrophilic fluorination reagents, which facilitates the correct selection of these fluorination reagent for the specific system, enabling more precise control over reactivity (Figure 1-4).[78] These fluorination reagents are commonly used within the laboratory and drug discovery setting to synthesise fluorinated molecules under mild conditions.[59, 79]

Nucleophilic Reagents

| HF/Pyridine | TBAF | TBAT | BrF$_3$-KHF$_2$ | TREAT.HF |

| IPy$_2$BF$_4$ | p-Tol-IF$_2$ | p-CF$_3$-C$_6$H$_4$-BrF$_2$ | DMPU/HF |

Electrophilic Reagents

| NFSI | SelectFluor | AccuFluor | fluoroiodane | chiral NFSI |

Deoxyfluorination Reagents

| DAST | Deoxyfluor | Fluolead | XtaslFluor-E | PhenoFluor |
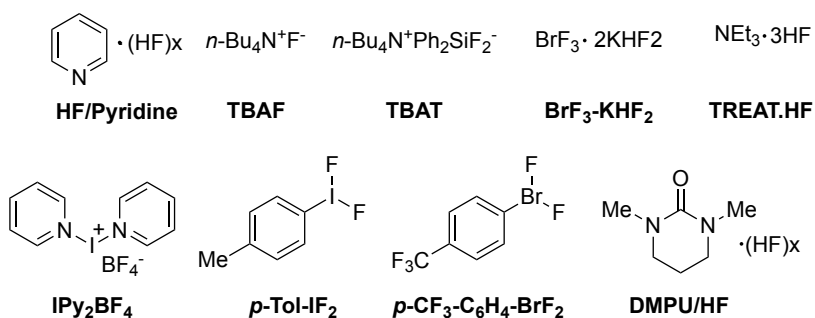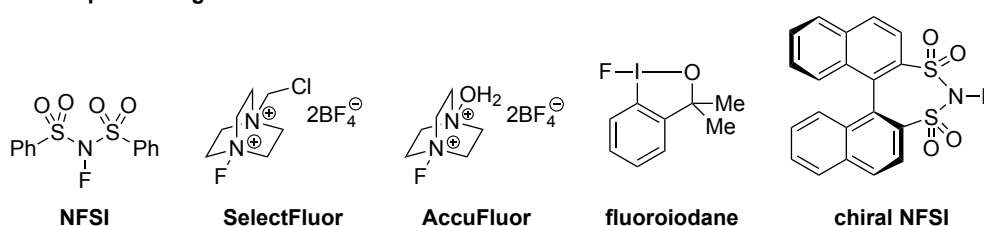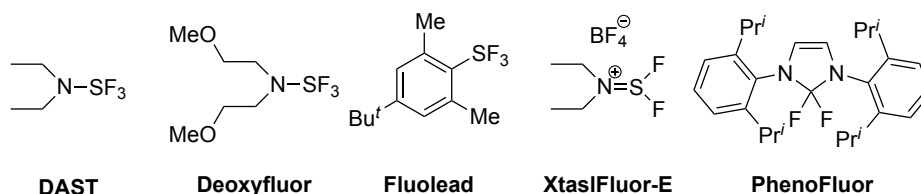
Figure 1-3. Selected common fluorination reagents, separated by nucleophilic fluorination, electrophilic fluorination and deoxyfluorination reagents. Each fluorination reagent is often targeted for a specific use case, such as the changing oxidation potential of the electrophilic fluorination reagents.

| -2.20 | -2.10 | -0.78 | -0.73 | -0.47 | -0.04 | 0.18 |

E$_p$ *red* vs. SCE

Increasing oxidation potential
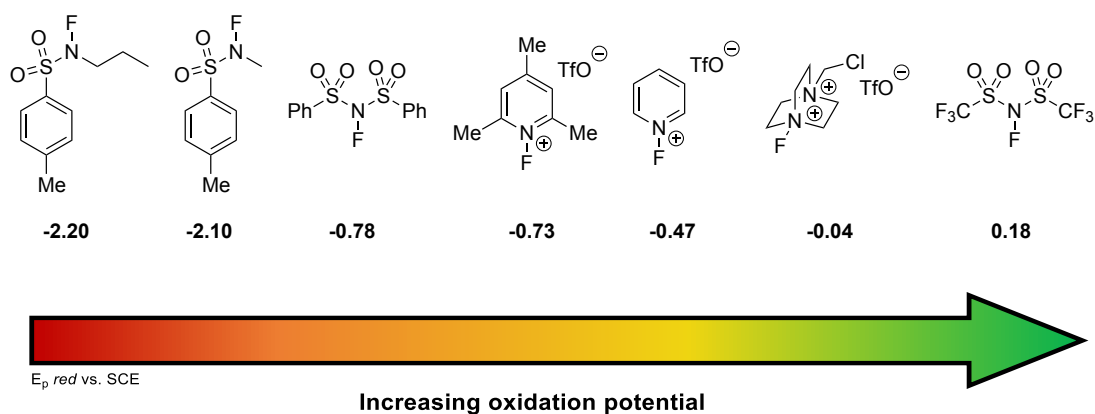
Figure 1-4. Scale of electrophilic power of a range of electrophilic reagents, given by the potential of the first one-electron reduction against a standard calomel electrode (SCE). A relationship between the reduction of the fluorination reagents and the fluorination power of the N-F bond was determined. Increasing the oxidation potential significantly increases fluorination power. Figure adapted from Xue's report on the relative power of electrophilic fluorination reagents.[78]

1.4 Sustainability considerations of current techniques and reagents

One of the principal philosophies influencing sustainable development within the chemical sciences is the 12 principles of green chemistry,[80] outlining key considerations that can be taken to lessen the environmental and human impact of chemical reaction design, including the reduction of waste and derivatisation, the reduction of energy and material consumption where possible and the development of safer methods using less hazardous reagents.

As mentioned in *Section 1.2*, the 2018 ACS GCIPR report highlighted that although "*substantial progress*" had been achieved in the development of fluorination methodologies "*through providing viable alternative approaches*" in the form of fluorination reagents,[43] these fluorination reagents do not directly address the issues associated with fluorination, outlined within the initial report.[30]

This new generation of fluorination reagents are made through multistep synthesis using fluorine gas, HF or metal fluorides as the fluoride source. They are essentially highly energetic fluorine vectors, which generate large volumes of waste to transfer a single fluorine atom to the target molecule. Major problems associated with the use of these fluorination reagents are the large investment of embedded energy associated with their preparation, undesirable atom efficiency, especially due to their super-stoichiometric use and the considerable health and safety requirements associated with some of the fluorination reagents.

SelectFluor™ is one of the most commonly utilized fluorination reagents,[71] and is used on a multi-tonne scale each year,[81] for the fluorination of a number of blockbuster fluorinated pharmaceuticals.[48, 49] However, for every fluorine atom transferred to the target, the use of SelectFluor™ produces nearly 18 times the mass of waste (molar mass 354.26 g) without taking into account its super-stoichiometric use. Even taking this into account, Selectfluor™ is considered a "greener" alternative reagent, as its use is advantageous compared to traditional fluorination routes. A retrosynthetic analysis of the production of SelectFluor™ from primary commodities such as oil and mining products required up to 41 individual steps (Scheme 1-2), which represents an extremely material and energy intensive synthetic process producing enormous quantities of waste, even without taking into account the downstream effects and full lifecycle of Selectfluor™.

A balance between atom economy/waste formation and fluorination performance is essential in the development of more sustainable fluorination techniques, however current solutions tend to favour greater control at the expense of environmental and energy considerations.

Chapter 1: Introduction

Alternative fluorination methodologies that maintain high performance, yet also take into account the lifecycle of the fluorine source are required.
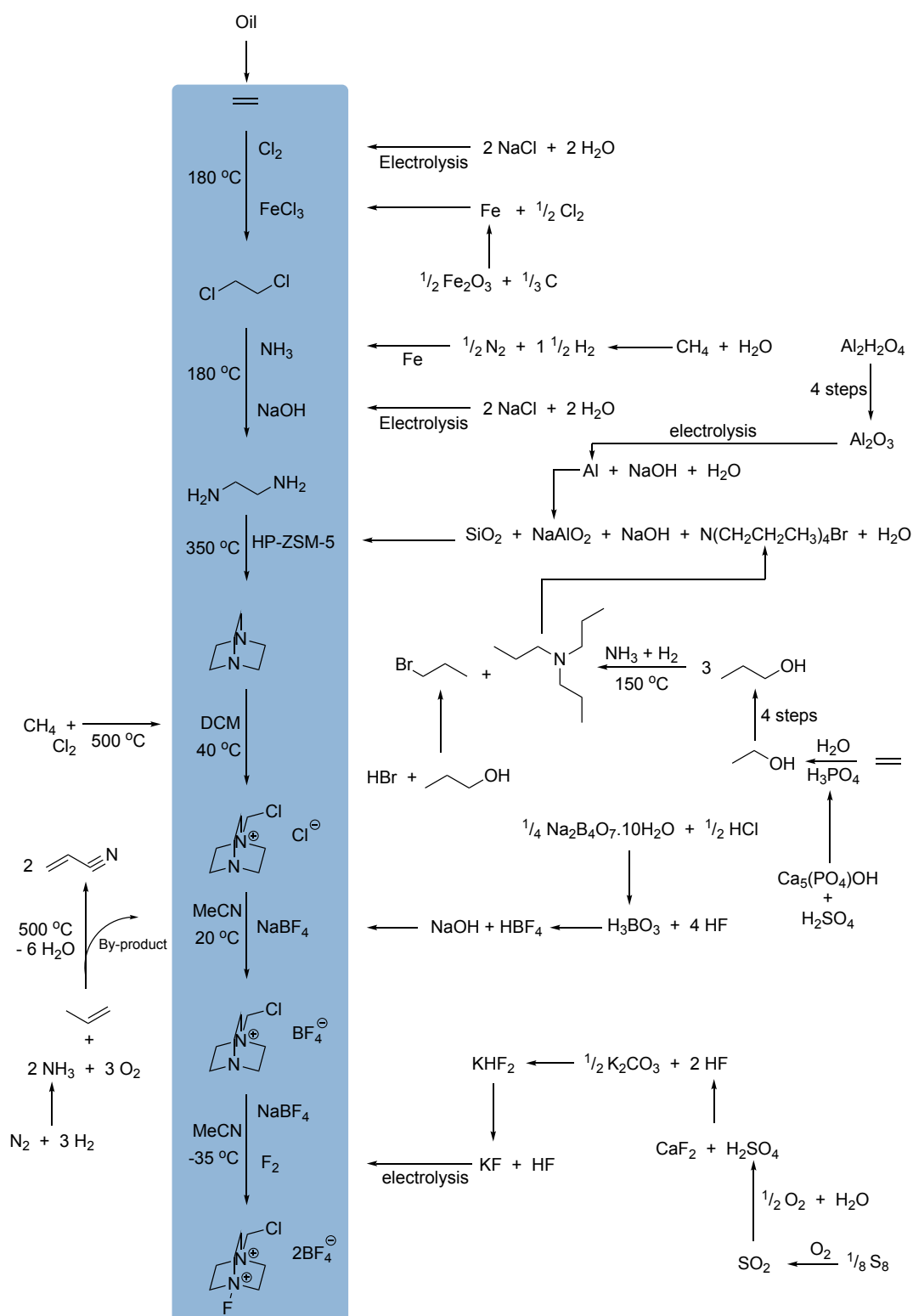
Scheme 1-2. Synthetic scheme for the synthesis of SelectFluor[TM], from refined reagents, requiring 41 synthetic steps. This reterosynthetic pathway exemplifies the large material and energy cost associated with the synthesis of Selectfluor[TM] at each step in the process. Designed using publicly available information for the synthesis of each substrate.

1.5 Nucleophilic fluorination with metal fluoride salts

An alternative fluorine source is metal fluoride salts such as; calcium fluoride, sodium fluoride, potassium fluoride, caesium fluoride and silver fluoride. These fluoride salts are present in rock or require a one- or two-step synthesis from mining by-products, representing a much more atom efficient and more sustainable source of fluorine than fluorination reagents.

Metal fluoride salts are readily available, cheap and less hazardous alternative to traditional fluorination materials. In terms of atom efficiency, metal fluoride salts represent one of the best methods to introduce fluorine into a target molecule, producing simple salt waste as a by-product. Fluorine gas and HF represent the only improvement in atom efficiency over metal fluoride salts, however for most, the drawback of F_2 and HF use are not worth the gain.

Metal fluoride salts are bench stable solids that can be easily used in a laboratory or industrial setting. However, it is the inherent stability of the metal fluoride salts that pose the major limitation for their use as fluorine sources. Firstly, the lattice dissociation enthalpies of these metal fluoride salts are high (LiF: 1037 kJ/mol; NaF: 926 kJ/mol; KF: 829 kJ/mol; CsF 759 kJ/mol),[82, 83] coupled with their low solubility in organic solvents, the reduced nucleophilic and highly basic character of the fluoride anion. These properties limit metal fluoride salt application towards nucleophilic fluorination.[84] To get around these fundamental issues better ways to control the reactivity of the metal fluoride salts must be found, to harness the nucleophilicity of the fluorine but without the problems associated with the basicity of the fluoride and the poor solubility of these salts in traditional organic media.

Due to the poor reactivity of alkali metal fluoride salts, traditional methods of introducing nucleophilic fluorine within a target relied upon the treatment of extremely electron poor aryl halides with a large excess of pre-treated anhydrous potassium fluoride at high temperatures (>200 °C) in high boiling point organic solvents.[85] The difficulty inherent to these reactions, namely the strong lattice enthalpy and poor solubility of the metal fluoride results in low rates of reactivity, therefore controlling the concentration of fluoride in solution is crucial. Large excesses of the fluoride salt are required in order for sufficient fluoride ion concentration in solution, even in aprotic polar solvents such as DMSO (solubility of potassium fluoride in DMSO at 300 K: 0.025 g/L).[86, 87] Therefore, alternative routes to control the reactivity of these metal fluoride salts are required.

Over the past decade numerous techniques have been developed to control the reactivity of fluorine from metal fluoride salts. Due to the limited solubility of metal fluoride salts in organic solvents, coupled with low nucleophilicity, methods of enhancing the reactivity of the

fluoride anion often take the form of an additive. Traditionally this has been achieved through the use of hydrogen bonding interactions[88] or crown ethers.[89] The addition of 18-Crown-6 to a solution of acetonitrile, to which potassium fluoride was added, resulted in the formation of "naked" fluoride (i.e. a solubilised fluoride anion devoid of a strongly bound solvation shell). This "naked" fluoride undergo fluorination of a range of organohalides resulting in formation of the fluorinated product *via* nucleophilic substitution. However, while the formation of this "naked" fluoride species results in the formation of a potent nucleophile, the fluoride anion also becomes a very powerful base, capable of carrying out elimination reactions. While this procedure resulted in limited control of fluoride, further development was required in order to improve control of the reactivity of the fluoride anion.[89]

Similarly, ionic liquids have also been found to enhance the reactivity of metal fluoride salts when used as a co-solvent, enabling partial solvation of the fluoride anion.[90] However, while addition of ionic liquids facilitated greater fluorination of the substrate from the fluoride salt, the basic character of the fluoride was enhanced, leading to competing elimination pathways (Scheme 1-3). Further developments through the design of task specific ionic liquids enabled greater selectivity towards the desired fluorinated products.[91-94]
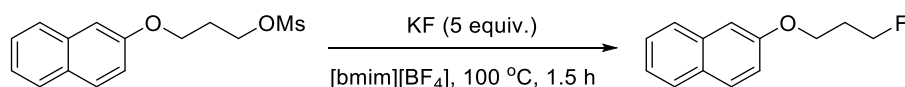
Scheme 1-3. Nucleophilic fluorination of mesylalkanes to fluoroalkanes using potassium fluoride in ionic liquids, whereby the ionic liquid enhances the reactivity of the metal fluoride salt. Use of an ionic liquid co-solvent aids in the control of fluorination from potassium fluoride. Scheme has been adapted from literature. [90] (OMs=methanesulfonate; [bmim][BF$_4$]=1-Methyl-3-Butylimidazole tetrafluoroborate).

These methodologies exploit the ability of crown ethers and ionic liquids to solubilise the metal fluoride salts, allowing for the fluoride anion to be available for reaction in solution. These methods therefore help to control the concentration of F$^-$ in solution. Through these methods we can see that the use of additives can result in the enhancement of fluorination due to an increase in the solubility of the metal fluoride salts, however specific control over selectivity and basicity remain an issue. Additionally, ionic liquids require extensive synthetic procedures to make,[95] often making up 80-95 % of the mass of the reaction medium, and while they can be recycled in some cases, the overall lifecycle of these systems must also be taken into account. These hydrogen bonding effects for nucleophilic fluorination using ionic liquids have recently been reviewed.[96]

A further development in the control of metal fluoride salts in recent years was the development of a hydrogen bonding phase transfer catalysis by Veronique Gouverneur and co-workers.[97] They developed a method in which a bis-urea compound with a chiral backbone (Scheme 1-4) was found to "solvate" a fluoride anion enabling the transfer of fluorine stereoselectively.
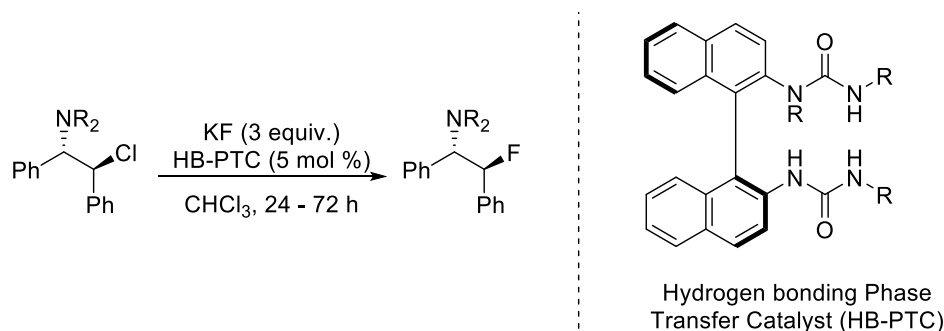
Scheme 1-4. Hydrogen Bonding Phase Transfer Catalysis in the enantioselective synthesis of ϐ-fluoroamines using potassium fluoride as the fluorine source. The structure of the HB-PTC was found to be vital in controlling the reactivity of the fluoride anion, where altering the R groups afforded changes in the observed reactivity, allowing for greater control through modification of the catalyst. Scheme has been adapted from literature. [97]

The design of this phase transfer catalyst enables the selective dissolution of metal fluoride salts into solution through interactions between the metal fluoride salt and the hydrogen bond donating bis-urea catalyst acting as a transport agent. This results in the formation of a hydrogen bonded fluoride complex, which is stable enough to be isolated and characterised *via* X-Ray diffraction (XRD).[98]
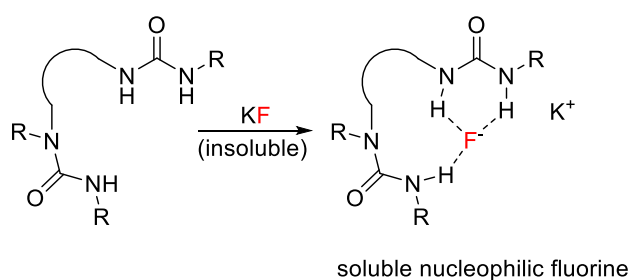
Scheme 1-5. Solubilisation of fluoride within the cavity of the urea based HB-PTC, bound through hydrogen bonding in a tridentate binding mode. The position of the fluoride within the cavity could be altered, thus changing fluoride reactivity, through changing the structure of the catalyst.

It was found that the fluoride was held within the cavity of the bis urea complex through a tridentate binding mode (Scheme 1-5). ^{1}H and ^{19}F NMR analysis was used to identify the extent of interaction between the N-H fragments of the catalyst and F[-].[98] This showed that

changing the R group on the catalyst changed the extent of interactions between the three sites of hydrogen bonding, meaning that the catalyst could be designed to tune the position of the fluoride within the cavity of the catalyst, altering substrate selectivity.[99-101]

This highlights a methodology whereby the reactivity of the fluoride ion could be altered through the design of the overall structure of the catalyst. This change in catalyst design enabled fluorination selectivity to be controlled to a greater extent and highlights how rational design can be used to further control the reactivity of fluoride.[98, 102]

1.6 Transition metal fluorides

The methods described in *Section 1.5* have all relied on attempting to increase the concentration of fluoride in solution through the addition of additives to carry out fluorination, with varying levels of control and accessibility. To do so high molar equivalents of the metal fluoride salts are often required in addition to stoichiometric additives. However, alternative methods of achieving fluorination are available, which do not require additives to alter the concentration of fluoride within solution. Of particular interest in this thesis is the formation of transition metal fluorides (TMF). While there is no single general method for the synthesis of TMF, the treatment of a metal fluoride salt (which is inherently unreactive towards nucleophilic substitution due to a high lattice enthalpy) with a suitable organometallic halide complex has been found to undergo Halex exchange resulting in the formation of the TMF. This changes the intrinsic reactivity of the fluoride, thereby allowing for effective control and tuning of its reactivity, *via* the ligands of the complex.

The formation of TMFs are of particular interest due to the ability to tune the coordination sphere of the complex thereby altering the properties and reactivity of the M–F bond. As the focus of this thesis is the synthesis and reactivity of group 9 organometallic complexes the emphasis of the following sections will discuss these transition metal complexes. Reviews are available on the topic of early and middle transition metal fluoride complexes.[103]

From a purely theoretical standpoint, the synthesis of late transition metal fluorido-complexes would appear to be challenging. Indeed, this was largely considered to be the case throughout early experimentation in the 1950s and early 1960s, where the synthesis of highly fluorinated tri-, tetra- and penta-valent metal fluoride complexes were prevalent.[104-108] Using assumptions taken from Pearson's acid-base theory,[109] the stability of a complex formed between the "hard" fluorine ligand with the "soft" and polarizable electron rich late stage transition metal was thought to be unfavourable.[110] One of the first organometallic late transition metal fluorido-

complex synthesised was reported in 1968,[111] with much work in this time focussed around the stabilisation of the M-F bond through the use of co-ligands, stabilising the M-F bond.

This stabilisation can be achieved due to the strong π donor ability of the fluoride ligand. While the σ bonding characteristics of the fluoride ligand is weak, due in part to the high electronegativity of fluorine, the major contribution to M–F bonding is the result of donation of electron density from the fluoride ligands' filled *p*-like orbitals into the empty d_π-orbital of the metal. Early work on the synthesis of fluorido-complexes included the addition to Lewis acidic π-acceptor ligands (such as NO and CO), adopting a *trans* orientation with respect to the M-F bond.

The π donating fluoride ligand donates π-electron density into the metal, thereby increasing electron density on the metal centre. The addition of these strongly Lewis acidic ligands allow for this additional electron density from the metals d_π orbital (HOMO) to be distributed through greater backbonding into the π* orbital (LUMO) of the π-accepting ligands. This results in an overall transfer of electron density from the fluoride, through the metal to the π-accepting co-ligand, decreasing the electron density at the metal, while also increasing the π-donor contribution from the fluoride ligand, further stabilising the complex. Conversely, late transition metals have partially filled *d* orbitals, resulting in a destabilisation effect due to electrostatic repulsion between the metals d_π orbitals and the p-like orbitals of the fluorine ligand, which must also be taken into account. The presence of a CO ligand in the coordination sphere of the metal not only stabilises the TMF through these interaction, it also acts as a convenient handle to assess the electronic character of the metal through FTIR measurements.

Consequently, by changing the coordination sphere around the metal centre, the reactivity of the M-F bond can be altered. By introducing a more electron rich highly donating ligand, greater electron density on the metal centre results in a reduction in the strength of the M-F bond, and *vice versa* with an electron withdrawing ligand. By weakening and strengthening the M-F bond the reactivity of the fluoride can be altered tuning the reactivity of the fluoride to organic electrophiles.

The synthesis of the fluorido-complex, *trans*-[IrF(CO)(PPh$_3$)$_2$] by Vaska and Peone[112] (Scheme 1-6) represented one of the first convenient routes to the synthesis of late TMFs. The fluorido-complex was synthesised *via* the metathesis of the chloride analogue, [IrCl(CO)(PPh$_3$)$_2$], with silver fluoride, which is formed *in-situ* through the reaction of silver carbonate with ammonium fluoride, affording the pure fluorinated complex. Subsequent work showed how these complexes could be used as precursors in the synthesis of a range of other d^8 complexes as [IrF(CO)(PPh$_3$)$_2$] was found to undergo rapid ligand exchange, due to the

lability of the M-F bond.[113] This class of Vaska's type complexes has been expanded to the rhodium analogue, [RhF(CO)(PPh$_3$)$_2$], and through the modification of the phosphine ligand used. More recently a methodology for the fluorination of Vaska's complexes directly from anhydrous ammonium fluoride has been developed affording the formation of the desired TMF.[114]

$$IrCl_3 \cdot H_2O \xrightarrow[\text{DMF, } \Delta, N_2, 0.5h]{2\ PPh_3} OC-\underset{\underset{PPh_3}{|}}{\overset{\overset{PPh_3}{|}}{Ir}}-Cl \xrightarrow[\text{MeOH, } \Delta, N_2, 0.5h]{\substack{\text{i) NH}_4\text{F (20 equiv.)} \\ \text{ii) Ag}_2\text{CO}_3\ \text{(0.5 equiv.)}}} OC-\underset{\underset{PPh_3}{|}}{\overset{\overset{PPh_3}{|}}{Ir}}-F$$
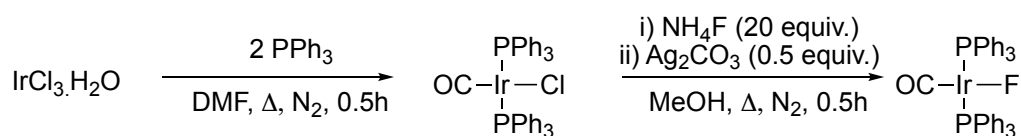
Scheme 1-6: Synthesis of [IrF(CO)(PPh$_3$)$_2$] from halide exchange with silver fluoride, generated in-situ from ammonium fluoride and silver carbonate.

Due to the difficulties associated with the formation, isolation and characterisation of late transition metal fluoride complexes, particularly in the absence of π acceptor ligands, it wasn't until 1995 that Bergman and co-workers reported the first neutral iridium[III] fluorinated species which was structurally characterised[115] and 2004 that the first iridium[I] based fluorido-complex was characterised with crystallographic structure determination.[116] Until this publication was reported by Roesky and co-workers, the Vaska's type complexes, [IrF(CO)(PR$_3$)$_2$], were the only iridium[I] based neutral organometallic fluoride known.

The most common route to the formation of the M-F bond is through direct metathesis of a M-X bond (X = halide) with super-stoichiometric quantities of silver fluoride. This has been met with some success in the synthesis of novel iridium[III] piano-stool complexes, through the metathesis of an Ir-I bond,[117] and has received much attention in the past two decades in the synthesis of iridium[I],[118] iridium[III],[119] and cobalt[III][120] fluorido-complexes. The formation of these TMF complexes has provided a greater understanding of the environment required to stabilised the M–F bond through careful consideration of the coordination sphere of the complex.

Gray and co-workers reported a bis(cyclometallated) iridium[III] system,[121] where silver fluoride was used to exchange the bridging chloride ligands for fluoride, forming a rare example of bridging cyclometallated iridium fluoride complex. The lability of the Ir−F bond was investigated by treating the complex with a range of sulfur and carbon based electrophiles, including toluoyl chloride, which converted quantitatively into toluoyl fluoride over the course of 6 hours (determined by ^{19}F NMR analysis), demonstrating that the M-F bond of this TMF is labile and nucleophilic. This methodology demonstrates the potential of generating TMFs

for the fluorination of organic electrophiles, through modifying and controlling the reactivity of the fluoride.

Similarly, Holland *et. al.,* reported the activation of fluorobenzenes by a low coordinate cobalt[I] complex to give a cobalt[II] bridging fluoride-complex (Scheme 1-7), demonstrating the ability of these first row late transition metals towards the formation of metal-fluorine bonds *via* C−F bond oxidative addition.[122, 123] Oxidative addition of the fluorobenzene resulted in the formation of an unstable mono-fluorinated species, which undergoes reduction with a second cobalt species to give [L^{t}BuCo(μ-F)]$_2$.
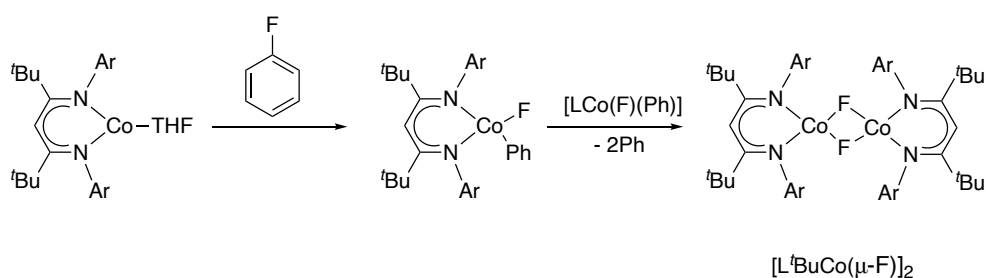
Scheme 1-7: Synthesis of cobalt fluoride complex through oxidative addition of fluorobenzene. Describes an alternate method for the formation of a TMF, through the oxidative addition of a fluoroarene, compared to the more common method of halide exchange with metal fluoride salt. Scheme adapted from literature.[149]

A cobalt[III]-fluoride systems was developed by Baker and co-workers,[120] utilising the metathesis between silver fluoride and the halide ligand to give the resultant fluorinated cobalt complex. Similarly the method outlined by Gray above,[121] treatment of the Co−F complex with toluoyl chloride resulted in quantitative fluorination giving toluoyl fluoride (Scheme 1-8). The generation of this nucleophilic fluoride was key to the development of the reaction. While it is known that third row transition metals tend to form weaker bonds to fluorine,[103] the use of cobalt allowed for the formation of this M-F bond, which could be crystallographically characterised. The authors subsequently developed a catalytic fluorination protocol of toluoyl chloride by forming the active catalytic species *in-situ* using silver fluoride as the fluoride source. This catalytic methodology will be discussed further in *Section 1.7*.
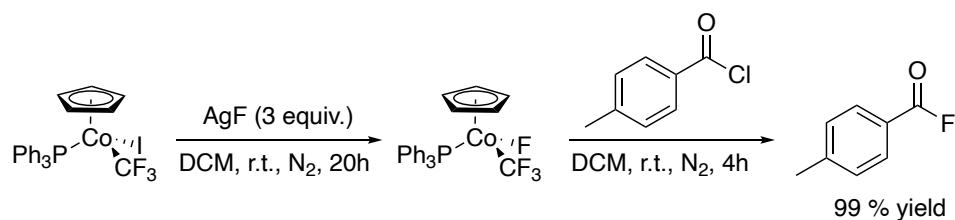
Scheme 1-8: Fluorination of toluoyl chloride by cobalt TMF complex, [CoCp(F)(CF₃)(PPh₃)]. The TMF complex was synthesised and isolated, prior to addition of toluoyl chloride. The method was subsequently developed towards a catalytic methodology where the TMF was generated in-situ through the addition of silver fluoride to [CoCp(I)(CF₃)(PPh₃)]. Scheme adapted from literature. [120]

The generation of TMFs for fluorination is advantageous, especially from a sustainability perspective, as it allows for the enhancement in reactivity of fluoride from metal fluoride salts, with the potential of developing catalytic protocols where the active TMF species is generated *in-situ*. These TMFs can then undergo nucleophilic attack of organic electrophiles, resulting in the establishment of a catalytic fluorination methodology which incorporates non-hazardous substrates with improved atom economy compared to fluorination reagents and traditional fluorination practices.

1.7 Transition metal catalysed nucleophilic fluorination methodologies

Advances within selective transition metal catalysed nucleophilic fluorination reactions, particularly in the last two decades have been developed which are tolerant to a growing range of functional groups.[60, 61, 124, 125] In this time metal catalysed selective fluorination largely follow one of three general methodologies (Scheme 1-9);

i) The formation of a TMF with an external fluoride source, followed by nucleophilic attack of the fluoride with an electrophilic substrate.

ii) The reductive elimination of the fluorinated product from the metal centre following oxidative addition of substrate and fluoride metathesis with an external fluorine source.

iii) The activation of the substrate by the catalyst *via* intermolecular interactions, enabling nucleophilic substitution by a fluoride source.
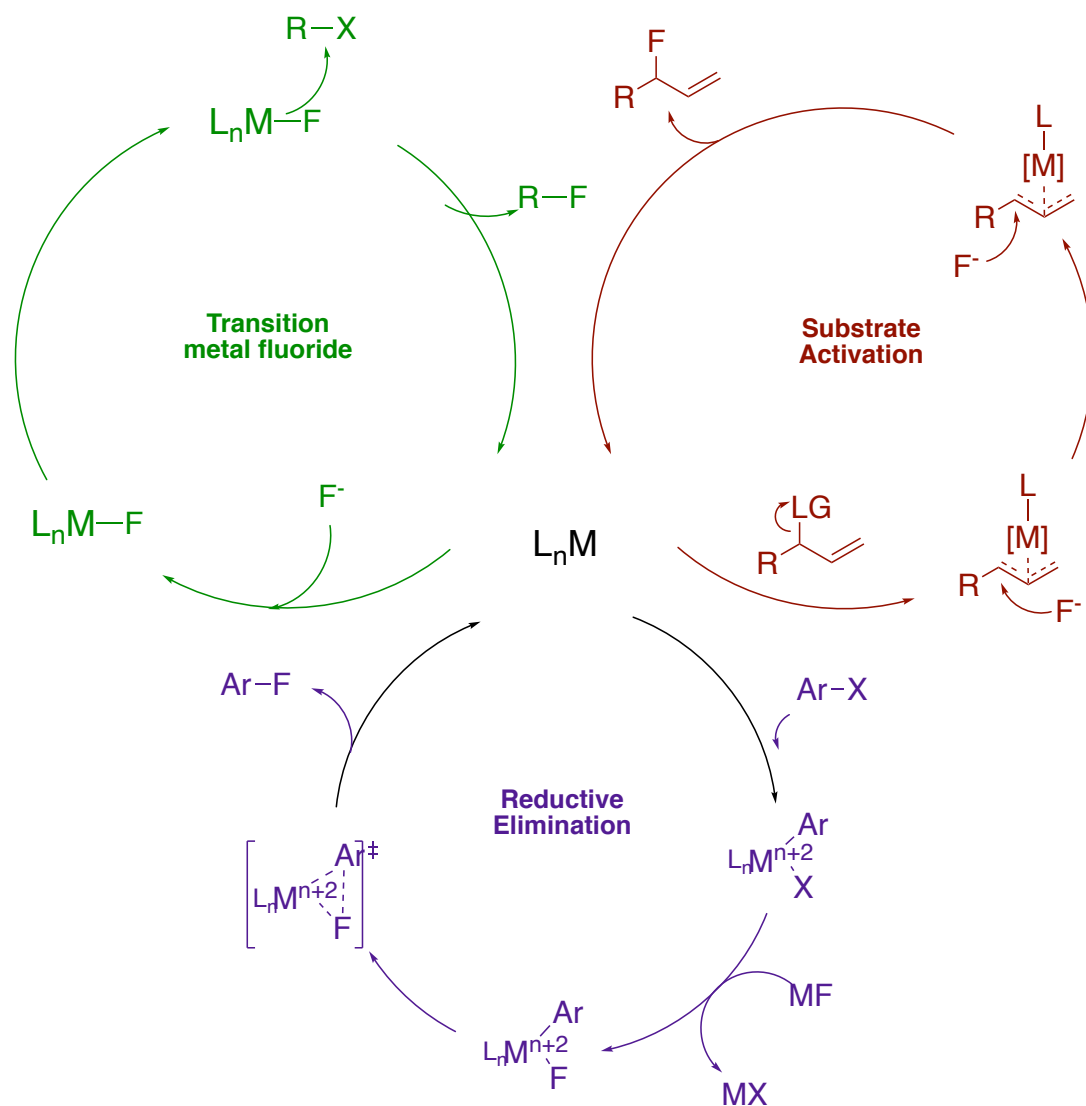
Scheme 1-9: General scheme for the metal mediated/catalysed fluorination of organic substrates: i) in-situ formation of transition metal fluoride, through halide exchange, resulting in the activation of the fluoride towards nucleophilic attack of organic electrophiles (top left; green); ii) oxidative addition of organic substrate across metal centre, followed by halide exchange with fluoride, resulting in formation of fluorinated product following reductive elimination (bottom; purple); iii) activation of an organic substrate through interaction with metal complex, increasing reactivity of substrate towards fluoride nucleophile (top left; red).

As discussed in *Section 1.6*, the formation of an organometallic complex containing a metal-fluorine bond can in some cases leads to the formation of nucleophilic fluorine which can transfer the fluorine from the organometallic complex to an electrophilic substrate, resulting in the formation of a new fluorinated product. As described in *Section 1.6* Gray,[119] Baker[120] and co-workers investigated the synthesis and formation of TMF complexes prior to stoichiometric nucleophilic fluorination. Additional methodologies have been developed towards the fluorination of organic electrophiles, with the proposed formation of the TMF *in-situ*, enabling the catalytic fluorination of organic substrates.

The stoichiometric fluorination of acyl chlorides by a cobalt TMF described by Baker and co-workers, was further developed towards a catalytic fluorination protocol. [120, 126] This system achieved quantitative fluorination of toluoyl chloride after four hours. The ionic character of the Co−F bond was noted by the authors as a major factor contributing towards the complexes fluorination potential. Further development of this system was attempted by changing the ancillary ligands. A high throughput screening method was utilised to probe the effect on the fluorination of benzoyl fluoride against a range of phosphine ligands and precatalytic precursors.[126] Increasing the electron density on the metal, by utilizing Cp* and electron donating phosphine ligands, resulted in improved fluorination over the timescale of the reaction (Scheme 1-10). It was rationalised that greater electron density on the metal, should weaken the cobalt-fluoride bond enhancing fluoride lability and fluorination potential.

It was proposed that this reaction proceeds *via* a halide exchange between the iodine bound to the cobalt and the fluoride source, forming the TMF bond *in-situ*. This nucleophilic fluorine reacts with the electrophilic carbon centre of the acyl chloride, followed by abstraction of the chloride forming a cobalt chloride complex and the acyl fluoride product. The cobalt fluoride complex is regenerated by another equivalent of silver fluoride. A range of acyl chlorides underwent fluorination using this protocol giving the fluorinated product in high yields. This work highlights how an understanding of the nature of TMF formation can lead to the development of a catalytic fluorination methodology.

$$R \overbrace{}^{O}Cl \xrightarrow[\text{DCM, r.t., Ar, 4h}]{\substack{[CoCp^*(I_2)(PPh_2Me)] \ (5 \ mol \ \%) \\ AgF \ (2.5 \ equiv.)}} R \overbrace{}^{O}F$$

up to 99 % yield
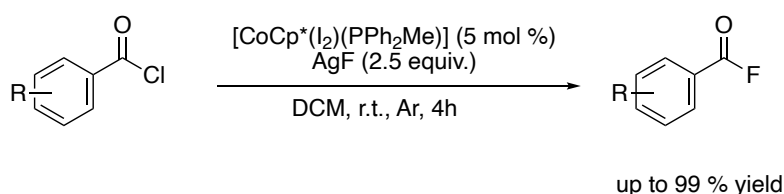
Scheme 1-10: Cobalt catalysed fluorination of acyl chloride using super-stoichiometric quantities of silver fluoride. Strongly electron donating ligands were proposed to enhance fluoride nucleophilicity facilitating near quantitative formation of the fluorinated product. Scheme adapted from literature.[126]

A manganese catalysed fluorination procedure, based on a chloromanganese[III] porphyrin pre-catalyst was developed by Groves and co-workers.[127] This oxidative fluorination procedure utilises silver fluoride as the fluoride source for the selective fluorination of cyclic alkanes. The proposed mechanism proceeds *via* catalyst oxidation with external oxidant, followed by H abstraction from the substrate, generating a substrate radical, prior to formation of a manganese-fluoride bond with silver fluoride. The TMF then reacts with the substrate radical

via fluorine atom transfer resulting in fluorination. This procedure gives moderate yield of the fluorinated product (32 – 57 % yield) with a roughly 1:1 ratio between the desired fluorinated product and oxidated side products. This protocol required the use of super-stoichiometric quantities of both an external oxidant and silver fluoride. This was further developed towards selective decarboxylative fluorination, using a manganese salen complex, showing sufficient activity over 10 minutes enabling the adaption of this decarboxylative fluorination technique towards radiofluorination with [^{18}F], without the requirement of [^{18}F] carrier additives.[128] Radioisotope labelled K^{18}F was found to be suitable for this reaction, however with lower activity than that observed for silver fluoride.

Copper mediated fluorination has also proven to be a successful methodology for the synthesis of aryl fluorides. Often these systems require the use of directing groups or activated substrates to facilitate fluorination, in particular the copper mediated fluorination of aryl stannanes[129] and aryl silanes.[130] These activated substrates are formed from aryl halides and unactivated arenes respectively. The substrate is activated towards fluorination by a TMF generated through the treatment of copper triflate with a fluoride source (metal fluoride salt or KHF$_2$). The TMF then reacts with the activated substrate resulting in the formation of the aryl fluoride. However, these procedures require super stoichiometric quantities of both metal and fluoride source (4-6 equivalents), resulting in moderate yield of the fluorinated product.

While the fluorination of organic substrates through the formation of TMF allows for the fluorination of a growing number of functional groups, the capacity of catalytic nucleophilic fluorination from TMFs remains under-utilised and developing greater understanding around the reactivity of the metal-fluoride bond would be advantageous.

Other metal catalysed and mediated fluorination protocols have been developed which do not rely on the activation of fluoride through the formation of a TMF. The synthesis of aryl fluorides through the oxidative addition of an aryl halide, followed by halide metathesis with a metal fluoride salt, resulting in the reductive elimination of the aryl fluoride product has been extensively reported (Scheme 1-9; ii). [60, 131-148] Additionally, a growing number of reports describe the activation of a substrate towards nucleophilic fluorination through bonding interactions with a metal complex, rather than altering the reactivity of the fluoride source (Scheme 1-9; iii).[149-158] These procedures will not be described in detail, as they are not the focus of this thesis.

The methodologies described in *Section 1.7* often require super-stoichiometric quantities of metal and the use of an external oxidant, coupled with large excesses of a fluorination reagent or metal fluoride salt, generating large volumes of waste. The challenges of atom efficiency,

facile separation and the reduction of the embedded energy associated with these methodologies must be overcome to provide a viable and more sustainable nucleophilic fluorination reaction.

1.8   Project aims

The fluorination of organic compounds is vitally important across many aspects of modern life. However, our current methods of making these fluorinated compounds often rely on unsustainable approaches, characterised by material and energy waste. More sustainable techniques must be developed in order to address the super stoichiometric use of fluoride, expensive additives and hazardous reagents. This project aims to address these issues by attempting to gain an understanding of how to more effectively control the reactivity of fluoride, from metal fluoride salts and perfluorinated compounds. Three different techniques will be probed to investigate how greater control of fluorine can be utilised to access fluorinated molecules through the development of more sustainable catalytic fluorination, defluorination and transfer fluorination methodologies.

A series of group 9 piano-stool NHC complexes, previously synthesised within our extended group and demonstrated to have high catalytic potential in a range of applications, will be probed for their catalytic fluorination potential upon treatment with organic electrophiles, using metal fluoride salts as the fluoride source. It has previously been shown that group 9 organometallic complexes can form TMF upon treatment with metal fluoride salts. Therefore iridium, rhodium and cobalt analogues of the piano-stool NHC complexes will be targeted

These complexes will then be investigated towards the formation of fluorido-complexes, and the reactivity of these complexes upon treatment with organic electrophiles will be examined to gain an understanding of the environment required to generate nucleophilic fluorine. Using this understanding, the development of a new catalytic fluorination protocol for the fluorination of acyl chlorides through the *in-situ* generation of nucleophilic fluorine will be targeted, resulting in nucleophilic substitution with the organic electrophiles. A mechanistic understanding for any catalytic fluorination protocol developed will be evidenced using a range of analytical techniques, including *in-situ* FTIR analysis.

Transfer fluorination methodologies, utilising organic fluorine as the fluoride source will be explored, to understand if perfluorinated groups can undergo C–F bond activation, transferring the fluorine to an external substrate. The reactivity of perfluorinated ligands towards C–F bond

activation and transfer fluorination will be investigated, to probe the possibility of forming acyl fluoride in the absence of an external fluorine source. Multi-spectral analysis of this transformation will be used to provide an understanding of how to generate nucleophilic fluorine and control the transfer of fluorine from the perfluorinated substrate to an organic electrophile. The aim is to further develop any transfer fluorination methodology produced into a catalytic process, to enable the transfer of fluorine from an external perfluorinated group to an organic electrophile.

The development of defluorinative substitution and hydrodefluorination methodologies of perfluorinated substrates will be investigated, with the aim to control the selective defluorination of perfluoroarenes. The combination of these defluorination reactions with catalytic fluorination methodologies will be investigated, with the aim of utilising these potential "waste" organofluorine substrates as fluorine sources.

2 Chapter 2: Synthesis and characterisation of catalytic complexes

2.1 Overview

Group 9 organometallic complexes have long been vital across a range of commercial applications[159] from automotive catalytic convertors and the carbonylation of methanol,[160-163] to the hydroformylation of olefins[164-166] and the production of terephthalic acid[167] amongst others. These numerous, highly efficient industrial protocols highlight the capability of not only group 9 catalysis, but homogeneous catalysis in general as vitally important to the chemical industries (Figure 2-1).

Recently, a new area has emerged exploring the highly active nature of group 9 metals towards nucleophilic catalytic fluorination. These include the fluorination of acyl chlorides using a $[CoCp^{(R)}I_2(PR_3)]$ catalyst (Scheme 2-1; a);[126, 168] an iridium and rhodium catalysed fluorination, using trichloroacetimide as a leaving and directing group (Scheme 2-1; b);[169, 170] and the rhodium catalysed formation of heteroaryl fluorides from heteroaryl ethers[171] (Scheme 2-1; c). Only the method developed by Baker, *et al.* (Scheme 2-1; a)*,* undergoes fluorination through the formation of an *in-situ* TMF bond (*Section 1.6)*.
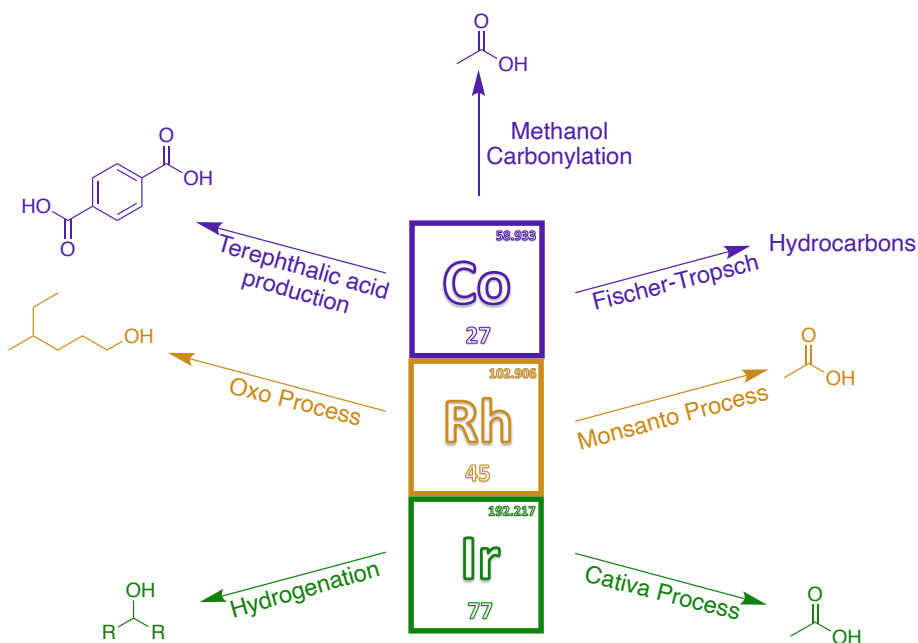
Figure 2-1: Schematic overview of some of the major industrial uses of group 9 homogeneous catalysts. These large scale industrial processes highlight the utility and feasibility of using group 9 homogeneous catalysts in industry.

a)

b)

c)
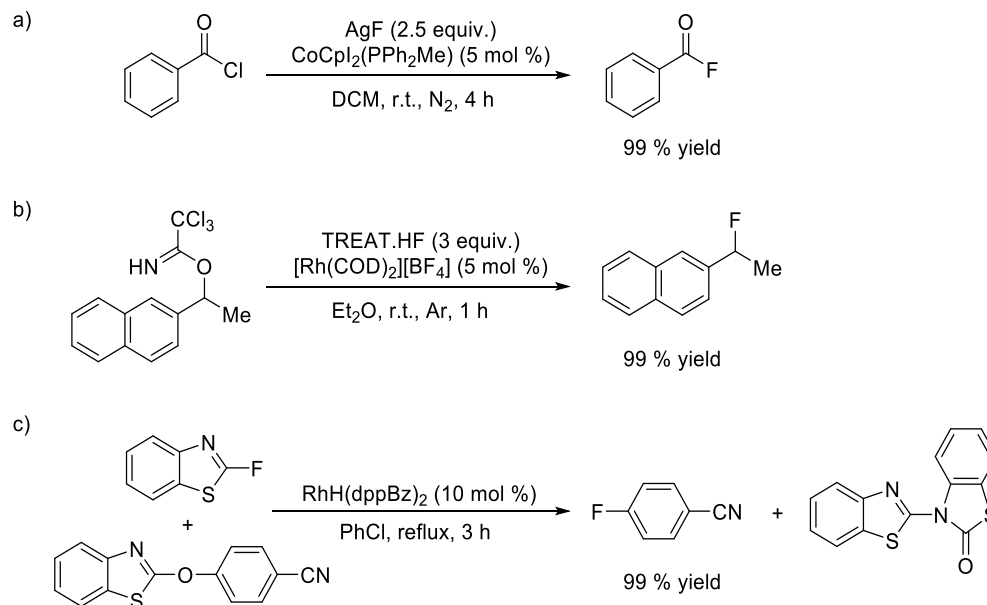
Scheme 2-1. Group 9 catalysed fluorination reactions. a) Fluorination of benzoyl chloride using an optimised cobalt system, where fluorination proceeds via *the formation of a Co–F bond* in-situ[199]; *b) fluorination of benzylic trichloroacetimides, where the trichloroacetimide group acts as a powerful directing and leaving group[200]; c) rhodium catalysed transfer of fluorine between heteroaryl fluorides and heteroaryl aryl ethers to give a range of (hetero)aryl fluorides, where rhodium catalyses the formation of a C–F bond from a C–O bond.* [171]

Even with recent advances within the field, the use of group 9 complexes as fluorination catalysts remain under-utilised, and represent an area in which further research is needed to make group 9 catalysed fluorination techniques more sustainable and economically viable. To address this, the development of a catalytic fluorination protocol was attempted, investigating the reactivity of a range of group 9 organometallic complexes as fluorination catalysts.

Phosphine ligands are commonly employed as ancillary ligands in homogeneous transition metal catalysed reactions[172] due to their strong σ-donating and π-accepting capabilities, in recent years it has been shown that N-heterocyclic carbenes (NHCs) rival or surpass the activity of phosphines in a range of transition metal catalysed reactions,[173, 174] in part due to their enhanced stability, tunability and strongly σ-donating characteristics. The use of NHC complexes has also seen the development of more sustainable processes with improved activity at lower metal loadings, under more sustainable reaction conditions enabling improved systems for catalyst recycling and waste reduction.[175]

Stable NHCs were first synthesised and isolated by Arduengo *et al.*,[176] in 1991. Since their first isolation and characterisation, carbenes have been utilised in a wide array of applications as organic catalysts[177-179] and ligands,[180-183] as well as within materials chemistry,[184-187] including a number of commercially significant processes.[188]

NHCs have also been used as ligands in metal mediated/catalysed nucleophilic fluorination processes, notably the nucleophilic radiofluorination of arylhalides through the use of a stoichiometric copper-NHC species, in the presence of a phase-transfer additive (Scheme 2-2; a).,[136] the copper−NHC catalysed fluorination of propargylic electrophiles (Scheme 2-2; b).[189] and the formation of acyl azolium fluorides from the reaction of acyl fluorides with free NHC (Scheme 2-2; c), which can facilitate the fluorination of a range of activated arylchlorides and nitroarenes.[190]

This work will focus on is a library of complexes developed by Marr, Saunders and co-workers,[191] containing η^5-pentamethyl-cyclopentadienyl and NHC ligands (Figure 2-2). These complexes have been shown to exhibit interesting reactivity across a range of catalytic processes including; water oxidation,[192, 193] transfer hydrogenation,[180, 194] dynamic kinetic resolution,[195] hydrogen transfer initiated dehydration,[181] the alkylation of amines,[196] and dehydrogenative oxidation of alcohols[197] and the activation of aryl carbon–hydrogen bonds[198, 199] and carbon–fluorine bonds.[200]
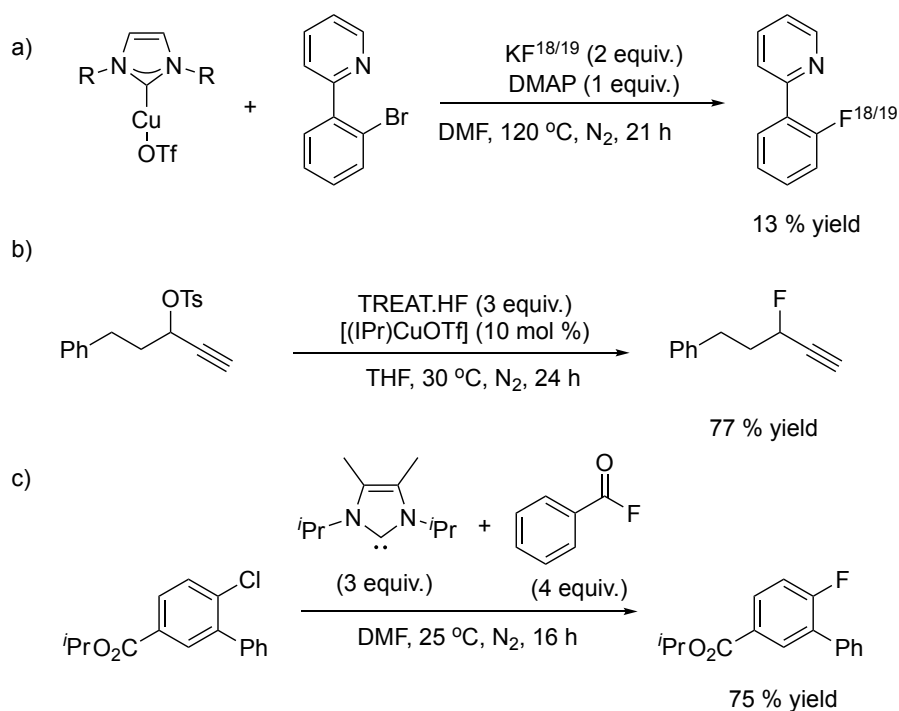
Scheme 2-2. NHC and NHC–metal mediated/catalysed nucleophilic fluorination methodologies. a) A copper–NHC mediated nucleophilic directed fluorination of aryl halides through the formation of a Cu–F bond in-situ. Radiofluorination of aryl halides was achieved using this method[136]; b) A copper–NHC catalysed nucleophilic fluorination of propargylic electrophiles through the formation of a Cu–F bond in-situ which is able to displace the tosylate leaving group forming a new C−F bond[189]; c) The reaction between benzoyl chloride and the NHC produces a soluble acyl azonium fluoride, which acts as an anhydrous soluble nucleophilic source of fluorine for the fluorination of chloroarenes. [190]
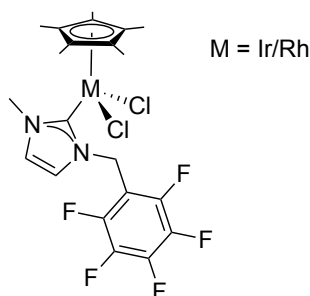
Figure 2-2. Structure of NHC complex which will be utilized and further developed within this work. This complex was targeted due to the electron donating Cp* and NHC ligands in addition to a halide ligand, that may undergo exchange with fluoride. The stability and reactivity of the resultant TMF bond could then be altered through modification of the NHC ligand.

It has previously been shown that by increasing the electron density on the metal through the use of strongly electron donating ligands, the reactivity of metal complexes towards fluorination can be enhanced.[126] This is due to the strongly π-donating character of the fluoride ligand, which when bound to a metal with a high degree of electron density, results in the destabilisation of the metal-fluorine bond. This destabilisation makes the fluoride more reactive, allowing for fluorination to occur more readily.

Bonding between the metal centre and the pentamethylcyclopentadienyl (Cp*) ligand occurs due to overlap of the s,p and d orbitals of the metal with the 5 π-molecular orbitals of the Cp* ligand resulting in the formation of strong π-bonds. The use of Cp* is advantageous due to the stability derived from the increased steric bulk coupled with the greater electron donating ability of the methyl groups. This is beneficial when investigating the formation and reactivity of the metal-fluorine bond as greater electron density on the metal increases the nucleophilicity of the fluoride ligand.

The use of NHCs are of particular interest within these complexes due to the ability to tune the ligands steric and electronic properties through modulation of the side chains on the nitrogen atoms as well as the imidazole backbone itself. NHCs are a type of singlet carbene that contain two non-bonding electrons paired within the same orbital with anti-parallel spin. These electrons are paired within the highest occupied molecular orbital (HOMO) σ, while the pπ remains vacant, making them strong 2 electron σ-donors (Figure 2-3). This allows singlet carbenes to display both nucleophilic and electrophilic character and can be stabilised through the presence of electronegative α-substituents and/or electron withdrawing groups. The ground state electronic configuration of NHCs is characterised by a widening of the band gap between the σ and p$_\pi$ orbitals. The σ-orbital can be stabilised through the inductive effect of electronegative nitrogen α- to the carbon, resulting in a widening of the σ-p$_\pi$ band gap. This

can determine the multiplicity of the carbene as electron withdrawing substituent inductively stabilise the σ nonbonding orbital resulting in an increasing s character while leaving the p_{π} orbital unchanged. This increased the σ-p_{π} band gap resulting the singlet state becoming favoured.
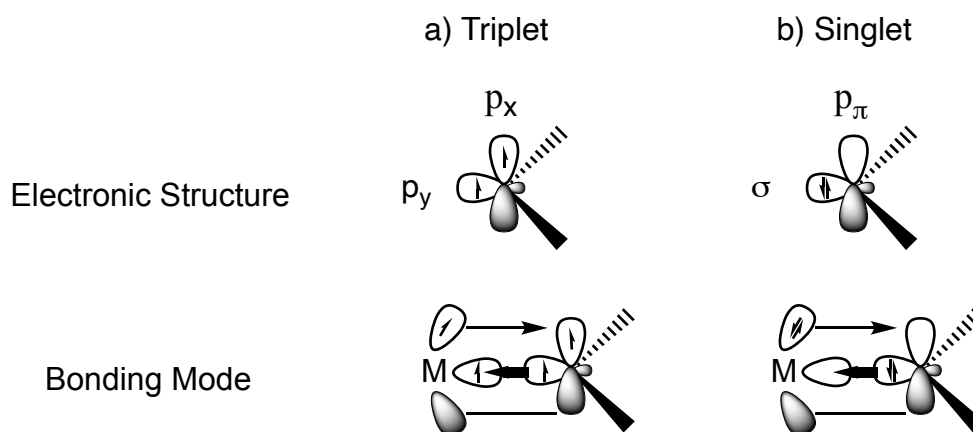
a) Triplet   b) Singlet

Figure 2-3: Electronic structure and bonding mode of triplet and singlet carbenes. Two electrons are located within the same orbital with anti-parallel spin, in the case of singlet carbenes.

While NHCs were initially thought to be purely σ-donating ligands, their π-acceptor ability has recently been show to play a more significant role in metal-carbene bonding than previously thought.[88] This ability to accept electron density from the strongly π-donating fluoride ligand along with their tuneable electron donating nature makes NHCs ideal ligands for investigating catalytic fluorination and the formation of TMFs.

In the context of fluorination from TMFs, the electronic nature of the metal centre is important, where a balance between TMF stabilisation and metal-fluoride lability is required to achieved fluorination and catalytic turnover. Therefore, from a catalytic perspective it is imperative to ensure over-stabilisation of the metal-fluorine bond does not occur. As such the use of NHC ligands containing electron withdrawing groups are interesting targets to investigate.

Chapter 2: Complex Synthesis

2.1 Research aims

The aim of this chapter is to outline the synthetic protocols developed and adapted for the synthesis of a range of group 9 organometallic complexes. The synthesis and characterisation of a range of cobalt, rhodium and iridium-based complexes, bearing NHCs, will be described and the unique reactivity of these complexes upon treatment with silver oxide will be examined. The differing reactivity between these complexes will be discussed. These synthesised complexes with be investigated as catalysts towards the nucleophilic fluorination of organic electrophiles in *Section 3*.

2.2 Synthesis and development of catalytic targets

2.2.1 General Procedure

The initial process in the development of transition metal catalysed nucleophilic fluorination was the synthesis of a range of potential catalysts. The catalytic targets of interest in this thesis are based on the piano-stool group 9 complexes, $[MCp*(Cl)_2(NHC)]$, bearing a $Cp^{(R)}$ group (R=H or Me), an NHC ligand and two terminal halides, where modification of the NHC ligand could result in a change in the catalytic activity of the metal. The rhodium and iridium analogues can readily be prepared using a method previously described by Marr and Saunders.[180, 201] These complexes were targeted due to their tuneable electronic properties, high stability and relatively straightforward synthesis from commercially available starting materials.

A range of iridium and rhodium piano-stool complexes have been synthesised *via* a three-step method with overall yields of 35–93 %. First, the NHC precursor is formed through the reaction of 1-methylimidazole with the substituted benzyl bromide, resulting in the formation of an imidazolium salt. Treatment of this NHC precursor (**1-5**) with silver oxide results in the formation of an NHC-silver adduct, followed by the formation of the iridium or rhodium complexes through transmetallation with the metal precursor, $[RhCp*Cl_2]_2$ or $[IrCp^*(X)_2]_2$, (X=Cl or I) resulting in the formation of the desired complex (**6-20**) (Scheme 2-3). All experimental results and characterisation are consistent with theoretical results and previously synthesised compounds (*Section 2.4*). The molecular structures of selected examples following single crystal XRD are given in Figure 2-4.
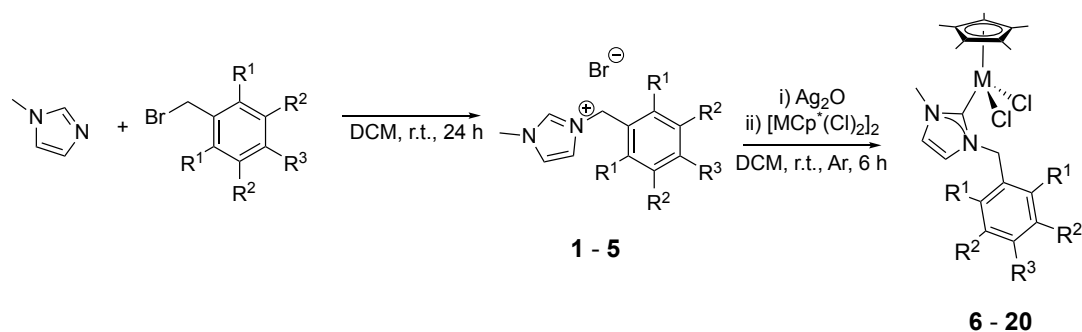
[F$_5$Bzmim]Br, **1**: R^1 = R^2 = R^3 = F (96 % yield)
[F$_4$HBzmim]Br, **2**: R^1 = R^2 = R^3 = F (88 % yield)
[F$_3$Bzmim]Br, **3**: R^1 = R^3 = F, R^2 = H (96 % yield)
[Me$_2$Bzmim]Br, **4**: R^1 = Me, R^2 = R^3 = H (98 % yield)
[Bzmim]Br, **5**: R^1 = R^2 = R^3 = H (84 % yield)

M = Rh
[RhCp*(Cl)$_2$(F$_5$Bzmim)], **6**: (77 % yield)
[RhCp*(Cl)$_2$(F$_5$Bzmim)], **7**: (85 % yield)
[RhCp*(Cl)$_2$(F$_3$Bzmim)], **8**: (93 % yield)
[RhCp*(Cl)$_2$(Me$_2$Bzmim)], **9**: (72 % yield)
[RhCp*(Cl)$_2$(Bzmim)], **10**: (88 % yield)

M = Ir
[IrCp*(Cl)$_2$(F$_5$Bzmim)], **11**: (75 % yield)
[IrCp*(Cl)$_2$(F$_4$HBzmim)], **12**: (75 % yield)
[IrCp*(Cl)$_2$(F$_3$Bzmim)], **13**: (50 % yield)
[IrCp*(Cl)$_2$(Me$_2$Bzmim)], **14**: (49 % yield)
[IrCp*(Cl)$_2$(Bzmim)], **15**: (49 % yield)
[IrCp*(I)$_2$(F$_5$Bzmim)], **16**: (75 % yield)
[IrCp*(I)$_2$(F$_4$HBzmim)], **17**: (69 % yield)
[IrCp*(I)$_2$(F$_3$Bzmim)], **18**: (50 % yield)
[IrCp*(I)$_2$(Me$_2$Bzmim)], **19**: (46 % yield)
[IrCp*(I)$_2$(Bzmim)], **20**: (35 % yield)

Scheme 2-3. General reaction scheme and isolated yields for the benzyl-imidazole ligand precursors 1-5 and group 9 MCp*X$_2$(NHC) complexes 6-20 via transmetallation of the silver imidazolylidene ligand as an NHC transfer reagent. Moderate to high yields of the isolated complexes were obtained
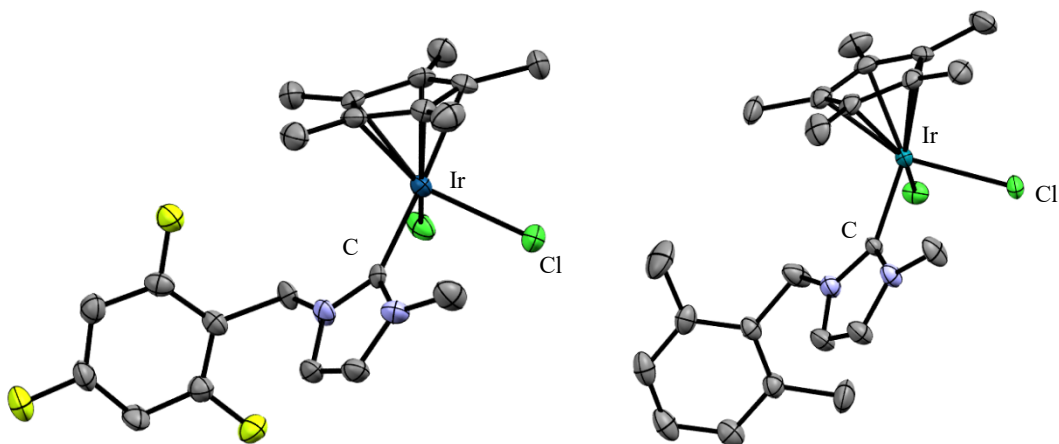
Figure 2-4: Single crystal X-Ray structure of IrCp*Cl$_2$(F$_3$Bzmim), **13** (left) and IrCp*Cl$_2$(Me$_2$Bzmim), **14** (right). Thermal ellipsoids represent 50 % probability. Hydrogen atoms have been omitted for clarity. Selected bond distances (Å); **13**: Ir–Cp* 2.208, Ir–Cl 2.423, Ir–C(NCN) 2.059; **14**: Ir–Cp* 2.211, Ir–Cl 2.428, Ir–C(NCN) 2.067.

2.2.2 Rhodium Complexes

Upon purification of [RhCp*Cl$_2$(F$_5$Bzmim)], **6**, it was found that in addition to the expected peaks of the desired product in the ^{19}F NMR spectrum at -140.6, -151.4 and -160.0 ppm, five additional peaks of a minor side product at -145.6, -149.4, -174.0, -176.8 and -185.7 ppm were detected (Figure 2-5).
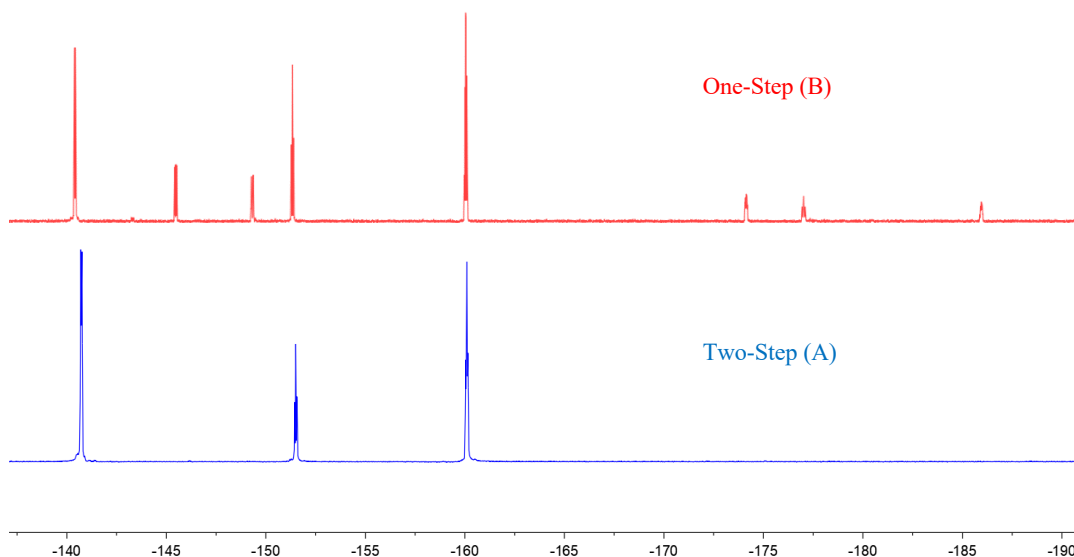
One-Step (B)

Two-Step (A)

Figure 2-5: ^{19}F NMR spectrum of **6** from two-step synthesis (A). A side product was observed in the ^{19}F NMR spectrum of **6** from one-step synthesis (B). The removal of silver by-products before addition of [RhCp*Cl$_2$]$_2$ eliminated the formation of side products. NMR carried out in deuterated chloroform.

This indicated a previously unidentified reaction was occurring with the complex, competing with the formation of the desired product, **6**, resulting in the fluorine atoms on the perfluorinated ring to become non-equivalent. It has previously been shown that the reaction of [IrCp*Cl$_2$(F$_5$Bzmim)], **11**, with silver particles results in *ortho*metallation *via* carbon-fluorine bond activation, resulting in the formation of a four fluorine environment complex, [Cp*IrCl(κC$_2$-MeNC$_3$H$_2$NCH$_2$C$_6$F$_4$)], **21** (Scheme 2-4).[98]
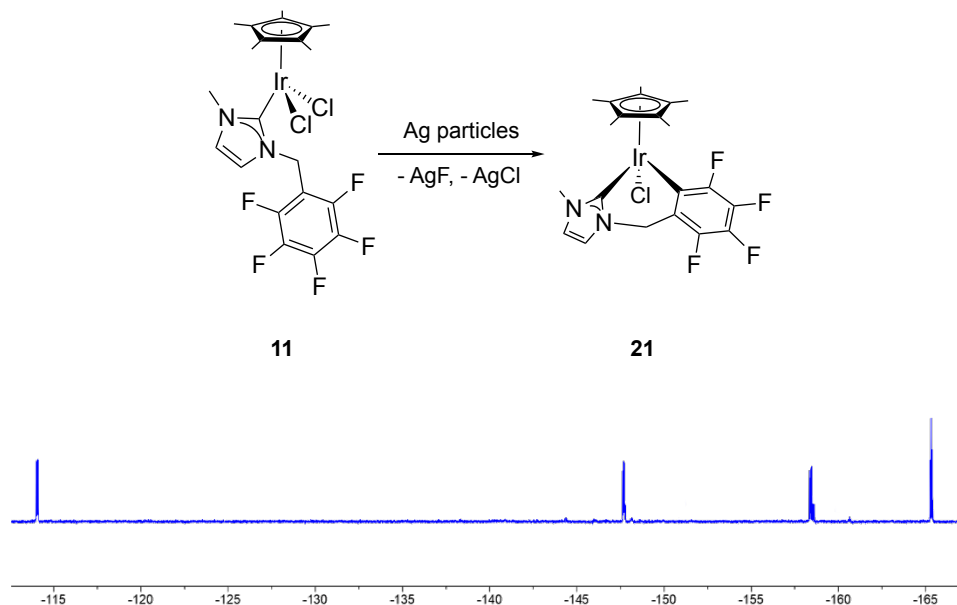
Scheme 2-4: Synthesis of [Cp*IrCl(κC$_2$-MeNC$_3$H$_2$NCH$_2$C$_6$F$_4$)], **21** from reaction between silver oxide and IrCp*Cl$_2$(F$_5$Bzmim). C−F bond activation leading to the formation of the Ir–C bond, resulting in the orthometallated product (top). The four fluorine environments of this complex can clearly be seen from the ^{19}F NMR spectrum (bottom). NMR carried out in deuterated chloroform.

It was highlighted within this publication that the formation of silver particles within the reaction appears to be caused through mechanochemical decomposition of Ag$_2$O *via* stirring.[98] While the spectral signature of this new unidentified minor species does not correspond with that observed previously, it was believed a similar silver mediated process may be occurring, resulting in the formation of this new five fluorine environment species.

As the formation of silver particles was proposed to be the cause of the side reaction, the general synthesis of the complexes described in Scheme 2-3, was adapted to a two-step method. After formation of the NHC-silver adduct any excess silver or unreacted silver oxide was removed *via* a double filtration through a plug of celite, before addition of the metal precursor to the filtrate. This additional filtration step resulted in the isolation of only the desired product, **6**, eliminating the observed side reaction (Figure 2-5). Switching to a two-step method avoids the formation of side products, consistent with a silver mediated side reaction.

Consequently, to test whether the formation of this new five fluorine environment side product was formed due to the presence of silver or silver oxide, **6**, was treated with silver oxide, following a similar procedure developed for the synthesis of **21**.[202] RhCp*Cl$_2$(F$_5$Bzmim), **6**, was treated with silver oxide and left to stand in darkness, under argon, for 24 hours. Over the course of the reaction **6** underwent complete conversion to a new complex.

The ^{19}F NMR spectrum of this new complex showed the peaks associated with **6** at -140.6, -151.4 and -160.0 ppm had completely disappeared and that the five resonance peaks at -145.6, -149.4, -174.1, -176.8 and -185.7 ppm (Figure 2-6), corresponding to the minor product observed previously, were observed.

-144 -146 -148 -150 -152 -154 -156 -158 -160 -162 -164 -166 -168 -170 -172 -174 -176 -178 -180 -182 -184 -186 -188
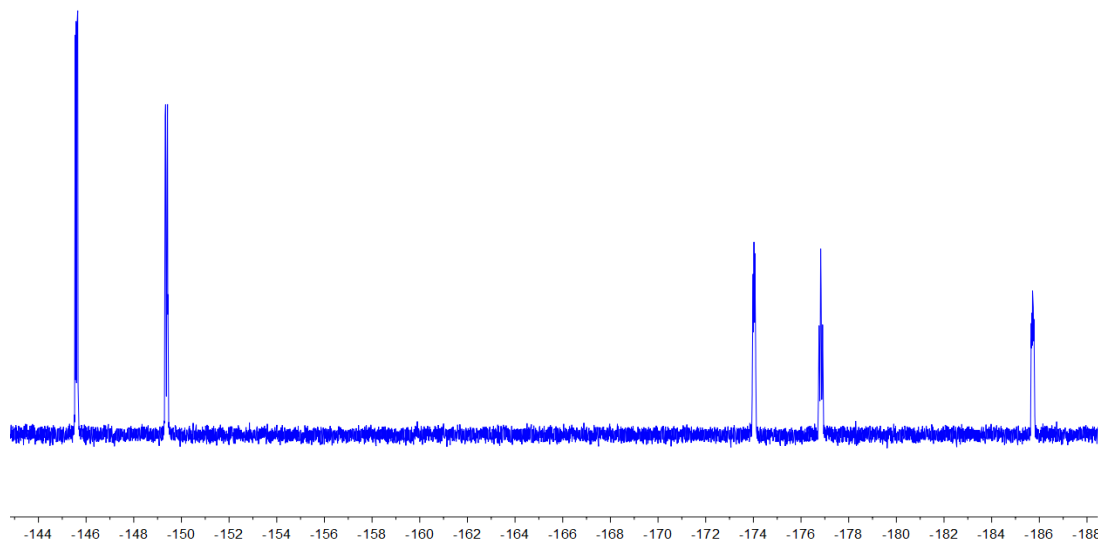
Figure 2-6: ^{19}F NMR spectrum for [(η^5,κ^2C-C$_5$Me$_4$CH$_2$C$_6$F$_5$CH$_2$NC$_3$H$_2$NMe)-RhCl], **22**, showing complete conversion upon treatment of RhCp*Cl$_2$(F$_5$Bzmim) **6** with silver oxide. Five resonance peaks are observed at -145.6, -149.4, -174.1, -176.8 and -185.7 ppm, representative of the five non-equivalent fluorine atoms on the polyfluorocyclohexadiene ring. NMR carried out in deuterated chloroform.

^{1}H NMR data showed the presence of four pentamethylcyclopentadienyl resonances at δ 0.74, 1.39, 1.80, and 1.86 and two mutually coupled doublet resonances at δ 1.38 and 1.76, consistent with the formation of a non-equivalent pentamethylcyclopentadienyl group.[203] The identity of this species was confirmed by XRD studies (Figure 2-7). The formation of the new complex, [(η^5,κ^2C-C$_5$Me$_4$CH$_2$C$_6$F$_5$CH$_2$NC$_3$H$_2$NMe)-RhCl], **22**, proceeds through the route described in Scheme 2-5.[204]
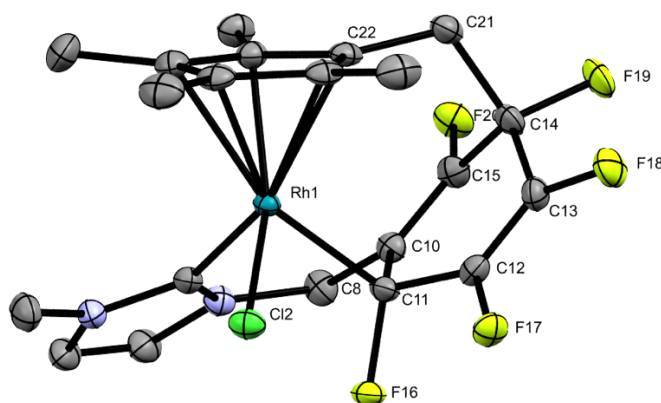
Figure 2-7. Single crystal X-Ray structure of [(η^5,κ^2C-C$_5$Me$_4$CH$_2$C$_6$F$_5$CH$_2$NC$_3$H$_2$NMe)-RhCl], **22**, showing the dearomatisation of the polyfluorophenyl ring and tethering to the Cp* ligand. Thermal ellipsoids represent 50 % probability. Hydrogen atoms and solvent molecules have been omitted for clarity.
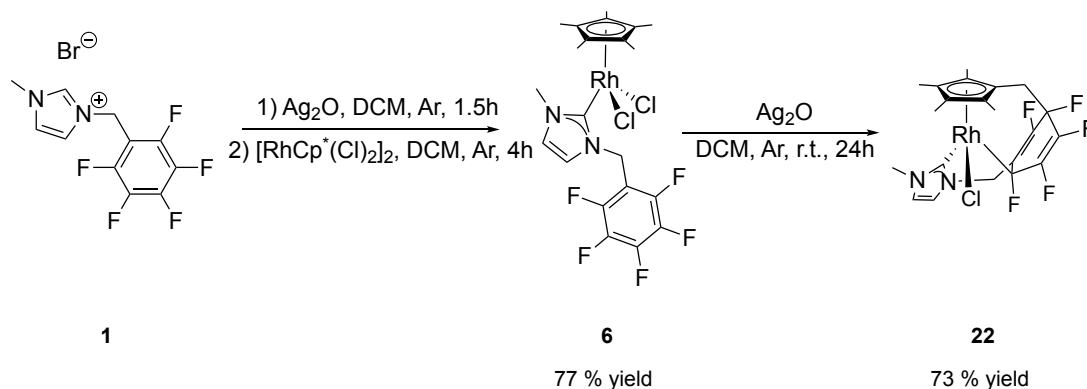
*Scheme 2-5: Synthesis of [(η^5,κ^2C-C$_5$Me$_4$CH$_2$C$_6$F$_5$CH$_2$NC$_3$H$_2$NMe)-RhCl], **22**, through treatment of RhCp*Cl$_2$(F$_5$Bzmim), **6**, with silver oxide.*

It can be seen that the rhodium centre and a methylene carbon on the pentamethylcyclopentadienyl ring has undergone 1,4-addition to the pentafluorophenyl ring resulting in loss of aromaticity and the formation of a new Rh–C bond. The resonance pattern observed with this complex was consistent with other polyfluorocyclohexa-1,4-dienes.[205] The loss of aromaticity is evident through the adoption of a boat conformation with atoms C(11) and C(14) exhibiting tetrahedral geometry with the bond distances between C(12)–C(13) and C(10)–C(15) (1.326(3) Å and 1.328(3) Å respectively) consistent with double bonds with four single bonds between C(10)–C(11), C(11)–C(12), C(13)–C(14) and C(14)–C(15) (1.477(3) Å, 1.468(3) Å, 1.486(3) Å and 1.485(3) Å respectively). Of particular interest was the lengthening of the C(11)–F(16) and C(14)–F(19) bonds (1.409(2) Å and 1.404(2) Å, respectively) on the tetrahedral carbon centres, α- to the rhodium and Cp*. These bonds were 0.057 Å longer than the average C−F bond distance of the other three fluorine atoms in the ring. MS data was consistent with the formation of **22**, giving a major mass peak at 535.0448 *m/z*, corresponding to the calculated mass fragment for C$_{21}$H$_{21}$ClRhF$_5$N$_2$ of 535.0447 *m/z*.

The formation of this new complex is proposed to proceed *via* the abstraction of a chloride, forming a cationic species, increasing the acidity of the pentamethycyclopentadienyl hydrogen atoms. Following loss of a proton with base, the nucleophilic methylene carbon and Lewis acidic rhodium centre undergo a concerted 1,4-addition of the pentafluorophenyl ring resulting in the formation of **22** (Scheme 2-6). No intermediate towards the formation of **22** was identified, however once the zwitterion is formed the reaction is expected to progress rapidly. The limiting factor for the reaction is thought to be the formation of the zwitterion due to the heterogeneous nature of silver oxide.
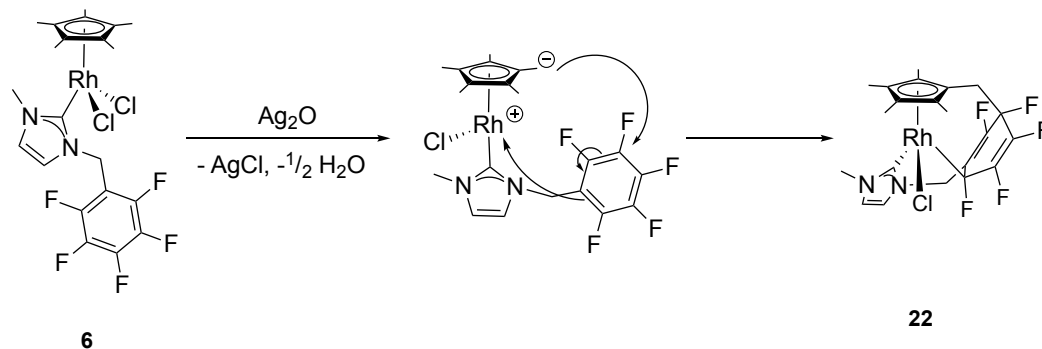
Scheme 2-6: Proposed mechanism for the reaction between RhCp*Cl$_2$(F$_5$Bzmim), **6** and silver oxide. Abstraction of chloride by silver, followed by base mediated deprotonation of Cp* results in a concerted 1,4-addition of the pentafluorophenyl ring from the nucleophilic methylene carbon and the Lewis acidic metal centre.

Unlike the case for the previously reported iridium analogue, the treatment of **6** with either silver oxide or silver nanoparticles did not result in the formation of [Cp*RhCl(κC$_2$-MeNC$_3$H$_2$NCH$_2$C$_6$F$_4$)], **23**. Therefore, an alternative route to its synthesis was required. It was found that treatment of RhCp*Cl$_2$(F$_4$HBzmin), **7**, with silver oxide resulted in C−H bond activation assisted *ortho*metallation.[206] Treatment of 3-methyl-1-(tetrafluoro)benzyl imidazolium bromide with silver oxide results in the formation of the NHC-silver adduct, followed by the formation of the desired complex, **7**, through *trans*metallation with [RhCp*Cl$_2$]$_2$ (Scheme 2-7). The reaction proceeded in the absence of light and crystallisation of the concentrated filtrate from pentane at *ca*. -20 $^\circ$C allowed for collection of the pure product in high yields (85 % yield). Recrystallization by vapour diffusion of hexane into a concentrated solution of the complex in DCM resulted in the collection of X-Ray quality single crystals.
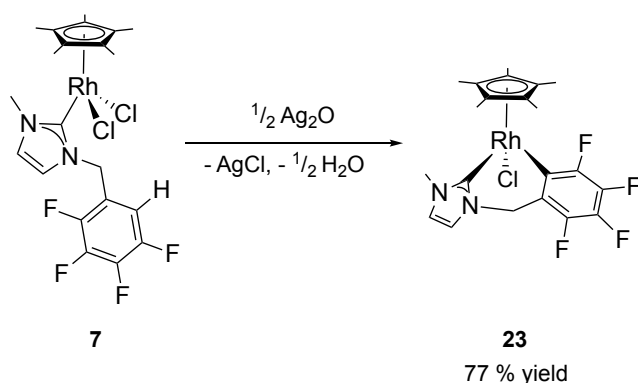
*Scheme 2-7. Formation of [Cp*RhCl(κC$_2$-MeNC$_3$H$_2$NCH$_2$C$_6$F$_4$)], **23** via C−H bond activation following reaction of RhCp*Cl$_2$(F$_4$HBzmin), **7**, with silver oxide. Replacing one of the ortho-fluorine atoms on the perfluorinated ring changes the observed reactivity upon addition of silver oxide.*

The spectroscopic data of **23**, synthesised using this alternative method was consistent to that observed for **21**. ^{19}F NMR analysis identified four resonance peaks at -137.3, -145.5, -155.1 and -156.1 ppm, corresponding to the four non-equivalent fluorine atoms on the tetrafluorophenyl ring. Additionally, mass spectrum analysis of **23** gave the expected peak for $C_{21}H_{23}F_4N_2ClRh$ of 517.0538 *m/z*. The structure was confirmed through XRD studies (Figure 2-8). Once the desired complex, **23** has been synthesised from **7**, subsequent studies into accessing **23** from **6** were conducted. These studies showed that when silver oxide was added to dilute DCM solutions of **6** (4 µM), **23** was the major product as a result of C−F bond activation, compared to previous results giving **22** from concentrated DCM solutions (15 µM). This allows for alternate routes to the desired complexes.
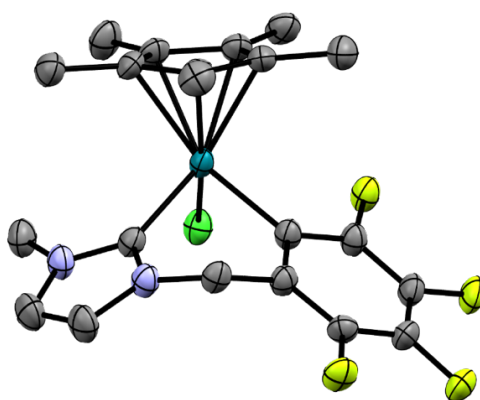
Figure 2-8. Single crystal X-ray structure of RhCp*Cl$_2$(F$_4$Bzmim), **23**. Thermal ellipsoids represent 50 % probability. Hydrogen atoms and solvent molecules have been omitted for clarity.

The formation of *cyclo*metallated and *ortho*metallated analogues, bearing less-fluorinated substituted benzimidazole ligands were then targeted. In addition to an interest in the synthesis of a range of additional *cyclo*metallated and *ortho*metallated complexes for potential use in future catalysis, it was envisioned that less fluorinated ligands would enable greater nucleophilicity of the fluoride, as greater electron density would be located on the metal centre, in complexes without the electron withdrawing pentafluorophenyl ring, thereby destabilising a potential TMF bond. However, attempts to synthesise the *cyclo*metallated complexes, including the tetrafluorophenyl-, trifluorophenyl- and (4-trifluoromethyl)phenyl-benzimidazolium substituted complexes gave no reaction upon addition of silver oxide. This will be discussed further in *Section 6*.

2.2.3   Iridium Complexes

Similarly to the rhodium analogue above, the formation of a five fluorine environment side product was observed upon purification of [IrCp*Cl$_2$(F$_5$Bzmim)], **11**, with the ^{19}F NMR spectrum of the side product at -146.1, -151.3, -172.2, -175.1 and -188.4 ppm (Figure 2-9). Unlike our previously reported example where treatment of **11** with silver particles results in *ortho*metallation *via* carbon-fluorine bond activation,[202] [Cp*IrCl(κC$_2$-MeNC$_3$H$_2$NCH$_2$C$_6$F$_4$)], **21**, was not observed under these conditions (Figure 2-9).

The structural characterisation of **22** gave insights into the possible structure of the minor side product identified due to similarities in the ^{19}F NMR spectrum of **11** from the one-step method (Figure 2-9). **24** was isolated following multiple recrystallisation and filtration steps resulting in the spectral characterisation of **24**. ^{19}F NMR spectrum gave a similar spectral signature to **22**, with resonance peaks at -146.1, -151.3, -172.2, -175.1 and -188.4 ppm.
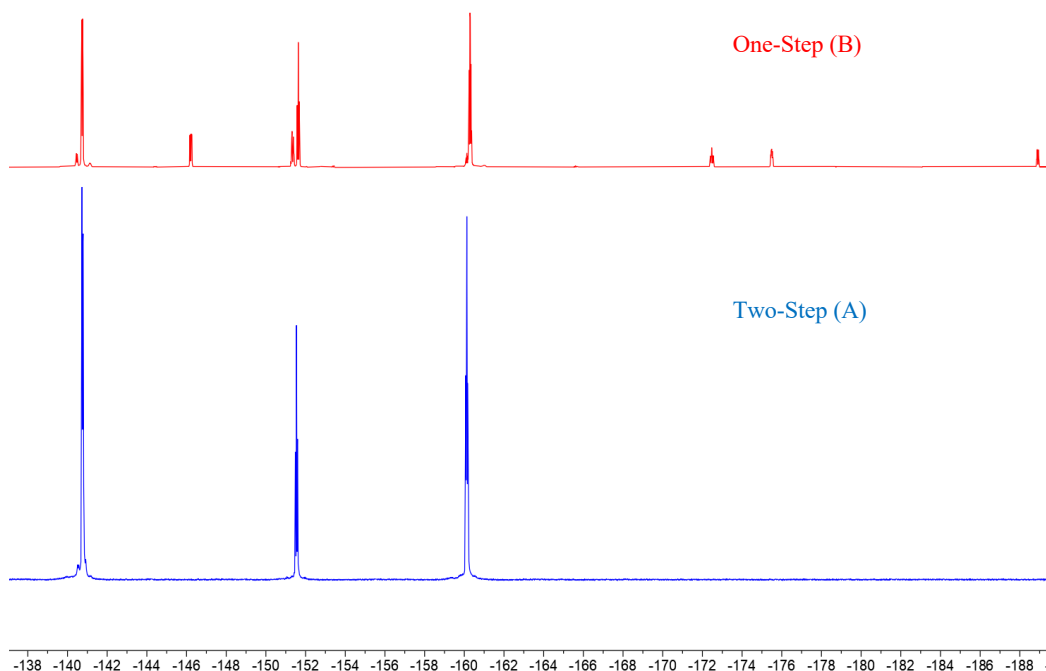
*Figure 2-9: ^{19}F NMR spectrum of **11** from two-step synthesis (A). A side product was observed in the ^{19}F NMR spectrum of **11** from one-step synthesis (B). The removal of silver by-products before addition of [IrCp*Cl$_2$]$_2$ eliminates the formation of side products. NMR carried out in deuterated chloroform.*
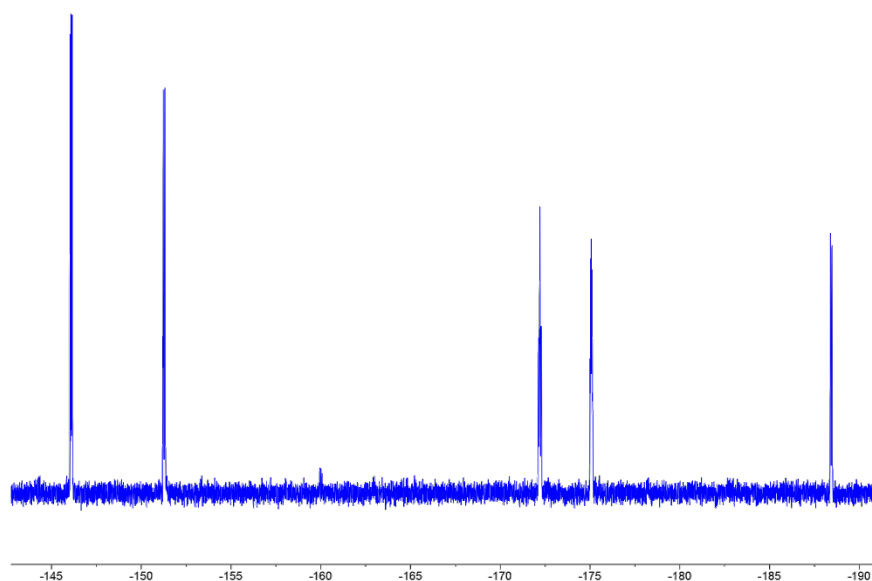
*Figure 2-10: ^{19}F NMR of **24**, showing complete conversion upon treatment of **11** with silver oxide. Five resonance peaks are observed at 146.1, -151.3, -172.2, -175.1 and -188.4 ppm, representative of the five non-equivalent fluorine atoms on the polyfluorocyclohexadiene ring. This is consistent with the spectrum gathered for **22**, showing minor (≈ 1 – 3 ppm shifts) between the rhodium and iridium analogues. NMR carried out in deuterated chloroform.*

The ^{1}H NMR spectrum also shows four cyclopentadienyl methyl resonances at 1.55, 1.69, 1.83 and 1.84 ppm which is consistent with previously described examples of **22**. This evidence coupled with the mass spectrum which gave a peak for $C_{21}H_{21}IrF_5N_2$ at 589.1249 *m/z*, compared to a theoretical value of 589.1254 *m/z*, allowed us to confirm the formation of [(η^5,κ^2C-C$_5$Me$_4$CH$_2$C$_6$F$_5$CH$_2$NC$_3$H$_2$NMe)- IrCl], **24** from the reaction of **11** with Ag$_2$O, following the same mechanism as that described for the rhodium analogue **22** (Scheme 2-6). The absolute conformation of **24** was also characterised by XRD (Figure 2-11). The structure of **24** is consistent with that observed for **22**.
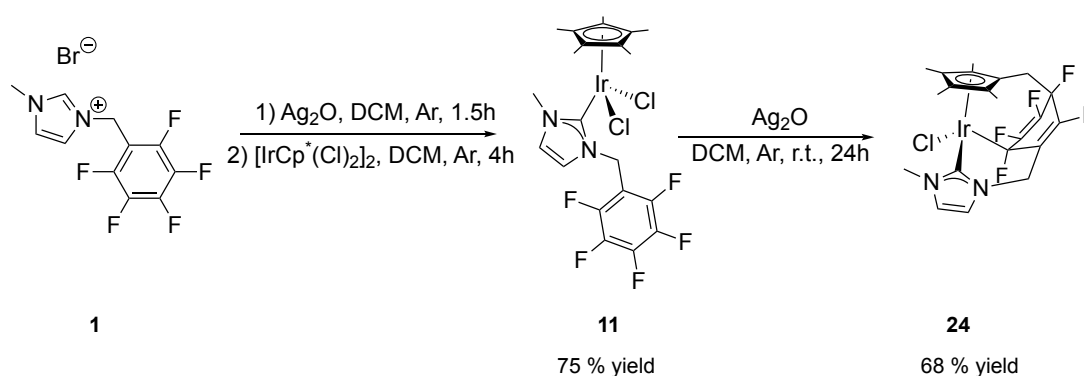
Scheme 2-8: 1,4-addition of the iridium centre and pentamethylcyclopentadienyl methylene carbon into the pentafluorophenyl ring induced by the reaction between complex **11** and silver particles.
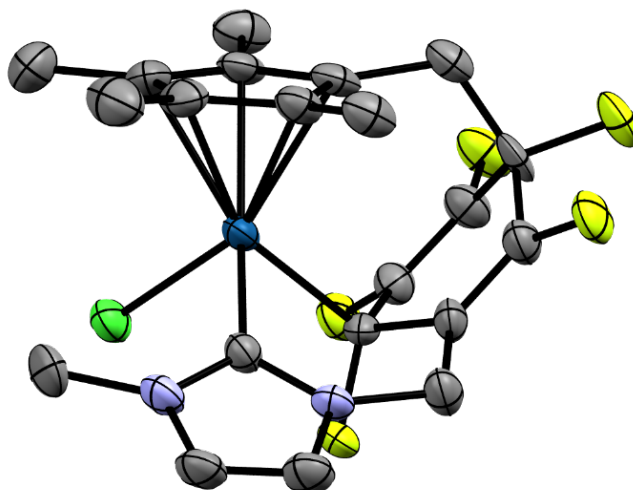
Figure 2-11. Single crystal X-ray structure of [(η^5,κ^2C-C$_5$Me$_4$CH$_2$C$_6$F$_5$CH$_2$NC$_3$H$_2$NMe)-IrCl], **24.** Thermal ellipsoids represent 50 % probability. Hydrogen atoms have been omitted for clarity.
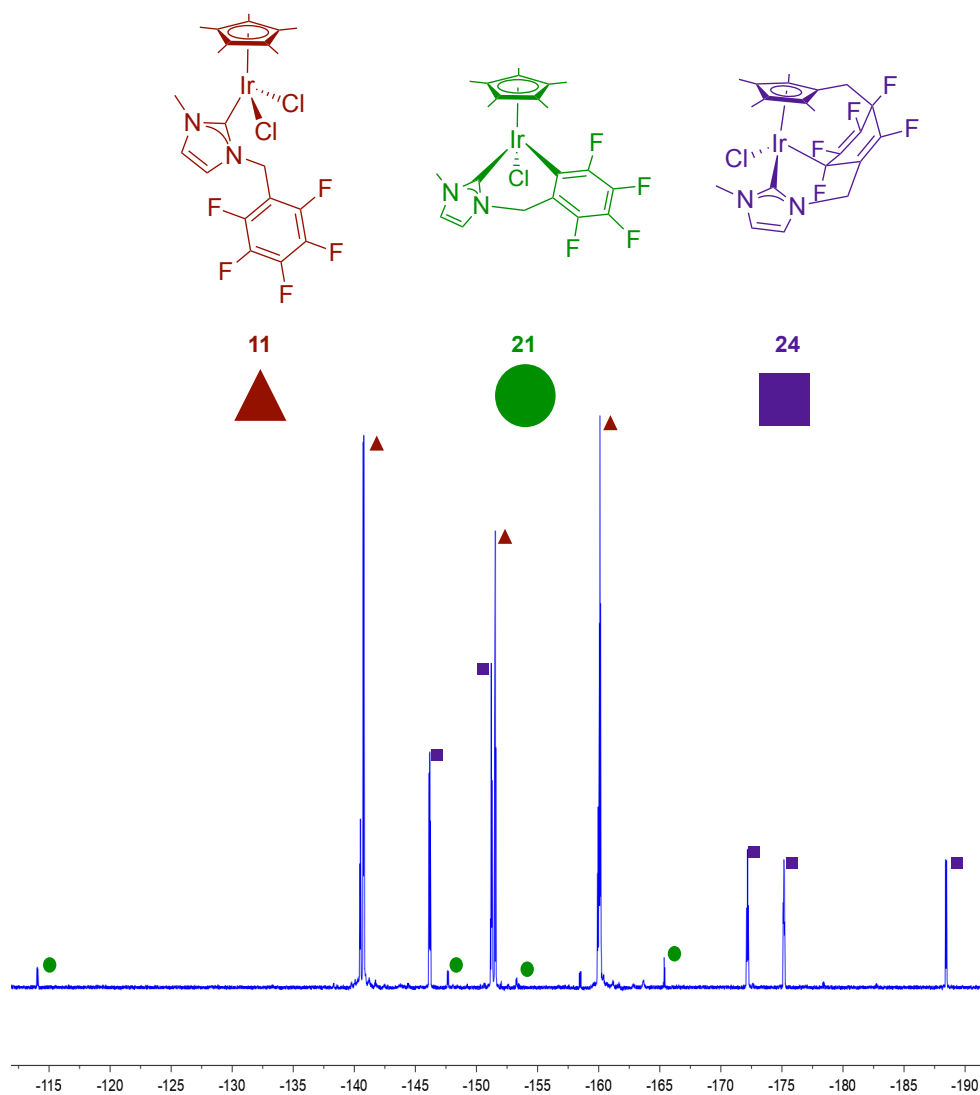
Figure 2-12. ^{19}F NMR spectrum following treatment of **11** with silver oxide. The reaction results in the formation of a number of products which could not be separated. The formation varying quantities of **24** (purple) in addition to **21** (green) was found, with a significant quantity of unreacted **11** (red). NMR carried out in deuterated chloroform.

Unlike for the synthesis of **22**, the treatment of **11** with silver oxide did not cleanly result in the formation of **24**. Following the same procedure as described in the synthesis of **22**, **11** was dissolved in DCM (20 mL) and treated with silver oxide (two equivalents) and left to stand in darkness under argon for 48 hours. Upon work-up, a mixture of products were identified following NMR analysis, giving varying ratios of **11**, **24** and **21** (Figure 2-12).

To better understand how each of these products formed over the course of the experiment, the reaction was monitored over the course of 120 hours (Figure 2-13). It was found that the formation of the five equivalent fluorine atom complex, **24**, forms preferentially over the formation of the four equivalent fluorine complex, **21**. Following 24 hours, the minor product, **24**, is observed. The concentration of **24** within the reaction increases over the following 72 hours. The spectral signature of **21** is observed after 24 hours as a minor resonance peak on the baseline. Its concentration increases significantly after 48 hours. Although clean conversion of **11** to **24** was not achieved this reaction gave insight into the formation of both the 1,4-addition product **24** and the *ortho*-metallation product **21**. The reaction was monitored for five days. The relative rates of formation of **21** and **24** can be rationalised through their proposed mechanism of formation.

11 reacts with silver oxide resulting in the formation of a zwitterion which undergoes 1,4-addition with the pentafluorophenyl ring.[205] While the zwitterion formation is slow due to the different phases of the reaction, once it has formed it reacts rapidly with the pentafluorophenyl ring (Scheme 2-6 for the rhodium analogue). This reaction proceeds over the course of 24 hours, resulting in the formation of **24**.

 The formation of **21** takes longer as *ortho*metallation requires the formation of silver particles through the decomposition of silver oxide which is a slow process, especially as no stirring took place to achieve mechanochemical decomposition. Upon formation of silver particles, the silver species acts as a reductant, abstracting the chloride from the metal centre, resulting in the formation of silver chloride. This is thought to then promote the oxidative addition of the aryl C−F bond, leading to **21** upon halex exchange (Scheme 2-9). The formation of silver particles is the limiting factor towards the formation of **21** which can clearly be seen as the relative concentration of **21** rises following 42 hours, allowing time for silver particle formation (Scheme 2-10). In fact, when freshly prepared silver nanoparticles[207] were added to a solution of **11**, the orthometallated product, **21**, was accessed cleanly over the course of four hours, consistent with the hypothesis described above.
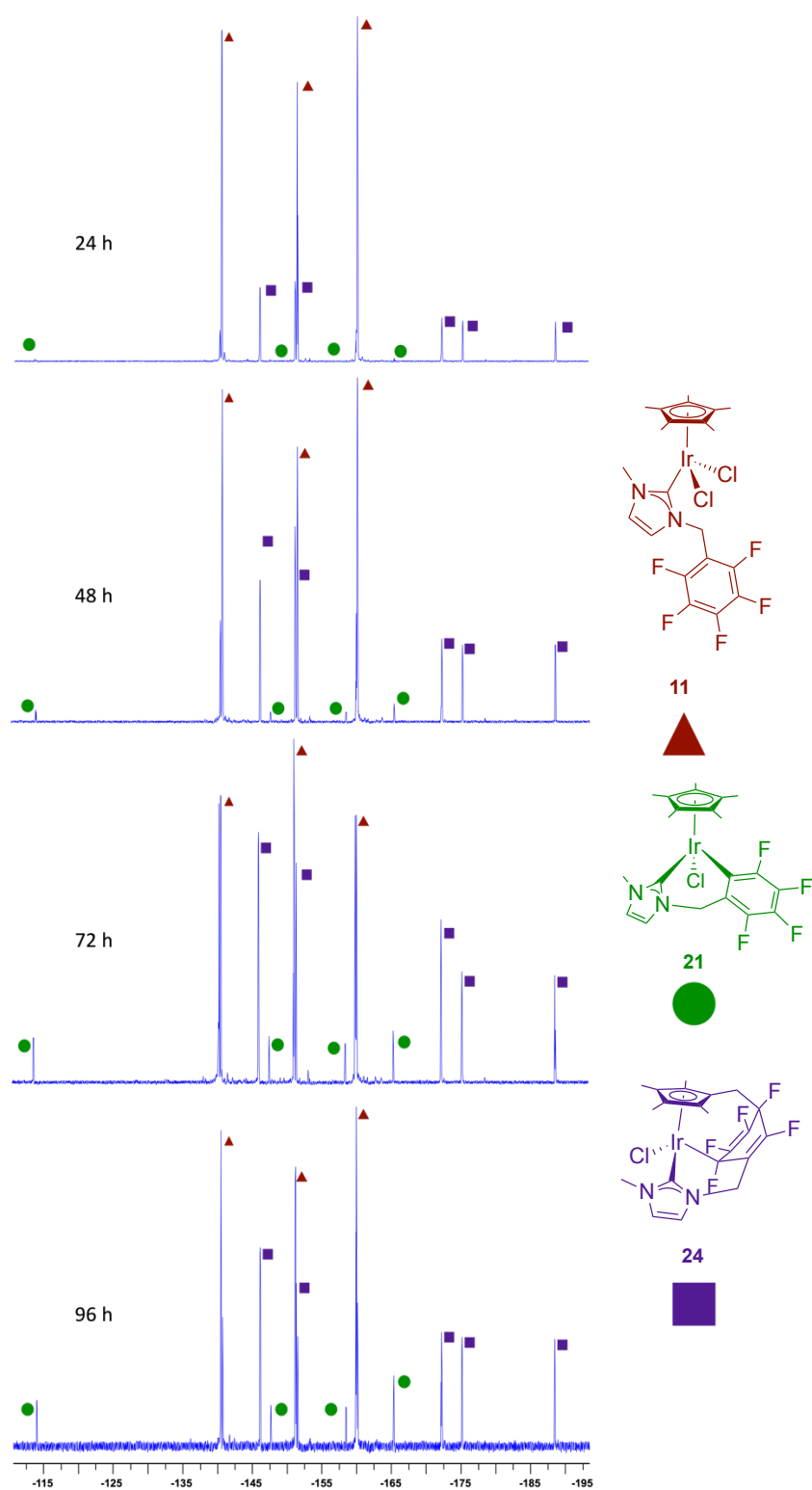
Figure 2-13: ^{19}F NMR spectrum for the reaction of **11** (red), with silver oxide over 96 hours. Initial formation of **24** (purple), is observed after 24 hours. **21** (green), is present after 24 hours, however its relative concentration compared to **24** increases over the following 72 hours. *NMR carried out in deuterated chloroform.*
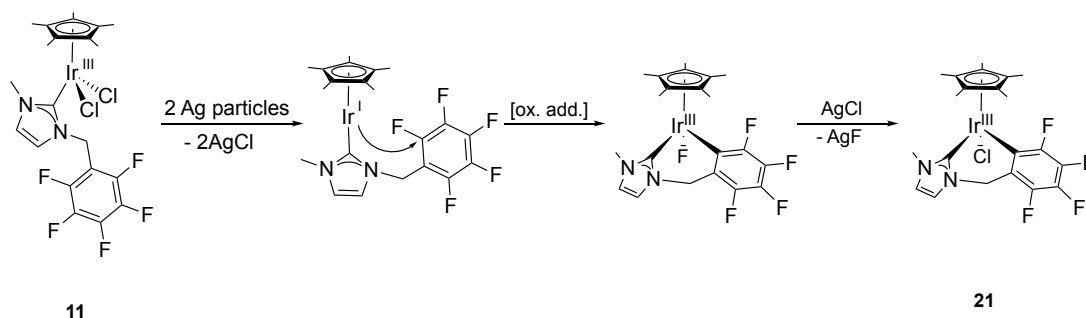
Scheme 2-9. Proposed mechanism for the reaction between **11** and Ag$_2$O, resulting in the formation of **21**. Silver particles act as a reductant leading to the astraction of terminal halide by silver and formation of an iridium^I species. This promotes the concerted oxidative addition of the pentafluorophenyl ring followed by abstraction of fluoride resulting in the formation of **21**.
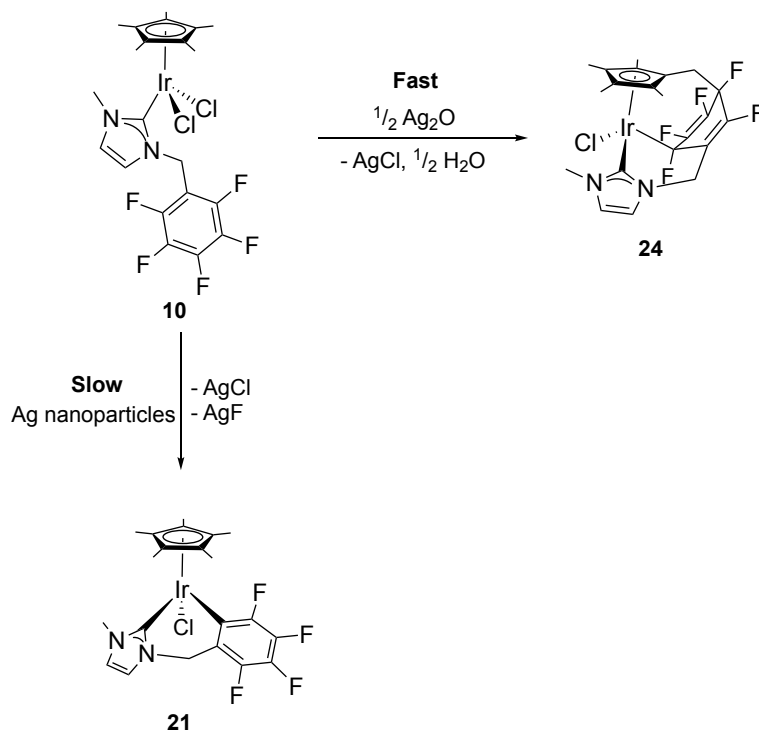
*Scheme 2-10: Proposed routes describing access to **24** promoted cyclometallation via silver oxide and **21** formation through action of silver nanoparticles. The formation of **24** proceeds via the abstraction of chloride from **10** followed by the deprotonation of a methylene carbon, initiating cyclometalation. Whereas, the formation of **21** occurs more slowly, as the formation of silver particles is the limiting factor. If silver nanoparticles are used instead of silver oxide, the formation of **21** occurs rapidly.*

When the iodo-analogue, IrCp*I$_2$(F$_5$Bzmim), **16**, was treated with silver oxide, the 1,4-addition product was never observed. It cleanly converted to the *ortho*metallated species, [Cp*IrI(κC$_2$-MeNC$_3$H$_2$NCH$_2$C$_6$F$_4$)], **25**, over the course of 24 hours. It is proposed that this was due to the more favourable abstraction of iodide from **16**, compared to the chloride ligand in **11**.

This could be due to the more favourable formation of silver iodide, as a thick layer of silver iodide was observed at the phase boundary between the silver species and solution indicating that the abstraction of iodide, forming silver iodide, was more favourable than for the chloride complexes (Figure 2-14).

Figure 2-14. Picture showing the pale off-white precipitate silver iodide by-product, following the reaction of 16 with silver oxide. Under the same conditions treatment of 10 with silver oxide produces a much lower quantity of pale yellow AgCl precipitate, with a significant proportion of unreacted silver oxide remaining.

Further studies also identified the clean formation of **24** upon treatment of **11** with silver oxide, when in dilute dichloromethane solutions, compared to the previously discussed formation of **21** upon treatment of **11** in concentrated dichloromethane solutions.

2.2.4   Cobalt Complexes

The ACS GCIPR highlighted that the need for the development of catalytic procedures using base group metals was imperative,[43] due to the negative environmental and sustainability concerns associated with the noble metals, coupled with the expense and scarcity of rhodium and iridium, piano stool NHC complexes of cobalt were targeted. Additionally, as cobalt forms a stronger metal-fluorine bond than rhodium and iridium, due to better orbital overlap between cobalt and fluorine, the formation of these complexes was proposed to give an improved likelihood of forming TMF complexes.

As no cobalt analogue, $[CoCp*Cl_2]_2$, was commercially available, a different route to the synthesis of the catalytic precursor was required. Following a search of the relevant literature two possible routes were identified that could lead to the synthesis of the desired cobalt complexes; one to synthesise a range of cyclopentadienyl complexes from $[CoCp(CO)_2]$,[208, 209] and the other to synthesise a range of pentamethylcyclopentadienyl complexes from $[Co_2(CO)_8]$.[210-212] These $[CoCp^{(*)}LX_2]$ complexes have previously been shown to be accessible for addition of pentafluorobenzyl complexes, therefore their synthesis was of interest to this work.[213] Both $[Co_2(CO)_8]$ and $[CoCp(CO)_2]$ are extremely toxic and air sensitive, therefore any manipulations using these reagents were done under strict Schlenk conditions.

Treatment of $[Co_2(CO)_8]$ with Cp*H, in toluene for 6 hours leads to the formation of $[CoCp^*(CO)_2]$. Over the course of the reaction effervescence was observed as the colour of the reaction lightened from dark mauve to red in colour. Following removal of the solvent *in vacuo*, iodine (in a diethyl ether solution) was added dropwise into an ether solution of $[CoCp*(CO)_2]$ over the course of two hours. This resulted in a deep purple solution, due to oxidative addition of iodine across the metal centre, with vigorous effervescence during the course of iodine addition, indicating CO displacement. An ice bath was required as the reaction between $[CoCp*(CO)_2]$ and iodine was exothermic. Excess iodine was removed through addition of hexane and filtration of this hexane solution *via* cannula. Any additional iodine was removed upon sublimation under vacuum. This led to the isolation of $[CoCp^*I_2(CO)]$ in excellent yields (95 % yield) following purification *via* layered diffusion of hexane into a saturated solution of DCM to afford a purple black crystalline solid (Scheme 2-11).
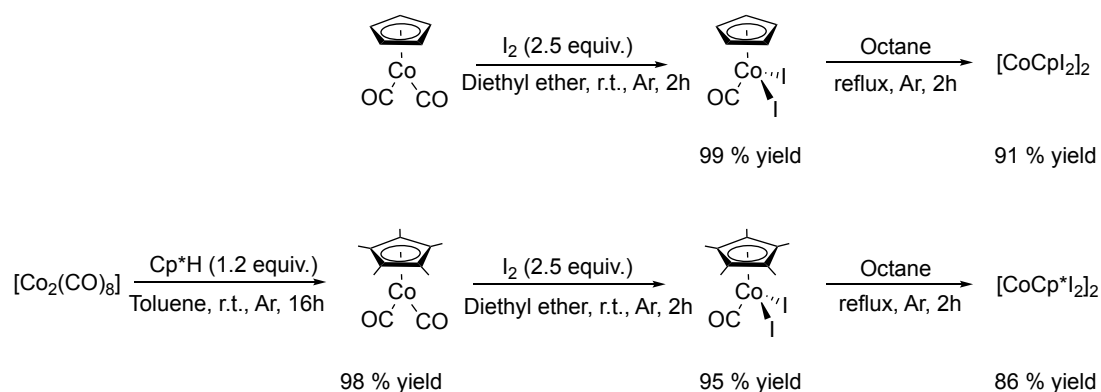
Scheme 2-11. Synthetic route towards the formation of [CoCpI$_2$]$_2$ and [CoCp*I$_2$]$_2$. Both [CoCp$^{(*)}$I$_2$(CO)] and [CoCp$^{(*)}$I$_2$]$_2$ will be used as precursors towards the synthesis of the desired cobalt NHC complexes. Either CpH or Cp*H can be used upon treatment with [Co$_2$(CO)$_8$] for afford the respective cyclopentadienyl or pentamethylcyclopentadienyl [CoCp$^{(*)}$I$_2$]$_2$ complexes.

X-Ray quality single crystals were grown in this manner. The product was found to be stable upon immediate exposure to air, however following literature advice it was stored under an inert atmosphere.[210] Characterisation of the product was consistent with literature values and absolute configuration was identified through single-crystal X-Ray diffraction (Figure 2-15). The synthesis of [CoCpI$_2$(CO)] from [CoCp(CO)$_2$] follows this adapted synthetic pathway. The synthesis of these complexes are summarised in Scheme 2-11.
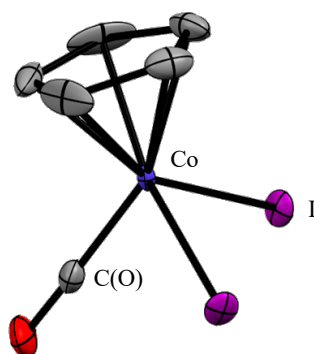
Figure 2-15: Single crystal X-ray structure of [CoCpI$_2$(CO)]. Thermal ellipsoids represent 50 % probability. Hydrogen atoms have been omitted for clarity. Selected bond distances (Å) Co-Cp* 2.083(6), Co-I 2.568(9), Co-C(O) 1.793(8).

With the desired cobalt precursors in hand the formation of the cobalt complex CoCpI$_2$(F$_5$Bzmim), **26**, was conducted using an adapted method to the iridium and rhodium analogues. This proceeded through the transmetallation of the NHC-silver adduct with **35** forming the desired complex (Scheme 2-12).

44
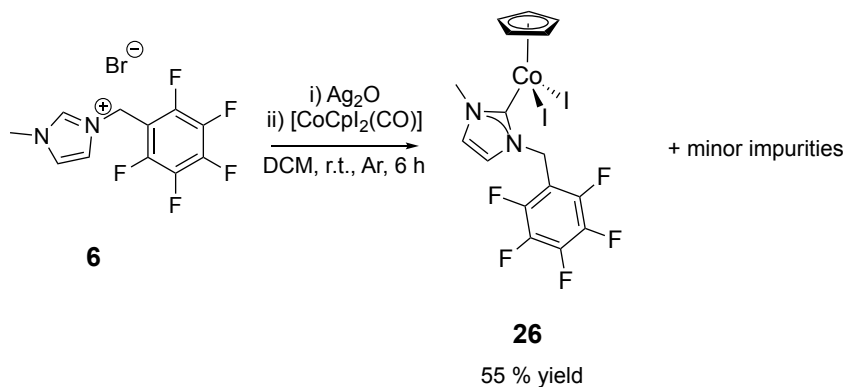
Scheme 2-12: Synthetic route for the formation of CoCpI₂(F₅Bzmim), 26. This resulted in the formation of unwanted by-products which could not be removed upon purification attempts.

Unlike in the case of the iridium and rhodium complexes, this reaction proceeds *via* a ligand exchange with the carbonyl group, as light effervescence is observed upon addition of [CoCpI$_2$(CO)]. The reaction proceeds in the absence of light and oxygen to prevent the decomposition of silver oxide and the cobalt precursor respectively. A crude product was isolated in 59 % yield, however spectroscopic analysis of this crude product identified the formation of an unidentified impurity which could not be removed upon further purification steps. Following recrystallisation of the crude reaction mixture, two distinct sets of crystals were observed. This was evident through the formation of dark purple crystals of the desired **26**, coupled with colourless crystals within the recrystalised crude product, that when analysed following XRD showed the formation of cobaltocene, a known decomposition product of [CoCpI$_2$(CO)], [CoI$_4$]$^{2-}$ and the imidazolylidene ligand (Figure 2-16). Due to the formation of impurities, which competed for the desired reaction and could not be separated from the crude product, an alternative route to the synthesis of the piano-stool cobalt complexes was devised.
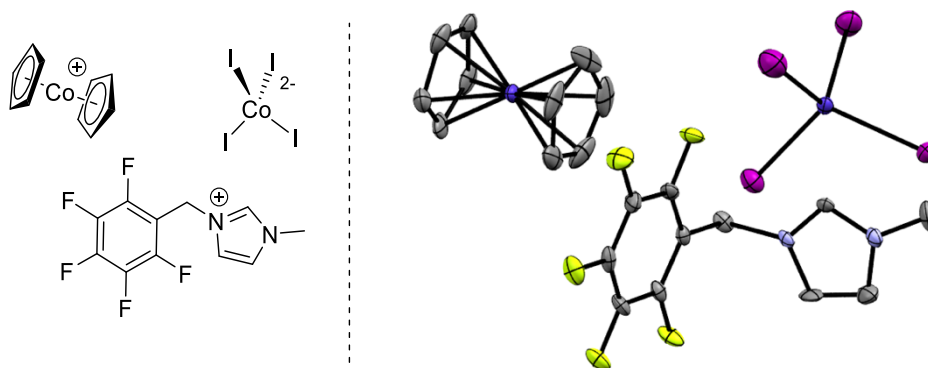
Figure 2-16: Imidizolylidene ligand and decomposition products from synthesis of **26**. Thermal ellipsoids represent 50 % probability. Hydrogen atoms and solvent molecules have been omitted for clarity.

This method was developed to avoid the formation of decomposition products found to be commonly associated with $[CoCp^{(*)}I_2(CO)]$. This alternative method involves the synthesis of the cobalt analogue of the iridium and rhodium precursors, $[CoCp^{(*)}I_2]_2$.[214] It was discovered that $[CoCp^{(*)}I_2(CO)]$ undergoes rapid decarbonylation, under refluxing *n*-octane,[215] and dimerization of the complex leading to the successful synthesis of $[CoCp^{(*)}I_2]_2$ (Scheme 2-13). Unreacted starting material was observed, shown by the presence of a carbonyl stretching band within the IR spectrum ($\nu_{CO} = 2025$ cm^{-1}). Purification *via* soxlet extraction in DCM lead to the isolation of the pure complex in 65 % yield. It was isolated as a dark green powder.
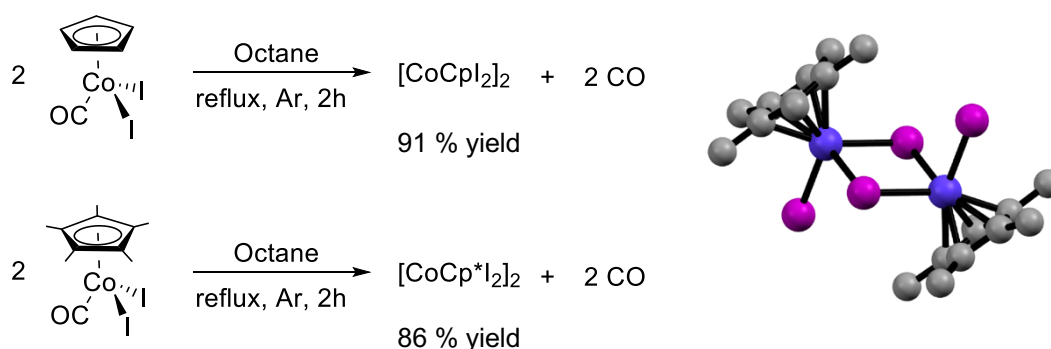
Scheme 2-13. *Formation of cobalt dimer, $[CoCp^{(*)}I_2]_2$, from the decarbonylation of $[CoCp^{(*)}I_2(CO)]$, under refluxing octane (left). Molecular structure of, $[CoCp*I_2]_2$ (right). Thermal ellipsoids not described due to quality of data set, however identification is determined. Hydrogen atoms have been omitted for clarity.*

The formation of the dimer was confirmed through MS and XRD. The mass found was consistent with the decarbonylated species and recrystallization from vapour diffusion of hexane into a concentrated solution of the product in dichloromethane resulted in the formation of X-Ray quality single crystals. XRD allowed for product identification however due to the quality of the data set absolute configuration and atomic displacement parameters could not be assigned (Scheme 2-13). $[CoCp*(I_2)]_2$ has previously been synthesised however structural characterisation through X-Ray diffraction has not previously been reported.[215]

XRD studies also identified the formation of an unexpected by-product following the reaction. A three element bridging complex, $[(Cp*Co)_2(-\mu-I_3)]$, was identified following XRD of the purified product (Figure 2-17). This complex, while theorised to exist in 1982,[216] had not previously been structurally characterised. This impurity was not observed within the bulk sample following mass spectrum and NMR spectroscopic analysis. Additional attempts to isolate a crystal of this complex from the same and subsequent recrystallisation attempts were unsuccessful.
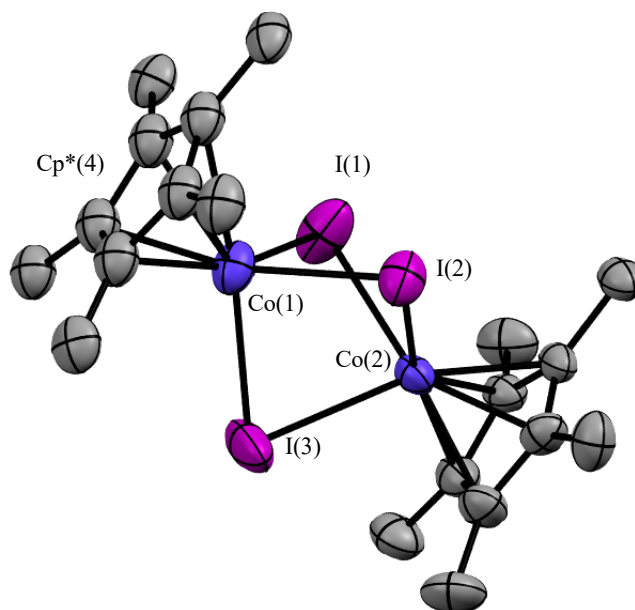
Figure 2-17: Molecular structure of [(CoCp*)₂(-µ-I₃)]. This is the first crystallographic characterisation of this complex. Thermal ellipsoids represent 50 % probability. Hydrogen atoms and counterions have been omitted for clarity. Selected bond distances (Å) and angles (deg): Co(1)–Cp*(4) 2.078, Co(1)–I(2) 2.628, Co(1)–C(9) 1.955; Cp*(4)−Co(1)−I(2) 87.01, Cp*(4)−Co(1)−C 43.84, I−Co−C 95.38.

With the cobalt analogue, $[CoCp^{(*)}I_2]_2$, in hand, this complex could be used as a direct drop-in to the synthesis of the NHC complexes, following the route described for the rhodium and iridium complexes. Addition of $[CoCp(*)I_2]_2$ to a dichloromethane solution of the NHC-silver adduct resulted in the formation of the desired complex, $CoCp^{(*)}I_2(F_5Bzmim)$, **27**, over the course of 4-6 hours (Scheme 2-14) in a 68 % yield.

68 % yield
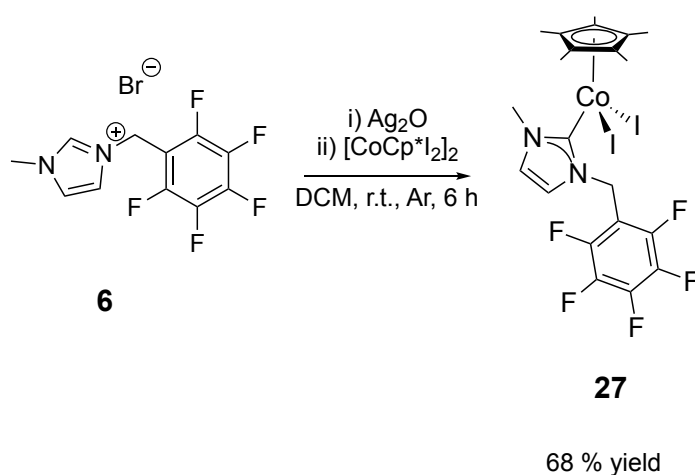
*Scheme 2-14. Synthesis of CoCp*I₂(F₅Bzmim), **27**, via the transmetallation of imidazolium silver adduct with [CoCp*I₂]₂.*

Subsequent workup, purification and recrystallization allowed for the isolation of X-Ray quality single crystals from vapour diffusion of hexane into a concentrated solution of the metal complexes in DCM forming black crystalline needles. NMR spectroscopic characterisation of the product was consistent with that observed in the iridium and rhodium analogues. Three resonance peaks were evident within the ^{19}F NMR spectrum, their chemical shift indicative of the NHC ligand bound to the metal centre; -140.3, -152.1 and -160.6.

Four additional resonance peaks (-105.4, -111.0, -148.3 and -158.0 ppm) were visible in ^{19}F NMR in trace quantities above the baseline. These are believed to correspond to the minor formation of the *ortho*metallated product with a similar spectral signature of the *ortho*metallated iridium complex **21**, however further studies on silver oxide addition to promote cyclometallation or *ortho*metallation of **27** proved inconclusive.

The molecular structure of both the **26** and **27** were identified through single-crystal X-Ray diffraction (Figure 2-18). The geometry and bond distances of this complex is consistent with that observed with in the crystal structures of the analogous iridium and rhodium complexes. As expected for a first row transition metal, the bond distances between the metal centre and the Cp* and NHC ligands are shorter than the analogous iridium complexes (Co–Cp*: 2.078(12) Å and Co–C(NCN): 1.962(11) Å vs Ir–Cp*:2.208(3) Å and Ir–C(NCN): 2.067(4) Å). This new cobalt complex, **27**, was found to be air stable over the course of one week in the solid state.
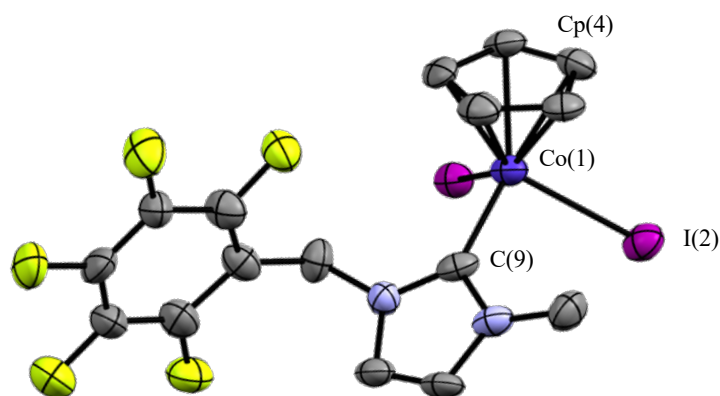
*Figure 2-18: Molecular structure of **26**. Thermal ellipsoids represent 50 % probability. Hydrogen atoms and solvent molecules have been omitted for clarity. Selected bond distances (Å) and angles (deg): Co(1)–Cp(4) 2.078(12), Co(1)–I(2) 2.628(18), Co(1)–C(9) 1.962(11); Cp(4)−Co(1)−I(2) 87.1(3), Cp(4)−Co(1)−C(8) 43.84(5), I(2)−Co(1)−C(9) 95.38(3).*

2.3 Summary

A simple and facile route to the synthesis of a range of group 9 organometallic complexes, which had previously been developed within our extended group, has been adapted and expanded upon. This has given access to a range of rhodium and iridium complexes bearing different NHC groups in moderate to excellent yields. All complexes have been characterised with, ^{1}H, ^{13}C and ^{19}F NMR analysis, HRMS, EA and single crystal XRD (where appropriate). A new route to the synthesis of cobalt analogues of these complexes has been developed from commercially available starting material, allowing for the synthesis of the cobalt complexes on a moderate scale (up to a 0.1 mol).The synthesis and characterisation of **22**, **23**, **24**, **21** has been explored, with separate routes designed to target the desired complex. With the development of practical synthetic routes towards the synthesis of all complexes described, the catalytic activity of these complexes towards the catalytic fluorination of acyl chlorides can be probed, allowing for comparisons between their reactivity and catalytic potential to be gained.

Further work would focus on the synthesis of cyclometallated and orthometallated iridium and rhodium complexes bearing less fluorinated ligands in order to increase the electron density at the metal centre. Additionally, further work on the clean formation of *cyclo*metallated and *ortho*metallated cobalt complexes would be of great interest.

2.4   Experimental

2.4.1   General

All reagents were purchased from Sigma Aldrich, Acros Organics, Alfa Aesar, Strem Chemicals or Fluorochem. Reagents purchased from Sigma Aldrich include; acetone, dichloromethane, chloroform, methanol, acetonitrile, ethyl acetate, pentane, hexane, diethyl ether, tetrohydrofuran, toluene, hexafluorobenzene, 1-Fluoronapthelene, 1-Methylimidazole, silver(I) oxide, cyclopentadienylcobaltcarbonyl, dicobalt octacarbonyl, diiodo(pentamethylcyclopentadienyl) iridium[III] dimer and dichloro(pentamethylcyclopentadienyl) rhodium[III] dimer. Reagents purchased from Fluorochem include; (2,3,4,5,6-Pentafluoro)benzylbromide, (2,4,6-Trifluoro)benzylbromide and (2,6-Dimethyl)benzylbromide. Dichloro(pentamethylcyclopentadienyl)iridium[III] dimer, 1-Benzylimidazole was purchased from Acros Organics. Pentamethylcyclopentadiene (98 %) was purchased from Strem Chemicals.

NMR spectral analysis was carried out using a Bruker Ascend 400 spectrometer (400 MHz) and Bruker Ascend 500 spectrometer (500 MHz) at room temperature ($\approx$ 300 K). The scan range was as follows; ^{1}H NMR: 16 to -3 δ/ppm; ^{19}F NMR: 20 to -210, -190 to -410 and -390 to -610 δ/ppm; ^{13}C NMR: 230 to -10 δ/ppm. ^{1}H and ^{13}C NMR spectra were referenced to the corresponding residual solvent signals (MeOD: 4.87 ppm for ^{1}H, 49.00 ppm for ^{13}C; CDCl$_3$: 7.26 ppm for ^{1}H, 77.16 ppm for ^{13}C; C$_6$H$_6$: 7.160 ppm for ^{1}H, 128.060 for ^{13}C). The ^{19}F NMR spectra were referenced by an internal method of the NMR. The chemical shifts are reported in ppm. Signal multiplicities are reported as singlet (s), doublet (d), triplet (t), quartet (q), pentet (p) and multiplet (m). J values are given in Hz. NMR resonances were assigned by assessing multiplicity and coupling constants, and comparing against previously reported compounds. For ^{19}F NMR density functional theory calculations were also performed (*Section 4.6.5*). NMR assignments for all synthesised complexes are given; ^{1}H NMR (green), ^{19}F NMR (red) and ^{13}C NMR (blue). IR spectra were recorded in cm^{-1} with a Bruker Alpha FTIR spectrometer equipped with a universal diamond ATR or a transmission IR in the form of a KBr disc and a Bruker Vertex 70 FTIR spectrometer equipped with a universal diamond ATR for far-IR measurements. Other measurements include ESI-MS (Bruker micrOTOF II with Agilent technologies 1200 Infinity Series G1315D DAD), Karl Fischer coulometric titration (CA-200 moisuremeter from Mitsubishi chemical analytech) and X-Ray diffraction measurements were conducted at the School of Chemistry, University of Nottingham (Agilent SuperNova diffractometer, Atlas CCD area detector, using Cu microfocus X-Ray sources).

Single crystals were identified for potential X-Ray diffraction measurements (Olympus BX51 system microscope) and crystal data was processed using OLex^2. Single crystals were prepared using layered diffusion or vapour diffusion methods using the appropriate solvent/anti-solvent combinations. Elemental analysis conducted at the School of Chemistry, University of Nottingham by Dr Tong Liu. Elemental analysis is often not as required due to the preparation method required to deal with the fluorine component of the compounds.

All experiments were carried out under an inert gas atmosphere using standard Schleck techniques and/or a glove box (MBraun MG-200-B Eco), using oven and flame-dried glassware that had been put under vacuum and back-filled with argon three consecutive times, unless otherwise noted. THF, toluene, diethyl ether and dichloromethane were dried over alumina under a nitrogen atmosphere in an Inert Solutions solvent purification system. [D$_6$]Benzene, CDCl$_3$, hexane, pentane and octane were dried over 3Å molecular sieves for 24 hours followed by degasification *via* standard freeze-thaw-degas techniques prior to use. Other reagents were used as received. Compounds synthesised in *Section 2.2.1* were prepared following an adapted general procedure developed within the Marr and Saunder's groups.[180, 181]

2.4.2   Synthesis of N-heterocyclic carbene ligands

2.4.2.1   Synthesis of 3-methyl-1-(pentafluorobenzyl)-imidazolium bromide (**1**).

1-methylimidazole (0.822 g, 10.0 mmol) was added to a dichloromethane (20.0 mL) solution of pentafluorobenzyl bromide (2.622 g, 10.0 mmol). The resulting colourless solution was stirred for 24 hours. Solvent removal led to a pale yellow liquid that was dried overnight *in vacuo*. The resulting colourless crystalline powder was recrystallized from vapour diffusion of diethyl ether in DCM.

Colourless crystalline powder. Yield: 3.29 g (96 %). **^{1}H NMR** (400 MHz, MeOD) δ 7.72 (d, *H*CCH, $^3J_{HH}$ =1.9 Hz, 1H) 7.66 (d, HCC*H*, $^3J_{HH}$=2 Hz, 1H) 5.67 (s, NC*H$_2$*, 2H) 3.97 (s, HC*H$_3$*, 3H). C^2 proton not found. **^{19}F NMR** (376 MHz, MeOD) δ -143.91 (dt, J=20.1, 7.0 Hz, 2F), -154.35 (tt, J=20.0, 7.0 Hz, 1F), -163.63 (m, 2F). **^{13}C NMR** (101 MHz, MeOD) δ 148.3 (d, *Ar*F, $^1J_{CF}$= 15.2 Hz), 145.9 (d, *Ar*F, $^1J_{CF}$= 15.3 Hz), 145.0 (d, *Ar*F, $^1J_{CF}$= 15.2 Hz), 142.5 (d, *Ar*F, $^1J_{CF}$= 15.1 Hz), 140.5 (d, *Ar*F, $^1J_{CF}$= 15.0 Hz), 125.5 (s, HC*C*H), 123.8 (s, HC*C*H), 109.2 (s, *Ar*CH$_2$), 41.4 (s, *C*H$_2$), 36.9 (s, *C*H$_3$). **MS** (ESI): Calcd for C$_{11}$H$_8$F$_5$N$_2$, 263.0607; Found [M]$^+$ 263.0611. **Elemental analysis**, Anal. Calcd for C$_{11}$H$_{10}$BrF$_3$N$_2$: C, 38.51%; H, 2.35 %; N, 8.17%. Found: C, 38.94 %; H, 2.64 %; N, 7.81 %. **IR**: 3127 (w), 3080, 3051, 2973 (b),

2841, 1769, 1663, 1511 (s), 1447, 1350, 1315, 1224, 1164, 1124, 1035, 1025, 970, 887, 790 cm^{-1}. **m.p.** 137 °C.
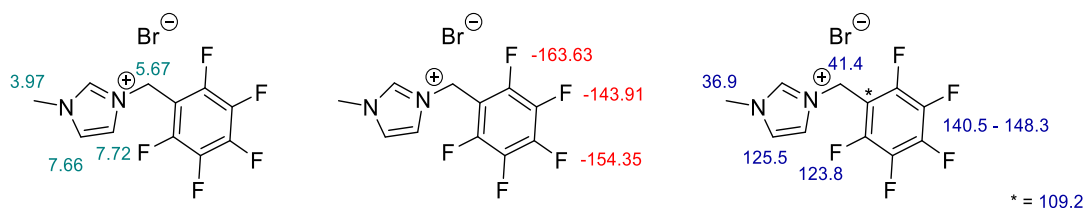
Characterisation consistent with previously reported literature.[201]

2.4.2.2 Synthesis of 3-methyl-1-(2,3,4,5-tetrafluorobenzyl)-imidazolium bromide (**2**).

1-methylimidazole (0.511 g, 6.22 mmol) was added to a dichloromethane (20.0 mL) solution of 2,3,4,5-tetrafluorobenzyl bromide (1.506 g, 6.20 mmol). The resulting colourless solution was stirred for 96 hours. Solvent removal led to a pale yellow liquid that was dried overnight *in vacuo*. The resulting colourless crystalline powder was recrystallized from vapour diffusion of diethyl ether in DCM.

Colourless crystalline powder. Yield: 1.776 g (88 %). **^{1}H NMR** (400 MHz, *d-chloroform*) δ 11.02 (s, NC*H*N, 1H), 8.00 (s, *H*CCH, 1H) 7.34 (s, HCC*H*, 1H) 7.19 (m, C$_6$-*H*, 1H) 5.91 (s, NC*H$_2$*, 2H) 4.04 (s, HC*H$_3$*, 3H). **^{19}F NMR** (376 MHz, *d-chloroform*) δ -135.14 (m, 2F), -142.62 (m, 1F), -151.32 (m, 1F), -153.52 (m, 1F). **^{13}C NMR** (101 MHz, *d$_1$-* chloroform) δ 146.9 (dm, $^1J_{CF}$ = 247 Hz, *Ar*F), 146.1 (dm, $^1J_{CF}$ = 247 Hz, *Ar*F), 142.1-139.0 (m, *Ar*F), 137.5 (s, N*C*N), 124.4 (s, H*C*CH), 122.8 (s, HC*C*H), 118.7 (s, *Ar*H), 113.5 (dm, $^1J_{CF}$ = 20 Hz, *Ar*CH$_2$), 45.5 (s, *C*H2), 36.4 (s, *C*H3). **MS** (ESI): Calcd for C$_{11}$H$_9$F$_4$N$_2$, 245.0702; Found [M]$^+$ 245.0701. **Elemental analysis**, Anal. Calcd for C$_{11}$H$_{10}$BrF$_3$N$_2$: C, 38.51%; H, 2.35 %; N, 8.17%. Found: C, 35.96 %; H, 2.09 %; N, 7.15 %.
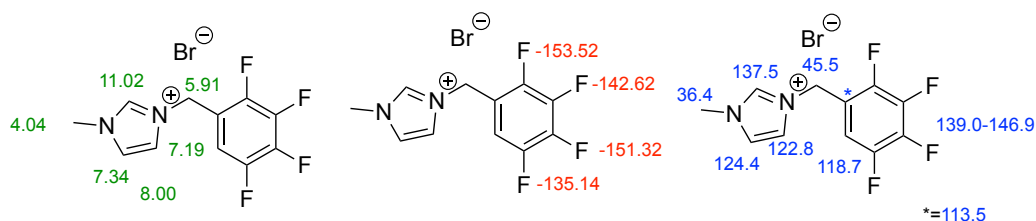
2.4.2.3 Synthesis of 3-methyl-1-(2,4,6-trifluorobenzyl)-imidazolium bromide (**3**).

1-methylimidazole (0.685 g, 8.3 mmol) was added to a dichloromethane (20.0 mL) solution of 2,4,6-trifluorobenzyl bromide (1.877 g, 8.3 mmol). The resulting colourless solution was stirred for 48 hours. Solvent removal led to a colourless crystalline powder that was dried overnight followed by recrystallization from vapour diffusion of diethyl ether in DCM.

Colourless crystalline powder. Yield: 3.29 g (96 %). **^{1}H NMR** (400 MHz, MeOD) δ 9.11 (s, NC*H*N, 1H) 7.63 (d, *H*CCH, $^3J_{HH}$ =1.9 Hz, 1H) 7.66 (d, HCC*H*, $^3J_{HH}$=1.9 Hz, 1H) 7.09 (m, Ar*H*, 2H) 5.56 (s, NC*H$_2$*, 2H) 3.98 (s, NC*H$_3$*, 3H). **^{19}F NMR** (376 MHz, MeOD) δ -105.70 (t, J=7.5 Hz, 1F) -112.89 (d, J=7.5 Hz, 2F). **^{13}C NMR** (101 MHz, MeOD) δ 166.9 (m, *Ar*F), 164.5 (d, $^1J_{CF}$ = 15.3 Hz), 125.66 (s, H*C*CH), 123.86 (s, HC*C*H), 108.19 (s, *Ar*CH$_2$), 102.42 (m, *Ar*H), 41.67 (s, *C*H$_2$), 36.91 (s, *C*H$_3$). **MS** (ESI): m/z: Calcd for C$_{11}$H$_{10}$F$_3$N$_2$, 227.0796; Found [M]$^+$ 227.0800. **Elemental analysis**, Anal. Calcd for C$_{11}$H$_{10}$BrF$_3$N$_2$: C, 43.02%; H, 3.28 %; N, 9.12 %. Found: C, 42.74 %; H, 3.42 %; N, 8.78 %. **IR**: 3469, 3399 (b), 3024, 2986, 1628, 1604, 1574, 1444, 1175, 1165, 1125, 1053, 1001, 871, 835, 746 cm^{-1}. **m.p.** 111 °C
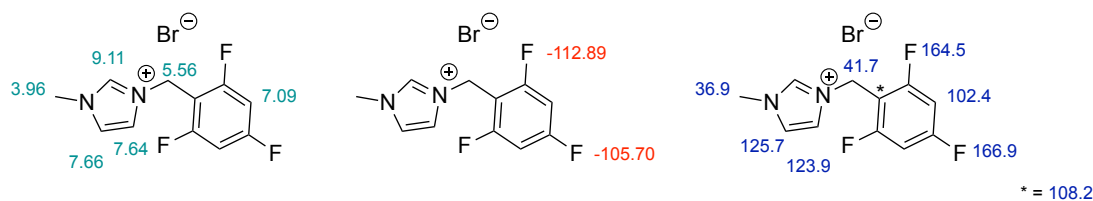
Characterisation consistent with previously reported literature.[180]

2.4.2.4 Synthesis of 3-methyl-1-(2,6-dimethylbenzyl)-imidazolium bromide (**4**).

1-methylimidazole (0.41 g, 5.02 mmol) was added to a dichloromethane (20.0 mL) solution of 2,6-dimethylbenzyl bromide (1.1 g, 5.5 mmol, 1.1 eq.). The resulting colourless solution was stirred for 48 hours. Solvent removal led to a colourless crystalline powder that was dried overnight followed by recrystallization from vapour diffusion of diethyl ether in DCM.

Colourless crystalline powder. Yield: 3.01 g (98 %). **^{1}H NMR** (400 MHz, MeOD) δ 8.68, (s, NC*H*N, 1H) 7.60 (d, *H*CCH, $^3J_{HH}$=1.9 Hz, 1H) 7.48 (d, HCC*H*, $^3J_{HH}$=1.9 Hz, 1H) 7.32 (m, Ar*H*, 1H) 7.18 (t, Ar*H*, 2H) 5.51 (s, NC*H$_2$*, 2H) 3.98 (s, NC*H$_3$*, 3H) 2.37 (s, Ar(C*H$_3$*)$_2$, 6H). **^{13}C NMR** (101 MHz, MeOD) δ 139.7 (s, N*C*N), 131.1 (s, *Ar*), 130.2 (s, *Ar*), 129.8 (s, *Ar*), 125.19 (s, H*C*CH), 123.38 (s, HC*C*H), 36.62 (s, *C*H$_3$), 19.71 (s, Ar*C*H$_3$). **MS** (ESI): Calcd for C$_{13}$H$_{17}$N$_2$ 201.1392; Found [M]$^+$ 201.1394. **Elemental analysis**, Anal. Calcd for C$_{13}$H$_{17}$BrN$_2$:

C, 38.51%; H, 2.35 %; N, 8.17 %. Found: C, 35.72 %; H, 2.01 %; N, 8.06 %. **IR**: 3156, 3118, 3010, 2963 (b), 2823, 1585, 1465, 1364, 1156 (s), 1026, 1014, 860, 831, 775, 750 cm^{-1}.
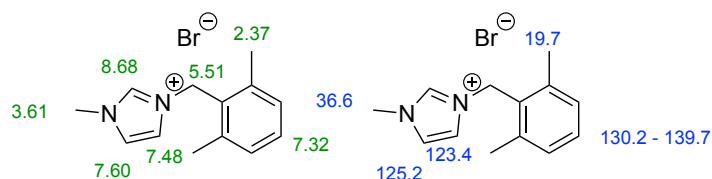
Characterisation consistent with previously reported literature.[180]

2.4.2.5 Synthesis of 3-methyl-1-benzylimidazolium bromide (**5**)

1-methylimidazole (2.055 g, 25.0 mmol) was added to a dichloromethane (30.0 mL) solution of benzyl bromide (4.275 g, 25.0 mmol). The resulting colourless solution was stirred for 24 hours. Solvent removal led to a colourless viscous liquid that was dried overnight. The product began to crystallise on the benchtop after 2 months.

Colourless oil. Yield: 5.33g, 25.0 mmol (84 %). **^{1}H NMR** (400 MHz, MeOD) δ 9.19, (s, NC*H*N, 1H) 7.72 (d, *H*CCH, $^{3}J_{HH}$ =1.6 Hz, 1H) 7.69 (d, HCC*H*, $^{3}J_{HH}$ =1.5 Hz, 1H) 7.52 (m, Ar*H*$_5$, 5H) 5.54 (s, NC*H*$_2$, 2H) 4.03 (s, NC*H*$_3$, 3H). **^{13}C NMR** (101 MHz, MeOD) δ 136.6 (s, N*C*N), 134.0 (s, *Ar*) , 129.1 (s, *Ar*), 129.0 (s, *Ar*), 128.4 (s, *Ar*), 123.9 (s, H*C*CH), 122.3 (s, HC*C*H), 52.7 (s, *C*H$_2$), 35.4 (s, *C*H$_3$). **MS** (ESI): Calcd for C$_{11}$H$_{13}$N$_2$ 173.1078; Found [M]$^{+}$ 173.1083. **Elemental analysis**, Anal. Calcd for C$_{13}$H$_{17}$BrN$_2$: C, 52.19 %; H, 5.18 %; N, 11.07 %. Found: C, 48.57 %; H, 4.46 %; N, 10.54 %. **IR**: 3423 (b), 3051 (b), 2851, 1559, 1454, 1157 (s), 1082, 820, 718 cm^{-1}. Water content: 488 ppm.
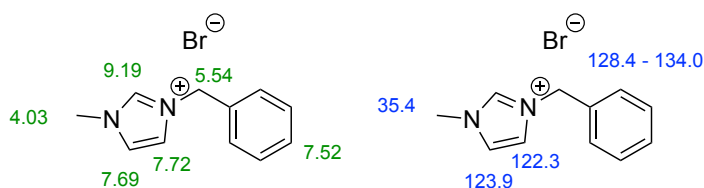
Characterisation consistent with previously reported literature.[180]

2.4.3 Synthesis of rhodium complexes

2.4.3.1 Synthesis of pentamethylcyclopentadienylrhodium-(-3-methyl-1-pentafluorobenzylimidazolium)chloride (**6**)

Silver (I) oxide (0.066g, 0.284 mmol) was added to a solution of 3-methyl-1-(pentafluorobenzyl)imidazolium bromide (0.064 g, 0.187 mmol) in dichloromethane (20 mL) in the absence of light. The mixture was stirred for 1.5 hours before filtration through a plug of celite and washed with dichloromethane (2 x 20 mL). [RhCp*Cl$_2$]$_2$ (0.0587 g, 0.095 mmol) was added to this solution which was stirred for a further four hours. The crude reaction mixture was filtered through a plug of celite, washed with dichloromethane (2 x 20 mL) and the filtrate was concentrated under reduced pressure. The crude product was recrystallized from the concentrated solution of dichloromethane and pentane at -20 °C. The pure product was collected *via* filtration, washed with hexanes, and dried *in vacuo*. X-ray quality single crystals were grown through vapour diffusion of hexane into a saturated DCM solution of **6**.

Red/orange crystalline product. Yield: 0.0836 g (77 %). **^{1}H NMR** (400 MHz, *d-chloroform*) δ 6.98 (d, *H*CCH, $^3J_{HH}$ = 2.0 Hz, 1H), 6.57 (d, HCC*H*, $^3J_{HH}$ = 1.9 Hz, 1H), 6.07 (d, imidazoleC*H*, $^2J_{HH}$= 16.1 Hz, 1H), 5.50 (d, imidazoleC*H*, $^2J_{HH}$= 15.0 Hz, 1H), 4.07 (s, NC*H$_3$*, 3H), 1.68 (s, Cp*, 15H). **^{19}F NMR** (282 MHz, *d-chloroform*) δ -140.58 (m, 2F), -151.40 (t, J = 20.8 Hz, 1F), -160.03 (td, J = 20.7, 7.1 Hz, 2F). **^{13}C NMR** (101 MHz, *d-chloroform*) δ 158.2 (s, N*C*N), 124.5 (s, HC*C*H), 120.7 (s, H*C*CH), 96.6 (s, *Cp*), 42.8 (s, *C*H$_2$), 38.4 (s, *C*H$_3$), 9.5 (s, Cp*C*H$_3$). **MS** (ESI): Calcd for C$_{21}$H$_{22}$RhClF$_5$N$_2$ 534.0441; Found [M]$^+$, 534.0434. **Elemental analysis**, Anal. Calcd for C$_{21}$H$_{22}$RhCl$_2$F$_5$N$_2$: C, 44.16%; H, 3.88 %; N, 4.90 %. Found: C, 44.56 %; H, 3.59 %; N, 4.58 %. **IR**: 3099 (w), 2921, 1658, 1502 (s), 1447, 1377, 1130, 1027, 1005, 920, 748 cm^{-1}.
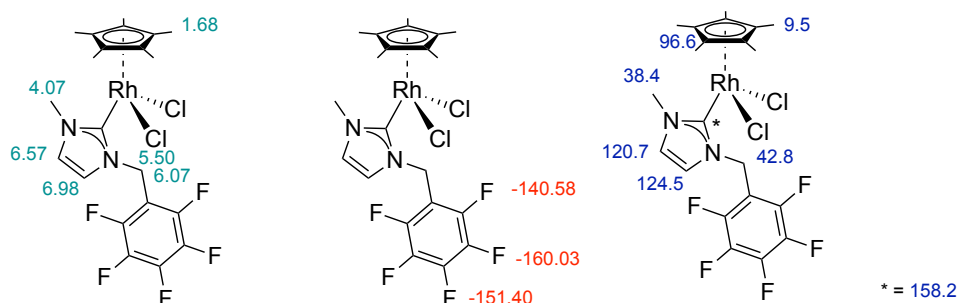
Characterisation consistent with previously reported literature.[201]

2.4.3.2 Synthesis of pentamethylcyclopentadienylrhodium-(-3-methyl-1-(2,3,4,5-tetrafluorobenzylimidazolium) chloride (**7**)

Silver (I) oxide (0.103 g, 0.444 mmol) was added to a solution of 3-methyl-1-(2,3,4,5-tetrafluorobenzyl)imidazolium bromide (0.218 g, 0.671 mmol) in dichloromethane (20 mL) in the absence of light. The mixture was stirred for 1.5 hours before filtration through a plug of celite and washed with dichloromethane (2 x 20 mL). [RhCp*Cl$_2$]$_2$ (0.21 g, 0.335 mmol) was added to this solution which was stirred for a further four hours. The crude reaction mixture was filtered through a plug of celite, washed with dichloromethane (2 x 20 mL) and the filtrate was concentrated under reduced pressure. The crude product was recrystallized from the concentrated solution of dichloromethane and pentane at -20 °C. The pure product was collected *via* filtration, washed with hexanes, and dried *in vacuo*. X-ray quality single crystals were grown through vapour diffusion of hexane into a saturated DCM solution of **7**.

 Red/orange crystalline product. Yield: 0.315 g (85 %). **^{1}H NMR** (400 MHz, *d-chloroform*) δ 7.56 (m, C$_6$-*H*, 1H), 7.03 (d, *H*CCH, $^3J_{HH}$= 2.0 Hz, 1H), 6.79 (d, HCC*H*, $^3J_{HH}$ = 1.9 Hz, 1H), 6.40 (d, imidazoleC*H*, $^3J_{HH}$= 10.9 Hz, 1H), 5.04 (d, imidazoleC*H*, $^3J_{HH}$= 13.6 Hz, 1H), 4.03 (s, NC*H$_3$*, 3H), 1.61 (s, Cp*, 15H). **^{19}F NMR** (282 MHz, *d-chloroform*) δ -137.31 (m, 1F), -145.46 (m, 1F), -155.06 (m, 1F), -156.07 (m, 1F). **^{13}C NMR** (101 MHz, *d-chloroform*) δ 171.3 (d, $^1J_{RhC}$ = 57 Hz, N*C*N), 147.3 (dd, $^1J_{CF}$ = 249 Hz, J_{CF} = 10 Hz, *Ar*F), 145.8 (ddd, $^1J_{CF}$ = 246 Hz, J_{CF} = 3, 11 Hz, *Ar*F), 140.4 (dm, $^1J_{CF}$ = 255 Hz, *Ar*F), 125.4 (s, H*C*CH), 122.2 (s, HC*C*H), 120.1 (m, *Ar*), 113.3 (m, *Ar*), 96.6 (d, $^1J_{RhC}$ = 7 Hz, *C*p), 45.8 (s, *C*H$_2$), 39.4 (s, *C*H$_3$), 9.5 (s, Cp*C*H$_3$). **MS** (ESI): Calcd for C$_{21}$H$_{23}$RhClF$_4$N$_2$ 517.0541; Found [M]$^+$, 517.0538.
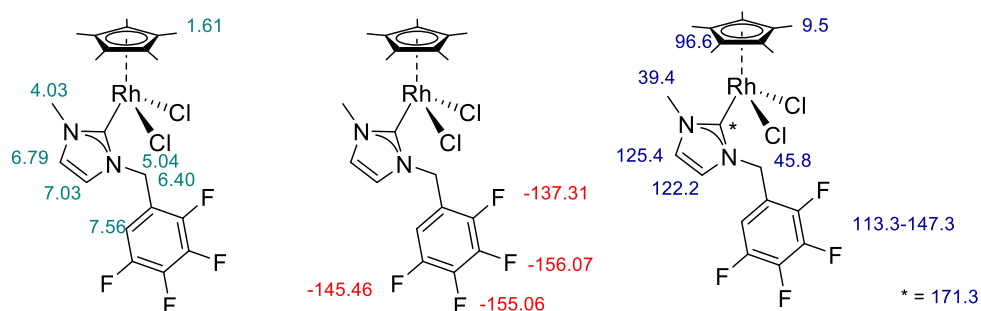
Characterisation consistent with previously reported literature.[201]

2.4.3.3 Synthesis of pentamethylcyclopentadienylrhodium-(-3-methyl-1-(2,4,6)-trifluorobenzylimidazolium)chloride (**8**)

Silver (I) oxide (0.066g, 0.284 mmol) was added to a solution of 3-methyl-1-(2,4,6-trifluorobenzyl)imidazolium bromide (0.057 g, 0.187 mmol) in dichloromethane (20 mL) in the absence of light. The mixture was stirred for 1.5 hours before filtration through a plug of celite and washed with dichloromethane (2 x 20 mL). [RhCp*Cl$_2$]$_2$ (0.0587 g, 0.095 mmol) was added to this solution which was stirred for a further four hours. The crude reaction mixture was filtered through a plug of celite, washed with dichloromethane (2 x 20 mL) and the filtrate was concentrated under reduced pressure. The crude product was recrystallized from the concentrated solution of dichloromethane and pentane at -20 °C. The pure product was collected *via* filtration, washed with hexanes, and dried *in vacuo*. X-ray quality single crystals were grown through vapour diffusion of hexane into a saturated DCM solution of **8**.

Yellow crystalline solid. Yield: 0.0951 g (93 %). **^{1}H NMR** (400 MHz, *d-chloroform*) δ 6.94 (d, *H*CCH, $^3J_{HH}$ = 2.0 Hz, 1H) 6.77 (t, C$_6$-*H*, ^2J = 8.0 Hz, 2H) 6.56 (d, HCC*H*, $^3J_{HH}$ = 1.8 Hz, 1H) 5.98 (d, imidazoleC*H*, $^2J_{HH}$ = 14.4 Hz, 1H) 5.35 (d, imidazoleC*H*, $^2J_{HH}$ = 14.7 Hz, 1H) 4.06 (s, NC*H*$_3$, 3H) 1.69 (s, Cp*, 15H). **^{19}F NMR** (376 MHz, *d-chloroform*) δ -105.23 (t, J = 7.1 Hz, 1F) -109.29 (d, J = 7.1 Hz, 2 F). **^{13}C NMR** (126 MHz, *d-chloroform*) δ 170.2 (d, $^1J_{RhC}$ = 52 Hz, N*C*N), 123.7 (s, H*C*CH), 120.8 (s, HC*C*H), 96.4 (s, *Cp*), 43.9 (s, *C*H$_2$), 39.4 (s, *C*H$_3$), 9.4 (s, Cp*C*H$_3$). Carbon atoms of benzyl region not detected. **MS** (ESI): calcd for C$_{21}$H$_{24}$ClF$_3$RhN$_2$, 499.0630; found [M]$^+$, 499.0616. **Elemental Analysis**, Anal. Calcd for C$_{21}$H$_{24}$Cl$_2$F$_3$RhN$_2$: C, 47.13; H, 4.52: N, 5.23. Found: C, 47.75; H, 4.08: N, 5.48%.
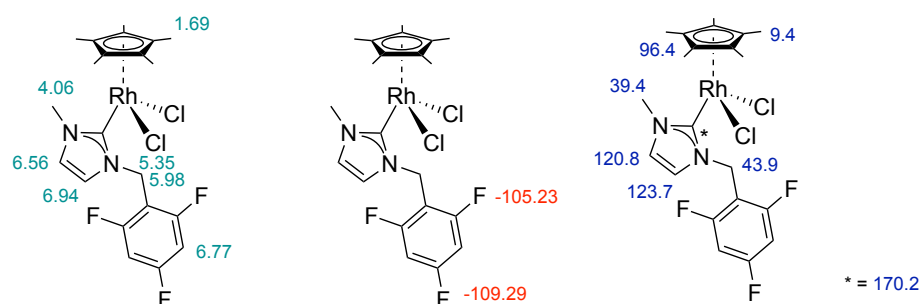
2.4.3.4 Synthesis of pentamethylcyclopentadienylrhodium-(-3-methyl-1-(2,6)-dimethylbenzylimidazolium)chloride (**9**)

Silver (I) oxide (0.066g, 0.284 mmol) was added to a solution of 3-methyl-1-(2,6-dimethylbenzyl)imidazolium bromide (0.052 g, 0.187 mmol) in dichloromethane (20 mL) in

the absence of light. The mixture was stirred for 1.5 hours before filtration through a plug of celite and washed with dichloromethane (2 x 20 mL). [RhCp*Cl$_2$]$_2$ (0.0587 g, 0.095 mmol) was added to this solution which was stirred for a further four hours. The crude reaction mixture was filtered through a plug of celite, washed with dichloromethane (2 x 20 mL) and the filtrate was concentrated under reduced pressure. The crude product was recrystallized from the concentrated solution of dichloromethane and pentane at -20 °C. The pure product was collected *via* filtration, washed with hexanes, and dried *in vacuo*. X-ray quality single crystals were grown through vapour diffusion of hexane into a saturated DCM solution of **9**.

Yellow crystalline solid. Yield: 0.070 g (72 %). **^{1}H NMR** (500 MHz, *d-chloroform*) δ 7.22 (t, C$_6$-*H*, ^{2}J$_{HH}$= 7.5 Hz, 1H), 7.12 (d, C$_6$-*H*, ^{2}J$_{HH}$= 7.5 Hz, 1H), 6.85 (d, *H*CCH, ^{3}J$_{HH}$ = 1.9 Hz, 1H), 6.36 (d, HCC*H*, ^{3}J$_{HH}$ = 1.9 Hz, 1H), 4.79 (s, C*H$_2$*, 2H) 4.09 (s, C*H$_3$*, 3H), 2.34 (s, C$_6$(C*H$_3$*)$_2$, 6H), 1.71 (s, Cp*, 15H). **^{13}C NMR** (126 MHz, *d-chloroform*) δ 169.1 (s, N*C*N), 131.5 (s, *Ar*), 128.8 (s, *Ar*), 122.9 (s, H*C*CH), 120.9 (s, HC*C*H), 96.2 (s, *Cp*), 49.2 (s, *C*H$_2$), 39.5 (s, *C*H$_3$), 20.5 (s, Ar*C*H$_3$), 9.7 (s, Cp*C*H$_3$). **MS** (ESI): calcd for C$_{23}$H$_{31}$ClRhN$_2$, 473.1225; found [M – Cl]$^+$, 473.1215. **Elemental Analysis**, Anal. Calcd for C$_{23}$H$_{31}$RhCl$_2$N$_2$: C, 54.24; H, 6.14: N, 5.50. Found: C, 53.32; H, 6.14: N, 4.94 %.

2.4.3.5 Synthesis of pentamethylcyclopentadienylrhodium-(-3-methyl-1-benzylimidazolium)chloride (**10**)

Silver (I) oxide (0.066g, 0.284 mmol) was added to a solution of 3-methyl-1-benzylimidazolium bromide (0.047 g, 0.187 mmol) in dichloromethane (20 mL) in the absence of light. The mixture was stirred for 1.5 hours before filtration through a plug of celite and washed with dichloromethane (2 x 20 mL). [RhCp*Cl$_2$]$_2$ (0.0587 g, 0.095 mmol) was added to this solution which was stirred for a further four hours. The crude reaction mixture was filtered through a plug of celite, washed with dichloromethane (2 x 20 mL) and the filtrate was concentrated under reduced pressure. The crude product was recrystallized from the concentrated solution of dichloromethane and pentane at -20 °C. The pure product was

collected *via* filtration, washed with hexanes, and dried *in vacuo*. X-ray quality single crystals were grown through vapour diffusion of hexane into a saturated DCM solution of **10**.

Yellow crystalline solid. Yield: 0.0801 g (88 %). **^{1}H NMR** (400.11 MHz, *d-chloroform*) δ 7.34 (dt, C$_6$-*H*, ^{2}J$_{HH}$= 13.2, 6.6 Hz, 5H), 6.95 (d, *H*CCH, ^{3}J$_{HH}$ = 1.8 Hz, 1H), 6.76 (d, HCC*H*, ^{3}J$_{HH}$ = 1.8 Hz, 1H), 6.13 (d, imidazoleC*H*, ^{2}J$_{HH}$ = 14.7 Hz, 1H) 5.26 (d, imidazoleC*H*, ^{2}J$_{HH}$ = 12.2 Hz, 1H) 4.06 (s, C*H$_3$*, 3H), 1.62 (s, Cp*, 15H). **^{13}C NMR** (126 MHz, *d-chloroform*) δ 170.3 (s, N*C*N), 136.9 (s, *Ar*), 128.9 (s, *Ar*), 128.7 (s, *Ar*), 128.2 (s, *Ar*), 124.3 (s, H*C*CH), 122.9 (s, HC*C*H), 96.4 (s, *Cp*), 54.9 (s, *C*H$_2$), 39.4 (s, *C*H$_3$), 9.7 (s, Cp*C*H$_3$). **MS** (ESI): calcd for C$_{21}$H$_{27}$ClRhN$_2$, 445.0912; found [M–Cl]$^+$, 445.0918. **Elemental Analysis**, Anal. Calcd for C$_{21}$H$_{27}$Cl$_2$RhN$_2$: C, 52.41; H, 5.66: N, 5.82. Found: C, 51.52; H, 5.49: N, 5.51 %.
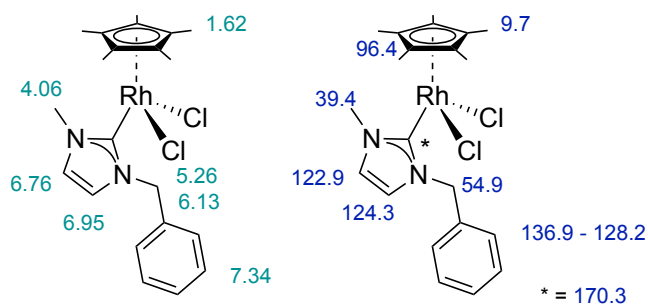
2.4.3.6 Synthesis of *cyclo*metallated rhodium species [(η^5,κ$_2$C-C$_5$Me$_4$CH$_2$C$_6$F$_5$CH$_2$NC$_3$H$_2$NMe)- RhCl] (**22**)

RhCp*Cl$_2$(F$_5$Bzmim) (**6**) (0.170 g, 0.3 mmol) and silver oxide (0.21 g, 0.9 mmol) were added to a round bottomed flask containing DCM (30 mL) in darkness, and left to stand under argon for 24 hours. The crude reaction mixture was filtered through a plug of celite, washed with dichloromethane (2 x 20 mL) and the filtrate was concentrated under reduced pressure. The crude product was recrystallized from the concentrated solution of dichloromethane and hexane at -20 °C. The pure product was collected *via* filtration, washed with hexanes, and dried *in vacuo*. X-ray quality single crystals were grown through vapour diffusion of hexane into a saturated DCM solution of **22**.

Red crystalline solid. Yield: 0.117 g (73%). **^{1}H NMR** (500 MHz, *d-chloroform*) δ 7.11 (d, *H*CCH, ^{3}J$_{HH}$ = 2.0 Hz, 1H) 7.06 (d, HCC*H*, ^{3}J$_{HH}$ = 2.0 Hz, 1H). 4.88 (s, imidazoleC*H$_2$*, 2H) 4.08 (s, NC*H$_3$*, 3H) 1.84 (s, 3H, Me) 1.77 (s, 3H, Me) 1.75 (dd, C5C*H*H, ^{2}J$_{HH}$ = 12.1 Hz, J = 5.5 Hz, 1H) 1.37 (s, 3H, Me) 1.37 (ddd, C5CH*H,* ^{2}J$_{HH}$ = 12.1 Hz, J = 6.8, 1.6 Hz, 1H) 0.72 (s, 3H, Me). **^{19}F NMR** (282 MHz, *d-chloroform*) δ -145.62 (dd, *J$_{FF}$* = 27.0, 13.5 Hz), -149.34 (dt, *J$_{FF}$* = 30.2, 6.8 Hz), -174.07 (ddt, *J$_{FF}$* = 25.9, 12.9, 6.5 Hz), -176.80 (td, *J$_{FF}$* = 26.1, 6.6 Hz), -

185.74 (ddd, J_{FF} = 20.5, 10.8, 5.8 Hz). **MS** (ESI): Calcd for $C_{21}H_{22}ClRhF_5N_2$, 535.0447; Found [M-Cl]$^+$ 535.0448.
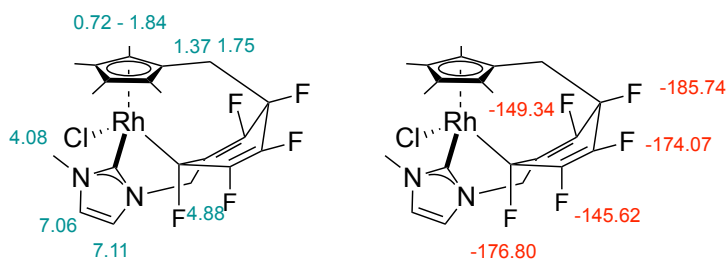
2.4.3.7 Synthesis of *ortho*metallated rhodium chloride species [Cp*RhCl(κC$_2$-MeNC$_3$H$_2$NCH$_2$C$_6$F$_4$)] (**23**)

RhCp*Cl$_2$(F$_4$Bzmim) (**7**) (0.055 g, 0.1 mmol) and silver oxide (0.070 g, 0.3 mmol) were added to a round bottomed flask containing DCM (15 mL) in darkness, and left to stand under argon for 24 hours. The crude reaction mixture was filtered through a plug of celite, washed with dichloromethane (2 x 20 mL) and the filtrate was concentrated under reduced pressure and was recrystallized from a concentrated solution of dichloromethane and hexane at -20 °C. The pure product was collected *via* filtration, washed with hexanes, and dried *in vacuo*. X-ray quality single crystals were grown through vapour diffusion of hexane into a saturated DCM solution of **23**.

Red/orange crystalline product. Yield: 0.040 g (77 %). **¹H NMR** (400 MHz, *d-chloroform*) δ 7.08 (d, *H*CC*H*, $^3J_{HH}$ = 1.9 Hz, 1H), 7.00 (d, HCC*H*, $^3J_{HH}$ = 1.9 Hz, 1H), 5.27 (d, imidazoleC*H*, ^2J = 14.8 Hz, 1H), 4.59 (d, imidazoleC*H*, ^2J = 14.8 Hz, 1H), 3.96 (s, NC*H$_3$*, 3H), 1.67 (s, Cp*, 15H). **¹⁹F NMR** (282 MHz, *d-chloroform*) δ -110.35 (dd, J_{FF} = 14.0, 31.4 Hz, 1F), -146.83 (dd, J_{FF} = 14.2, 20.8 Hz, 1F), -157.99 (dd, J_{FF} = 19.5, 31.2 Hz, 1F), -164.44 (t, J_{FF} = 20.2 Hz, 1F). **MS** (ESI): Calcd for $C_{21}H_{22}RhClF_4N_2$ 481.0774; Found [M]$^+$ 481.0768. **Elemental analysis**, Anal. Calcd for $C_{21}H_{22}RhClF_4N_2 \cdot CHCl_3$: C, 41.54%; H, 3.64 %; N, 4.40 %. Found: C, 41.73 %; H, 3.89 %; N, 4.67 %.
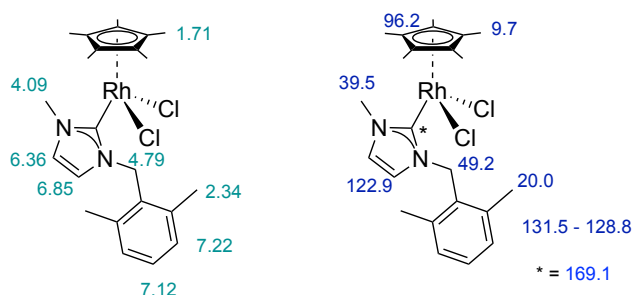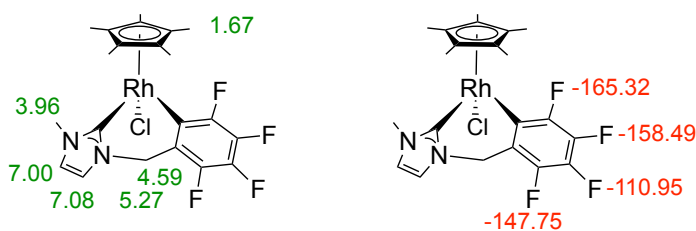
2.4.4 Synthesis of iridium complexes

2.4.4.1 Synthesis of pentamethylcyclopentadienyliridium-(-3-methyl-1-(pentafluorobenzylimidazolium)chloride (**11**)

Silver (I) oxide (0.066g, 0.284 mmol) was added to a solution of 3-methyl-1-(pentafluorobenzyl)imidazolium bromide (0.064 g, 0.187 mmol) in dichloromethane (20 mL) in the absence of light. The mixture was stirred for 1.5 hours before filtration through a plug of celite and washed with dichloromethane (2 x 20 mL). [IrCp*Cl$_2$]$_2$ (0.0756 g, 0.095 mmol) was added to this solution which was stirred for a further four hours. The crude reaction mixture was filtered through a plug of celite, washed with dichloromethane (2 x 20 mL) and the filtrate was concentrated under reduced pressure. The crude product was recrystallized from the concentrated solution of dichloromethane and pentane at -20 °C. The pure product was collected *via* filtration, washed with hexanes, and dried *in vacuo*. X-ray quality single crystals were grown through vapour diffusion of hexane into a saturated DCM solution of **11**.

Orange crystalline solid. Yield: 0.0927 g (75%). **^{1}H NMR** (500 MHz, *d-chloroform*) δ 6.93 (d, *H*CC*H*, $^3J_{HH}$ = 2.1 Hz, 1H) 6.49 (d, HCC*H*, $^3J_{HH}$ = 2.1 Hz, 1H) 6.05 (d, imidazoleC*H*, $^2J_{HH}$ = 15.4 Hz, 1H) 5.46 (d, imidazoleC*H*, $^2J_{HH}$ = 15.8 Hz, 1H) 4.00 (s, NC*H$_3$*, 3H) 1.69 (s, Cp*, 15H). **^{19}F NMR** (376 MHz, *d-chloroform*) δ -140.79 (dd, J_{FF} = 22.4, 8.8 Hz, 2F) -151.58 (t, J= 20.9 Hz, 1F) -160.16 (td, J= 20.6, 7.0 Hz, 2F). **^{13}C NMR** (126 MHz, *d-chloroform*) δ 157.9 (s, N*C*N), 147.0 (s, *Ar*F), 144.6 (s, *Ar*F), 139.1 (s, *Ar*F), 123.5 (s, H*C*CH), 119.9 (s, HC*C*H), 89.2 (s, *Cp*), 43.3 (s, *C*H$_2$), 39.0 (s, *C*H$_3$), 9.2 (s, Cp*C*H$_3$). **MS** (ESI): Calcd for C$_{21}$H$_{22}$IrF$_4$N$_2$, 571.1348; Found [M]$^+$ 571.1332. **Elemental analysis**, Anal. Calcd for C$_{21}$H$_{22}$IrCl$_2$F$_5$N$_2$: C, 40.39%; H, 3.87 %; N, 4.49 %. Found: C, 39.06 %; H, 3.14 %; N, 4.49%. **IR**: 3168 (w), 3100 (w), 2983 (w), 2913 (w), 1658, 1502 (s), 1448, 1301, 1130, 1005, 920, 748 cm^{-1}.
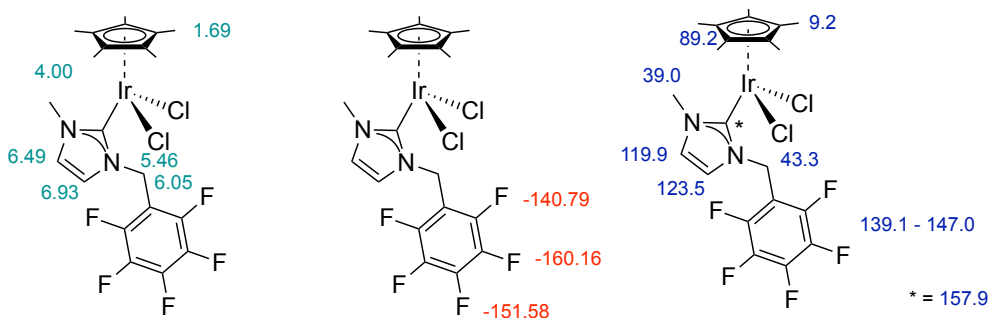
Characterisation consistent with previously reported literature.[201]

2.4.4.2 Synthesis of pentamethylcyclopentadienyliridium-(-3-methyl-1-(2,3,4,5-tetrafluorobenzylimidazolium)chloride (**12**)

Silver (I) oxide (0.070 g, 0.3 mmol) was added to a solution of 3-methyl-1-(2,3,4,5-tetrafluorobenzyl)imidazolium bromide (0.065 g, 0.2 mmol) in dichloromethane (20 mL) in the absence of light. The mixture was stirred for 1.5 hours before filtration through a plug of celite and washed with dichloromethane (2 x 20 mL). [IrCp*Cl$_2$]$_2$ (0.08 g, 0.1 mmol) was added to this solution which was stirred for a further four hours. The crude reaction mixture was filtered through a plug of celite, washed with dichloromethane (2 x 20 mL) and the filtrate was concentrated under reduced pressure. The crude product was recrystallized from the concentrated solution of dichloromethane and pentane at -20 °C. The pure product was collected *via* filtration, washed with hexanes, and dried *in vacuo*. X-ray quality single crystals were grown through vapour diffusion of hexane into a saturated DCM solution of **12**.

Orange crystalline solid. Yield: 0.0964 g (75%). **^{1}H NMR** (500 MHz, *d-chloroform*) δ 7.53 (m, C$_6$-*H*, 1H), 6.96 (d, *H*CCH, $^3J_{HH}$ = 2.0 Hz, 1H) 6.71 (d, HCC*H*, $^3J_{HH}$ = 2.0 Hz, 1H) 6.25 (d, imidazoleC*H*, $^2J_{HH}$ = 15.2 Hz, 1H) 5.02 (d, imidazoleC*H*, $^2J_{HH}$= 14.3 Hz, 1H), 3.99 (s, NC*H*$_3$, 3H) 1.64 (s, Cp*, 15H). **^{19}F NMR** (376 MHz, *d-chloroform*) δ -137.29 (m, 1F), -145.47 (m, 1F), -155.08 (m, 1F), -155.99 (t, J= 20.0 Hz, 1F). **^{13}C NMR** (126 MHz, *d-chloroform*) δ 157.6, 148.7 (d, $^1J_{CF}$ = 246 Hz, *Ar*F), 146.6 (d, $^1J_{CF}$ = 249 Hz, *Ar*F), 144.6 (d, $^1J_{CF}$= 247 Hz, *Ar*F), 139.9 (d, $^1J_{CF}$= 255 Hz, *Ar*F), 124.4 (s, H*C*CH), 121.2 (s, HC*C*H), 89.2 (s, *Cp*), 45.9 (s, *C*H$_2$), 38.9 (s, *C*H$_3$), 9.3 (s, Cp*C*H$_3$). **MS** (ESI): Calcd for C$_{21}$H$_{23}$IrClF$_4$N$_2$, 607.1115; Found [M]$^+$ 607.1092.
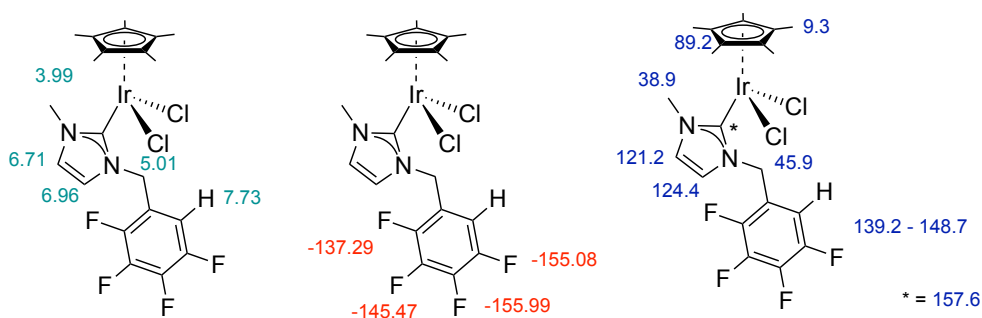
2.4.4.3   Synthesis   of   pentamethylcyclopentadienyliridium-(-3-methyl-1-(2,4,6-trifluorobenzylimidazolium)chloride (**13**)

Silver (I) oxide (0.066g, 0.284 mmol) was added to a solution of 3-methyl-1-(2,4,6-trifluorobenzyl)imidazolium bromide (0.057 g, 0.187 mmol) in dichloromethane (20 mL) in the absence of light. The mixture was stirred for 1.5 hours before filtration through a plug of celite and washed with dichloromethane (2 x 20 mL). [IrCp*Cl$_2$]$_2$ (0.0756 g, 0.095 mmol) was added to this solution which was stirred for a further four hours. The crude reaction mixture was filtered through a plug of celite, washed with dichloromethane (2 x 20 mL) and the filtrate was concentrated under reduced pressure. The crude product was recrystallized from the concentrated solution of dichloromethane and pentane at -20 °C. The pure product was collected *via* filtration, washed with hexanes, and dried *in vacuo*. X-ray quality single crystals were grown through vapour diffusion of hexane into a saturated DCM solution of **13**.

Orange crystalline solid. Yield: 0.0594 g (50 %). **^{1}H NMR** (500 MHz, *d-chloroform*) δ 6.92 (d, *H*CCH, $^3J_{HH}$ = 2.1 Hz, 1H) 6.77 (dt, C$_6$-*H*, $^3J_{HF}$ = 7.6, 0.8 Hz, 2H) 6.48 (d, HCC*H*, $^3J_{HH}$ = 2.0 Hz, 1H) 5.95 (s, imidazole*CH*, 1H) 5.33 (s, imidazole*CH*, 1H) 4.00 (s, NC*H*$_3$, 3H) 1.69 (s, Cp*, 15H). **^{19}F NMR** (376 MHz, *d-chloroform*) δ -105.32 (tt, J$_{FF}$ = 15.5 Hz, J$_{FH}$ = 7.6 Hz, 2F) -109.41 (t, J = 7.3 Hz, 1F). **^{13}C NMR** (126 MHz, *d-chloroform*) δ 158.1 (s, N*C*N), 146.9 (s, *Ar*), 144.9 (s, *Ar*), 139.0 (s, *Ar*), 123.5 (s, H*C*C*H*), 120.0 (s, HC*C*H), 89.3 (s, *Cp*), 43.5 (s, *CH*$_2$), 39.1 (s, *CH*$_3$), 9.3 (s, Cp*CH*$_3$). **MS** (ESI): calcd for C$_{21}$H$_{24}$ClF$_3$IrN$_2$, 589.1204; found [M–Cl]$^+$, 589.1196. **Elemental Analysis,** Anal. Calcd for C$_{21}$H$_{24}$Cl$_2$F$_3$IrN$_2$: C, 40.39; H, 3.87: N, 4.49. Found: C, 39.65; H, 3.54: N, 4.03%. **IR**: 3160 (w), 3116 (w), 2974, 2921, 1633, 1609, 1405, 1388, 1222, 1122, 1061, 1001, 841, 742 cm^{-1}.
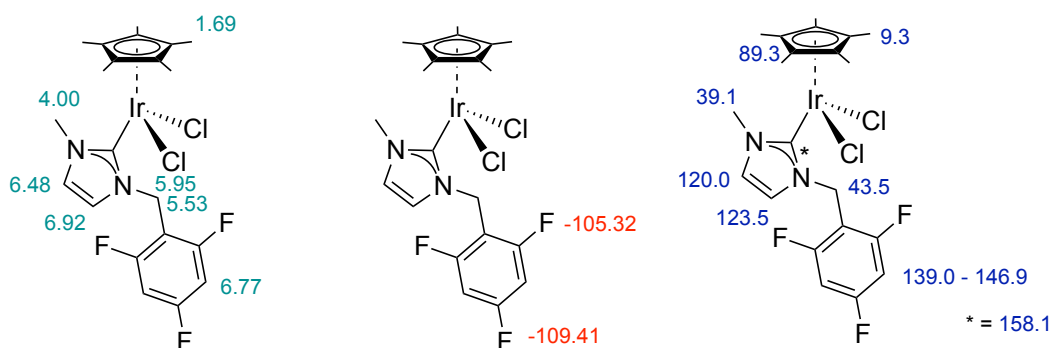
Characterisation consistent with previously reported literature.[180]

2.4.4.4 Synthesis of pentamethylcyclopentadienyliridium-(-3-methyl-1-(2,6)-dimethylbenzylimidazolium)chloride (**14**)

Silver (I) oxide (0.066g, 0.284 mmol) was added to a solution of 3-methyl-1-(2,6-dimethylbenzyl)imidazolium bromide (0.052 g, 0.187 mmol) in dichloromethane (20 mL) in the absence of light. The mixture was stirred for 1.5 hours before filtration through a plug of celite and washed with dichloromethane (2 x 20 mL). [IrCp*Cl$_2$]$_2$ (0.0756 g, 0.095 mmol) was added to this solution which was stirred for a further four hours. The crude reaction mixture was filtered through a plug of celite, washed with dichloromethane (2 x 20 mL) and the filtrate was concentrated under reduced pressure. The crude product was recrystallized from the concentrated solution of dichloromethane and pentane at -20 °C. The pure product was collected *via* filtration, washed with hexanes, and dried *in vacuo*. X-ray quality single crystals were grown through vapour diffusion of hexane into a saturated DCM solution of **14**.

Orange crystalline solid. Yield: 0.055 g (49 %). **^{1}H NMR** (400.11 MHz, *d-chloroform*) δ 7.16 (m, C$_6$-*H*, 3H) 6.77 (d, *H*CCH, ^{3}J$_{HH}$ = 2.1 Hz, 1H) 6.27 (d, HCC*H*, ^{3}J$_{HH}$ = 2.0 Hz, 1H) 4.75 (s, imidazoleC*H*$_2$, 1H) 4.03 (s, NC*H*$_3$, 3H) 2.32 (s, ArC*H*$_3$, 6H) 1.73 (s, Cp*, 15H). **^{13}C NMR** (126 MHz, *d-chloroform*) δ 155.3 (s, N*C*N), 138.0 (s, *Ar*), 131.5 (s, *Ar*), 129.3 (s, *Ar*), 128.9 (s, *Ar*), 122.0 (s, H*C*CH), 120.1 (s, HC*C*H), 88.7 (s, *Cp*), 48.7 (s, *C*H$_2$), 38.9 (s, *C*H$_3$), 20.0 (s, Ar*C*H$_3$), 9.5 (s, Cp*C*H$_3$). **MS** (ESI): calcd for C$_{23}$H$_{30}$IrN$_2$ 527.2038; found, C$_{23}$H$_{30}$IrN$_2$ 527.2074. **Elemental Analysis**, Anal. Calcd for C$_{23}$H$_{31}$Cl$_2$IrN$_2$: C, 46.15; H, 5.22: N, 4.68. Found: C, 45.56; H, 4.91: N, 4.73%. **IR**: 3099, 3024, 2983, 2913, 1575, 1469, 1446, 1378, 1276, 1210, 1030, 842, 766, 749 cm^{-1}.
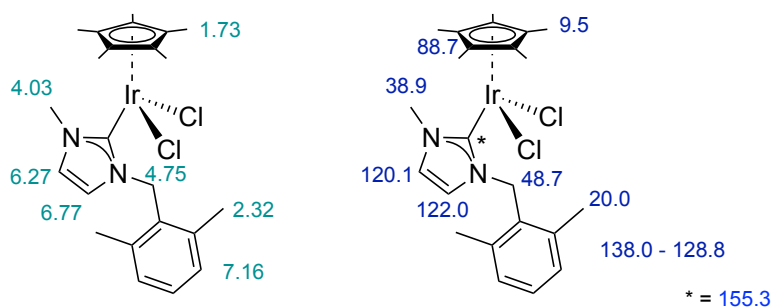
Characterisation consistent with previously reported literature.[180]

2.4.4.5 Synthesis of pentamethylcyclopentadienyliridium-(-3-methyl-1-benzylimidazolium)chloride (**15**)

Silver (I) oxide (0.066g, 0.284 mmol) was added to a solution of 3-methyl-1-benzylimidazolium bromide (0.047 g, 0.187 mmol) in dichloromethane (20 mL) in the

absence of light. The mixture was stirred for 1.5 hours before filtration through a plug of celite and washed with dichloromethane (2 x 20 mL). [IrCp*Cl$_2$]$_2$ (0.0756 g, 0.095 mmol) was added to this solution which was stirred for a further four hours. The crude reaction mixture was filtered through a plug of celite, washed with dichloromethane (2 x 20 mL) and the filtrate was concentrated under reduced pressure. The crude product was recrystallized from the concentrated solution of dichloromethane and pentane at -20 °C. The pure product was collected *via* filtration, washed with hexanes, and dried *in vacuo*. X-ray quality single crystals were grown through vapour diffusion of hexane into a saturated DCM solution of **15**.

 Orange crystalline solid. Yield: 0.053 g (49 %). **^{1}H NMR** (400.11 MHz, *d-chloroform*) δ 7.15 (m, C$_6$-*H*, 5H) 6.88 (d, *H*CCH, $^3J_{HH}$ = 2.0 Hz, 1H) 6.75 (d, imidazoleC*H*, $^2J_{HH}$ = 14.8 Hz, 1H) 6.51 (d, HCC*H*, $^3J_{HH}$ = 2.0 Hz, 1H) 6.25 (d, imidazoleC*H*, $^2J_{HH}$ = 14.7 Hz, 1H) 4.01 (s, NC*H*$_3$, 3H) 1.70 (s, Cp*, 15H). **^{13}C NMR** (126 MHz, *d-chloroform*) δ 157.0 (s, N*C*N), 137.0 (s, *Ar*), 128.9 (s, *Ar*), 128.2 (s, *Ar*), 123.3 (s, H*C*CH), 122.0 (s, HC*C*H), 89.0 (s, *Cp*), 54.7 (s, *C*H$_2$), 38.9 (s, *C*H$_3$), 9.4 (s, Cp*C*H$_3$). **MS** (ESI): calcd for C$_{21}$H$_{27}$Cl$_2$IrN$_2$ 535.1492; found [M-cyclometallated]$^+$, 499.1718. **Elemental Analysis**, Anal. Calcd for C$_{21}$H$_{27}$Cl$_2$IrN$_2$: C, 44.21; H, 4.77 N, 4.91. Found: C, 44.66; H, 4.91: N, 4.73 %. **IR**: 3140 (w), 3125 (w), 2994, 2912, 1494, 1446, 1382, 1261, 1223,1028, 749 cm^{-1}.
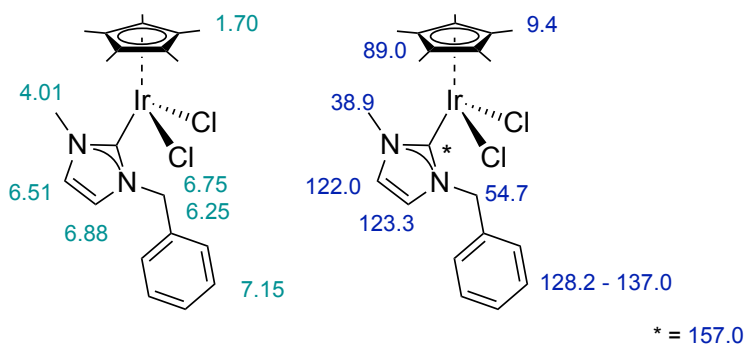

Characterisation consistent with previously reported literature.[217]

2.4.4.6 Synthesis of pentamethylcyclopentadienyliridium-(-3-methyl-1-(pentafluorobenzylimidazolium)iodide (**16**)

Silver (I) oxide (0.066g, 0.284 mmol) was added to a solution of 3-methyl-1-(pentafluorobenzyl)imidazolium bromide (0.064 g, 0.187 mmol) in dichloromethane (20 mL) in the absence of light. The mixture was stirred for 1.5 hours before filtration through a plug of celite and washed with dichloromethane (2 x 20 mL). [IrCp*I$_2$]$_2$ (0.11 g, 0.095 mmol) was added to this solution which was stirred for a further four hours. The crude reaction mixture was filtered through a plug of celite, washed with dichloromethane (2 x 20 mL) and the filtrate

was concentrated under reduced pressure. The crude product was recrystallized from the concentrated solution of dichloromethane and pentane at -20 °C. The pure product was collected *via* filtration, washed with hexanes, and dried *in vacuo*. X-ray quality single crystals were grown through vapour diffusion of hexane into a saturated DCM solution of **16**.

Orange crystalline solid. Yield: 0.117 g (73%). **^{1}H NMR** (500 MHz, *d-chloroform*) δ 7.09 (d, *H*CCH, $^3J_{HH}$ = 2.0 Hz, 1H) 6.53 (d, HCC*H*, $^3J_{HH}$ = 2.0 Hz, 1H) 5.55 (s, imidazoleC*H*, 1H) 5.33 (s, imidazoleC*H*, 1H) 3.81 (s, NC*H*$_3$, 3H) 1.78 (s, Cp*, 15H). **^{19}F NMR** (376 MHz, *d-chloroform*) δ -140.38 (dd, J_{FF} = 14.8, 8.0 Hz, 2F) -151.11 (t, J= 20.8 Hz, 1F) -159.89 (td, J= 20.6, 7.1 Hz, 2F). **^{13}C NMR** (126 MHz, *d-chloroform*) δ 158.2 (s, NC*N*), 147.2 (s, *Ar*), 144.7 (s, *Ar*), 139.3 (s, *Ar*), 123.5 (s, HC*C*H), 120.0 (s, H*C*CH), 88.9 (s, *Cp*), 43.5 (s, *C*H$_2$), 39.1 (s, *C*H$_3$), 9.3 (s, Cp*C*H$_3$). **MS** (ESI): Calcd for C$_{21}$H$_{22}$IIrF$_5$N$_2$, 717.0377; Found [M]$^+$ 717.0369. **Elemental analysis**, Anal. Calcd for C$_{21}$H$_{22}$IrI$_2$F$_5$N$_2$: C, 29.91%; H, 2.63 %; N, 3.32 %. Found: C, 29.21 %; H, 2.64 %; N, 3.19%.
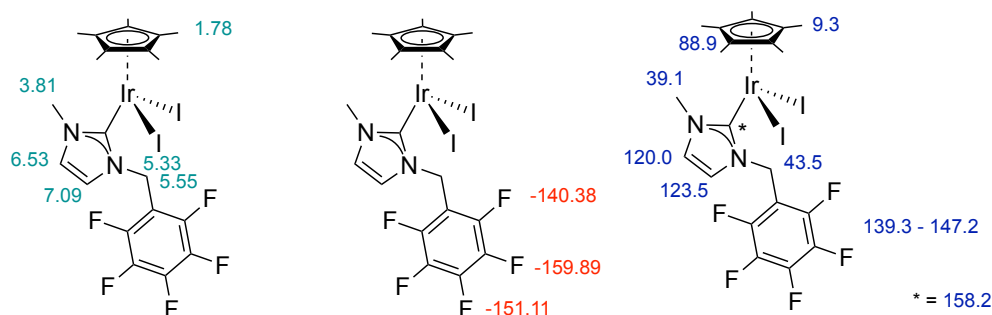
2.4.4.7 Synthesis of pentamethylcyclopentadienyliridium-(-3-methyl-1-(2,3,4,5-tetrafluorobenzylimidazolium) iodide (**17**)

Silver (I) oxide (0.07 g, 0.3 mmol) was added to a solution of 3-methyl-1-(2,3,4,5-tetrafluorobenzyl)imidazolium bromide (0.65 g, 0.2 mmol) in dichloromethane (20 mL) in the absence of light. The mixture was stirred for 1.5 hours before filtration through a plug of celite and washed with dichloromethane (2 x 20 mL). [IrCp*I$_2$]$_2$ (0.116 g, 0.1 mmol) was added to this solution which was stirred for a further four hours. The crude reaction mixture was filtered through a plug of celite, washed with dichloromethane (2 x 20 mL) and the filtrate was concentrated under reduced pressure. The crude product was recrystallized from the concentrated solution of dichloromethane and pentane at -20 °C. The pure product was collected *via* filtration, washed with hexanes, and dried *in vacuo*. X-ray quality single crystals were grown through vapour diffusion of hexane into a saturated DCM solution of **17**.

Orange crystalline solid. Yield: 0.137 g (69 %). **¹H NMR** (500 MHz, *d-chloroform*) δ 7.53 (m, C₆-*H*, 1H) 6.96 (d, *H*CCH, ³J*HH* = 2.0 Hz, 1H) 6.71 (d, HCC*H*, ³J*HH* = 2.3 Hz, 1H) 6.25 (d, imidazoleC*H*, ²J*HH* = 14.4 Hz, 1H) 5.02 (s, imidazoleC*H*, ²J*HH* = 14.4 Hz, 1H) 3.99 (s, NC*H₃*, 3H) 1.64 (s, Cp*, 15H). **¹⁹F NMR** (376 MHz, *d-chloroform*) δ -137.28 (ddd, J*FF* = 21.1, 12.7, 2.6 Hz), -145.46 (ddd, J*FF* = 20.8, 12.8, 3.2 Hz), -155.06 (td, J*FF* = 20.5, 2.9 Hz), -155.99 (td, J*FF* = 20.0, 2.6 Hz).**¹³C NMR** (126 MHz, *d-chloroform*) δ 157.6 (s, NCN), 148.7 (d, ¹J*CF* = 247 Hz, *Ar*F), 146.5 (d, ¹J*CF* = 246 Hz, *Ar*F), 139.8 (d, ¹J*CF* = 253 Hz, *Ar*F), 124.4 (s, HCCH), 121.2 (s, HCCH), 89.2 (s, *Cp*), 45.9 (s, *CH₂*), 38.9 (s, *CH₃*), 9.3 (s, Cp*CH₃*). **MS** (ESI): Calcd for C₂₁H₂₃IrIF₄N₂, 699.0472; Found [M]⁺ 699.0467. **Elemental analysis**, Anal. Calcd for C₂₁H₂₃IrI₂F₄N₂: C, 40.39%; H, 3.87 %; N, 4.49 %. Found: C, 39.06 %; H, 3.14 %; N, 4.49%.
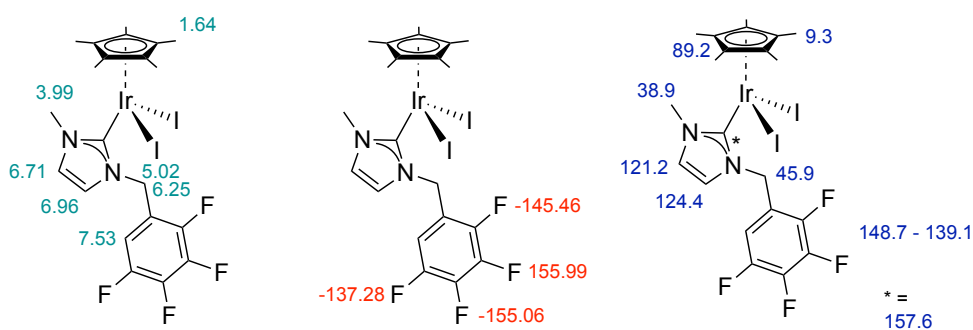
2.4.4.8 Synthesis of pentamethylcyclopentadienyliridium-(-3-methyl-1-(2,4,6)-trifluorobenzylimidazolium) iodide (**18**)

Silver (I) oxide (0.066g, 0.284 mmol) was added to a solution of 3-methyl-1-(2,4,6-trifluorobenzyl)imidazolium bromide (0.045 g, 0.2 mmol) in dichloromethane (20 mL) in the absence of light. The mixture was stirred for 1.5 hours before filtration through a plug of celite and washed with dichloromethane (2 x 20 mL). [IrCp*I₂]₂ (0.1116 g, 0.1 mmol) was added to this solution which was stirred for a further four hours. The crude reaction mixture was filtered through a plug of celite, washed with dichloromethane (2 x 20 mL) and the filtrate was concentrated under reduced pressure. The crude product was recrystallized from the concentrated solution of dichloromethane and pentane at -20 °C. The pure product was collected *via* filtration, washed with hexanes, and dried *in vacuo*. X-ray quality single crystals were grown through vapour diffusion of hexane into a saturated DCM solution of **18**.

Red crystalline solid. Yield: 0.096 g (74 %). **¹H NMR** (500 MHz, *d-chloroform*) δ 7.34 (s, *H*CCH, 1H) 7.17 (s, HCC*H*, 1H) 6.80 (t, C₆-*H*, ³J = 8.0 Hz, 2H) 5.65 (s, imidazoleC*H₂*, 2H) 4.14 (s, NC*H₃*, 3H) 1.65 (s, Cp*, 15H). **¹⁹F NMR** (282 MHz, *d-chloroform*) δ -102.26 (t, J*FF*

= 7.6 Hz, 1F) -110.12 (d, J_{FF} = 7.6 Hz, 1F). **^{13}C NMR** (126 MHz, *d-chloroform*) δ 160.7 (s, N*C*N), 138.6 (s, *Ar*), 131.0 (s, *Ar*), 128.9 (s, *Ar*), 123.9 (s, H*C*CH), 121.4 (s, HC*C*H), 101.5 (s, *Cp*), 41.2 (s, *C*H$_2$), 37.3 (s, *C*H$_3$), 11.1 (s, Cp*C*H$_3$). **MS** (ESI): calcd for C$_{21}$H$_{24}$IF$_3$IrN$_2$, 680.0576; found [M]$^+$, 680.0881. **Elemental Analysis**, Anal. Calcd for C$_{21}$H$_{24}$I$_2$F$_3$IrN$_2$: C, 31.24; H, 3.00: N, 3.47 %; Found: C, 37.63; H, 3.58: N, 3.09 %. Analysis not as required.
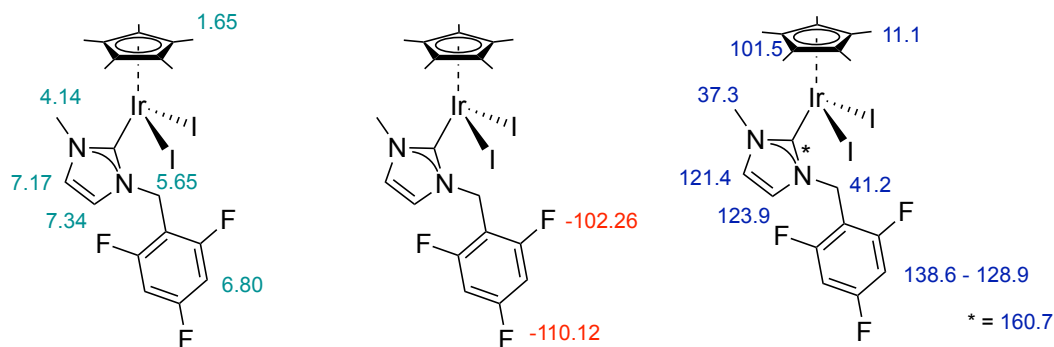
2.4.4.9 Synthesis of pentamethylcyclopentadienyliridium-(-3-methyl-1-(2,6)-dimethylbenzylimidazolium) iodide (**19**)

Silver (I) oxide (0.066g, 0.284 mmol) was added to a solution of 3-methyl-1-(2,6-dimethylbenzyl)imidazolium bromide (0.052 g, 0.187 mmol) in dichloromethane (20 mL) in the absence of light. The mixture was stirred for 1.5 hours before filtration through a plug of celite and washed with dichloromethane (2 x 20 mL). [IrCp*I$_2$]$_2$ (0.11 g, 0.095 mmol) was added to this solution which was stirred for a further four hours. The crude reaction mixture was filtered through a plug of celite, washed with dichloromethane (2 x 20 mL) and the filtrate was concentrated under reduced pressure. The crude product was recrystallized from the concentrated solution of dichloromethane and pentane at -20 °C. The pure product was collected *via* filtration, washed with hexanes, and dried *in vacuo*. X-ray quality single crystals were grown through vapour diffusion of hexane into a saturated DCM solution of **19**.

Dark green crystalline solid. Yield: 0.065 g (46 %). **^{1}H NMR** (400.11 MHz, *d-chloroform*) δ 7.11 (m, C$_6$-*H*, 3H) 6.79 (d, *H*CCH, $^3J_{HH}$ = 2.0 Hz, 1H) 6.26 (d, HCC*H*, $^3J_{HH}$ = 2.0 Hz, 1H) 5.83 (s, imidazoleC*H*, 1H) 4.93 (s, imidazoleC*H*, 1H) 3.82 (s, NC*H*$_3$, 3H) 1.82 (s, Cp*, 15H).**^{13}C NMR** (126 MHz, *d-chloroform*) δ 163.0 (s, N*C*N), 129.7 (s, *Ar*), 128.9 (s, *Ar*), 121.2 (s, H*C*CH), 119.2 (s, HC*C*H), 85.8 (s, *Cp*), 47.8 (s, *C*H$_2$), 37.6 (s, *C*H$_3$), 20.5 (s, Ar*C*H$_3$), 9.8 (s, Cp*C*H$_3$). **MS** (ESI): calcd for C$_{23}$H$_{30}$IrN$_2$, 525.2015.; found, [M]$^+$, 525.2093. **Elemental Analysis**, Anal. Calcd for C$_{23}$H$_{30}$IIrN$_2$: C, 42.26; H, 4.63; N, 4.29%. Found: C, 46.69; H, 5.22; N, 4.28%. Analysis not as required.
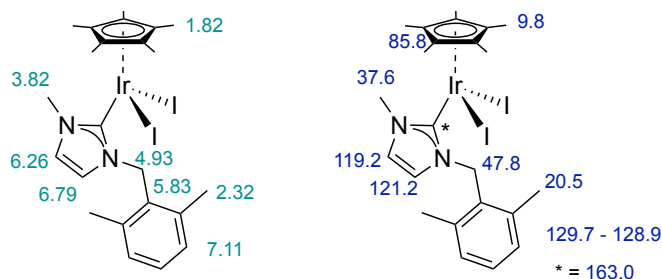
2.4.4.10 Synthesis of pentamethylcyclopentadienyliridium-(-3-methyl-1-benzylimidazolium) iodide (**20**)

Silver (I) oxide (0.066g, 0.284 mmol) was added to a solution of 3-methyl-1-benzylimidazolium bromide (0.047 g, 0.187 mmol) in dichloromethane (20 mL) in the absence of light. The mixture was stirred for 1.5 hours before filtration through a plug of celite and washed with dichloromethane (2 x 20 mL). [IrCp*I$_2$]$_2$ (0.11 g, 0.095 mmol) was added to this solution which was stirred for a further four hours. The crude reaction mixture was filtered through a plug of celite, washed with dichloromethane (2 x 20 mL) and the filtrate was concentrated under reduced pressure. The crude product was recrystallized from the concentrated solution of dichloromethane and pentane at -20 °C. The pure product was collected *via* filtration, washed with hexanes, and dried *in vacuo*. X-ray quality single crystals were grown through vapour diffusion of hexane into a saturated DCM solution of **20**.

Yellow crystalline solid. Yield: 0.049 g (35 %). **^{1}H NMR** (400.11 MHz, *d-chloroform*) δ 7.35 (m, C$_6$-*H*, 5H) 6.90 (d, *H*CCH, [3]J$_{HH}$ = 2.0 Hz, 1H) 6.68 (d, HCC*H*, [3]J$_{HH}$ = 2.0 Hz, 1H) 6.11 (s, imidazoleC*H*, 1H) 5.17 (s, imidazoleC*H*, 1H) 4.03 (s, NC*H*$_3$, 3H) 1.70 (s, Cp*, 15H).**^{13}C NMR** (126 MHz, *d-chloroform*) δ 156.9 (s, N*C*N), 136.8 (s, *Ar*), 128.7 (s, *Ar*), 128.5 (s, *Ar*), 128.0 (s, *Ar*), 123.2 (s, H*C*CH), 121.9 (s, HC*C*H), 88.8 (s, *Cp*), 54.6 (s, *C*H$_2$), 38.7 (s, *C*H$_3$) 9.2 (s, Cp*C*H$_3$). **MS** (ESI): calcd for C$_{21}$H$_{27}$IIrN$_2$ 627.0848; found [M-I]$^+$ 627.0828. **Elemental Analysis**, Anal. Calcd for C$_{21}$H$_{27}$I$_2$ IrN$_2$: C, 44.21; H, 4.77 N, 4.91. Found: C, 53.32; H, 6.14: N, 4.94 %. Analysis not as required.
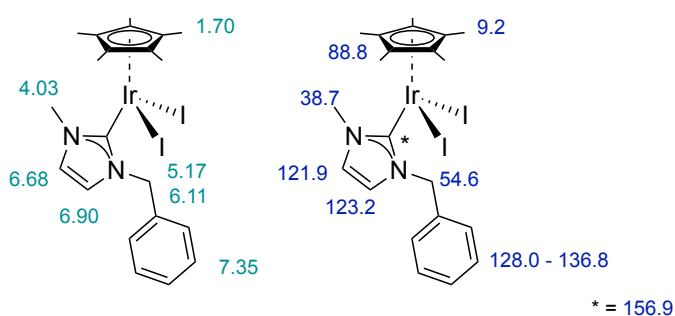
2.4.4.11 Synthesis of *cyclo*metallated iridium species [(η^5,κ_2C-C$_5$Me$_4$CH$_2$C$_6$F$_5$CH$_2$NC$_3$H$_2$NMe)- IrCl] (**24**)

IrCp*Cl$_2$(F$_5$Bzmim) (**11**) (0.066 g, 0.1 mmol) and silver oxide (0.070 g, 0.3 mmol) were added to a round bottomed flask containing DCM (40 mL) in darkness, and left to stand under argon for 24 hours. The crude reaction mixture was filtered through a plug of celite, washed with dichloromethane (2 x 20 mL) and the filtrate was concentrated under reduced pressure. The crude product was recrystallized from the concentrated solution of dichloromethane and hexane at -20 °C. The pure product was collected *via* filtration, washed with hexanes, and dried *in vacuo*. X-ray quality single crystals were grown through vapour diffusion of hexane into a saturated DCM solution of **24**.

Red crystalline solid. Yield: 0.045 g (68%). **^{1}H NMR** (500 MHz, *d-chloroform*) δ 7.03 (d, *H*CC*H*, $^3J_{HH}$ = 1.8 Hz, 1H) 6.97 (d, HCC*H*, $^3J_{HH}$ = 1.8 Hz, 1H) 4.84 (d, imidazoleC*H*, $^2J_{HH}$= 14.3, 1H) 4.51, (d, imidazoleC*H*, $^2J_{HH}$=14.3 Hz, 1H) 4.00 (s, NC*H$_3$*, 3H) 1.84 (s, Cp*, 3H), 1.82 (s, Cp*, 3H), 1.74 (s, Cp*, 3H), 1.63 (s, Cp*, 1H), 1.55 (s, Cp*, 3H) 1.27 (ddd, C$_5$CH*H*, J_{HH} = 12.0 Hz, J = 6.7, 1.5 Hz, 1H) 0.94 (s, Cp*, 3H). **^{19}F NMR** (282 MHz, *d-chloroform*) δ -146.09 (dd, J_{FF} = 26.5, 13.4 Hz, 1F) -151.27 (dq, J_{FF} = 29.6, 6.5 Hz, 1F), -172.22 (ddp, J_{FF} = 29.8, 24.6, 5.5 Hz, 1F) -175.07 (dddd, J_{FF} = 25.2, 12.7, 7.4, 4.6 Hz, 1F), -188.43 (dp, J_{FF} = 26.2, 5.5 Hz, 1F). **MS** (ESI): Calcd for C$_{21}$H$_{22}$ClIrF$_5$N$_2$, 587.1231; Found [M-Cl]$^+$ 587.1263.
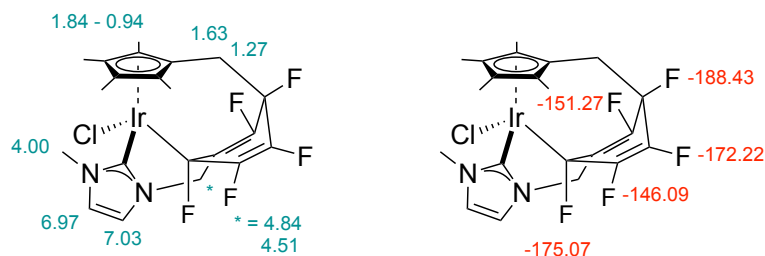
2.4.4.12 Synthesis of *ortho*metallated iridium chloride species [Cp*IrCl(κC$_2$-MeNC$_3$H$_2$NCH$_2$C$_6$F$_4$)] (**21**)

IrCp*Cl$_2$(F$_5$Bzmim) (**11**) (0.066 g, 0.1 mmol) and silver oxide (0.070 g, 0.3 mmol) were added to a round bottomed flask containing DCM (15 mL) in darkness, and left to stand under argon for 24 hours. The crude reaction mixture was filtered through a plug of celite, washed with dichloromethane (2 x 20 mL) and the filtrate was concentrated under reduced pressure. The crude reaction mixture was found to contain a mixture of **24** and **21**. Following concentration of the reaction filtrate, a pale orange suspension was present which was filtered under gravity

and washed with heptane. The resulting solid was dried under vacuum and was recrystallized from a concentrated solution of dichloromethane and hexane at -20 °C, enabling the separation of **24** from the sample. The pure product was collected *via* filtration, washed with hexanes, and dried *in vacuo*. X-ray quality single crystals were grown through vapour diffusion of hexane into a saturated DCM solution of **21**.

Orange crystalline solid. Yield: 0.052 g (79 %). **^{1}H NMR** (500 MHz, CDCl$_3$) δ 6.92 (d, *H*CCH, $^{3}J_{HH}$ = 2.1 Hz, 1H) 6.49 (d, HCC*H*, $^{3}J_{HH}$ = 2.1 Hz, 1H) 6.05 (d, imidazoleC*H*, $^{2}J_{HH}$ = 15.5 Hz, 1H) 5.46 (d, imidazoleC*H*, $^{2}J_{HH}$ = 15.6 Hz, 1H) 4.00 (s, NC*H*$_3$, 3H) 1.69 (s, Cp*, 15H,). **^{19}F NMR** (282 MHz, CDCl$_3$) δ - 114.00 (dd, J$_{FF}$ = 29, 14 Hz, 1F) -147.68 (dd, J$_{FF}$ = 21, 14 Hz, 1F) -158.42 (dd, J$_{FF}$ = 29, 20 Hz, 1F) -165.33 (dd, J$_{FF}$ = 21, 20 Hz, 1F). **MS** (ESI): Calcd for C$_{21}$H$_{22}$IrF$_4$N$_2$, 571.1348; Found [M]$^{+}$ 571.1330. **Elemental Analysis**, Anal. Calcd for C$_{21}$H$_{22}$ClF$_4$IrN$_2$.1$^{1}/_{2}$CH$_2$Cl$_2$: C, 38.72; H, 3.60 N, 4.01. Found: C, 38.85; H, 3.70: N, 3.80 %.
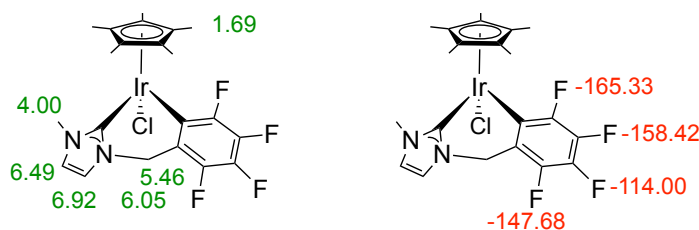
Characterisation consistent with previously reported literature.[202]

2.4.4.13 Synthesis of *ortho*metallated iridium iodide species [Cp*IrI(κC$_2$-MeNC$_3$H$_2$NCH$_2$C$_6$F$_4$)] (**25**)

IrCp*I$_2$(F$_5$Bzmim) (**16**) (0.084 g, 0.1 mmol) and silver oxide (0.070 g, 0.3 mmol) were added to a round bottomed flask containing DCM (15 mL) in darkness, and left to stand under argon for 24 hours. The crude reaction mixture was filtered through a plug of celite, washed with dichloromethane (2 x 20 mL) and the filtrate was concentrated under reduced pressure. The crude reaction mixture was found to contain a mixture of unreacted **16** and **25**. The crude mixture was recrystallized from the concentrated solution of dichloromethane and hexane at -20 °C. Subsequent recrystallisation attempts were not able to separate the reaction mixture. The mixed product was collected *via* filtration, washed with hexanes, and dried *in vacuo*.

Dark green crystalline solid. Mixed isolated yield of [Cp*IrI(κC$_2$-MeNC$_3$H$_2$NCH$_2$C$_6$F$_4$)] (**25**) and [IrCp*I$_2$(F$_5$Bzmim)] (**16**): 0.049 g. **^{1}H** NMR (500 MHz, *d-chloroform*) δ 7.01 (d, HCCH, $^{3}J_{HH}$ = 2.0 Hz, 1H) 6.96 (d, HCCH, $^{3}J_{HH}$ = 2.0 Hz, 1H) 5.30 (s, imidazoleC*H*, 1H) 5.21 (d, imidazoleC*H*, $^{2}J_{HH}$ = 14.5 Hz, 1H) 3.91 (s, NCH$_3$, 3H) 1.74 (s, Cp*, 15H). **^{19}F NMR** (282

MHz, *d-chloroform*) δ -110.95 (dd, J_{FF} = 29.3, 13.8 Hz, 1F), -147.75 (dd, J_{FF} = 21.4, 13.9 Hz, 1F) -158.49 (dd, J_{FF} = 28.6, 19.7 Hz, 1F) -165.32 (m, 1F). **MS** (ESI): Calcd for $C_{21}H_{22}IrF_4N_2$, 571.1348; Found $[M]^+$ 571.1339.
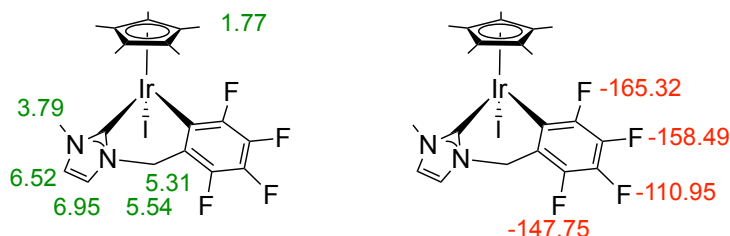
2.4.5 Synthesis of cobalt complexes

2.4.5.1 Synthesis of diiodocyclopentadienylcobalt carbonyl[218]

CoCp(CO)$_2$ (100 μL, 0.75 mmol) charged into a flask containing diethyl ether (10 mL). To this, a solution of iodine (0.22 g, 0.91 mmol) in diethyl ether (10 mL) was added dropwise *via* cannula over the course of 20 minutes, followed by stirring for 2 hours. Following reaction completion, the solvent was evapourated *in vacuo*. Product recrystallized from a solution of dichloromethane and hexane (1:4) at ca. -20 °C.

Black/dark purple crystalline solid. Yield: 0.32 g (99 %). **^{1}H NMR** (400.11 MHz, d_6-DMSO) δ 1.60 (s, Cp*, 15H). **^{13}C NMR** (126 MHz, *d-chloroform*) δ 9.9 (s, *Cp*). **MS** (ESI): calcd for C_6H_5CoIO, 278.8717; found $[M]^+$, 279.9187. **Elemental Analysis**, Anal. Calcd for $C_6H_5CoI_2O$: C, 17.76; H, 1.24 %. Found: C, 18.42; H, 1.73 %. **FTIR**: (v_{CO}) 2058 cm^{-1}.
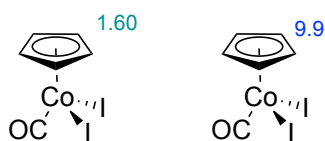
2.4.5.2 Synthesis of diiodopentamethylcyclopentadienylcobalt carbonyl

Dichloromethane (100 mL) added to a flask containing [Co$_2$(CO)$_8$] (4.787 g, 14.0 mmol) in a glovebox. Following transfer to a Schlenk line Cp*H (5.5 mL, 34.0 mmol) was charged into the flask and the mixture was heated to reflux for 6 hours. The reaction mixture was cooled to room temperature followed by solvent removal *in vacuo*. Diethyl ether (50 mL) added to crude

product, which was allowed to dissolve before a solution of iodine (9.0 g, 35.5 mmol) in diethyl ether (50 mL) was charged into the flask dropwise over 20 minutes *via* cannula filtration. (Note: Upon addition of iodine solution, the mixture refluxed due to exothermic reaction.) The reaction was stirred for a further hour, before the solvent was removed *in vacuo*. Product was recrystallized *via* dichloromethane:hexane (2:1) at ca. -20 $^{\circ}$C.

Dark purple crystalline solid. Yield: 13.31 g (95%). **^{1}H NMR** (400.11 MHz, *d-chloroform*) δ 2.23 (s, Cp*, 15H). **^{13}C NMR** (126 MHz, *d-chloroform*) δ 89.4 (s, *Cp*), 11.7 (s, Cp*CH$_3$*). **MS** (ESI): calcd for C$_{10}$H$_{15}$ICo, 320.9550; found [M]$^+$, 320.9542. **Elemental Analysis**, Anal. Calcd for C$_{11}$H$_{15}$CoI$_2$O: C, 27.76; H, 3.18. Found: C, 29.28; H, 3.62 %. **FTIR**: v_{CO} – 2054 cm^{-1} and 2028 cm^{-1}.
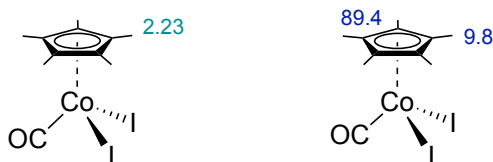
2.4.5.3 Synthesis of di-μ-iodo-bis[iodo-η^5-pentamethyl cyclopentidienylcobalt(III)

Octane (20 mL) was charged into a Schlenk flask containing [CoCp*I$_2$(CO)] (0.98 g, 2.05 mmol) and heated to reflux for 16 hours. Over the course of the reaction an insoluble dark green solid was observed within the reaction mixture. The solvent was removed *via* cannula filtration, washed with hexane (2 x 20 mL) and dried under vacuum. Recrystallization was achieved *via* vapour diffusion of a saturated solution of the complex in DCM with hexane within the glovebox. Each sample was examined under a microscope for evidence of single crystal growth. Samples that displayed the best visual single crystals underwent X-Ray analysis.

Dark green powder. Yield: 0.81 g, (86 % yield). **^{1}H NMR** (400.11 MHz, *d-chloroform*) δ 1.78 (s, Cp*, 15H). **^{13}C NMR** (126 MHz, *d-chloroform*) δ 11.4 (s, Cp*CH$_3$*). Quaternary Cp carbons not found. **MS** (ESI): calcd for C$_{10}$H$_{15}$CoI, 320.9550, C$_{20}$H$_{30}$Co$_2$I$_3$, 768.8146; found [CoCp*I]$^+$ 320.9535, [M-I]$^+$ 768.8110. **Elemental Analysis**, Anal. Calcd for C$_{20}$H$_{30}$Co$_2$I$_4$: C, 26.81; H, 3.38 %. Found: C, 23.55; H, 2.80: %. Analysis was not as required due to slow decomposition. No CO band observed upon FTIR analysis.
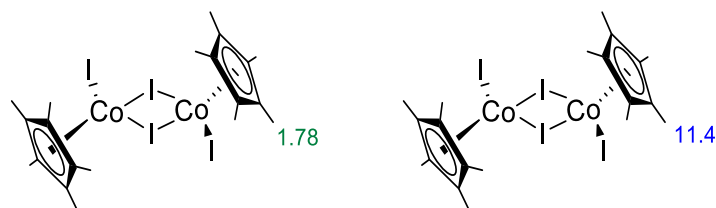
Characterisation consistent with literature.[215]

2.4.5.4   Synthesis of diiodocyclopentadienylcobalt-1-pentafluorobenzyl-3-methyl imidazole (**26**)

Silver (I) oxide (0.066g, 0.284 mmol) was added to the 3-methyl-1-pentafluorobenzyl-imidazolium chloride (0.068g, 0.2 mmol) in dichloromethane (20 mL) in the absence of light. The mixture was stirred for 1.5 hours before inert filtration through a plug of celite and washed with dichloromethane (2 x 20 mL). The filtrate was transferred to a Schlenk flask containing CoCp(CO)I$_2$ (0.082g, 0.2 mmol) and reaction stirred for a further 20 hours in the dark followed by solvent removal *in vacuo*. Product recrystallized *via* dichloromethane:hexane (2:1) at *ca.* 20°C within a glovebox. Two different crystal types were observed, black needles and colourless plates.

Dark purple crystalline solid. Mixed yield: 0.079 g (55 % yield). **¹H NMR** (400 MHz, *d-chloroform*) δ 7.20 (s, *H*CCH, poorly resolved, 1H) 6.89 (s, HCC*H*, poorly resolved, 1H) 5.68 (s, imidazoleC*H$_2$*, 2H) 4.34 (s, HC*H$_3$*, 3H) 1.56 (s, Cp, 5H). **¹⁹F NMR** (282 MHz, *d-chloroform*) δ -141.95 (dd, J= 20.5, 7.5 Hz, 2F) -150.73 (t, J= 20.4 Hz, 1F) -159.51 (td, J= 21.5, 7.0 Hz, 2F). **¹³C NMR** (126 MHz, *d-chloroform*) δ 128.81 (s, *Ar*), 122.93 (s, H*C*CH), 120.94 (s, HC*C*H), 96.18 (s, *Cp*), 49.20 (s, *C*H$_2$), 39.20 (s, *C*H$_3$), 9.74 (s, Cp*C*H$_3$). Aryl carbons not found. **MS** (ESI): calcd for C$_{16}$H$_{12}$IF$_5$CoN$_2$, 512.9297; found [M]$^+$, 512.9283. **FTIR**: v_{CO} – 2036.24 cm^{-1} and 2027.16 cm^{-1}.
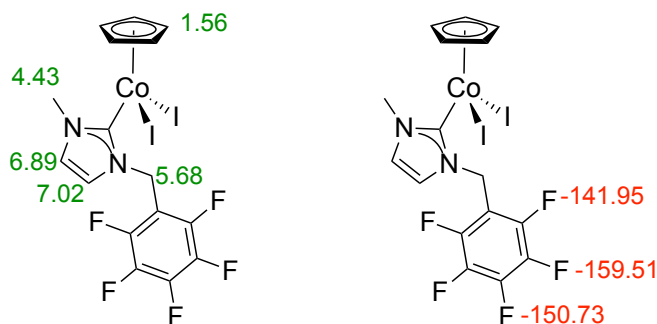
2.4.5.5 Synthesis of diiodopentamethylcyclopentadienyl cobalt-1-pentafluorobenzyl-3-methylimidazole (**27**)

Silver (I) oxide (0.066g, 0.284 mmol) was added to the 3-methyl-1-pentafluorobenzyl-imidazolium chloride (0.064g, 0.187 mmol) in dichloromethane (20 mL) in the absence of light. The mixture was stirred for 1.5 hours before inert filtration through a plug of celite and washed with dichloromethane (2 x 20 mL). The solvent was removed *in vacuo*, transferred to the glove box, washed with DCM (20 mL) and transferred to a Schlenk flask containing [CoCp*I$_2$]$_2$ (0.085 g, 0.095 mmol) and reaction stirred for a further 20 hours in the dark followed by solvent removal *in vacuo*. Product recrystallized *via* dichloromethane:hexane (2:1) at *ca*. -20 °C.

Black crystalline solid. Yield: 0.068 g (68 %). **¹H NMR** (500 MHz, *d$_6$*-benzene) δ 7.64 (d, *H*CCH, ³J$_{HH}$ = 2.0 Hz, 1H) 6.93 (d, HCC*H*, ³J$_{HH}$ = 2.0 Hz, 1H) 5.83 (s, imidazoleC*H*, 1H) 5.55 (s, imidazoleC*H*, 1H) 4.34 (s, NC*H$_3$*, 3H) 1.41 (s, Cp*, 15H). **¹⁹F NMR** (282 MHz, *d$_6$*-benzene) δ -140.27 (dd, J= 20.6, 7.4 Hz, 2F) -152.09 (t, J= 20.5 Hz, 1F) -160.62 (td, J= 21.5, 7.0 Hz, 2F). **¹³C NMR** not as required. **MS** (ESI): Calcd for C$_{21}$H$_{22}$CoIF$_5$N$_2$ 583.0079; Found [M]$^+$, 583.0070.
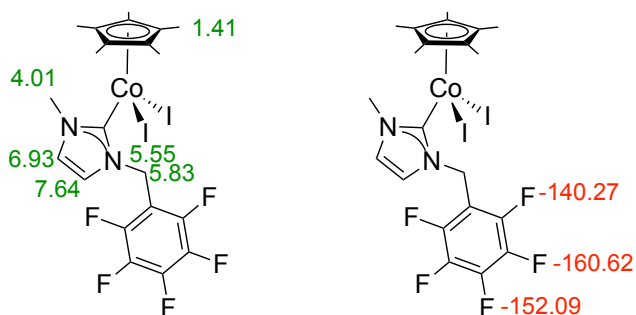
3   Chapter 3: Catalytic Nucleophilic Fluorination of Organic Electrophiles

3.1 Overview

3.1.1   Formation of Transition Metal Fluorides (TMF) for nucleophilic fluorination

As previously discussed in *Section 1.5–1.7* the generation and control of nucleophilic fluorine is vital to achieve selective fluorination of electrophiles. One method to control the reactivity of fluorine is through the formation of a metal-fluorine bond, as previously described in *Section 1.6*. The reactivity and stability of these TMF can then be modified through alteration of the coordination sphere of the complex. If tuned appropriately, a stable fluoride-complex can be formed which when treated with an electrophile is of sufficient reactivity to undergo fluorination.[121]

The formation of group 9 TMFs is of interest as the nucleophilicity and lability of the hard, polarizing fluoride ligand will be enhanced due to the presence of the soft, electron-rich metal centre, and thus these late transition metal fluorides are expected to be reactive.[57] Group 9 TMF complexes have traditionally been difficult to synthesise and isolate, requiring π-acceptor ligands to stabilise complexes featuring the strongly π-donating fluoride ligand,[219, 220,58] therefore the stability of fluoride-complexes are enhanced were *trans* π-acceptor ligands are utilised as strong π-donors form anti-bonding interactions with filled metal d-orbitals. The use of highly electron donating ligands could be employed to increase the nucleophilicity and lability of the fluoride ligand, by increasing electron density resulting in reduced π-acceptor capacity of the metal centre.

As described in *Section 1.6*, multiple group 9 TMF complexes have previously been synthesised, including the iridium and rhodium fluoride analogues of Vaska's complex, [MF(CO)(PPh$_3$)$_2$], M=Ir or Rh,[112] [IrF(C$_8$H$_{12}$)(PPh$_3$)],[116] and the piano-stool iridium complex, [IrCp*F(PMe$_3$)(R$_F$)], reported by Hughes, *et al.* (Scheme 3-1).[117] Nolan and co-workers synthesised the iridium[I] fluoride complex using an electron rich NHC ligand to stabilise the disparity between the "hard" fluoride and "soft" iridium centre.[221] The use of these electron rich NHC ligands have been shown to be capable of stabilising hard/soft ligand/metal interactions between iridium and the hydroxyl ligand.[222, 223,224] It was proposed by the authors that this interaction was believed to enhance the stability of the complex to allow for full characterisation of be carried out. Other methodologies for the formation of TMF utilising

nucleophilic fluoride sources include the use of HF or TREAT.HF (Figure 1-3) as the source of fluorine, allowing for methodologies to access metal-fluorine bonds that do not require halide substitution.[220, 225, 226]

M = Ir, Rh
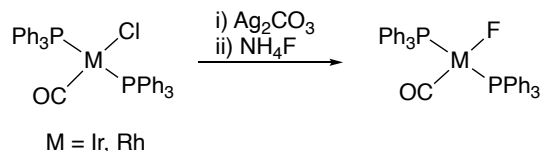
Vaska, L. *Inorganic Synthesis*, **1974**, *15*, 64 - 68.
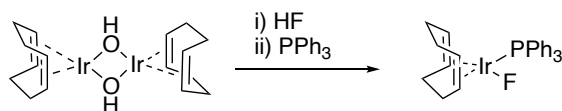
Roesky, H., *Eur. J. Inorg. Chem.,* **2004**, *13*, 2678 - 2682.
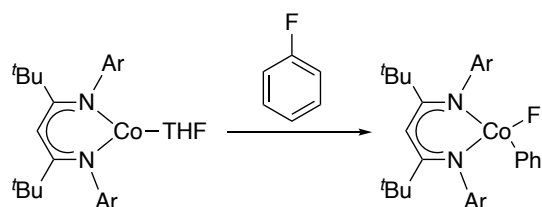
Holland, P., *Organometallics*, **2012**, *31*, 1349 - 1360.
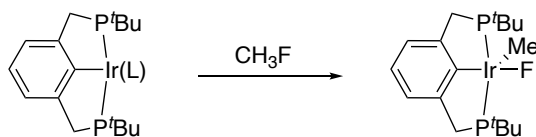
Goldman, A., *Science*, **2011**, *332*, 1545 - 1548.
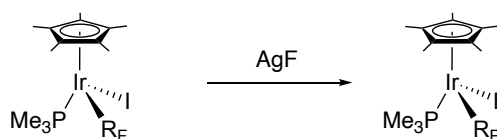
Hughes, R., *Organometallics*, **2006**, *25*, 3474 - 3480.
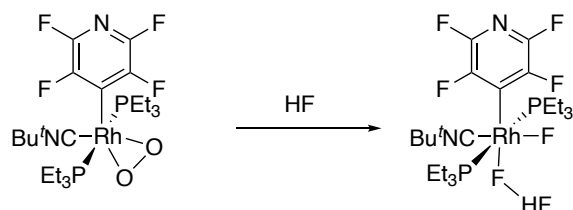
Braun, T., *Eur. J. Inorg. Chem.,* **2016**, *28*, 4565 - 4572.

Scheme 3-1: Selected examples of group 9 TMF complexes highlighting different synthetic routes towards the formation of the metal–fluorine bond. Formation of the TMF can occur through the oxidative addition of a fluoroorganic across a metal centre, giving a metal–fluorine bond, halide exchange with a metal fluoride salt, or through the addition of fluoride from HF/TREAT.HF.

However, few of these complexes have been utilised in the investigation into the reactivity of the TMF with an organic electrophile resulting in the formation of an organofluorine species. Gray *et al.*, reported the fluorination of acyl chlorides upon treatment with stoichiometric [bis(2-phenylbenzothiazolyl) (dimethylpyrazole) iridium fluoride,[121] where the TMF was formed through treatment of the iridium complex precursor with silver fluoride. While Baker *et al.*, demonstrated similar reactivity upon treatment of a piano-stool cobalt fluoride complex with acyl chlorides resulting in the formation of the acyl fluoride products.[227] These procedures will be discussed in *Section 3.4*.

To determine the efficacy of the fluorination of organic electrophiles from TMFs prior to catalytic development, group 9 TMF complexes were synthesised and treated with the acyl chlorides. Successful fluorination using these stoichiometric methods will then be developed towards a catalytic system.

3.1.2   Nucleophilic fluorination of acyl chlorides and why acyl chlorides are being targeted

Acyl fluorides have recently received increased attention in regards to their synthetic utility, showing improved stability and reactivity over their more commercially accessible chloride analogues, particularly within cross-coupling reactions,[228-233] enantioselective transformations,[234, 235] in fluorine transfer reactions[236] and the trifluoromethylation of aryl species (Scheme 3-2).[237]
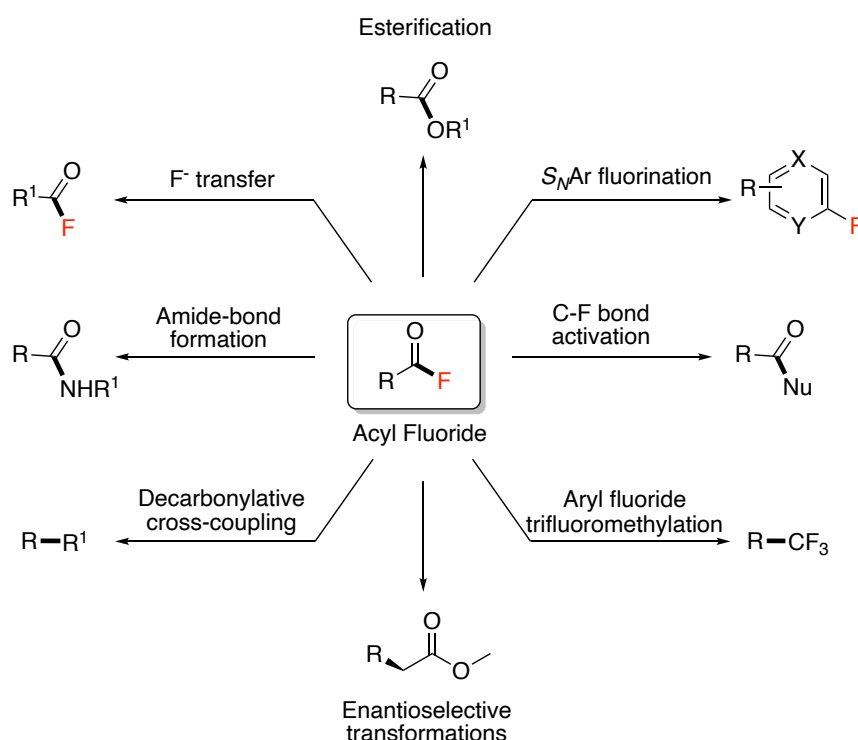
Scheme 3-2: Synthetic utility of acyl fluorides for a range of different transformations. Scheme showing the growing range of literature transformations that target the greater synthetic utility of acyl fluorides.

Due to growing interest in the synthetic utility of acyl fluorides, improved syntheses of the acyl fluoride starting materials are required to ensure commercial availability. Currently, the traditionally synthesis of these fluorinated compounds required toxic and hazardous reagents such as the SeF$_4$/pyridine complex[238] or cyanuric fluoride,[239] fluorination reagents such as DAST[240] or XtalFluor.[241]   Coupled with harsh reaction conditions, functional group compatibility is narrow, limiting the utility of acyl fluoride functionalisation methodologies within research and industry, especially where functional group tolerance and molecular scaffolds are significant.

Recently a number of small scale acyl fluoride protocols have been developed including: the deoxyfluorination of carboxylic acids;[242-246] direct fluorination with $(Me_4N)SCF_3$;[247] and transition metal catalysis.[126] Of these methodologies, the examples most frequently reported describe the deoxyfluorination of carboxylic acids, resulting in the formation of the analogous acyl fluorides. This is due, in part, to the prevalence of carboxylic acids within nature, and the ability to directly access acyl fluorides from potentially sustainable feedstocks.[248] The majority of these reported procedures rely on the formation of an activated substrate, where the carboxylic acid reacts *in-situ* with an additive (SOF_2,[243] $CF_3SO_2OCF_3$,[244] TCCA/amine,[245] TPFN,[246] $(Me_4N)SCF_3$,[249] PPh_3/NBS[250]) (Scheme 3-3), prior to treatment with a metal fluorine salt or other F^- equivalent, resulting in the formation of the acyl fluoride *via* a deoxyfluorination pathway.

However, many of these procedures require the use of obscure, non-commercially available reagents, expensive super-stoichiometric additives or toxic and hazardous reagents, such as HF equivalents or SO_2F_2 as the fluoride source. Therefore, synthetic procedures for the formation of acyl fluorides from inexpensive, non-toxic, readily available commercial sources that do not require specialist equipment are required.

a) SO$_2$F$_2$

b) CF$_3$SO$_2$OCF$_3$

Formed *in-situ*
from CF$_3$SO$_2$OCF$_3$

c) TCCA/amine

TCCA

d) (Me$_4$N)SCF$_3$

e) PPh$_3$/NBS
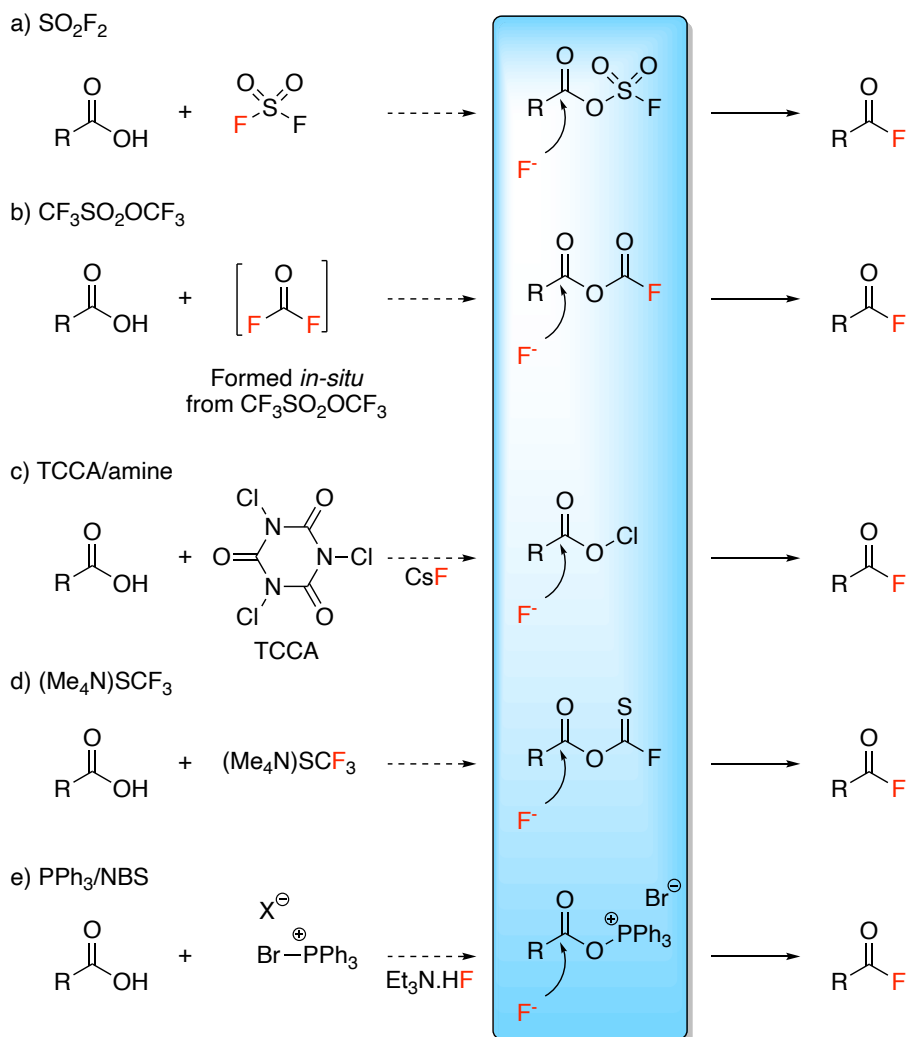
Scheme 3-3: Simplified synthetic route for the activation of carboxylic acids towards deoxyfluorination, highlighting the prevalence of formation of an activated acyl intermediate (highlighted) which then undergoes fluorination upon treatment with fluoride.

3.2   Research Aims

The formation of TMF bonds is an important first step in the process of understanding how to generate nucleophilic fluorine. To facilitate catalysis, it is important to understand the formation and reactivity of these TMF bonds,[52–56] therefore group 9 fluorido-complexes, bearing a labile metal-fluorine bond were synthesised. The fluoride complexes were treated with organic electrophiles to investigate the reactivity of the fluoride towards nucleophilic substitution. Subsequently, the generation of the TMF bond *in-situ*, was probed, to determine the catalytic potential of the reaction. A range of group 9 organometallic complexes act as catalysts for the procedure, where metal fluoride salts such as silver fluoride, potassium

fluoride and caesium fluoride used as the fluorine source. The development of a catalytic system, through the generation of nucleophilic fluorine *in-situ*, was investigated where the electrophilic organic targets, acyl chlorides, undergoes a nucleophilic substitution reaction with this reactive metal – fluoride bond resulting in the formation of the fluorinated product.

3.3 Formation of fluorido-complexes

To test the theory of whether nucleophilic fluorine can be generated through the formation of a TMF bond, first a suitable organometallic complex must be selected. [RhF(CO)(PPh₃)₂] was selected as a starting candidate due to its reliable synthesis, ease of purification and characterisation, coupled with the wealth of literature data on the synthesis, diversification and reactivity of this class of complexes.[114, 251, 252] [RhF(CO)(PPh₃)₂] was readily prepared through treatment of rhodium trichloride with triphenylphosphine in refluxing dimethylformamide, for four hours, under argon. Dimethylformamide acts as the carbonylation reagent to afford [RhCl(CO)(PPh₃)₂] as a red crystalline powder, in > 85 % yield following work-up. Following this, ligand exchange of [RhCl(CO)(PPh₃)₂] with tetramethylammonium fluoride gave near quantitative conversion of the desired fluorinated complex, [RhF(CO)(PPh₃)₂] (Scheme 3-4), with the pure complex characterised by ^{1}H NMR, ^{19}F NMR, ^{13}C NMR, ^{31}P NMR, HRMS and single crystal XRD. The spectroscopic data of this fluoride-rhodium complex is consistent with literature precedent.[114]
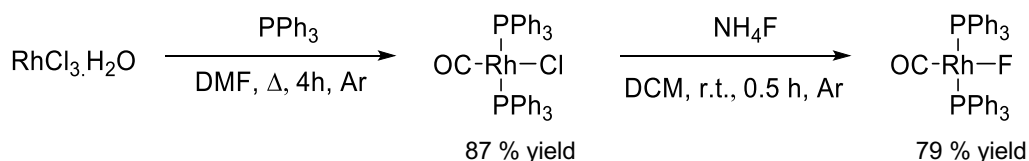
Scheme 3-4. Synthetic scheme for the synthesis of fluoride-complex, [RhF(CO)(PPh₃)₂].

Table 3-1. *Selected IR and NMR spectroscopic data of [RhF(CO)(PPh₃)₂]. Wavenumber in cm⁻¹, δ in ppm and J in Hz.*

Compound	ν(CO)	δ(^{19}F)	$^{1}J_{\text{Rh,F}}$	$^{2}J_{\text{P,F}}$	δ(^{31}P)	$^{1}J_{\text{Rh,P}}$
RhF(CO)(PPh₃)₂	1932	-270.61	51.4	27.1	29.47	129

Formation of the rhodium−fluorine bond was confirmed through the observed resonance peak within the ^{19}F NMR spectrum at -270.61 ppm (Table 3-1). The observed doublet peak is split

due to coupling with the spin active rhodium centre with a coupling constant of 55 Hz, consistent with other Rh−F bonds within similar systems.[114] Additionally, the ^{31}P NMR spectrum displays a doublet at 29.48 ppm, with coupling constant of $^1J_{Rh,P} = 127$ Hz, which exhibits a change in chemical shift for the fluorido-complex compared to the chloride precursor, [RhCl(CO)(PPh$_3$)$_2$] at 25.52 ppm. A difference is also observed in the IR stretching frequency in the carbonyl region between [RhCl(CO)(PPh$_3$)$_2$] (1961 cm^{-1}) and [RhF(CO)(PPh$_3$)$_2$] (1932 cm^{-1}), which indicates a weakening of the carbonyl bond in the fluoride-complex due to increased π-back donation from the from the metal centre as the result of increasing π-donation from the fluorine atom.

[RhF(CO)(PPh$_3$)$_2$] shows a slightly distorted square planar geometry (Figure 3-1), where the fluoride and carbonyl groups are in a mutual *trans* position, with a F(3)−Rh(1)−(CO)(1) bond angle of 178.2(1)° *vs* 179.2(1)° for Cl(3)−Rh(1)−(CO)(1), similar to that described in the literature.[114] The metal-halide bond distance within the two complexes was found to be; Rh(1)−Cl(3) 2.364(2) Å and Rh(1)−F(3) 2.025(1) Å, highlighting the greater bonding interaction of the π donating fluoride. This is coupled with the strengthening of the carbonyl - rhodium bond following fluorination, indicated by a shortening of the bonding contacts between C(1) and O(1) for the fluoride complex at 1.146(3) Å and C(1) and O(1) for the chloride complex at 1.251(8) Å, showing the effect of heightened π-back donation on the system.

[RhF(CO)(PPh$_3$)$_2$]   [RhCl(CO)(PPh$_3$)$_2$]
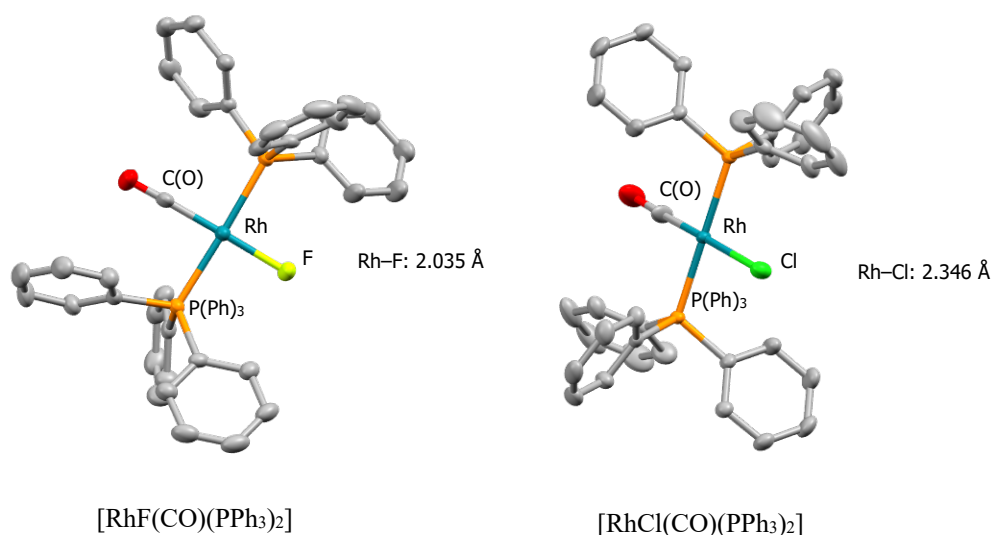
Figure 3-1. ORTEP diagram of trans-[Rh(F)(CO)(PPh$_3$)$_2$] and trans-[Rh(Cl)(CO)(PPh$_3$)$_2$], highlighting the differing bond strength and angles of the rhodium–halide bonds. Ellipsoids are drawn at 50% probability. All hydrogen atoms are omitted for clarity. Selected bond lengths /Å and angles /°: RhF(CO)(PPh$_3$)$_2$; Rh – PPh$_3$: 2.337(1), Rh – CO: 1.802(2), Rh – F: 2.025(1) Å / CO – Rh – F: 178.2(1)°, PPh$_3$ – Rh – PPh$_3$: 177.9 (2)°. RhCl(CO)(PPh$_3$)$_2$; Rh – PPh$_3$: 2.327(2), Rh – CO: 1.685(1), Rh – Cl: 2.364(2) Å / CO – Rh – Cl: 179.2(1)°, PPh$_3$ – Rh – PPh$_3$: 180.0(1)°.

These observation are comparable to other Vaska's type chloride and fluoride complexes.[114] This is indicative of the hypothesised bonding interaction with the strongly electronegative π-donating fluoride ligand and the metal centre resulting in the decreased bond order within the *trans*-carbonyl group, coupled with the observed strengthening of the rhodium-carbonyl bond.

With the successful synthesis of the desired TMF complex, the treatment of the complex with an organic electrophile could be conducted. If the formation of the TMF bond has enhanced the reactivity of the fluoride, over the fluoride salts, fluorination should be observed. Benzoyl chloride was chosen as the target electrophile, due to the recent interest in acyl fluorides as synthetic reagents and literature examples where treatment with group 9 fluorido-complexes result in the formation of benzoyl fluoride, as discussed in *Section 3.1*.[121] Treatment of [RhF(CO)(PPh₃)₂] with benzoyl chloride, in deuterated chloroform in a Young's tap NMR tube, proceeded rapidly over the course of 20 minutes, resulting in the quantitative conversion of benzoyl chloride to benzoyl fluoride (Scheme 3-5). In the nearly half century since Vaska first synthesised the fluorinated analogues, [MF(CO)(PPh₃)₂] (M= Ir/Rh),[112] to our knowledge this is the first occasion where their use has resulted in the direct fluorination of an organic electrophile.
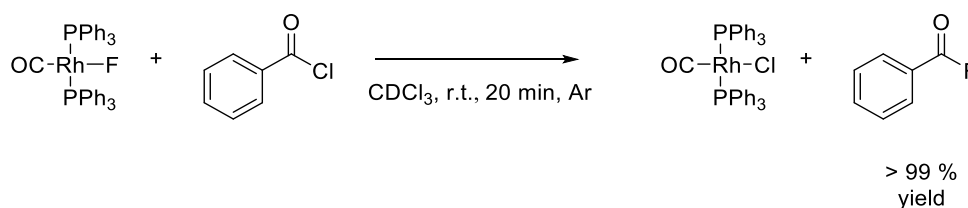
Scheme 3-5. Stoichiometric fluorination of benzoyl chloride using the fluorido-complex, [RhF(CO)(PPh₃)₂], as a reactive source of nucleophilic fluorine. Reaction occurs rapidly with full conversion to the fluorinated product.

The outcome of the reaction has been confirmed through NMR spectrometry, HRMS, FTIR and XRD. The benzoyl fluoride product was identified through ^{19}F NMR (18.05 ppm) giving quantitative contained yield *vs*. the internal standard. Following the reaction no Rh−F bond was observed at -270.61 ppm by ^{19}F NMR, indicating full consumption of [RhF(CO)(PPh₃)₂]. Additionally, the fluorine coupling within the ^{31}P NMR and ^{1}H NMR had disappeared and the ^{31}P NMR chemical shift of the resulting complex was indicative of [RhCl(CO)(PPh₃)₂], at 25.5 ppm. Following workup of the reaction, benzoyl fluoride was isolated in 83 % yield as a colourless oil and the resultant [RhCl(CO)(PPh₃)₂] complex has been identified through FTIR; 1961 cm⁻¹, consistent with previous experimental determination and literature values. The formation of X-Ray quality single crystals following evaporation of hexane into a saturated

solution of benzene resulted in the characterisation of the [RhCl(CO)(PPh$_3$)$_2$] complex, consistent with previously recrystallised samples.

The formation of the fluorinated product following treatment with a TMF complex shows that nucleophilic fluoride can be generated through complexation to the transition metal centre. The level of lability of this fluoride ligand is key if fluorination through ligand exchange is feasible. The reactivity of fluorinated Vaska's complexes towards the fluorination of an organic electrophile can be tuned through modification of the coordination sphere of the complex. Through changing the phosphine ligands present, the overall electronic and steric effects could modulate the reactive potential of the fluoride, either enhancing or retarding its fluorination ability. For a further discussion on this, please look to *Section 6* for future work.

The stoichiometric addition of these TMFs with an organic electrophile proved the concept that the generation of nucleophilic fluorine through the formation of a M−F bond can enhance the fluorides' reactivity over what is possible of simple metal fluoride salts. Unfortunately, [MCl(CO)(PPh$_3$)$_2$] showed limited catalytic ability upon initial investigation (described in *Section 3.4*), therefore the insights and techniques used within the development of this stoichiometric fluorination were applied in the catalytic development of the group 9 organometallic complexes developed in *Section 2* (Figure 3-2).
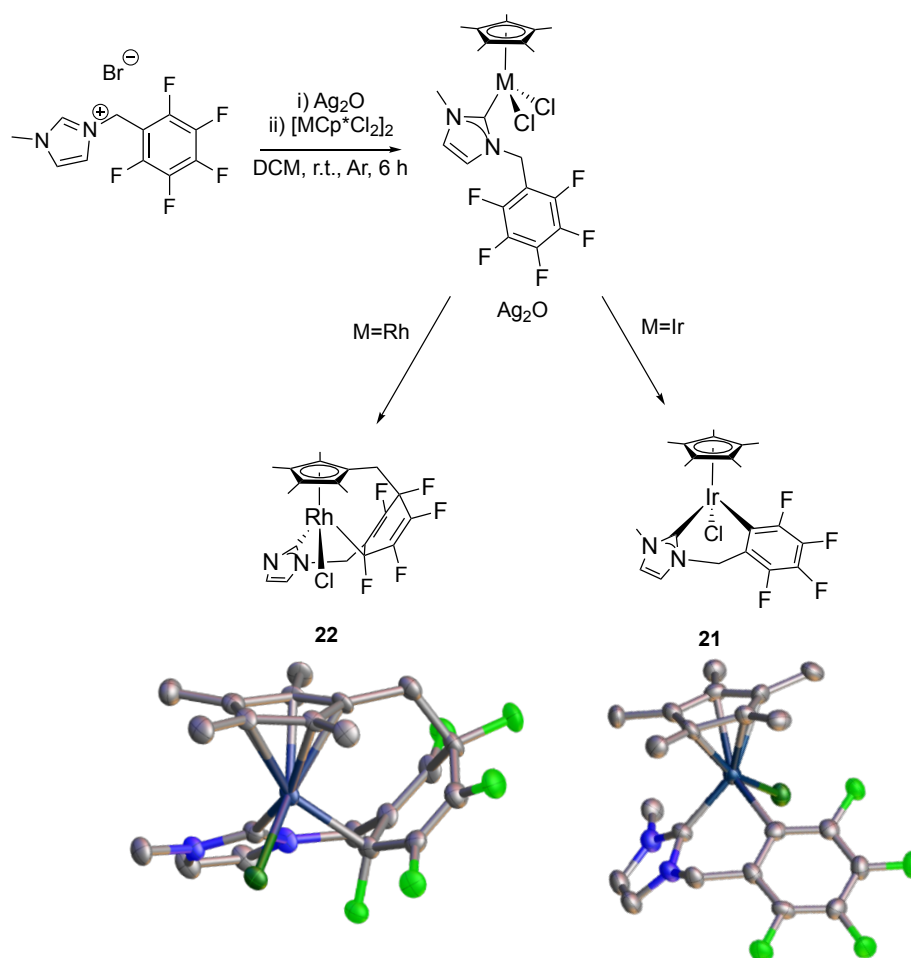
*Figure 3-2. Synthetic route to the formation of cyclometallated and orthometallated catalytic targets, **21** and **22** for the fluorination of acyl chlorides. These complexes were targeted to investigate whether halide exchange with the mono-halide by silver fluoride resulted in the formation of a TMF.*

To test the hypothesis on whether the complexes developed in *Section 2.2* could be developed as active fluorination catalysts, initial attempts were made to synthesis the fluorinated analogues of **6**, **11**, **22** and **21**. Initially, these complexes were treated with excess silver fluoride, following the method developed by Gray, *et al.*,[121] and utilised by Baker and co-workers to form piano stool cobalt fluoride complexes.[227] However, treatment of silver fluoride with the complexes described above did not result in the formation of the fluoride analogues, even when using upwards of 10 equivalents of the metal fluoride salt. Additional attempts using TREAT.3HF,[220] TBAF[114] and ammonium fluoride as the fluoride source also proved unsuccessful in the formation and isolation of the fluoride analogues. Further work to develop a system, utilizing a metal fluorine salt as a fluorine source in the presence of catalytic quantities of group 9 complexes are described in *Section 3.4*.

3.4   Development of catalytic fluorination

The catalytic activity of the complexes developed in *Section 2*, towards the fluorination of acyl chlorides was investigated. As highlighted in *Section 1.6*, the nucleophilic fluorination of acyl chlorides can be achieved through the treatment of the organic electrophile with stoichiometric quantities of the TMF, resulting in the quantitative formation of the fluorinated product. As such, the reaction conditions reported by Gray and co-workers[121] (Scheme 3-6) were adapted to form the reactive TMF *in-situ* with catalytic quantities of metal.
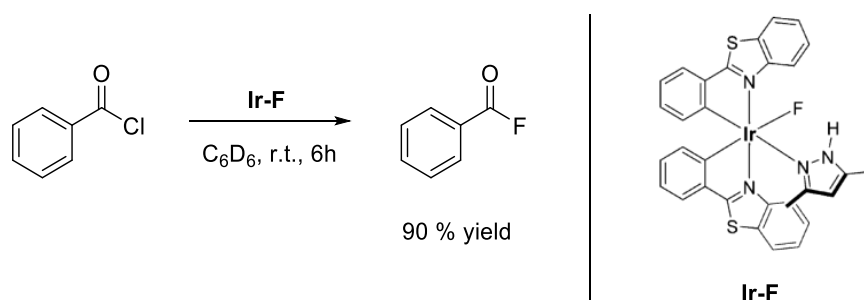
*Scheme 3-6: Fluorination of benzoyl chloride using the stoichiometric TMF iridium fluoride-complex, **Ir−F**. Illustrates how the formation of a TMF can lead to the nucleophilic fluorination of organic electrophiles. Scheme adapted from literature.[121]*

Toluoyl chloride was selected as the model substrate, as it has previously been shown to be active towards fluorination with TMF complexes.[121, 227] Similarly, silver fluoride was selected as the fluorine source, as this had been used by Gray and co-workers to form their reactive Ir–F bond.[121] The Vaska's complex, [IrCl(CO)(PPh$_3$)$_2$], and it rhodium analogue, [RhCl(CO)(PPh$_3$)$_2$], were then tested for their catalytic activity towards the fluorination of toluoyl chloride, following the fluorinated analogues successful stoichiometric reaction described in *Section 3.3*. However, it was observed that treatment of catalytic quantities of these complexes (5 mol %) with silver fluoride under the reaction conditions did not result in the formation of isolatable TMF bond and only a minor level of fluorination was observed (Table 3-2; entry 4 and 5). Interestingly, the rhodium analogue (entry 4) proved to have a higher activity that the iridium complex (entry 5).

Treatment of toluoyl chloride, in the presence of 5 mol % [CoCpI$_2$(CO)], with silver fluoride (3 equivalents) resulted in the formation of toluoyl fluoride, with a contained yield of 67 %, calculated against and internal standard *via* ^{19}F NMR (Scheme 3-7). Initial ^{19}F NMR

experiments identified the formation of a new singlet fluorine resonance at 17.43 ppm, corresponding to literature values of toluoyl fluoride.[253]
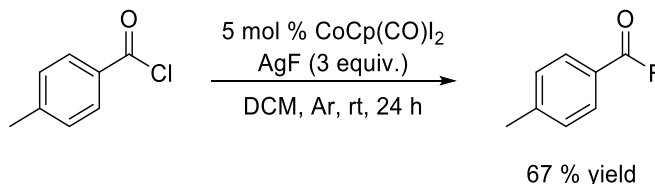
Scheme 3-7. Initial conditions applied for the catalytic formation of toluoyl fluoride, using 5 mol % catalyst, three equivalents of a fluoride source, leading to the catalytic fluorination of toluoyl chloride.

These initial results proved encouraging, as the non-catalysed reaction resulting in a toluoyl fluoride formation of ~ 0-5 % for potassium fluoride, caesium fluoride and silver fluoride (Table 3-2; entry 1, 2 and 3). The use of potassium fluoride as the fluorine source gave no conversion to toluoyl fluoride, whereas caesium fluoride and silver fluoride gave 5 % conversion and 2 % conversion respectively. These results show the need of the transition metal catalyst to control and enhance the reactivity of the fluorine in the system.

While the *in-situ* formation of a reactive TMF intermediate has not been observed following the reaction of [CoCpI$_2$(CO)] with silver fluoride, the current hypothesis follows that the silver fluoride reacts with the cobalt complex, resulting in the formation of a new metal-fluorine bond, *via* ligand substitution with iodide, forming reactive nucleophilic fluorine and silver iodide. This fluorine can then undergo nucleophilic attack of the toluoyl chloride electrophile, displacing chloride, resulting in the formation of toluoyl fluoride. The formation of this active cobalt-fluoride complex *in-situ* is proposed to occur as little reactivity was observed in the absence of the catalyst, showing the nucleophilicity of fluoride in silver fluoride is too low to facilitate the reaction.

Treatment of [CoCpI$_2$(CO)] with caesium fluoride exhibited similar fluorination capability to the non-catalysed reaction (Table 3-2; entry 6), whereas treatment of catalytic quantities of [CoCpI$_2$(CO)] with silver fluoride gave 67 % conversion of the fluorinated product (Table 3-2; entry 7), highlighting the differing reactivities of the metal fluorine salts within this system. This disparity in reactivity can be associated with the relative lattice enthalpies and solubility of the metal fluoride salts and resultant metal halide by-products. The use of the more electron donating Cp* group, in [CoCp*I$_2$(CO)], resulted in an increase in the conversion to the fluorinated product at 81 %, with an isolated yield of toluoyl fluoride at 71 % (Table

3-2; entry 8). This is as expected, as an increase in electron density on the metal centre results in an increase in the yield of fluorination, as greater electron density on the metal renders the metal-fluorine bond more nucleophilic.

Unfortunately, during the development of this system Baker and co-workers reported as similar fluorination procedure for the fluorination of acyl chlorides using piano stool cobalt catalyst of similar design.[126] This system followed a similar procedure for the formation of acyl fluorides from $[CoCp^{(*)}I_2(CO)]$ complexes, that were have developed independently, resulting in similar activity with 65 % contained yield of the acyl fluoride product with $[CoCpI_2(CO)]$ for the work reported by Baker, compared to 67 % contained yield within our work. Therefore, further work on this cobalt catalysed system was halted and our focus moved towards the development of rhodium and iridium catalysed systems.

The commercially available precatalytic complexes, $[MCp^*X_2]_2$, were tested for their catalytic potential in this system (Table 3-2; entry 9, 10, 11), giving poor to moderate conversion of the fluorinated product. The rhodium complex $[RhCp^*Cl_2]_2$ (entry 9) showed improved fluorination capability over the iridium analogue, $[IrCp^*Cl_2]_2$ (entry 10), a similar trend to that observed for the commercially available complexes, $[RhCl(CO)(PPh_3)_2]$ and $[IrCl(CO)(PPh_3)_2]$ described above. Whereas swapping the chloride for iodide (entry 11) gave an improved yield of the fluorinated product, from 9 to 40 % contained yield. The improved conversion for the iodo-complex was justified through the more favourable formation of AgI during the reaction, facilitating a greater turnover of the catalytic species. Unfortunately, treatment of toluoyl chloride with catalytic quantities of $CoCp^*I_2(F_5Bzmim)$, **26**, $RhCp^*Cl_2(F_5Bzmim)$, **6**, $IrCp^*Cl_2(F_5Bzmim)$, **11** (Table 3-2; entry 12, 13, 14 respectively) showed minor conversion to toluoyl fluoride, similar in activity to the non-catalysed systems. Due to the enhanced reactivity of $[IrCp^*I_2]_2$ over its chloride analogue, the iodo analogues, $RhCp^*I_2(F_5Bzmim)$ and $IrCp^*I_2(F_5Bzmim)$, **16**, were targeted to see if improved fluorination could be achieved. However, these complexes were not tested due to difficulty related to the separation and isolation of these complexes from the reaction mixture containing the *ortho*metallated analogues. Further work could be conducted into observing the effect of the halide ligand on these complexes towards catalytic performance.

Next the catalytic activity of the *ortho*metallated complexes **23** and **21**, were probed (Table 3-2; entry 15 and 16). It was initially proposed that these complexes may exhibit suitable fluorination activity as it was envisioned that displacement of the mono-halide ligand may be more favourable for the *ortho*metallated complexes, compared to their dihalide, piano stool precursors. However, repeated experiments resulted in roughly 15 % contained yield of

toluoyl fluoride for both *ortho*metallated complexes, displaying only a slightly higher degree of fluorination compared to the non-*ortho*metallated complexes **6** and **11**.

The reaction of toluoyl chloride with the *cyclo*metallated complex **22** (Table 3-2; entry 17), proved more successful**,** with a contained yield of 88 % of the toluoyl fluoride product, upon initial testing. It is proposed that the electron withdrawing nature of the polyfluorocyclohexadiene ring, coupled with the tethered Cp* ligand creates a more suitable environment for the exchange of chloride for fluoride. The removal of electron density from the metal stabilises the formation of a proposed rhodium–fluorine bond containing intermediate, which undergoes nucleophilic substitution with the toluoyl chloride electrophile. As mentioned in *Section 3.1*, a balance between M-F bond stability and lability is required in order to activate the fluoride, for TMF bond formation, and to ensure sufficient fluoride nucleophilicity. Additionally, the tethered NHC-C_6F_5-Cp* ligand system may act to block multiple faces of approach to the metal centre providing a suitable environment at the metal to facilitate this reaction, in addition to the formation of a nucleophilic fluoride. Therefore, the use of **22** enables a greater degree of control over the reactivity of fluorine, resulting in the desired reactivity. The synthesis of this *cyclo*metallated complex bearing less electron withdrawing ligands, which may enhance the nucleophilicity of the fluoride is discussed in *Section 6*.

It must be noted that over the time course of the reaction, the active catalytic species, **22**, was found to revert to the inactive form of **6**, identified by the loss of the −145.6 ppm, −149.4 ppm, −174.1 ppm, −176.8 ppm, and −185.7 ppm signals within the ^{19}F NMR spectrum and the formation of the -140.5 ppm, -151.4 ppm and -160.1 ppm peaks, representative of **6**.

Following the reaction, isolation of the toluoyl fluoride product could be accomplished by work-up in air. Filtration of the reaction mixture through a plug of celite, followed by elution with cold diethyl ether resulted in the formation of a pale orange solution with precipitation of an orange solid. Further precipitation was afforded by storing the filtrate at *ca*. -20 ºC for 16 hours. Filtration of this mixture enabled the separation and recovery of the catalytic material and the isolation of toluoyl fluoride as a colourless crystalline solid in 84 % yield.

Using this work-up procedure, the separation and isolation of the fluorinated product and the catalyst could be completed. Optimisation of this procedure by incorporating a further recrystallising step following diethyl ether filtration, from hot heptane, enabled the formation of X-Ray quality single crystals of toluoyl fluoride (Table 3-2), coupled with up to 91 % recovery of the rhodium species. The active catalytic species could then be regenerated through addition of silver oxide for 24 hours, in a similar procedure described for the synthesis

of **22** in *Section 2.4.4.6*. The recovered and regenerated catalyst could then be reused without loss in catalytic activity. With a working catalytic system in hand, exhibiting good fluorination activity and recyclability of the catalyst, **22** was chosen as the catalyst of choice for future experiments.

Table 3-2. Catalyst screen for the catalytic fluorination of toluoyl chloride.[a]

Entry	Fluoride Source	Catalyst	TON	Contained yield (%)[b]	Isolated yield (%)
1	KF	-	-	0	-
2	CsF	-	-	5	-
3	AgF	-	-	2	-
4	AgF	RhCl(CO)(PPh$_3$)$_2$	5.2	26	-
5	AgF	IrCl(CO)(PPh$_3$)$_2$	3.2	16	-
6	CsF	CoCpI$_2$(CO)	-	2.5	-
7	AgF	CoCpI$_2$(CO)	13.4	67	60
8	AgF	CoCp*I$_2$(CO)	16.2	81	71
9	AgF	[RhCp*Cl$_2$]$_2$	4.8	24	-
10	AgF	[IrCp*Cl$_2$]$_2$	1.8	9	-
11	AgF	[IrCp*I$_2$]$_2$	8	40	-
12	AgF	**27**	-	5	-
13	AgF	**6**	-	5	-
14	AgF	**11**	-	4	-
15	AgF	**23**	3.2	16	-
16	AgF	**21**	3.2	16	-
17	AgF	**22**	17.6	88	84

[a]Reaction conditions: Toluoyl chloride (1.0 mmol), Silver Fluoride (3.0 mmol), catalyst (5.0 mol %), DCM (5.0 mL), 400 rpm stirring, argon, room temperature, 24 hours. [b] ^{19}F NMR yields determined against internal standard of trifluorotoluene (20 µL).

Moving forward, an optimization screen was carried out to elucidate the effect of stirring, solvent, fluoride source, atmosphere and additives on the fluorination of toluoyl chloride (Table 3-3). The standard conditions of the reaction were varied in incremental steps, to determine the best system to take forward towards a substrate scope. The standard conditions, taken from the catalyst screening, are given in Table 3-3; entry 1. Toluoyl chloride (1 mmol), was treated with 5 mol % **22** in the presence of AgF (3 equivalents), in dry, degassed dichloromethane for 24 hours at room temperature. Conversion to the acyl fluoride product were calculated by ^{19}F NMR against an internal standard (20 µL trifluorotoluene) and the fluorinated product was isolated following the reaction by work-up procedure described above. The variation from standard conditions is highlighted in **bold** in Table 3-3. All results have been replicated and the contained yields highlighted in Table 3-3 are averaged across runs, with outliers removed.

In an attempt to improve the sustainability of the reaction, first the effect of fluoride source was examined. One of the major drawbacks of similar catalytic systems, utilising metal fluoride salts as the fluoride source, is the high loading of fluoride salt required to achieve fluorination, from 3-50 equivalents. Likewise, our initial system uses 3 equivalents of silver fluoride to achieve fluorination, which represents a significant quantity of silver waste at the end of the reaction. Improving the overall sustainability of this procedure, by reducing salt loading thus reducing waste, or by changing to a cheaper, more sustainable fluoride salt would be advantageous. However, during the course of these experiments it was observed that silver fluoride was required to achieve a high degree of fluorination (Table 3-3; entry 1) and changing the fluoride source has a significant effect on the conversion to the fluorinated product (Table 3-3; entry 2 and 3). This observed decrease in reactivity from silver fluoride>caesium fluoride>potassium fluoride is commonly observed when using these cheaper and more abundant fluorine salts due to the stronger lattice enthalpies and poorer solubility of these salts in organic systems. The high degree of fluorination using silver fluoride (up to 92 %) was retained when reducing the loading of the fluoride source to half (Table 3-3 entry 4), significantly reducing the quantity of waste produced, with no apparent reduction in yield. It should be noted that while the reported fluorination with caesium fluoride (36 % contained yield) and potassium fluoride (25 % contained yield) does not seem promising, these results represent a relatively good fluorination activity with these salts, compared to similar examples within the literature, which often require additives and/or forcing conditions.[254]

Unlike similar published fluorination methodologies,[126, 152, 153] the recovery of the catalyst was demonstrated. Catalyst recovery is a key consideration in homogeneous catalysis, especially from an industrial perspective and a fundamental requirement when analysing the overall sustainability and commercial viability of the system. At these small scales mechanical losses and human error can account for significant portions of catalyst loss within the system upon recovery, where rhodium recovery rates varied from 68 % up to 91 %. The addition of **22**, which had been recovered from previous reactions and regenerated through addition of silver oxide, showed little reduction is conversion of toluoyl fluoride (Table 3-3; entry 17).

To further reduce loss of metal from the system it will be important to explore different methodologies to improve reliability or increase recovery rates the catalyst in the future, compared to the current solvent extraction and recrystallisation route. Alternative methodologies including polymer supported catalysis, catalyst entrapment or organic solvent nanofiltration could be envisioned to further improve this efficiency.[255-259]

As it was observed that the active catalytic species **22**, reverted to the inactive form **6** over time, the use of an additive was proposed in which the active catalytic species was regenerated *in-situ*. To address this, differing quantities of silver oxide were added to the reaction mixture to initiate the regeneration of the active catalytic species *in-situ*. Initially, silver oxide (2 equivalents) was added to the reaction mixture alongside **6**, to investigate whether the active catalytic species could be formed *in-situ*. NMR sampling after 4 hours detected the formation of **22** alongside toluoyl fluoride, showing this method was effective in forming the active *cyclo*metallated complex during the course of the reaction (Table 3-3; entry 5). While the addition of silver oxide to **6** and the resultant formation of **22** *in-situ* results in a higher degree of fluorination (33 % contained yield) than solely **6**, it was observed to be less than that observed for **22** and unfortunately resulted in the decomposition of rhodium complexes over the course of the reaction. Stoichiometric addition of silver oxide to **22**, in an attempt to regenerate the active catalytic species *in-situ*, also resulted in complete decomposition of the catalyst (Table 3-3; entry 6). Stirring of silver salts in an organic solvent has been shown to lead to the mechanochemical generation of silver particles in some cases, which may lead to this observed decomposiiton.[200] The addition of 10 mol % silver oxide resulted in the re-formation of the active catalyst, **10**, which was observed in larger concentrations in solution following the reaction (Table 3-3; entry 7). A control reaction using catalytic quantities of silver oxide (Table 3-3; entry 8), in the absence of catalyst, shows little improvement over the non-catalysed system (Table 3-2; entry 1).

The use of silver oxide as a catalytic additive was discontinued as it had a small effect on the reaction yield (94 % contained yield *vs*. 88 % contained yield), resulting in the occasional decomposition of the catalyst, coupled with a reduction in fluorination, observed through the formation of a colourless solution with a black/brown suspension. The cause of decomposition is thought to be due to the mechanochemical decomposition of silver oxide to silver particles, resulting in the breakdown of the catalytic species.

As the fluoride source is heterogeneous in nature, sufficient mixing was required to ensure an even dispersion of silver fluoride in solution. Increasing the stir rate from 200 rpm to 600 rpm had a dramatic effect on the formation of the fluorinated product, from 68 % contained yield at 200 rpm (Table 3-3; entry 10) to 94 % contained yield (Table 3-3; entry 11) at 600 rpm. However, when the stir rate was increased above 600 rpm, up to 1000 rpm, a reduction in yield was observed as the rapid stirring resulted in the decomposition of silver fluoride to silver particles, resulting in the decomposition of the catalyst and formation of a black/brown suspension (Table 3-3; entry 12), where no catalytic or catalyst precursor material was detected by ^{19}F NMR. 600 rpm was chosen as the standard rotation speed and carried to future

experiments, as this represented the most appropriate balance between reduced product formation and catalyst decomposition.

In an attempt to aid the rate of fluorination, the reaction was carried out using anhydrous acetonitrile (Table 3-3; entry 13). Acetonitrile was targeted as it is a dipolar aprotic solvent, which can enhance the rate of nucleophilic substitution reactions and has been shown to aid in nucleophilic fluorination reactions.[245, 260] However, addition of acetonitrile to silver fluoride resulted in the immediate tarnishing of the silver fluoride, from orange to black, upon addition. This was observed to result in the rapid formation of toluoyl fluoride upon addition, followed by no additional observed reactivity. The speciation of silver or fluoride following addition of acetonitrile has not been determined but resulted in a reduction in formation of fluorinated product at 58 % contained yield. Additionally, no fluorination was observed when THF or toluene was used as the solvent (Table 3-3; entry 14 and 15 respectively). Alternatively, the use of CDCl$_3$, tested to investigate direct sampling of the reaction mixture for NMR, gave an excellent conversion of 92 % yield (Table 3-3; entry 16).

To probe whether the reaction was proceeding *via* a radical mechanism the radical scavenger, (2,2,6,6-Tetramethylpiperidin-1-yl)oxyl (TEMPO), was added, however little effect was observed (Table 3-3; entry 18). Attempts to aid the reaction *via* photoexcitation proved unsuccessful, as on each occasion the catalyst underwent decomposition with very minimal formation of the fluorinated product (Table 3-3; entry 19).

 Interestingly, the addition of **22** in the absence of a fluoride source, resulted in the detection of trace quantities of toluoyl fluoride upon work up (Table 3-3; entry 20). Initially, this was thought to be accidental contamination, however subsequent experiments proved otherwise. These results will be discussed further in *Section 4.3*.

Using the data gathered through the development of catalytic conditions for the rhodium catalysed fluorination of toluoyl chloride, an expanded substrate scope was conducted, using the following reaction conditions; 1 mmol of substrate, 1.5 equivalents of silver fluoride, 5 mol % **22**, using dry, degassed dichloromethane (5 mL), with a stirring speed of 600 rpm, carried out under an argon atmosphere at room temperature, in darkness for 24 hours.

*Table 3-3. Optimisation of reaction conditions for the fluorination of toluoyl chloride with catalytic quantities of **22**.*

Standard conditions: Toluoyl chloride (1.0 mmol), AgF (1.5 mmol), **22** (5.0 mol %), DCM (5.0 mL), 400 rpm, argon, room temperature, 24 hours. [A] Calculated against trifluorotoluene (20 µL) internal standard [B]

Entry	Fluorine Source	Solvent	Stir rate (rpm)	Atmos.	Catalyst	Additive	TON	^{19}F NMR contained yield[A] (%)	Isolated yield (%)
1[b,c]	AgF	DCM	400	Ar	**22**	-	17.6	88	84
2[c]	**KF**	DCM	400	Ar	**22**	-	5	25	-
3[c]	**CsF**	DCM	400	Ar	**22**	-	7.2	36	-
4	AgF	DCM	400	Ar	**22**	-	17.6	88	79
5[d]	AgF	DCM	400	Ar	**6**	**Ag₂O (2 equiv.)**	6.6	33	-
6[d]	AgF	DCM	400	Ar	**22**	**Ag₂O (2 equiv.)**	2.8	14	-
7[d]	AgF	DCM	400	Ar	**22**	**Ag₂O (10 mol %)**	18.8	94*	82
8	AgF	DCM	400	Ar	None	**Ag₂O (10 mol %)**	-	N.D.	-
9[d]	AgF	DCM	400	**Air**	**22**	-	7.2	36	-
10	AgF	DCM	**200**	Ar	**22**	-	13.6	68	-
11	AgF	DCM	**600**	Ar	**22**	-	18.8	94	86
12[d]	AgF	DCM	**1000**	Ar	**22**	-	12.2	61	-
13	AgF	**MeCN**	600	Ar	**22**	-	11.6	58	-
14	AgF	**THF**	600	Ar	**22**	-	-	Trace	-
15	AgF	**Tol**	600	Ar	**22**	-	-	Trace	-
16	AgF	**CDCl3**	600	Ar	**22**	-	18.4	92	81
17	AgF	DCM	600	Ar	**22 (recovered)**	-	18.6	93	85
18	AgF	DCM	600	Ar	**22**	**TEMPO (10 mol %)**	18	90	-
19[d]	AgF	DCM	600	Ar	-	**UV 300W lamp**	-	6	-
20	-	DCM	600	Ar	**22**	-	-	trace	-

Conditions taken from catalyst screen. [c] 3.0 equivalents of fluoride source used. [D] Decomposition of catalyst identified. [*] Decomposition of the catalyst occurred on occasion.

Following the optimisation of reaction conditions, the fluorination of toluoyl chloride was monitored over time. This could be achieved by following the reaction *via* FTIR using a ReactIR. ReactIR allows for changes in concentration to be monitored in real-time, with *in-situ* FTIR measurements collected every minute. An ATR probe is inserted into the reaction vessel under a dynamic flow of argon. The "solvent subtraction" feature of the iCIR software (Mettler Toledo ReactIR control and analysis software) enables the IR characteristics of the solvent, catalyst and fluoride source to be extracted and minimised, enabling the relative absorbance effects of the substrate to be analysed. The characteristic carbonyl stretches of the acyl chloride and acyl fluoride functional groups were used to determine the conversion and formation of the respective species, monitoring the consumption of acyl chloride, and the reduction of its associated absorption band over time as the acyl fluoride product was formed. This enabled the collection of concentration:time profiles to be gathered allowing for further modification and optimisation of the reaction conditions.

It can clearly be seen from the surface plot collected for the catalytic fluorination of toluoyl chloride (Figure 3-3), that the toluoyl chloride substrate (1773 cm^{-1}) is consumed, while the toluoyl fluoride product (1805 cm^{-1}) is formed. Reaction monitoring proceeds until all of the acyl chloride substrate is consumed and the formation of the acyl fluoride product plateaus. The rate of formation of the acyl fluoride product was found to equal that rate of consumption of the acyl chloride substrate. This is as expected within this system with a 1:1 stoichiometry between reactants and products, where nucleophilic attack of the acyl chloride substrate results in the direct formation of the acyl fluoride product, indicating a clean reaction without the formation of long-lasting intermediates. Monitoring by ReactIR enabled more precise determination of reaction time, reducing the 24 hour reaction time used for reaction development above to 3 hours. This direct observation of the time taken to reach reaction completion allowed for direct comparisons of the effects of aryl substitution on the rate of fluorination, which will be discussed in *Section 3.5*.
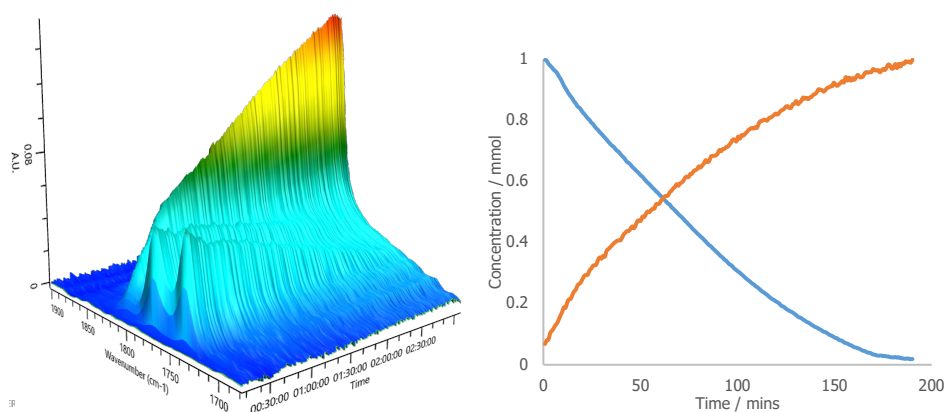
Figure 3-3: 3D surface profile and concentration:time plot for the catalytic fluorination of toluoyl chloride, showing the consumption of toluoyl chloride (1773 cm⁻¹) and the formation of toluoyl fluoride (1805 cm⁻¹) over time.

The use of the standard addition method,[261] facilitated quantification of the starting materials and products allowing rapid and accurate (± 1% deviation from calibration curve obtained for addition of benzoyl chloride) concentration analysis for the reactions. This method enables data quantification, as two aliquots of the substrate are added to the reaction mixture, with a gap of one complete scan. This allows for the relative absorbance associated with the IR active bands of the substrate to be proportional to the concentration of the substrate, in this case 1 mmol of toluoyl chloride. For example, when the relative absorbance of the carbonyl band of toluoyl chloride at 1773 cm⁻¹ decreases to the point of 50 % relative abundance, this is proportional to 0.5 mmol of substrate remaining. This allows for relative absorbance to be normalised to mmol of substrate. Additionally, the addition of two aliquots of a known concentration of the product to the reaction mixture at the end of the reaction enables for the quantification of the product, as the concentration of the product in solution following the reaction can be compared against this known concentration.

Offline quantitative ^{19}F NMR analysis of the reaction confirmed the *in-situ* measurements showing quantitative conversion of the toluoyl chloride starting material, a >99 % calculated contained ^{19}F NMR yield of toluoyl fluoride, with an isolated yield of 92 %.

3.5 Catalytic fluorination of organic electrophiles

Following the development of the reaction conditions a substrate scope was conducted, monitoring the reaction in real time using ReactIR. The effect of substituents on the rate of fluorination was investigated by observing the rate of fluorination of different substrates by varying the aryl substituents of the acyl chloride. Initially, a range of electron withdrawing and donating acyl chlorides were selected for investigation, in order to probe substituent effects on the rate of fluorination, as it was envisioned that electron withdrawing substituents would undergo fluorination at a greater rate than their electron donating counterparts, if catalytic fluorination proceeds *via* a nucleophilic substitution pathway.

It was observed through substrate screening that the aryl substituent played a significant role in the outcome of fluorination (Scheme 3-8). The fluorination of benzoyl chloride, monitored *via* ReactIR, resulted in the complete formation of the fluorinated product over the course of $3^1/_2$ hours, with an isolated yield of 87 %, very similar to that observed for the fluorination of toluoyl fluoride above. Acyl chlorides bearing electron withdrawing substituents exhibited faster reaction times, with the quantitative formation of 4-Nitrobenzoyl fluoride occurring after 110 minutes, and an isolated yield of 94 %. Off-line ^{19}F NMR analysis of the reaction with 4-Nitrobenzoyl chloride, 4-(Trifluoromethyl)benzoyl chloride and (2,3,4,5,6-Pentafluoro)benzoyl chloride also resulted in near quantitative conversion to the associated acyl fluorides.

When less electron-withdrawing substituents were placed in the *para*-position, the length of time to achieve quantitative fluorination increased, up to 620 minutes in the case of 4-Methoxybenzoyl chloride. Consequently, it was determined that aryl chlorides that contained electron withdrawing substituents on the aryl ring underwent more rapid fluorination. Electron withdrawal from the carbonyl region will render the acyl chloride more δ^+, and thus more electrophilic, resulting in a greater propensity to undergo nucleophilic substitution with nucleophilic fluorine generated at the active catalyst, which is in line with the hypothesis proposed earlier. Similarly, fast reaction times were observed for substrates containing electron withdrawing substituents in the *ortho*-position, with 2,6-difluorobenzoyl chloride reacting to give 2,6-difluorobenzoyl fluoride in 70 minutes, which was the faster rate to achieve quantitative fluorination of the substrates tested.

The effect of changing the steric bulk of the substituents in the *para*-position was showed to have little impact on the rate of fluorination, with 4-Ethylbenzoyl chloride, 4-*iso*propylbenzoyl chloride and 4-*tert*butylbenzoyl chloride all achieving quantitative conversion to their analogous acyl fluorides between 215 and 290 minutes.
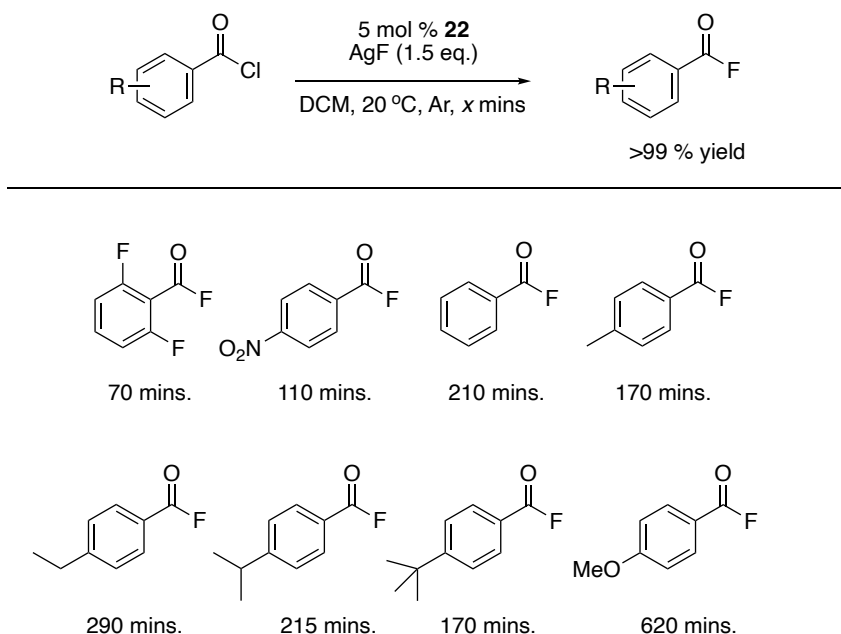
*Scheme 3-8: Fluorination of a range of aryl substituted acyl chlorides catalysed by **22**. Substrates containing electron withdrawing aryl groups undergo fluorination faster that substrates bearing electron donating aryl groups. Reaction time for each substrate are determined by the time taken for the formation of acyl fluoride to plateau at >99 % relative absorption.*

Due to the interest of fluorination in the fine chemical and pharmaceutical industries, the fluorination of the pharmaceutical analogue, Probenecid, was performed (Scheme 3-9). Probenecid is an anti-inflammatory drug often used for the treatment of gout and arthritis. Under the reaction conditions the acyl chloride analogue of the active pharmaceutical ingredient underwent fluorination over the course of 90 minutes, representing one of the fastest rates of fluorination of the substrates tested with an initial rate of 0.98 mmolh^{-1} and a TOF of 13.3 h^{-1}. The fluorination of these biologically active targets are of interest as acyl fluoride substituents can undergo further reactions and derivatisation as described in *Section 3.1.2* leading to functionalised biologically active pharmaceutical of interest in drug discovery.[262-264]

5 mol % **22**
AgF (1.5 eq.)

DCM, 20 °C, Ar, 1.5 h

>99 % yield
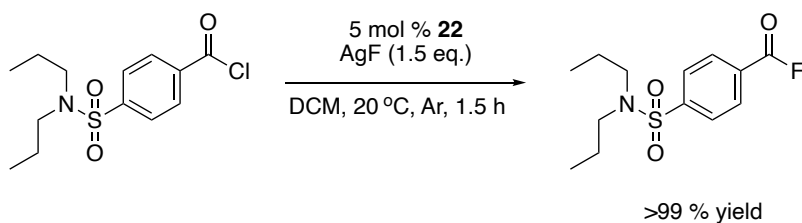
Scheme 3-9: Catalytic fluorination of the acyl chloride analogue of the active pharmaceutical ingredient, probenecid. Quantitative conversion occurred over the course of 90 minutes, representing on of the fastest reaction times for nucleophilic fluorination.

4-Methoxybenzoyl chloride

4-Nitrobenzoyl chloride

4-*tertbutyl*benzoyl chloride

Probenecid chloride

Benzoyl chloride

2,6-Difluorobenzoyl chloride
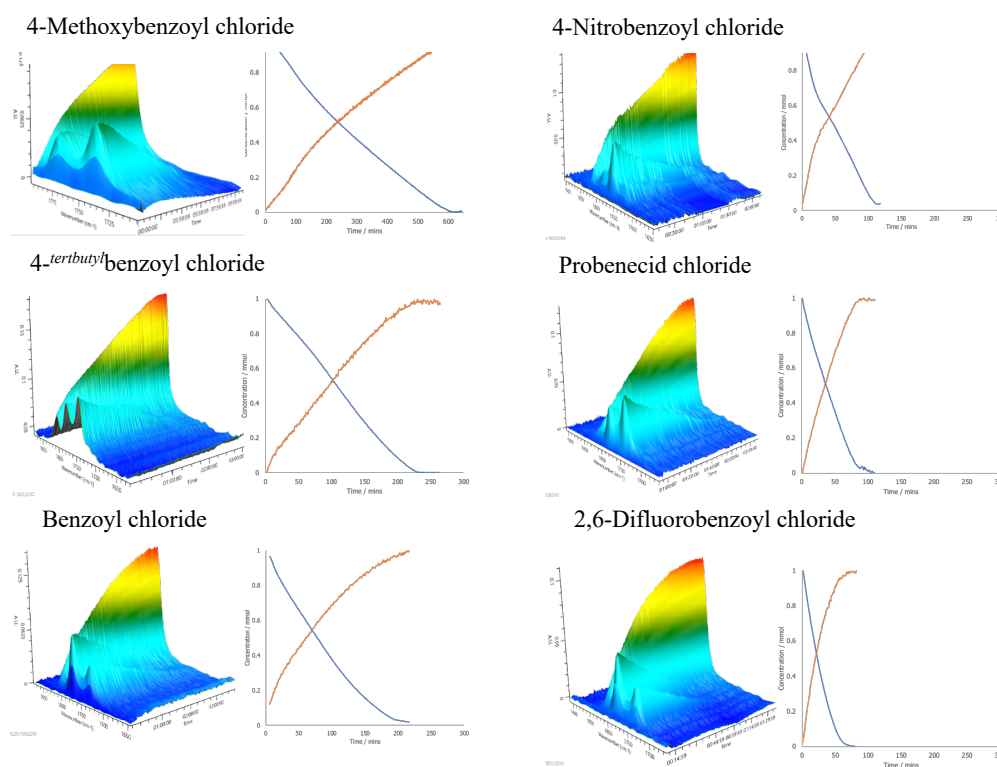
Figure 3-4: 3D surface plots and concentration:time profiles for the fluorination of acyl chlorides. All substrates react until quantitative conversion is achieved. Note the change of timescale between 4-Methoxybenzoyl chloride (620 minutes) against the other plots (300 minutes).

The results for the fluorination of acyl chlorides are consistent with a nucleophilic fluorination in which the attack of nucleophilic fluorine on the electrophile is the rate determining step. Initial rates of reaction for the fluorination of the acyl chloride substrate have been calculated from the ReactIR concentration:time profiles (Table 3-4). The effect of the electron density of the electrophile on the reaction rate has been visualised by plotting the carbonyl stretching frequency of the acyl chloride reagent against the initial rate of reaction (Figure 3-5). The plot shows that acyl chlorides bearing electron withdrawing groups and thus have a higher carbonyl

stretching frequency and are found to have a faster initial rate of reaction. These more δ^+ electrophilic carbon centres are more susceptible to attack from the activated nucleophilic fluoride, resulting in an increased initial rate of reaction, compared to substrates containing electron donating groups, which possess reduced electrophilic character. The plot gives an approximate linear relationship.

Table 3-4. Initial rate calculations for the catalytic fluorination of acyl chloride substrates as an order of decreasing carbonyl stretching frequency.

Substrate	C(O)Cl wavenumber /cm^{-1}	Initial Rate / mmolh^{-1}
2,6-Difluorobenzoyl chloride	1789	1.402
4-Nitrobenzoyl chloride	1788	0.974
Probenecid chloride	1782	0.942
4-*tert*butylbenzoyl chloride	1778	0.511
Benzoyl chloride	1775	0.483
4-Ethybenzoyl chloride	1774	0.305
Toluoyl chloride	1773	0.513
4-*iso*propylbenzoyl chloride	1771	0.348
4-Methoxybenzoyl chloride	1765	0.038
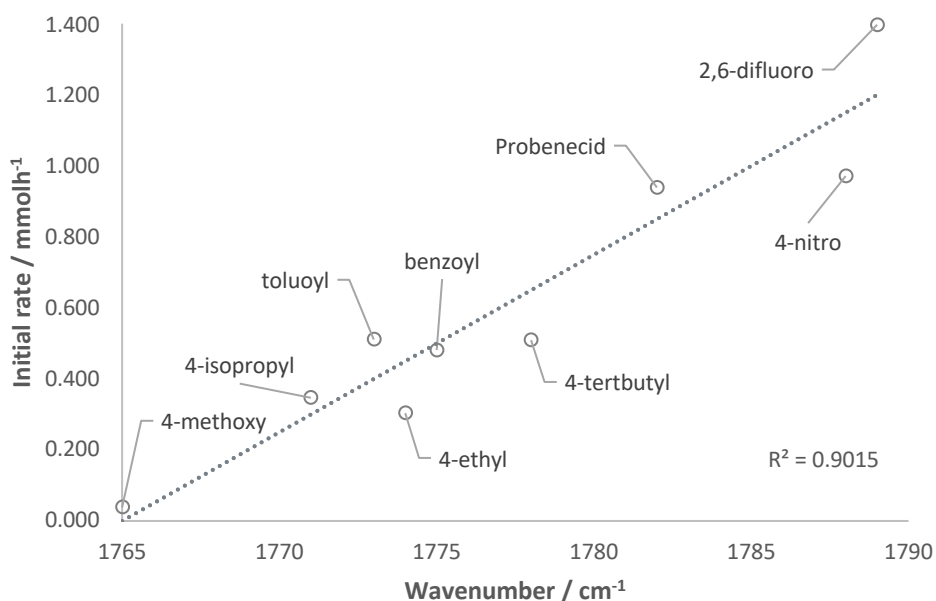
Figure 3-5: IR carbonyl stretching frequency of the acyl chloride substrates (cm^{-1}) measured against the initial rate of reaction (mmolh^{-1}) calculated for fluorination of the acyl chloride substrate. The approximate linear relationship between the electron density of the electrophilic carbon of the substrate and the rate of fluorination indicates a reaction where the acyl chloride substrate is involved in the rate determining step of the reaction.

Attempts to carry out the fluorination of other functional groups were conducted including: benzyl halides; anhydrides; aldehydes; ketones; and aryl halides, with limited success. Treatment of benzyl bromide, benzyl chloride and 2,3,4,5,6-pentafluorobenzyl bromide under the standard conditions optimised for the fluorination of toluoyl fluoride resulted in the formation of trace quantities of the analogous benzyl fluorides detected *via* ^{19}F NMR analysis. These substrates are not believed to be sufficiently electrophilic. No reaction was observed following use of bromobenzene, chlorobenzene, phenyltriflate and pentafluoro chlorobenzene as substrates, where the fluorinated products were not detected following NMR analysis. The failure of fluorination for the aldehydes and ketones is most likely due to the unfavourable formations of the analogous counter anions to give the salt by-product as a thermodynamic sink upon fluorination. Fluorination of anhydrides lead to the quantitative formation of the acyl fluoride product over extended timeframes, with the quantitative fluorination of benzoic anhydride to benzoyl fluoride occurring over 34 hours, compared to 3.5 hours for benzoyl chloride (Figure 3-6).
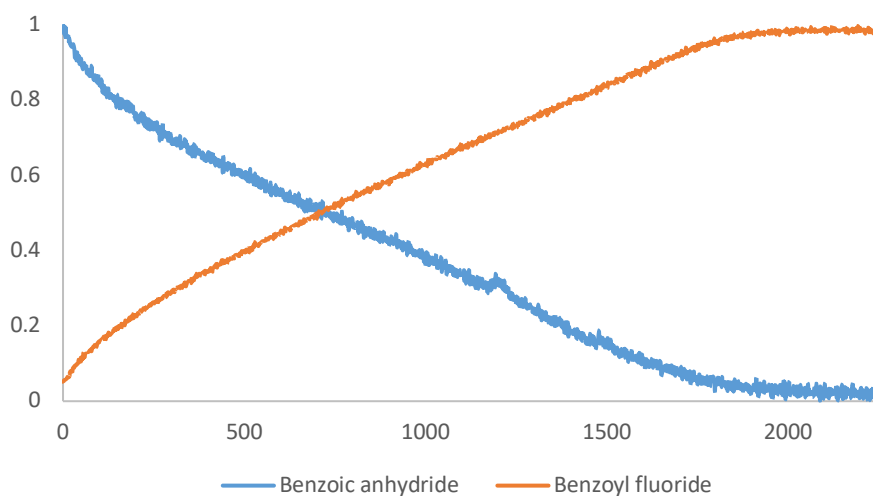
Figure 3-6: Concentration:time profile for the catalytic fluorination of benzoic anhydride. This reaction occurs over a much longer time period than the analogous acyl chloride.

3.6 Visual Time Normalised Analysis

In-situ IR monitoring of the catalytic fluorination of acyl chlorides enables time course concentration profiles of the reaction to be gathered. This data, in conjunction with Variable Time Normalised Analysis (VTNA),[265] provides a tool to qualitatively assess reaction features of interest, including product inhibition and catalyst deactivation. Visual kinetic analysis enables a rapid and straightforward approach to extracting pertinent kinetic information of progress reaction profiles, enabling the comparison of two or more reaction profiles visually. In addition, information can be gleaned on reaction order with respect to the catalyst and other components in the system. This can be achieved by visual analysis of time normalised reaction profiles, where the concentration plots are overlaid.

Over the time course of the catalytic fluorination of benzoyl chloride no catalyst deactivation or product inhibition was apparent (Figure 3-7). This shows a time normalised concentration profile, where the concentration of the benzoyl chloride reagent has been reduced. The lower concentration of starting material has undergone time normalisation and been shifted to overlay at [benzoyl chloride]$_{1/2}$. As can be seen in Figure 3-7, the time normalised concentration profiles for both 1 mmol (blue) and 0.5 mmol (green) starting concentration of benzoyl chloride overlay closely. This indicated that over the time course of the reaction at the sampled concentrations no product inhibition or catalyst deactivation is occurring.
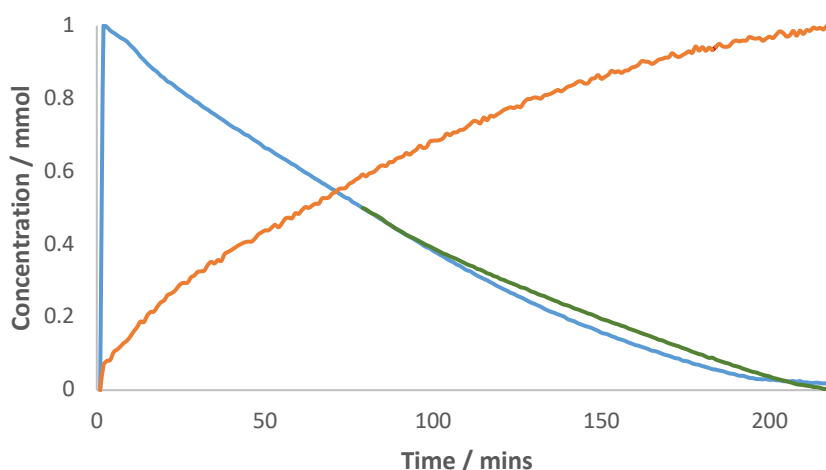
Figure 3-7: Time adjusted concentration:time plot for the catalytic fluorination of [benzoyl chloride]$_{1\ mmol}$ (blue) forming benzoyl fluoride (orange) including concentration:time normalised overlay for [benzoyl chloride]$_{0.5\ mmol}$ (green). Little difference is observed between the time adjusted concentration profiles, indicating no catalyst deactivation or product inhibition occurs over the timescale of this reaction.

Probing the impact of catalyst activation revealed significant effects on the initial rate of the system due to catalyst pre-activation (Figure 3-8). Under normal conditions, the catalyst and silver fluoride are stirred for 10 minutes prior to addition of the acyl chloride reagent. This was conducted to generate the active catalytic TMF species from the pre-catalyst, **22**. The effect of catalyst activation was probed by following the start of the fluorination of benzoyl chloride, upon immediate addition of the substrate and addition of the substrate following standard conditions. It can be observed in Figure 3-8 that the initial rate of reaction between these two systems do not overlay, with an increased rate observed when catalyst pre-activation occurred (Figure 3-8; orange) compared to under non-standard conditions, where catalyst pre-activation was not allowed to occur prior to addition of the acyl chloride substrate (Figure 3-8; blue). After this period of increased initial rate at the beginning of the reaction post catalyst activation the rate of fluorination runs parallel to the non-preactivated reaction.
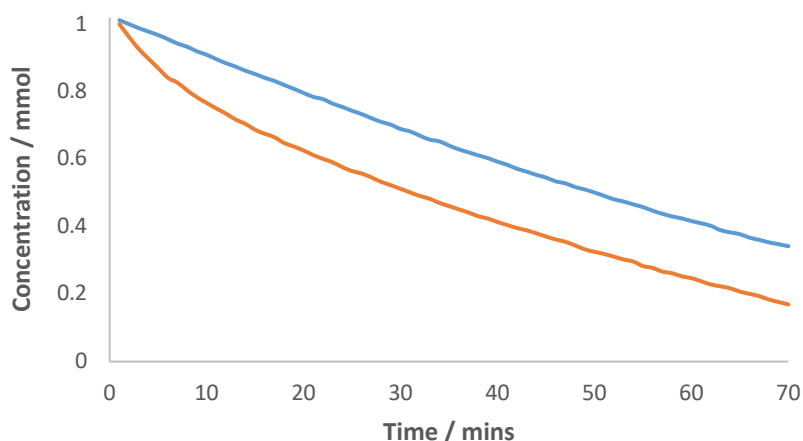
Figure 3-8: The effect of catalyst pre-activation on the initial rate of consumption of benzoyl chloride, 10 minutes of catalyst pre-activation (orange) and no catalyst pre-activation (blue). Pre-activation leads to a greater initial rate of fluorination, indicating that catalyst activation is required to achieve optimum fluorination.

Where excess silver fluoride was used, it was also possible to observe the effect of catalyst activation in real time (Figure 3-9). Following initial consumption of benzoyl chloride, when a second aliquot of substrate was added to the reaction vessel, fluorination was restarted with a faster initial rate than that observed for the first aliquot before following the same concentration profile. This indicates that a steady state concentration of the active catalytic species was present in solution (Figure 3-9). This steady state concentration was allowed to build up following consumption of the first aliquot of benzoyl chloride, resulting in an increased initial

rate of fluorination upon addition of the second aliquot, analogous to the standard initial catalyst pre-activation conditions.
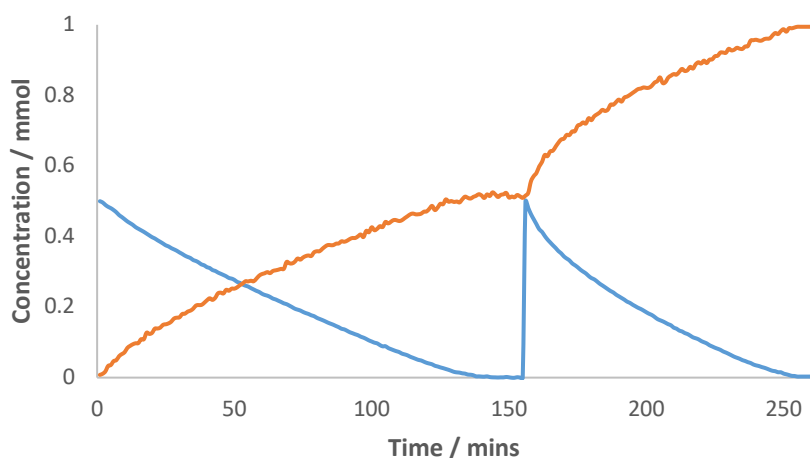
Figure 3-9: Two separate additions of benzoyl chloride (0.5 mmol, blue) illustrate the effect of catalyst activation and presence of a steady state concentration of the active catalytic species in solution and the rate of formation of benzoyl fluoride (orange).

VTNA analysis also enables elucidation of the initial rate order with respect to the different components within the system. This can be achieved through plotting the concentration:time normalised data for the consumption of benzoyl chloride and formation of benzoyl fluoride at different starting concentrations of benzoyl chloride against one another (Table 3-5). By arbitrarily changing the rate order term from 0 – n+1, where n is the rate order, the order of reaction with respect to the benzoyl chloride substrate can be determined. This can be determined through the visual analysis of data plotted for the different concentrations (Figure 3-10). In this case the rate order for the catalytic fluorination of benzoyl chloride, with respect to the benzoyl chloride substrate was calculated to be 1. The same data processing can be carried out to determine the rate order with respect to the catalyst, by changing the concentration of catalyst in solution (Table 3-6). While the concentration:time normalised data at catalyst concentrations of 5 mol % and 10 mol % were not observed to overlap precisely, most likely due to added complexity within the system, the closest overlap of the concentration:time normalised data was observed at a catalyst rate order of 1 (Figure 3-11). The reaction was first order with respect to both [**22**] and [benzoyl chloride]. The initial rate constant for the reaction was calculated, from the measurements gathered from VTNA analysis, as k_{obs} = 15.6 mmol^{-2}h^{-1}. These observations give us insight into the rate determining step of the catalytic fluorination of acyl chlorides and gives us information required to propose a plausible reaction mechanism.

106

Table 3-5. Rate order calculation for the catalytic fluorination of benzoyl chloride with respect to substrate.

	1.0 mmol Benzoyl Chloride			0.5 mmol Benzoyl Chloride		
t (min)	tA	[A] M	t (min)	tA	[A] M	[P] M
0	0.00	1.00	0	0.00	1.00	0.02
12	11.44	0.91	9	8.54	0.90	0.14
25	24.44	0.81	18	23.88	0.81	0.25
41	40.44	0.71	30	41.97	0.70	0.36
59	58.44	0.60	42	57.64	0.60	0.45
76	75.44	0.51	55	72.10	0.51	0.55
86	85.44	0.45	63	79.74	0.45	0.60
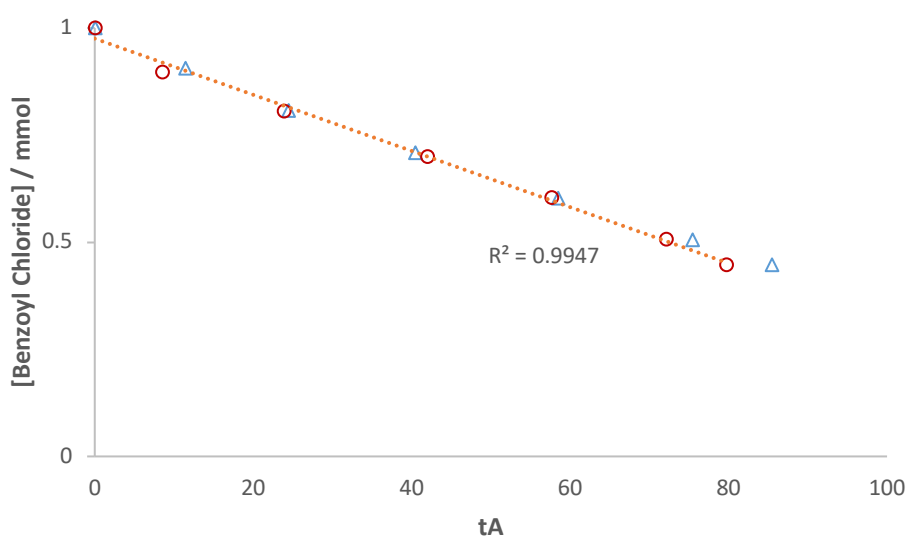
Figure 3-10: Rate order calculation with respect to substrate, taken from concentration-time normalized data in Table 3-5. Overlay was observed upon defining rate order with respect to substrate as 1.

Table 3-6. Rate order calculation for the catalytic fluorination of benzoyl chloride with respect to catalyst.

	5 mol % catalyst			10 mol % catalyst		
t (min)	tA	[A] M	t (min)	tA	[A] M	[cat] M
0	0.00	1.00	0	0.00	1.00	0.10
12	6.00	0.91	9	0.90	0.90	0.10
25	12.50	0.81	18	9.90	0.81	0.10
41	20.50	0.71	30	19.20	0.70	0.10
59	29.50	0.60	42	31.20	0.60	0.10
76	38.00	0.51	55	43.30	0.51	0.10
86	43.00	0.45				
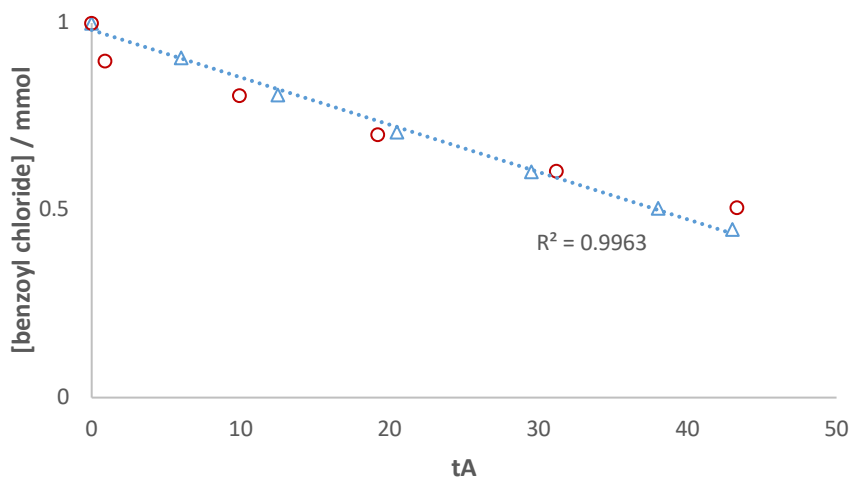
Figure 3-11: Rate order calculation with respect to catalyst, taken from concentration-time normalized data in Table 3-6. Closest overlay was observed upon defining rate order with respect to catalyst as 1.

Based on these observations above a plausible mechanism for the catalytic cycle has been proposed (Scheme 3-10). In the main catalytic cycle the active catalytic species is formed through treatment of **22** with an equivalent of silver fluoride, resulting in the formation of a metal-fluorine bond. This activated catalytic species, "[(η^5,κ_2C-C$_5$Me$_4$CH$_2$C$_6$F$_5$CH$_2$NC$_3$H$_2$NMe)-RhF]," **'28'**, the fluorine is of sufficient nucleophilicity to attack the electrophilic acyl chloride reagent and resulting in the formation of the fluorination product. **'28'** is subsequently converted back to **22** ready to interact with another equivalents of again.
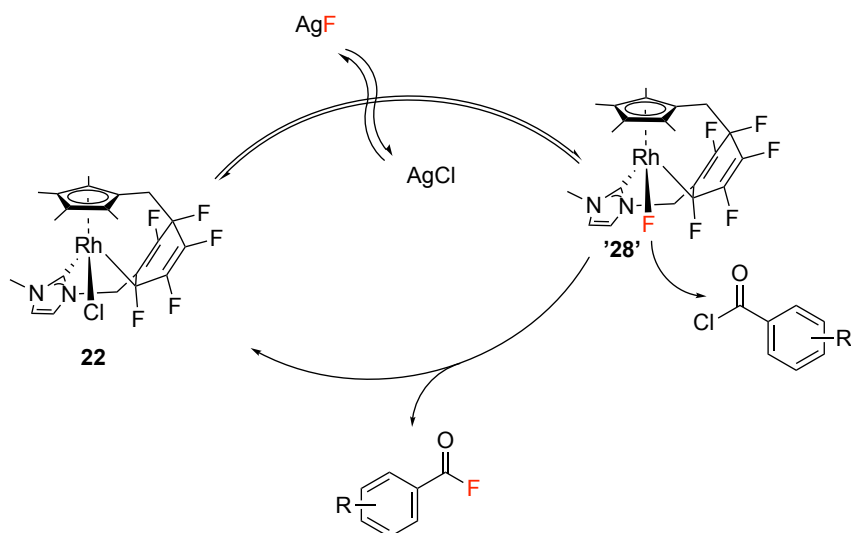
Scheme 3-10: Plausible mechanism for the rhodium catalysed nucleophilic fluorination of acyl chlorides, proceeding via a rhodium TMF intermediate, '28'. The pre-catalytic species 22, reacts with an equivalent of silver fluoride, to give the active catalytic species, '28', which contains a TMF bond. As catalyst pre-activation was observed, it takes time for a steady state concentration of '28' to develop, indicating an equilibrium between 22 and '28' within solution. The active TMF complex then reacts with the organic electrophile, resulting in the formation of the fluorinated product and reforming the pre-catalytic species, 22.

The experimental data shows pre-activation of **22** is required, as an initial slow rate of reaction is present as catalyst activation occurs. Following pre-activation a steady state concentration of the active catalytic species is present in solution, as evidenced by the constant reaction rate. This may be rationalised as the initial activation to form a steady state concentration of active fluoride '**28**' is believed to require an induction period. While the ideal speciation of silver fluoride within the reaction mixture has not been determined, a period of silver halide equilibration in solution may account for the induction time observed. The successful formation of '**28**' is dependent on the speciation of silver and halide as the reactions initiated in solution by the addition of silver fluoride can lead to a high steady state concentration of '**28**' under ideal conditions. However, as the reaction progresses higher concentration of silver chloride are present which may lead to unwanted off-cycle formation of dihalide complexes analogous to **6**, resulting in loss of active catalyst under the wrong conditions, such as excessive stirring or high AgX concentration.

Substituent effects clearly show an enhanced rate when electron withdrawing substituents are present on the aryl ring, indicative of nucleophilic attack of the acyl chloride electrophile being the rate determining step for most of the reaction. The reaction was found to be first order with respect to both **22** and the substrate during the first third of the reaction at which the rate order was calculated (Table 3.5 and 3.6). The order with respect to the substrate is straightforward, but the order with respect to **22** is more difficult to explain. It is propose that, at steady state, the introduction of an increased **22** concentration results in a rapid proportional increase in the concentration of '**28**'. This suggests that the formation of '**28**' is in equilibrium with **22**.

An alternative mechanism could be proposed involving the generation of the nucleophilic fluoride originating from the ligand, as observed in the fluorine transfer reaction, which will be discussed in *Section 4.3*.[206] In this rate determining step acyl chloride interacts with **22** to yield acyl fluoride and a partially defluorinated complex which is then regenerated to **22** or the fluorinated analogue upon interaction with silver fluoride. However, early outputs from computational calculation, conducted by Prof. Stuart Macgregor at Heriott-Watt University, suggests that the transition state energy associated with the nucleophilic substitution of acyl chlorides from '**28**' has a markedly lower energy barrier compared to fluorine activation from the perfluorinated ligand within this system. Further analysis and complementary calculations are ongoing, however, at present time computational theory supports

our current hypothesis of a mechanism proceeding through an active TMF produced *in-situ*.

3.7   Summary

An efficient protocol for the fluorination of a range of acyl chlorides has been developed, giving the acyl fluoride product in up to quantitative yield in as little as one hour under mild conditions. Success in the formation of TMFs and the demonstration of stoichiometric fluorination of acyl chlorides from these TMFs offered initial insights into the activity and reactivity of these species towards potential catalysis. The developed catalytic protocol displays advantages over previously developed routes, as it requires commercially available materials, coupled with a catalyst which can be readily prepared in a simple one-pot system, using a small excess of fluoride source, using standard laboratory equipment. In addition, unlike other transition metal catalysed acyl chloride fluorination reactions described in the literature, purification and recovery of the catalyst can be completed *via* a simple solvent/anti-solvent elution and recrystallisation, which also enables the isolation of the fluorinated product in high yields. This offers a powerful methodology towards the development of a more sustainable synthesis of acyl fluorides. In addition, the reaction has been found to tolerate a range of substituents, including the fluorination of an active pharmaceutical ingredient of interest. *In-situ* infrared measurements enabled real-time monitoring of the fluorination reaction, allowing for the generation of progress reaction profiles. This enables further insight into the reaction to be gained, *via* VTNA analysis, suggesting nucleophilic attack of the acyl chloride electrophile by fluoride is the rate determining step, with a first order reaction with respect to the acyl chloride substrate and the catalyst.

3.8 Experimental

3.8.1 Instrumentation

NMR spectral analysis was carried out using a Bruker Ascend 400 spectrometer (400 MHz) and Bruker Ascend 500 spectrometer (500 MHz) at room temperature ($\approx$ 300 K). ^{1}H and ^{13}C NMR spectra were referenced to the corresponding residual solvent signals (CDCl$_3$: 7.26 ppm for ^{1}H, 77.16 ppm for ^{13}C;). The ^{19}F NMR spectra were referenced by an internal method of the NMR. The chemical shifts are reported in ppm and coupling constants are given in Hz. A 60s delay was used for quantitative ^{19}F NMR integration. NMR data was processed using MestReNova software. Multiplicity assignments in NMR spectra are labelled as follows: "s" = singlet, "d"= doublet, "t"= triplet, "q" = quartet, "p" = pentet, "m" = multiplet. NMR assignments for all synthesised complexes are given; ^{1}H NMR (green), ^{19}F NMR (red) and ^{13}C NMR (blue). Electrospray mass spectra were recorded on a Bruker micrOTOF II with Agilent technologies 1200 Infinity Series mass spectrometer. *In-situ* ReactIR measurements conducted using Mettler Toledo ReactIR 15, collecting a spectral average of 256 scans at a scan rate of 256 scans per minute. Experiment set up and analysed using Mettler Toledo iC IR software, using a Mettler Toledo Easy Max basic synthetic workstation. Glassware was oven-dried, evacuated and backfilled with argon before use.

3.8.2 Materials

Catalysts used within the procedure have been synthesized as described in Section 2.4. [IrCl(CO)(PPh$_3$)$_2$] and [RhCl(CO)(PPh$_3$)$_2$] were synthesized following literature procedure.[266] [IrCp*Cl$_2$]$_2$ and [IrCp*I$_2$]$_2$, 1-Methylimidazole, silver oxide, toluoyl chloride, benzoyl chloride, 2,6-Difluorobenzoyl chloride, 4-Methoxybenzoyl chloride, 4-*tert*butylbenzoyl chloride and probenecid were purchased from Sigma Aldrich (Merck). [RhCp*Cl$_2$]$_2$, 4-Nitrobenzoyl chloride, 4-Ethylbenzoyl chloride, 4-*iso*propylbenzoyl chloride, 4-*tert*butylbenzoyl chloride, 4-(Trifluoromethyl)benzoyl chloride, 2,3,4,5,6-Pentafluorobenzoyl chloride, benzyl bromide and 2-Chloroacetaphenone were purchased from Alfa Aesar. Acetic anhydride was purchased from VWR. 2,3,4,5,6-Pentafluorobenzyl bromide and 3,4,5,6-Tetrafluorobenzyl bromide were purchased from Fluorochem. 3-Chloropenta-2,4-Dione was purchased from Acros Organics. All solvents were obtained from a

solvent purification system, with the exception of dichloromethane, which was supplied anhydrous in a sure seal bottle, and used as required without further purification.

3.8.3   Synthesis of transition metal fluoride complexes

3.8.3.1 Synthesis of [IrF(CO)(PPh$_3$)$_2$]

IrCl$_3$.3H$_2$O (0.35 g, 1.0 mmol) was added to a Schlenk flask alongside triphenylphosphine (1.31 g, 5.0 mmol) and DMF (20 mL) heated to reflux for 16 hours, during which time the colour changed from deep green to light red to pale yellow. The reaction mixture was then filtered under vacuum while hot and washed with warm methanol (3 x 15 mL). The filtrate was then placed in an ice bath resulting in the precipitation of a yellow crystalline solid, which was collected via filtration and washed with cold methanol (2 x 5 mL). A second crop of crystals were collected by cooling the filtrate at *ca*. -20 °C for 72 hours. The resulting product (0.5 g, 0.64 mmol) was dissolved in methanol (20 mL) and stirred with tetramethylammonium fluoride (0.59 g, 6.4 mmol) and silver carbonate (0.09 g, 0.32 mmol) for 30 minutes, before the solvent was removed under vacuum and the resulting yellow powder was extracted with toluene (30 mL), filtered through a plug of celite, washed with toluene (2 x 10 mL) and the filtrate was concentrated under reduced pressure. The crude product was recrystallized from the concentrated solution of dichloromethane and heptane at -20 °C. The pure product was collected *via* filtration, washed with hexanes (2 x 5 mL), and dried *in vacuo*. X-ray quality single crystals were grown through vapour diffusion of hexane into DCM. The crystalline product was stored under argon, as it was found to change colour to yellow/green upon exposure to air for 24 hours. Drying the yellow/green crystalline powder under vacuum for 2 hours afforded the return of the desired yellow crystalline product.

IrF(CO)(PPh$_3$)$_2$; Yellow crystalline powder. Yield: 0.42 g, 0.55 mmol (84 %). **^{1}H NMR** (400 MHz, d_6-benzene): δ 7.72 (broad s, C$_6$-*H,* 6H), 7.40 (m, C$_6$-*H*, 9H). **^{19}F NMR** (376 MHz, d_6-benzene): -257.62 (s, Ir*F*, 1F). **IR** (Ir–CO): 1942 cm^{-1}.[267]

3.8.3.2 Synthesis of [RhF(CO)(PPh$_3$)$_2$]

RhCl$_3$ (0.30 g, 1.15 mmol) was added to a Schlenk flask alongside DMF (10 mL) and ultrapure water (130 μL) and heated to reflux for 15 minutes, during which time the colour changed from deep red to pale yellow. Triphenylphosphine (0.58 g, 2.2 mmol) was then added under a dynamic flow of argon. Vigorous effervescence was observed following addition, and the reaction was stirred for a further 2 hours, during which time a yellow precipitate had formed. The reaction mixture was filtered under vacuum and the resulting yellow solid was dried under vacuum. The resulting product (0.70 g, 1.0 mmol) was dissolved in DCM (20 mL) and stirred with anhydrous ammonium fluoride (0.93 g, 10.0 mmol) for 30 minutes, before the solvent was removed under vacuum and the resulting yellow powder was extracted with toluene, filtered through a plug of celite, washed with toluene (2 x 10 mL) and the filtrate was concentrated under reduced pressure. The crude product was recrystallized from the concentrated solution of dichloromethane and heptane at -20 °C. The pure product was collected *via* filtration, washed with hexanes, and dried *in vacuo*. X-ray quality single crystals were grown through vapour diffusion of hexane into DCM.

RhF(CO)(PPh$_3$)$_2$; Yellow crystalline powder. Yield: 0.53 g, 0.78 mmol (79 %). **^{1}H NMR** (400 MHz, d_6-benzene): δ 7.95 (broad s, C$_6$-*H,* 6H), 7.03 (m, C$_6$-*H*, 9H). **^{19}F NMR** (376 MHz, d_6-benzene): -270.61 (dd, J$_{RhF}$ = 51.4 Hz, ^{2}J$_{PF}$ = 27.1 Hz, 1F). **^{31}P NMR** (162 MHz, d_6-benzene): δ 29.47 (d, *P*Ph$_3$, J$_{RhP}$ = 127.8 Hz). **^{13}C NMR** (101 MHz, d_6-benzene): 187.6 (s, *C*O), 134.9 (t, ^{2}*J* = 6.4 Hz, P-*Ar*), 133.5 (t, ^{1}*J* = 21.6 Hz,

P-*Ar*), 129.8 (s, *Ar*). **MS** (ESI): Theoretical [M]$^{+}$ [C$_{37}$H$_{30}$OP$_2$Rh]$^{+}$ 655.0827 ; found

for [C$_{37}$H$_{30}$OP$_2$Rh]$^{+}$ 655.0829. **IR** (Rh–CO): 1932 cm^{-1}.

Characterisation is consistent with previously reported literature.[114]

3.8.3.3 Stoichiometric fluorination of benzoyl chloride with [RhF(CO)(PPh₃)₂]

[RhF(CO)(PPh$_3$)$_2$] (67.5 mg, 0.1 mmol) was dissolved in CDCl$_3$ (0.5 mL) and added to a J. Young's NMR tube alongside benzoyl chloride (14 mg, 0.1 mmol) under argon. The contents of the NMR tube were shaken and transferred to an NMR spectrometer for analysis. ^{19}F NMR analysis showing the formation of RhCl(CO)(PPh$_3$)$_2$ and benzoyl fluoride after 20 minutes. ^{19}F NMR yield of benzoyl chloride *vs.* the internal standard 4-Trifluorotoluene (2 µL) > 99 %. Work up *via* elution with diethyl ether and hexane enabled the recovery of the rhodium complex and benzoyl fluoride was isolated in 83 % yield as a colorless oil.

RhCl(CO)(PPh$_3$)$_3$: Pale yellow solid. **^{1}H NMR** (400 MHz, *d$_6$*-benzene): δ 7.95 (broad s, C$_6$-*H,* 6H), 7.04 (m, C$_6$-*H*, 9H). **^{31}P NMR** (162 MHz, *d$_6$*-benzene): δ 25.52 (d, *P*Ph$_3$, J$_{RhP}$ = 126.8 Hz). **IR**: 1961 cm^{-1}.

Benzoyl fluoride: Colourless oil. Isolated yield: (83 %). **^{1}H NMR** (400 MHz, *d-chloroform*): δ 8.03 (m, C$_6$-*H,* 2H), 7.70 (tt, $^2J_{HH}$ = 7.6, 1.2 Hz, C$_6$-*H*, 1H), 7.52 (m, C$_6$-*H*, 2H). **^{19}F NMR** (376 MHz, *d-chloroform*): δ 18.05 (s, CO*F*, 1F). **^{13}C NMR** (101 MHz, *d-chloroform*): δ 157.4 (d, $^1J_{CF}$ = 344.2 Hz, *C*OF), 135.4 (s, *Ar*), 131.4 (d, ^3J = 4.0 Hz, *Ar*CO), 129.1 (s, *Ar*), 124.9 (d, $^2J_{CF}$ = 60.9 Hz, *Ar*CO). **MS** (ESI): Theoretical [2M+K] [C$_7$H$_5$O]$^{+}$ 249.0312; found for [C$_7$H$_5$O]$^{+}$ 249.0523. **IR**(*CO*F): 1812 cm^{-1}.[245]

3.8.4 Catalytic Fluorination

3.8.4.1 General Procedure for the catalyst screen

Catalyst (0.05 mmol) and silver fluoride (380 mg, 3.0 equiv.) were added to a 50 mL round bottomed flask, with a side arm, along with a stirring bar. The flask was evacuated and backfilled with argon 3 times, with care taken when exposing the evacuated flask to the inert atmosphere to avoid disturbance of the solid. Anhydrous DCM (5 mL) was added *via* syringe and the reaction mixture was allowed to stir under argon, in darkness for 10 minutes. Toluoyl chloride (1.0 mmol) was added *via* pipette under a dynamic flow of argon and the reaction was sealed and stirred at 400 rpm in darkness for four hours. After the reaction time had elapsed the reaction mixture was filtered through a plug of celite, washed with DCM (3 x 5 mL) and the solvent was removed under reduced pressure (250 mbar). The resulting orange oily residue was transferred to an NMR tube, with the aid of deuterated chloroform (0.5 mL) alongside trifluorotoluene (20 µL). Internal contained yield of the toluoyl fluoride product was determined against trifluorotoluene as the internal standard.

3.8.4.2 General Procedure for further development

Unless otherwise stated, $[C_5Me_4CH_2C_6F_5CH_2NC_3H_2NMe)$- RhCl]**, 22** (27 mg, 0.05 mmol, 5 mol %) and silver fluoride (190 mg, 1.5 equiv.) were added, alongside any additive, to a 50 mL round bottomed flask, with a side arm, along with a stirring bar. The flask was evacuated and backfilled with argon 3 times, with care taken when exposing the evacuated flask to the inert atmosphere to avoid disturbance of the solid. Anhydrous DCM (5 mL) was added *via* syringe and the reaction mixture was allowed to stir (400 rpm) under argon, in darkness for 10 minutes. Toluoyl chloride (1.0 mmol) was added *via* pipette under a dynamic flow of argon and the reaction was sealed and stirred in darkness for four hours. After the reaction time had elapsed the reaction mixture was filtered through a plug of celite, washed with DCM (3 x 5 mL) and the solvent was removed under reduced pressure. The resulting orange oily residue was transferred to an NMR tube, with the aid of deuterated chloroform (0.5 mL) alongside trifluorotoluene (20 µL). Internal contained yield of the toluoyl fluoride product was determined against the trifluorotoluene internal standard.

3.8.4.3 General Procedure for substrate scope

[C$_5$Me$_4$CH$_2$C$_6$F$_5$CH$_2$NC$_3$H$_2$NMe)- RhCl]**, 22** (27 mg, 0.05 mmol, 5 mol %) and silver fluoride (190 mg, 1.5 equiv.) were added to a Schlenk finger, alongside a stir bar and the flask was evacuated and backfilled with argon. The sealed Schlenk finger was placed in an EasyMax (details in *Section 3.8.1*) and heated to 20 °C. The IR probe was inserted under a positive pressure of argon and a background was taken using Mettler Toledo iC IR software (Figure 3-12). Anhydrous DCM (5 mL) was added *via* syringe and the experiment was started, with a stir rate of 600 rpm. The acyl chloride (1.0 mmol) was added *via* pipette in two additions, allowing for a complete scan interval (256 scans at a scan rate of 256 scans per minute) to occur between additions, following 10 minutes of stirring. The solids, 4-Nitrobenzoyl chloride and probenecid chloride, were added carefully under a positive pressure of argon. Changes that occurred were monitored over time *via* the "solvent abstraction" feature of the iC IR software, and trendlines showing the consumption of acyl chloride and the formation of acyl fluoride were plotted. The reaction was stopped once the formation of the acyl fluoride product plateaued.

In the case of benzoyl chloride, the benzoyl fluoride product is commercially available. Following completion of the reaction, benzoyl fluoride (1.0 mmol) was doped into the reaction following the double addition method.[265] Following completion of the reaction, where the absorption band of the benzoyl fluoride product (1812 cm^{-1}) plateaued, commercially purchased benzoyl fluoride (2 x 55 µL, 0.5 mmol) were added allowing for a complete scan to occur between additions. This allows for quantification of both the acyl chloride reagent and acyl fluoride product against a known concentration. Normalisation of the absorption intensities of the reagent and product to 1 mmol allowed for quantitative measurements to be assigned.

Figure 3-12: Schematic setup for ReactIR measurements. Diamond ATR probe, connected to a ReactIR 15, inserted into a Schlenk flask, under a positive pressure of argon.

After the absorption peak of the acyl fluoride product plateaued the reaction mixture was filtered through a plug of celite, washed with DCM (3 x 5 mL) and the solvent was removed under vacuum. Off-line ^{19}F NMR analysis of reaction mixture, integrated against the internal standard trifluorotoluene (20 µL), enabled secondary quantitative measurement to be completed. Following NMR measurements, the NMR solution was eluted with diethyl ether (5 mL) and placed at *ca*. -20 °C for a minimum of 16 hours. Filtration of the resultant mixture enable recovery of the catalyst and a pale orange solution. Solvent was then removed under vacuum and washed with a minimal quantity (2-5 mL) of hot heptane, the solution was decanted and then cooled *ca*. -20 °C for a minimum of 16 hours to air recrystallisation of the solid acyl fluoride products. The solvent was then removed under vacuum, to give a colourless / pale yellow oil or solid, with was dried under vacuum and isolated to give 79 - 92 % isolated yield of the acyl fluoride products. This double elution methodology also enabled the recovery of up to 91 % of the catalyst, which could be regenerated with Ag_2O (1.5 eq.) and reused, following the experimental procedure developed in *Section 2.4.4.6*.

3.8.4.3.1 Catalytic fluorination of benzoyl chloride

Benzoyl chloride (1.0 mmol) was added to a Schlenk tube containing **22** (27 mg, 0.05 mmol) and AgF (190 mg, 1.5 eq.) in dry DCM (5 mL), which had previously been stirred for 10 minutes. The reaction was stirred at 20 °C for 210 minutes, until all of the starting material had been consumed, followed by work-up via filtration through celite, removal of solvent and transfer to a NMR tube, alongside deuterated chloroform (0.5 mL) and trifluorotoluene (20 µL). ^{19}F NMR yield *vs*. the internal standard > 99 %, isolated yield of colourless oil, 108 mg, 87 % yield.

^{1}H NMR (400 MHz, *d-chloroform*): δ 8.03 (m, C_6-*H,* 2H), 7.70 (tt, $^2J_{HH}$ = 7.6, 1.2 Hz, C_6-*H*, 1H), 7.52 (m, C_6-*H*, 2H).**^{19}F NMR** (376 MHz, *d-chloroform*): δ 18.05 (s, CO*F*, 1F). **^{13}C NMR** (101 MHz, *d-chloroform*): δ δ 157.4 (d, $^1J_{CF}$ = 344.2 Hz, *C*OF), 135.4 (s, *Ar*), 131.4 (d, ^3J = 4.0 Hz, *Ar*CO), 129.1 (s, *Ar*), 124.9 (d, $^2J_{CF}$ = 60.9 Hz, *Ar*CO). **MS** (ESI): Theoretical [2M+K] $[C_7H_5O]^+$ 249.0312; found for $[C_7H_5O]^+$ 249.0523. **IR**(*C*OF): 1812 (s) cm^{-1}.

Characterisation is consistent with previously reported literature.[245]

3.8.4.3.2 Catalytic fluorination of toluoyl chloride

Toluoyl chloride (1.0 mmol) was added to a Schlenk tube containing **22** (27 mg, 0.05 mmol) and AgF (190 mg, 1.5 eq.) in dry DCM (5 mL), which had previously been stirred for 10 minutes. The reaction was stirred at 20 °C for 170 minutes, until all of the starting material had been consumed, followed by work-up via filtration through celite, removal of solvent and transfer to a NMR tube, alongside deuterated chloroform (0.5 mL) and trifluorotoluene (20 µL). ^{19}F NMR yield *vs.* the internal standard > 99 %, isolated yield of colourless solid, 126 mg, 92 % yield.

^{1}H NMR (400 MHz, *d-chloroform*): δ 8.01 (d, $^2J_{HH}$ = 8.3 Hz, C_6-*H*, 2H), δ 7.28 (d, $^2J_{HH}$ = 8.1 Hz, C_6-*H*, 2H), 2.43 (s, Me, 3H). **^{19}F NMR** (376 MHz, *d-chloroform*): δ 17.46 (s, CO*F*, 1F).[6] **MS** (ESI): Theoretical [M]$^+$ [C_8H_8O]$^+$ 120.0569; found for [C_8H_8O]$^+$ 120.0556. **IR**(*CO*F): 1805 (s) cm^{-1}.
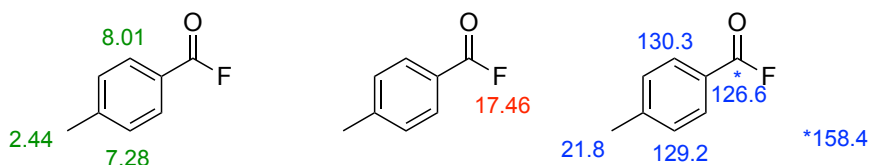
Characterisation is consistent with previously reported literature.[253]
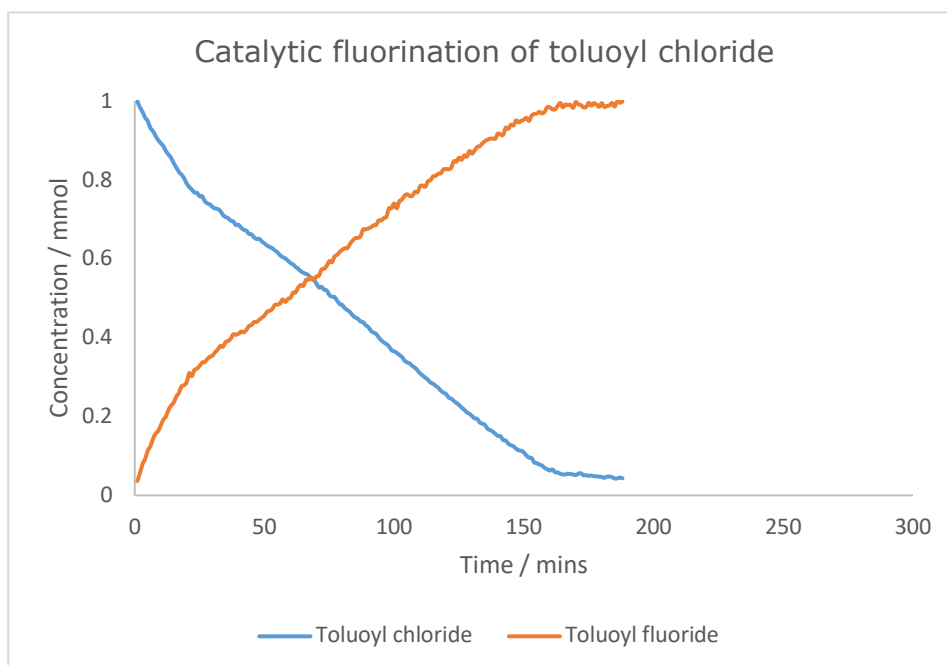
3.8.4.3.3 Catalytic fluorination of 4-Nitrobenzoyl chloride

4-Nitrobenzoyl chloride (1.0 mmol) was added to a Schlenk tube containing **22** (27 mg, 0.05 mmol) and AgF (190 mg, 1.5 eq.) in dry DCM (5 mL), which had previously been stirred for 10 minutes. The reaction was stirred at 20 °C for 110 minutes, until all of the starting material had been consumed, followed by work-up via filtration through celite, removal of solvent and transfer to a NMR tube, alongside deuterated chloroform (0.5 mL) and trifluorotoluene (20 µL). ^{19}F NMR yield *vs*. the internal standard > 99 %, isolated yield of pale yellow solid, 156 mg, 92 % yield.

^{1}H NMR (400 MHz, *d-chloroform*): δ 8.39 (d, $^2J_{HH}$ = 8.2 Hz, C_6-*H*, 2H), δ 8.25 (d, $^2J_{HH}$ = 8.8 Hz, C_6-*H*, 2H). **^{19}F NMR** (376 MHz, *d-chloroform*): δ 20.36 (s, CO*F*, 1F).

^{13}C NMR (101 MHz, d_1-chloroform): δ155.6 (d, J_{CF} = 346.4 Hz, *C*(O)F), 152.0 (s, O_2N-*C*), 132.7 (d, J_{CF} = 3.5 Hz, 2,6-*C*), 130.4 (d, J_{CF} = 63.2 Hz, *C*C(O)F), 124.3 (s, 3,5-*C*).[7] **MS** (ESI): Theoretical [M+MeCN] $[C_7H_4NO_3]^+$ 191.0451 ; found for $[C_7H_4NO_3]^+$. 191.0931. **IR**(*CO*F): 1821 (s) cm^{-1}.
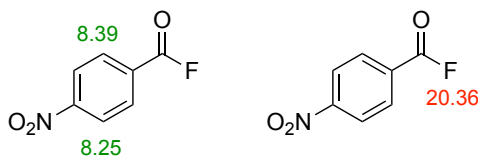
Characterisation is consistent with previously reported literature.[268]

Catalytic fluorination of 4-Nitrobenzoyl chloride

3.8.4.3.4 Catalytic fluorination of 2,6-Difluorobenzoyl chloride

2,6-Difluorobenzoyl chloride (1.0 mmol) was added to a Schlenk tube containing **22** (27 mg, 0.05 mmol) and AgF (190 mg, 1.5 eq.) in dry DCM (5 mL), which had previously been stirred for 10 minutes. The reaction was stirred at 20 °C for 70 minutes, until all of the starting material had been consumed, followed by work-up via filtration through celite, removal of solvent and transfer to a NMR tube, alongside deuterated chloroform (0.5 mL) and trifluorotoluene (20 µL). ^{19}F NMR yield *vs.* the internal standard > 99 %, isolated yield of colourless solid, 158 mg, 83 % yield.

^{1}H NMR (400 MHz, *d-chloroform*): δ 7.48 (tt, $^2J_{HH}$ = 8.5, 6.1 Hz, C$_6$-*H*, 2H), 7.00 (t, $^2J_{HH}$ = 8.4 Hz, C$_6$-*H*, 2H). **^{19}F NMR** (376 MHz, *d-chloroform*): δ 47.50 (t, J_{FF} = 38.7 Hz, CO*F*, 1F), -108.39 (s, C*F*, 2F). **MS** (ESI): Theoretical [M] [C$_7$H$_3$OF$_2$]$^+$ 141.0146; found for [C$_7$H$_3$OF$_2$]$^+$ 141.0160. **IR**(*CO*F): 1822 (s) cm^{-1}.
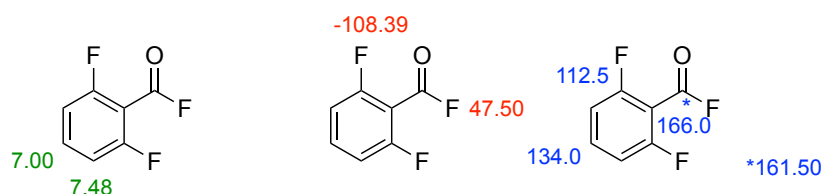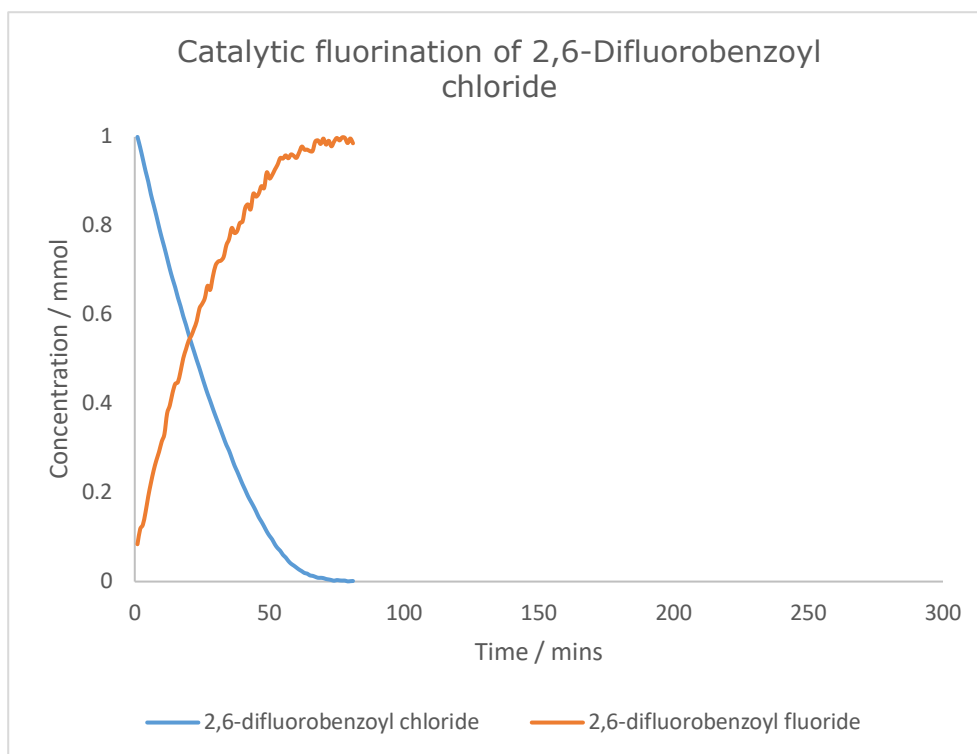
3.8.4.3.5 Catalytic fluorination of (2,3,4,5,6)-Pentafluorobenzoyl chloride

2,3,4,5,6-Pentafluorobenzoyl chloride (1.0 mmol) was added to a Schlenk tube containing **22** (27 mg, 0.05 mmol) and AgF (190 mg, 1.5 eq.) in dry DCM (5 mL), which had previously been stirred for 10 minutes. The reaction was stirred at 20 °C for four hours, followed by work-up via filtration through celite, removal of solvent and transfer to a NMR tube, alongside deuterated chloroform (0.5 mL) and trifluorotoluene (20 µL). ^{19}F NMR yield *vs*. the internal standard > 99 %, isolated yield of pale orange solid, 168 mg, 78 % yield.

^{19}F NMR (376 MHz, *d-chloroform*): δ 48.06 (t, J_{FF} = 40.2 Hz*, COF*, 1F), -136.49 (dp, J_{FF} = 18.1, 6.3 Hz, C_6-*F*, 2F), -146.56 (tt, J_{FF} = 20.9, 5.7 Hz, C_6-*F*, 1F), -159.96 (tq, J_{FF} = 20.1, 7.1 Hz, C_6-*F*, 2F). **MS** (ESI): Theoretical [M] $[C_7OF_5]^+$ 194.9864; found for $[C_7OF_5]^+$ 194.9885. **IR**(*CO*F): 1830 (s) cm^{-1}.
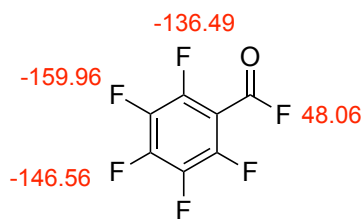
Characterisation is consistent with previously reported literature. [269]

3.8.4.3.6 Catalytic fluorination of 4-(Trifluoromethyl)benzoyl chloride

4-(Trifluoromethyl)benzoyl chloride (1.0 mmol) was added to a Schlenk tube containing **22** (27 mg, 0.05 mmol) and AgF (190 mg, 1.5 eq.) in dry DCM (5 mL), which had previously been stirred for 10 minutes. The reaction was stirred at 20 °C for four hours, followed by work-up via filtration through celite, removal of solvent and transfer to a NMR tube, alongside deuterated chloroform (0.5 mL) and trifluorotoluene (20 µL). ^{19}F NMR yield *vs.* the internal standard > 99 %.

^{1}H NMR (400 MHz, *d-chloroform*): δ 8.24 (d, $^2J_{HH}$ = 7.9 Hz, C_6-*H*, 1H), 7.78 (d, $^2J_{HH}$ = 8.2 Hz, C_6-*H*, 1H). **^{19}F NMR** (376 MHz, *d-chloroform*): δ 19.91 (s, CO*F*, 1F), -62.78 (s, C*F$_3$*, 3F). **MS** (ESI): Theoretical [M+Na] $[C_8H_4OF_3]^+$ 196.0106; found for $[C_8H_4OF_3]^+$ 196.1271. **IR**(*CO*F): 1817 (s) cm^{-1}.
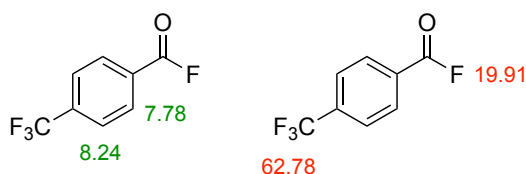
Characterisation is consistent with previously reported literature. [253]
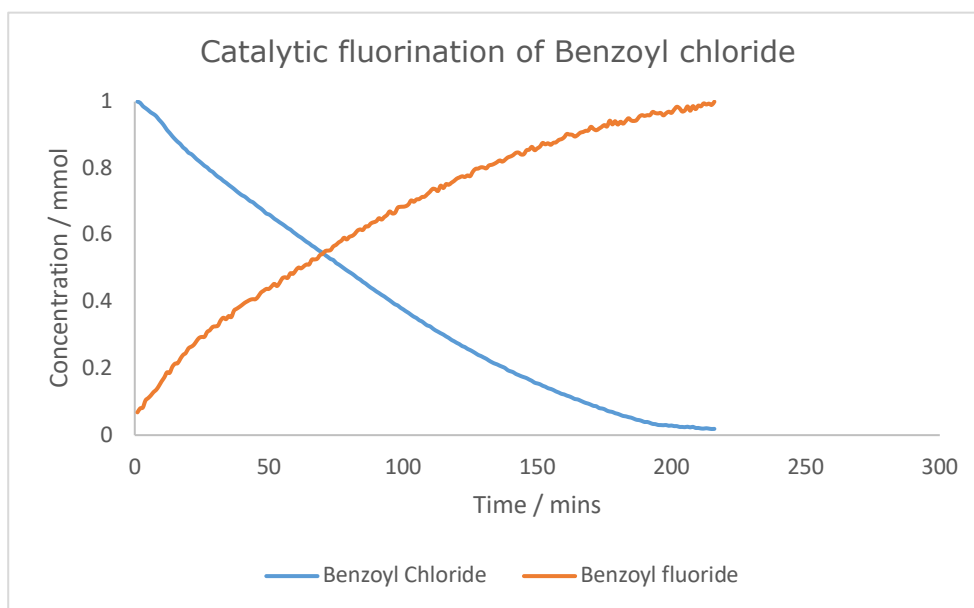
3.8.4.3.7 Catalytic fluorination of 4-Ethylbenzoyl chloride

4-Ethylbenzoyl chloride (1.0 mmol) was added to a Schlenk tube containing **22** (27 mg, 0.05 mmol) and AgF (190 mg, 1.5 eq.) in dry DCM (5 mL), which had previously been stirred for 10 minutes. The reaction was stirred at 20 °C for 290 minutes, until all of the starting material had been consumed, followed by work-up via filtration through celite, removal of solvent and transfer to a NMR tube, alongside deuterated chloroform (0.5 mL) and trifluorotoluene (20 µL). ^{19}F NMR yield *vs.* the internal standard > 99 %, isolated yield of pale yellow oil, 123 mg, 80 % yield.

¹H NMR (400 MHz, *d-chloroform*): δ 7.95 (d, $^2J_{HH}$ = 8.3 Hz, C_6-*H*, 2H), δ 7.35 (d, $^2J_{HH}$ = 7.9 Hz, C_6-*H*, 2H), 2.75 (q, $^3J_{HH}$ = 7.6 Hz, C*H₂*, 2H), 1.27 (t, $^3J_{HH}$ = 7.7 Hz, C*H₃*, 3H). **¹⁹F NMR** (376 MHz, *d-chloroform*): δ 17.14 (s, CO*F*, 1F). **¹³C NMR** (101 MHz, *d-chloroform*): δ 157.5 (d, ^1J = 342.9 Hz, *C*OF), 131.6 (d, ^3J = 4.1 Hz, *Ar*), 128.6 (s, *Ar*), 122.3 (d, ^2J = 61.3 Hz, *Ar*), 29.1 (s, *C*H₂), 15.0 (s, *C*H₃). **MS** (ESI): Theoretical [M+K] [C_9H_9O]$^+$ 172.0284; found for [C_9H_9O]$^+$ 172.1335. **IR**(*C*O*F*): 1804 (s) cm^{-1}.
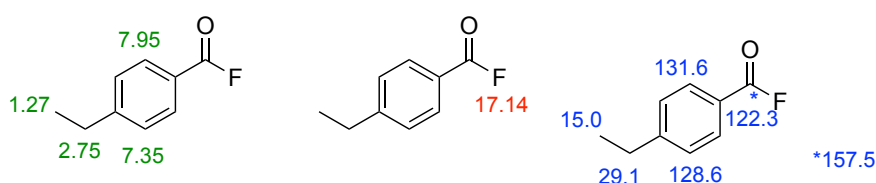
Characterisation is consistent with previously reported literature. [250]

3.8.4.3.8 Catalytic fluorination of 4-*iso*propylbenzoyl chloride

4-*iso*propylbenzoyl chloride (1.0 mmol) was added to a Schlenk tube containing **22** (27 mg, 0.05 mmol) and AgF (190 mg, 1.5 eq.) in dry DCM (5 mL), which had previously been stirred for 10 minutes. The reaction was stirred at 20 °C for 290

minutes, until all of the starting material had been consumed, followed by work-up via filtration through celite, removal of solvent and transfer to a NMR tube, alongside deuterated chloroform (0.5 mL) and trifluorotoluene (20 µL). ^{19}F NMR yield *vs.* the internal standard > 99 %, isolated yield of pale yellow oil, 144 mg, 87 % yield.

^{1}H NMR (400 MHz, *d-chloroform*): δ 7.96 (d, $^2J_{HH}$= 8.3 Hz, C$_6$-*H,* 2H), 7.37 (d, $^2J_{HH}$= 7.9 Hz, C$_6$-*H,* 2H), 3.00 (h, $^3J_{HH}$= 7.0 Hz, C*H,* 1H), 1.28 (d, $^3J_{HH}$= 6.9 Hz, C*H$_3$*, 6H).**^{19}F NMR** (376 MHz, *d-chloroform*): δ 17.16 (s, CO*F*, 1F). **^{13}C NMR** (101 MHz, *d-chloroform*): δ 157.5 (d, ^1J = 342.9 Hz, *C*OF), 131.7 (d, ^3J = 4.1 Hz, *Ar*), 128.6 (s, *Ar*), 122.4 (d, ^2J = 60.9 Hz, *Ar*), 34.5 (s, *C*H), 23.5 (s, *C*H$_3$). **MS** (ESI): Theoretical [M] [C$_{10}$H$_{11}$O]$^+$ 147.0804; found for [C$_{10}$H$_{11}$O]$^+$ 147.0799. **IR**(*C*OF): 1800 (s) cm^{-1}.
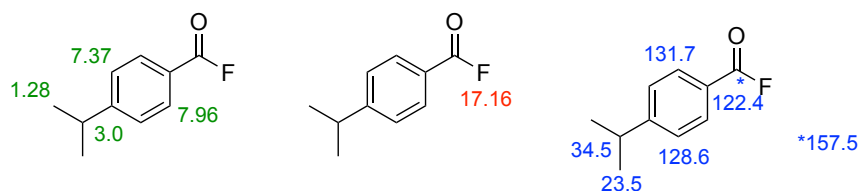
Characterisation is consistent with previously reported literature. [270]
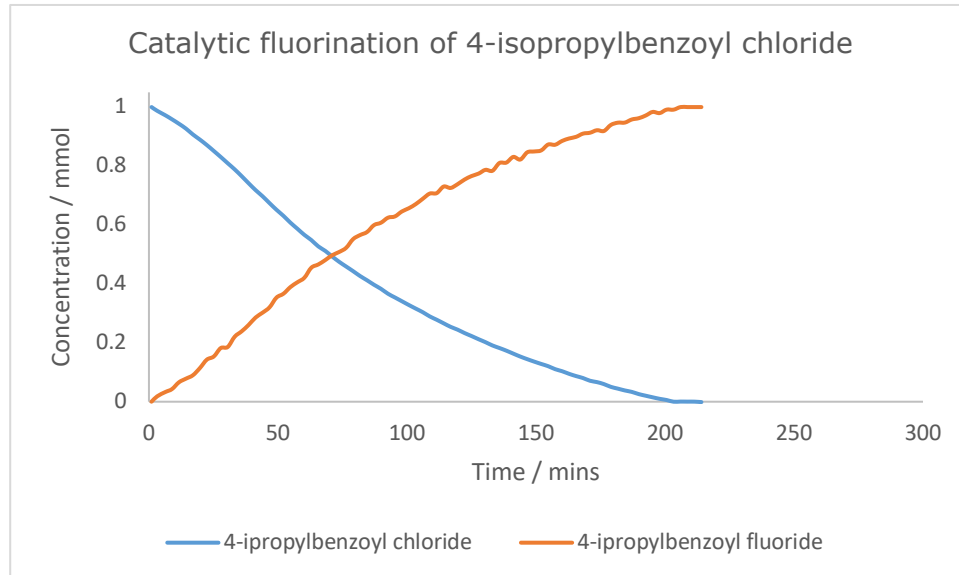
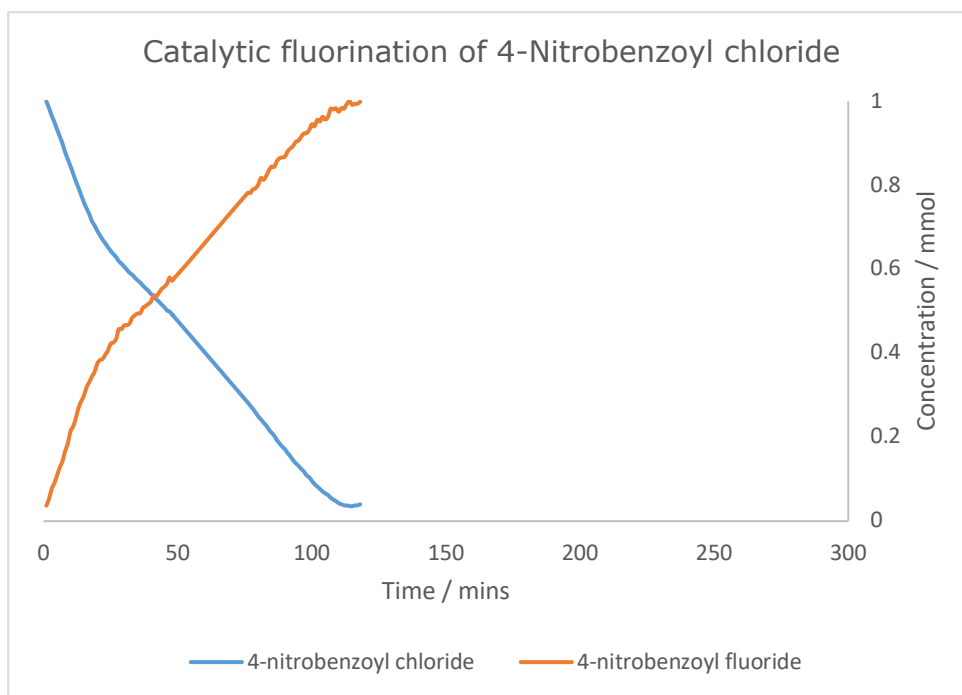### 3.8.4.3.9 Catalytic fluorination of 4-*tert*butylbenzoyl chloride

4-*tert*benzoyl chloride (1.0 mmol) was added to a Schlenk tube containing **22** (27 mg, 0.05 mmol) and AgF (190 mg, 1.5 eq.) in dry DCM (5 mL), which had previously been stirred for 10 minutes. The reaction was stirred at 20 °C for 290

minutes, until all of the starting material had been consumed, followed by work-up via filtration through celite, removal of solvent and transfer to a NMR tube, alongside deuterated chloroform (0.5 mL) and trifluorotoluene (20 μL). ^{19}F NMR yield *vs*. the internal standard > 99 %, isolated yield of pale yellow oil, 150 mg, 83 % yield.

^{1}H NMR (400 MHz, *d-chloroform*): δ 7.98 (d, $^2J_{HH}$ = 8.5 Hz, C$_6$-*H*, 2H), δ 7.56 (d, $^2J_{HH}$ = 7.4 Hz, C$_6$-*H*, 2H), 1.37 (s, C*H*$_3$, 9H). **^{19}F NMR** (376 MHz, *d-chloroform*): δ 17.47 (s, CO*F*, 1F). **^{13}C NMR** (101 MHz, *d-chloroform*): δ 157.5 (d, $^1J_{CF}$ = 342.7 Hz, *C*OF), 130.2 (s, *Ar*), 125.6 (s, *Ar*), 122.1 (d, $^2J_{CF}$ = 61.1 Hz, *Ar*), 35.4 (s, *C*), 31.0 (s, *C*H$_3$). **MS** (ESI): Theoretical [M] [C$_{11}$H$_{13}$O]$^+$ 161.0961; found for [C$_{11}$H$_{13}$O]$^+$ 161.0949. **IR**(*C*OF): 1805 (s) cm^{-1}.
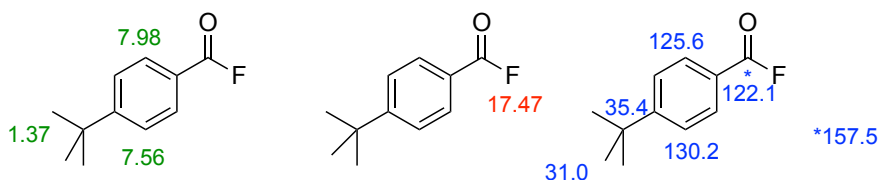
Characterisation is consistent with previously reported literature. [253]
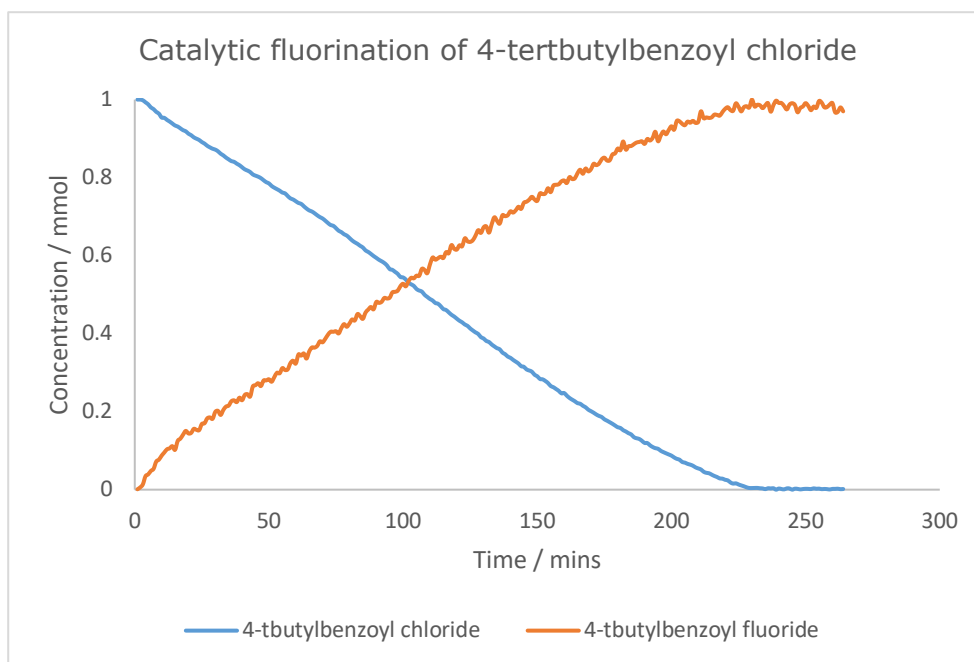
3.8.4.3.10 Catalytic fluorination of 4-Methoxybenzoyl chloride

4-Methoxybenzoyl chloride (1.0 mmol) was added to a Schlenk tube containing **22** (27 mg, 0.05 mmol) and AgF (190 mg, 1.5 eq.) in dry DCM (5 mL), which had previously been stirred for 10 minutes. The reaction was stirred at 20 °C for 620 minutes, until all of the starting material had been consumed, followed by work-up via filtration through celite, removal of solvent and transfer to a NMR tube, alongside deuterated chloroform (0.5 mL) and trifluorotoluene (20 μL). ^{19}F NMR yield *vs.* the internal standard > 99 %, isolated yield of colourless solid, 134 mg, 87 % yield.

^{1}H NMR (400 MHz, *d-chloroform*): δ 8.07 (d, $^2J_{HH}$ = 8.9 Hz, C_6-*H*, 2H), δ 6.95 (d, $^2J_{HH}$ = 8.9 Hz, C_6-*H*, 2H), 3.88 (s, C*H*$_3$, 3H). **^{19}F NMR** (376 MHz, *d-chloroform*): δ 16.00 (s, CO*F*, 1F). **^{13}C NMR** (101 MHz, *d*-chloroform): δ 167.8 (d, J_{CF} = 747.0 Hz, *C*(O)F),132.4 (s, *Ar*), 121.6 (s, *C*C(O)F), 113.8 (s, *Ar*), 55.5 (s, O*C*H$_3$).**MS** (ESI): Theoretical [M+CH$_3$] [C$_{13}$H$_{18}$O$_3$NS]$^+$ 301.1342; found for [C$_{13}$H$_{18}$O$_3$NS]$^+$ 301.1288. **IR**(*CO*F): 1798 (s) cm^{-1}.
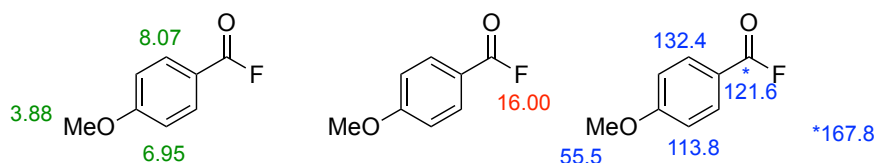
Characterisation is consistent with previously reported literature. [270]

Catalytic fluorination of 4-Methoxybenzoyl chloride
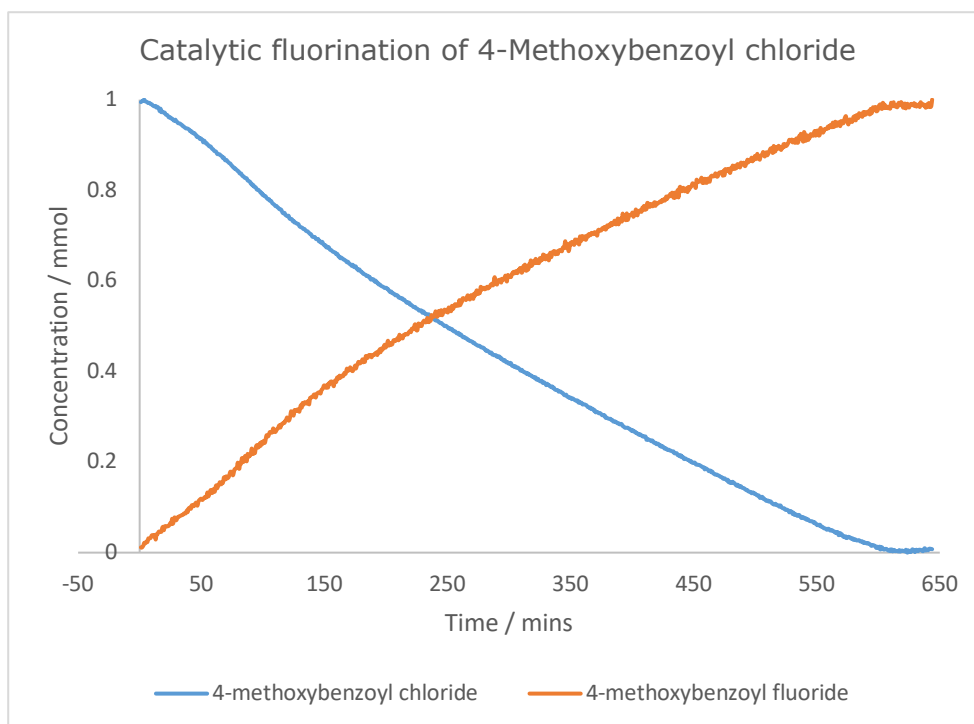
Note: Scale for this reaction profile different to other plots.

3.8.4.3.11 Catalytic fluorination of probenecid chloride

Probenecid chloride (1.0 mmol) was added to a Schlenk tube containing **22** (27 mg, 0.05 mmol) and AgF (190 mg, 1.5 eq.) in dry DCM (5 mL), which had previously been stirred for 10 minutes. The reaction was stirred at 20 °C for 90 minutes, until all of the starting material had been consumed, followed by work-up via filtration through celite, removal of solvent and transfer to a NMR tube, alongside deuterated chloroform (0.5 mL) and trifluorotoluene (20 μL). ^{19}F NMR yield *vs.* the internal standard > 99 %, isolated yield of colourless solid, 227 mg, 79 % yield.

^{1}H NMR (400 MHz, *d-chloroform*): δ 8.10 (dd, $^2J_{HH}$ = 8.97, 2.4 Hz, C$_6$-*H*, 2H), 7.89 (dd, $^2J_{HH}$ = 8.5, 2.3 Hz, C$_6$-*H*, 2H), 3.05 (tq, $^3J_{HH}$ = 6.9, 2.3 Hz, N-C*H$_2$*, 4H), 1.48 (qt, $^3J_{HH}$ = 7.4, 2.3 Hz, C*H$_2$*, 4H), 0.79 (tt, $^3J_{HH}$ = 7.5, 2.3 Hz, C*H$_3$*, 6H), **^{19}F NMR** (376 MHz, *d-chloroform*): δ 19.91 (s, CO*F*, 1F). **^{13}C NMR** (101 Mhz, *d*-chloroform): δ 156.0 (d, ^{1}J$_{CF}$ = 345.6 Hz, *C*OF), 146.6, 132.0 (d, ^{3}J$_{CF}$= 3.5 Hz, *Ar*), 128.7 (d, ^{2}J$_{CF}$= 61.6 Hz, *C*C(O)F), 127.4 (s, *Ar*), 49.8 (s, N*C*H$_2$), 21.8 (s, *C*H$_2$), 10.9 (s, *C*H$_3$). **MS**

(ESI): Theoretical [M+CH$_3$] [C$_{13}$H$_{18}$O$_3$NS]$^+$ 301.1342; found for [C$_{13}$H$_{18}$O$_3$NS]$^+$ 301.1288. **IR**(*CO*F): 1816 (s) cm^{-1}. **m.p**: 62-64 ºC.
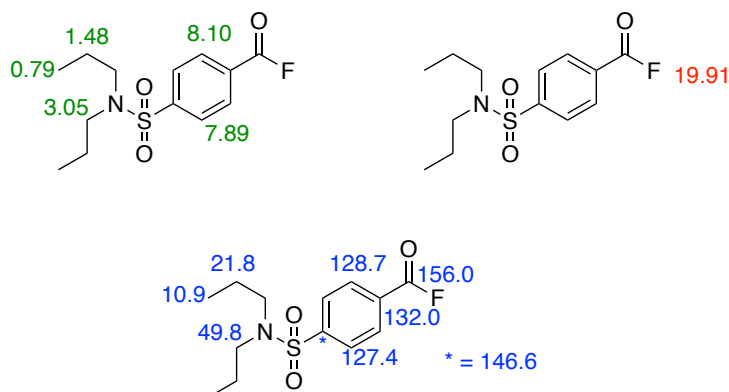
Characterisation is consistent with previously reported literature.[253]
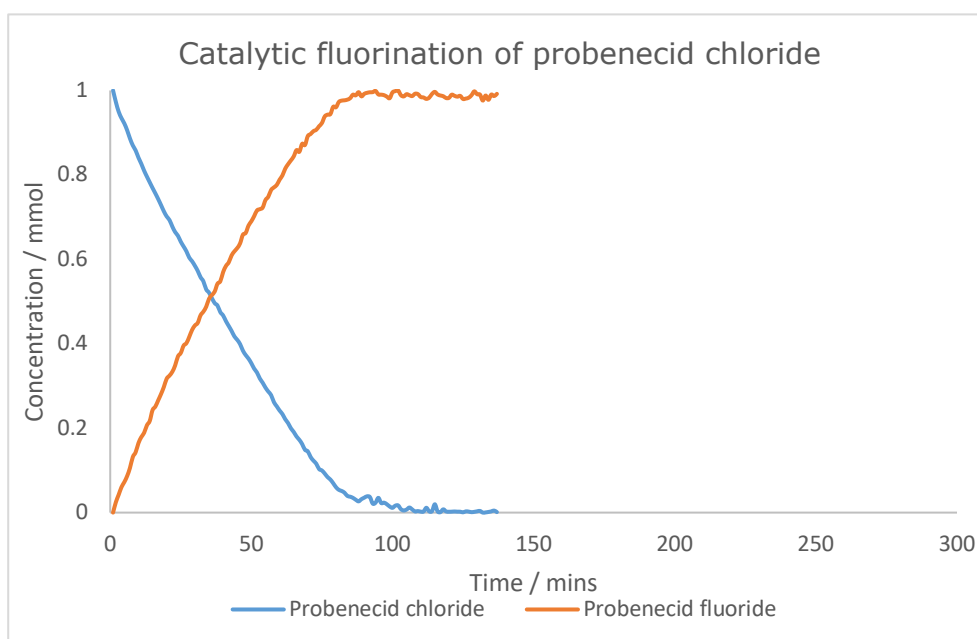
3.8.4.3.12 Catalytic fluorination of benzoic anhydride
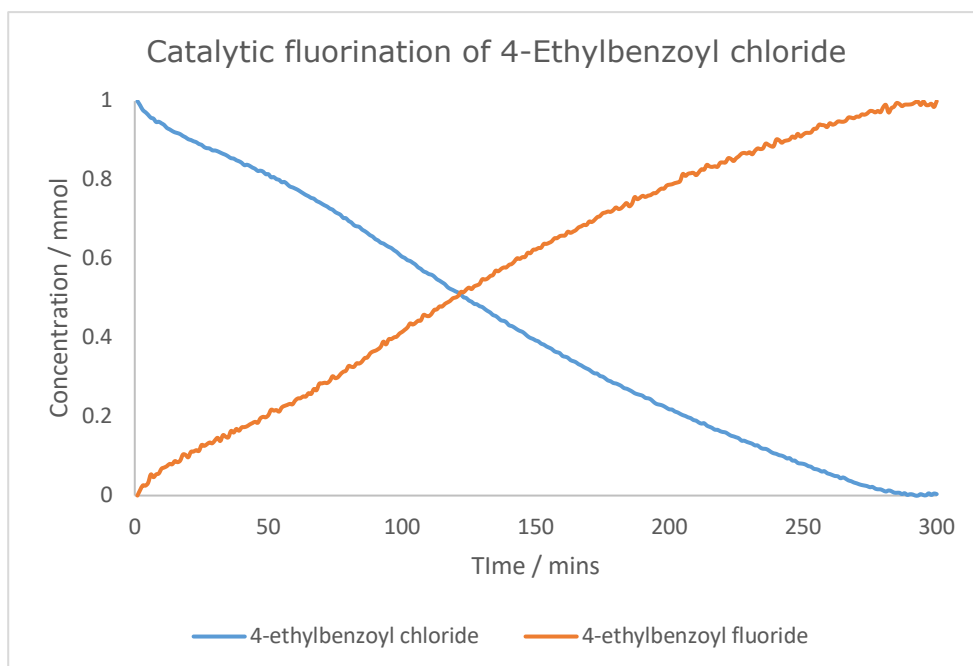
Benzoic anhydride (1.0 mmol) was added to a Schlenk tube containing **22** (27 mg, 0.05 mmol) and AgF (190 mg, 1.5 eq.) in dry DCM (5 mL), which had previously been stirred for 10 minutes. The reaction was stirred at 20 °C for 42 hours, until all of the starting material had been consumed, followed by work-up via filtration through celite, removal of solvent and transfer to a NMR tube, alongside deuterated chloroform (0.5 mL) and trifluorotoluene (20 µL). ^{19}F NMR yield *vs*. the internal standard > 99 %.

¹H NMR (400 MHz, *d-chloroform*): δ 8.03 (m, C_6-*H*, 2H), 7.70 (tt, $^2J_{HH}$ = 7.6, 1.2 Hz, C_6-*H*, 1H), 7.52 (m, C_6-*H*, 2H). **¹⁹F NMR** (376 MHz, *d-chloroform*): δ 18.05 (s, CO*F*, 1F). **¹³C NMR** (101 MHz, *d-chloroform*): δ δ 157.4 (d, $^1J_{CF}$ = 344.2 Hz, *C*OF), 135.4 (s, *Ar*), 131.4 (d, ^3J = 4.0 Hz, *Ar*CO), 129.1 (s, *Ar*), 124.9 (d, $^2J_{CF}$ = 60.9 Hz, *Ar*CO). **MS** (ESI): Theoretical [2M+K] $[C_7H_5O]^+$ 249.0312; found for $[C_7H_5O]^+$ 249.0523. **IR**(*C*OF): 1812 (s) cm^{-1}.

Characterisation is consistent with previously reported literature.[245]

4   Chapter 4: Transfer Fluorination

4.1 Overview

Perfluorinated compounds such as Teflon and polyfluoroalkyl substances (PFAS), long harnessed by industry, are now ubiquitous in everyday life for their unique chemical inertness, resulting in their colloquial description as "forever chemicals." In part this is due to the strong dissociation energies of the C−F bond, the single strongest bond in organic chemistry (481 kJ/mol).[271]   However, the ability to cleave C−F bonds and thus degrade perfluorinated compounds is becoming increasingly important due to our growing awareness of the negative environmental effects of organofluorine due to anthropogenic use, and their persistent nature within the environment.[272-274] The potential harmful effects of this class of chemicals have been highlighted through the bioaccumulation of fluorinated pharmaceuticals in the environment,[275, 276] in addition to the documented bioaccumulation of PFAS compounds within foetal tissue, potentially causing unknown health effects.[277] The negative atmospheric effects of fluorinated compounds have long been acknowledged[278] and are still being observed from primary emissions of CFCs, HFCs or fluorocarbon, over three decades after their use was drastically reduced under the 1987 Montreal Treaty.[279] However, methodologies to degrade these fluorinated compounds are under-developed and new methodologies are required to access the fluorine for further functionalisation.

The field of C−F bond activation, which started as a series of one-off transition metal organometallic reactions,[280-284] has developed in recent years into a rapidly advancing field of catalytic research.[285-291] This has enabled new synthetic pathways to access molecules of interest and other fluorinated building blocks, that are less accessible from a "bottom-up" approach. Additionally, C−F bond activation at metal centres has become a powerful tool for introducing new functionality at the site of C−F bonds,[33] especially carbon-heteroatom coupling in the form of borylation,[292-295] silylation[292, 296-298] and amination.[299, 300]

Carbon-carbon cross coupling reactions, while well established for other halides, are still under-utilized for fluorinated molecules. Even though one of the leading methods for C−C coupling *via* C−F activation was developed in the 1970's by Kumada,[301] new methods to introduce new carbon-carbon bonds within fluorinated molecules remain elusive, especially compared to the other halocarbons. Of those currently developed, nickel catalysed C−F activated C−C cross coupling appears to be the most favourable,[302, 303] with recent studies reporting the feasibility of palladium catalysed Suzuki–Miyaura coupling *via* C−F activation from acyl fluorides and boronic acids.[253, 304, 305]

These processes predominantly proceed *via* the oxidative addition of the C−F bond of the fluorinated compound across the metal centre forming new metal-fluorine and metal-carbon bonds. The fluorine then undergoes abstraction with a sacrificial scavenger, resulting in the formation of a thermodynamic sink, in the form of H−F, Si−F or B−F bonds.

These methodologies however result in the removal of fluorine from the system. The issues associated with fluorine loss from these often energy and resource intensive processes are compounded when you consider the large quantities of material and energy resources required to incorporate fluorine into the molecule in the first place. Therefore, a more sustainable and circular route could be envisioned where the reaction is adapted, instead of losing fluorine to these thermodynamic sinks, the fluorine lost under C−F bond activation is transferred onto a non-fluorinated substrate, leading to the recycling of the fluorinated compound and resulting in the valorisation of both substrates in a 'fluorine transfer reaction.' This would direct these compounds away from waste streams, where their negative environmental effects are just becoming understood. However, this is a considerable challenge as, in general, little progress has been made in utilizing fluoroorganics as fluorine sources *via* C−F activation, and generally applicable catalytic nucleophilic fluorinations remain elusive.

To our knowledge the first example where this "fluoride shuttle" concept was described, was reported by Richmond *et. al.*, in 1994, where cobaltocenium fluoride, derived from the treatment of perfluorodecalin with cobaltocene, allowed for the fluorination of organic halides including benzoyl chloride, methyl iodide and benzyl chloride (Scheme 4-1).[306]
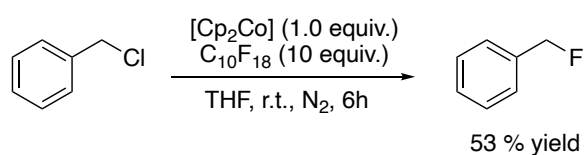
Scheme 4-1: *One-pot fluorine transfer reaction between fluorodecalin and benzyl chloride, mediated by cobaltocene. Treatment of fluorodecalin with cobaltocene results in the formation of cobaltocenium fluoride and fluoronapthalene. Cobaltocenium fluoride reacts with benzyl chloride to give benzyl fluoride.*

Since development of the work described within this chapter, a number of transfer fluorination methodologies have been reported, highlighting the current interest of this area of research. Ogiwara and Sakai have recently highlighted a metal-based fluorine transfer reaction where benzoyl fluoride is used as a nucleophilic fluorination reagent (Scheme 4-2).[228] Oxidative addition across a palladium centre facilitates acyl exchange with anhydrides to give a range

of acyl fluorides and the analogous anhydride in moderate to good yields. This represents a possible use of the fluorinated products produced within the previous chapter (*Chapter 3*).
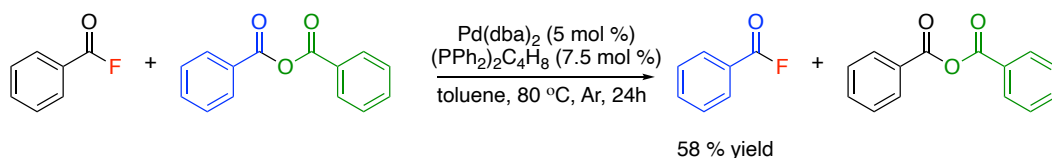
Scheme 4-2: Acyl transfer reaction developed by Ogiwara, utilising acyl fluorides as fluorination reagents for the fluorination of anhydrides. Represent a method for forming acyl fluorides which can be difficult to synthesise using traditional methods, through the exchange of fluorine from benzoyl fluoride. Scheme adapted from literature. [228]

Following this, Crimmin and co-workers reported an organocatalysed methodology towards the formation of acyl fluorides, where the perfluoroarene pentafluoropyridine was used as the fluorine source (Scheme 4-3).[307] Fluorine transfer to the acyl substrates occurred through activation of the perfluoroarene with dimethylaminopyridine (DMAP), resulting in the displacement of the *para*-fluorine *via* nucleophilic displacement, forming a nitroarene salt where the nucleophilic fluorine anion undergoes attack of the acyl electrophiles. This method enables the transfer of fluorine resulting in the defluorination of activated heteroarenes and the fluorination of suitable acyl partners in variable yields.
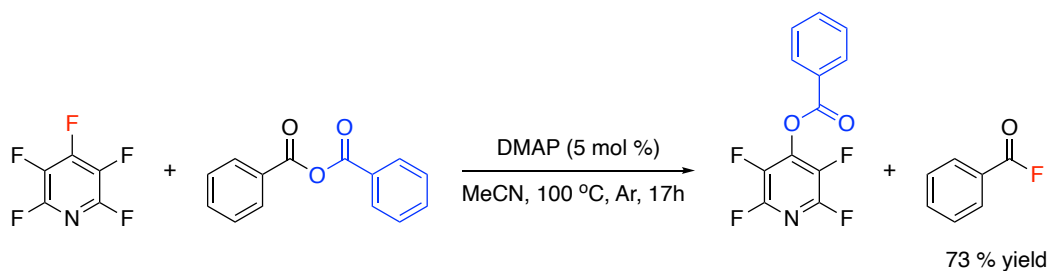
Scheme 4-3: Fluorine transfer reaction between pentafluoropyridine and anhydrides, resulting in formation of acyl fluorides and substituted tetrafluoropyridines. Represents a methodology for the activation of organic fluorine, which is then utilised for the fluorination of an organic electrophile. Scheme adapted from literature. [307]

More recently, Cobb and Brittain has described a similar methodology for the formation of acyl fluorides *via* transfer fluorination using pentafluoropyridine as the fluorine source (Scheme 4-4).[308] Under the reaction conditions, treatment of a range of carboxylic acids in the presence of pentafluoropyridine and di-(*iso*propyl)ethylamine resulted in the transfer of fluorine between the two substrates resulting in the formation of the acyl fluoride and 4-hydroxy-2,3,5,6-tetrafluoropyridine in high yields. This protocol enables the utilisation

fluorine from perfluorinated groups as the fluorine source for the fluorination of desired organic targets in moderate yields.
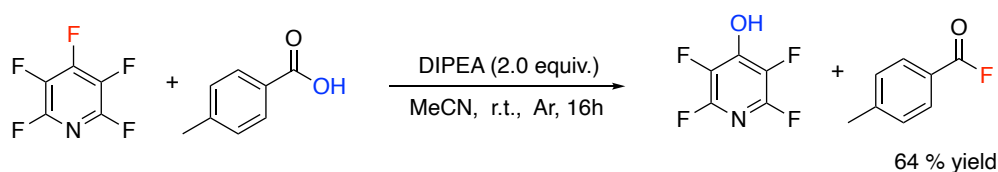
Scheme 4-4: Deoxyfluorination of carboxylic acids using pentafluoropyridine as the fluoride source. Activates an organic source of fluorine towards to fluorination of carboxylic acids. Scheme adapted from literature. [308]

4.2 Research Aims

C−F bond activation and C−F bond formation are very important areas of current research and the development of fluorination strategies to transfer fluorine from one substrate to another is an important step towards a circular fluorine economy. A transfer fluorination methodology was developed where C−F bond activation of a perfluorinated group results in the transfer of fluorine to an organic target. This enables the simultaneous C−F bond cleavage reactions of highly fluorinated molecules coupled with the fluorination of non-fluorinated substrates. The reactivity of this activated fluorine was probed to better understand the conditions required to generate nucleophilic fluorine, upon treatment with organic electrophiles. The overall aim is to be able to control the transfer of fluorine from where it is undesirable to where it is desirable. The work described in this chapter was reported in Organometallics in 2020.[206]

4.3 Discovery of transfer fluorination between **22** and toluoyl fluoride

As discussed previously in *Section 3.4*, treatment of 5 mol % **22** with toluoyl chloride in the absence of an external fluorine source resulted in the formation of a small quantity of the toluoyl fluoride product (¹⁹F NMR: 17.5 ppm) (*Table 3-3; entry 20*). Potential contamination of the reaction mixture with extraneous fluoride was ruled out upon further testing, where similar quantities of the toluoyl fluoride product was found following the reaction upon repeated control experiments. In addition to this, trace quantities of a new four fluorine

environment species was detected by ^{19}F NMR, with a chemical shift of −117.4 ppm, −131.1 ppm, −135.1 ppm, and −160.9 ppm, alongside the formation of toluoyl fluoride (Figure 4-1).
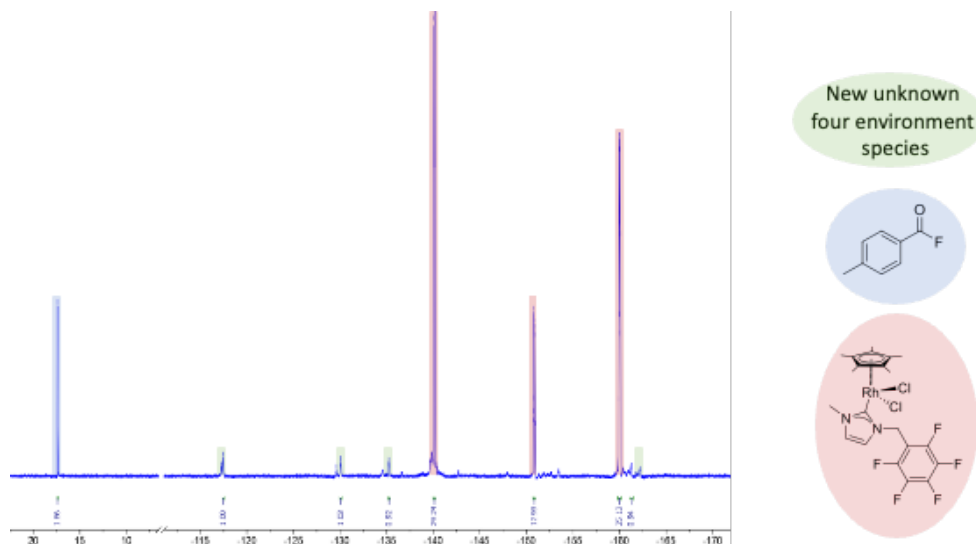
Figure 4-1: ^{19}F NMR spectrum of reaction of 5 mol % 22 with toluoyl chloride in the absence of an external fluorine source. Post-reaction analysis identified the formation of toluoyl fluoride (blue; -17.5 ppm), 6 (red; -140.6, -151.4 and -160.0 ppm) and a minor unidentified four fluorine environment species (green; -117.4, -131.1, -135.1 and -160.9 ppm). NMR analysis recorded in deuterated chloroform.

Subsequent investigation focused on the stoichiometric addition of **22** to dichloromethane and acetonitrile solution of toluoyl chloride found toluoyl fluoride was formed in a 1:1 ratio with this new distinct four fluorine environment species, where the concentration of toluoyl fluoride in the sample increased over the course of one week. After 7 days, no further reaction was observed.

Following our previous observation of C−F bond activation induced *cyclo*metallation forming **21**, it was initially thought that this four fluorine environment species was the rhodium analogue, **23**, where C−F bond activation at the C−F bond α- to the metal centre of **22**, followed by re-aromatization of the phenyl ring resulted in the formation of **23**. However, the ^{19}F NMR spectral signature of the new four fluorine environment rhodium complex observed upon reaction with toluoyl fluoride differed from that subsequently observed for **23**. This deviation between the observed ^{19}F NMR spectrum for the new four fluorine environment rhodium complex and **23** showed further complementary studies were required to deduce the structure of the new rhodium complex.

X-Ray quality single crystals of this new rhodium complex were eventually grown through elution of the reaction mixture with cold ether, affording the separation of the metal complexes from the organic product. Minimal dichloromethane was then added to the dried mixture of **6**, **22** and the four fluorine environment rhodium complex, where slow evaporation of this saturated dichloromethane solution resulted in the selective growth of single crystals of the new four fluorine environment rhodium complex. The structure of which was solved by single crystal XRD (Figure 4-2), which comprises a bimetallic metallocycle in which the methylene group of the Cp* ligand of one complex is attached to the partially fluorinated phenyl ring of the substituted NHC of another molecule at the site of C−F activation. This observation explains the disparity within chemical shift between the observed four fluorine environment species, **29** and **23** (Figure 4-3).
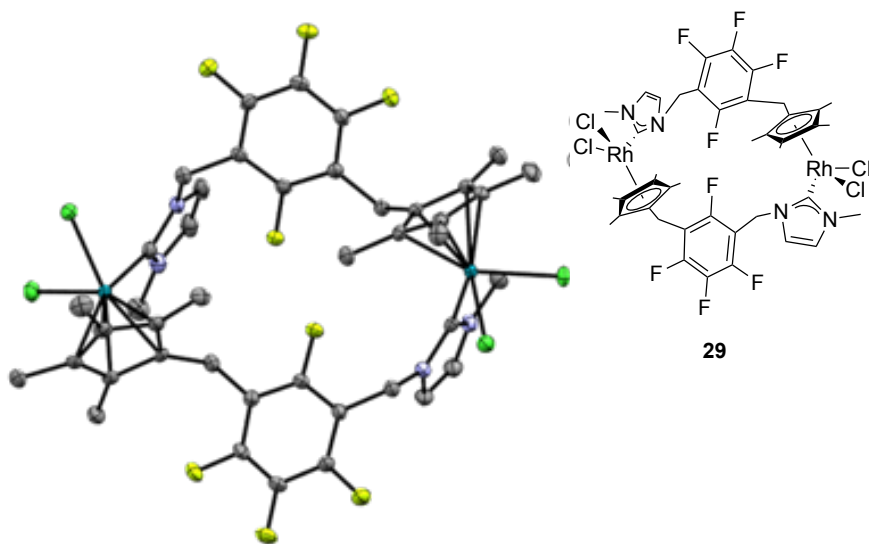
*Figure 4-2: Molecular structure of **29**, showing formation of a bimetallic rhodacycle. One of the fluorine atoms of the rearomatised polyfluorophenyl ring has undergone activation and fluorine transfer with an organic electrophile. Thermal ellipsoids for the anisotropic displacement parameters represent 50% probability. Hydrogen atoms and solvent molecules have been omitted for clarity. Selected bond distances (Å) and angles (deg) given in Table 4-1.*

The structural characteristics of this new rhodacyclic complex, **29**, where four fluorine atoms are bound to the phenyl ring, is consistent with the proposed mode of reactivity, where concurrent C−F bond activation, fluorine transfer, and C−F bond formation, initiated by the treatment of **22** with the organic electrophile toluoyl chloride. During the course of the reaction, the fluoride liberated following C−F activation reacts with the electrophile toluoyl chloride to give the fluorinated product, toluoyl fluoride, and new complex, **29** *via* fluorine transfer. Interestingly, when an external fluorine source is present, the formation of **29** has never been observed.
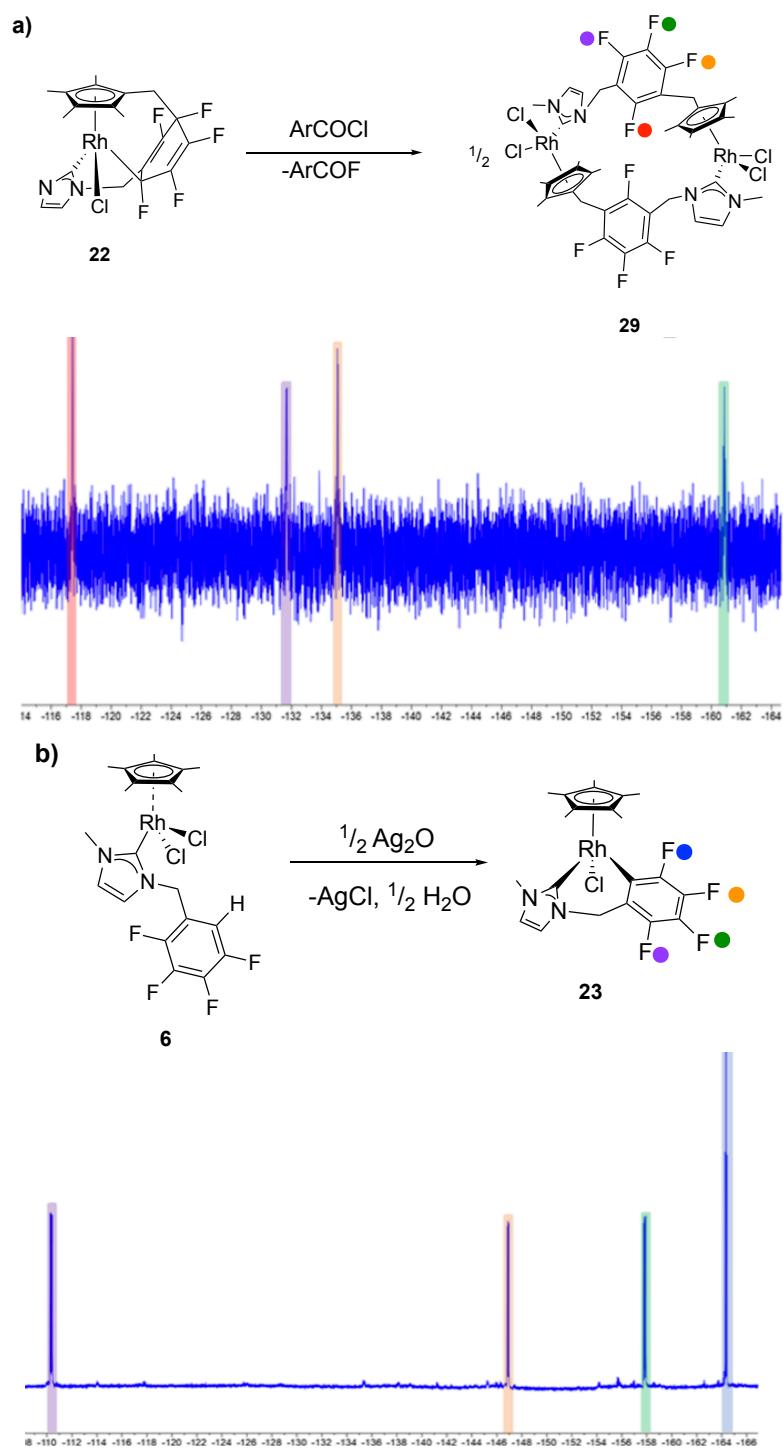
*Figure 4-3: (a, top) Transfer fluorination induced metallocycle formation of **29**, including ^{19}F NMR spectrum (a, bottom) showing four fluorine environments: −117.4 ppm (red), −131.1 ppm (purple), −135.1 ppm (orange), and −160.9 ppm (green). (b, top) Silver-particle induced orthometallation of **23**, including ^{19}F NMR spectrum (b, bottom) showing four fluorine environments: −110.4 ppm (purple), −146.9 ppm (orange), −158.0 ppm (green), and −164.4 ppm (blue). NMR carried out in deuterated chloroform.*

4.4 Structural characteristics of the rhodacycle, **29**

29 reformed a piano-stool structure with bond angles consistent with octahedral geometry (Figure 4-4); Cl(1)−Rh−Cl(2) 86.60(2)°, Cl(1)−Rh −C(11) 89.43(7)°, C(11)−Rh−Cl(2) 91.70(7)° following the distortion observed in **22** due to cyclometallation. Bond lengths for the partially fluorinated phenyl rings are between 1.374 and 1.389 Å, which are consistent with data for typical phenyl ring systems,[309] corresponding to the regeneration of aromaticity. It is also evident that the carbon atoms of the ring system have shifted in-plane, with an RMS deviation of 0.004 Å, corresponding to the "flatness" of the ring system.
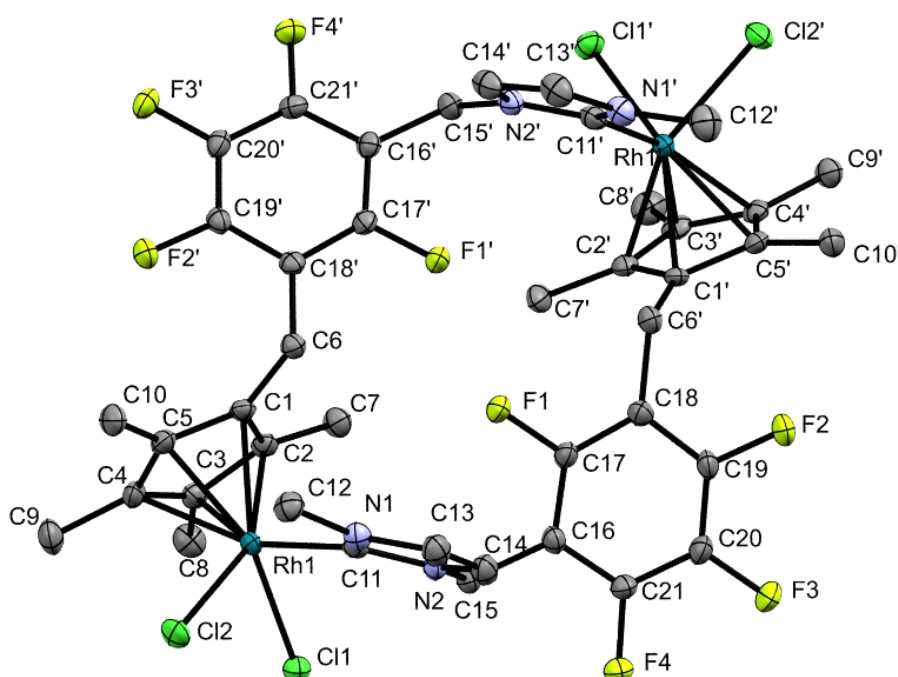
*Figure 4-4: Molecular structure of **29** highlighting the corresponding atom labels. These labels are used for reference for discussion in Section 4.4.*

Density functional theory (DFT) calculations, carried out in collaboration with Magnus Hanson-Heine at the University of Nottingham, proved valuable in comparing the experimental observations to computational theory calculated for **29**. The bond lengths calculated for the optimized geometry of **29** are within 0.077 Å from the experimental data (Table 4-1). The largest deviation occurs for the Rh−Cp* bond lengths where Rh(1)'−C(4)' has a difference of 0.077 Å. Rh(1)−C(4) has a bond length variation of 0.07 Å. The calculated Rh(1)'−C(5)' bond length shows only a slight variation from the experimental result, with a

difference of just 0.003 Å. There is a relatively large deviation in the observed and calculated bond distances between the calculated C−F bond lengths, where the difference observed for the C(17)−F(1) is 0.027 Å, whereas the C(21)−F(4) difference is 0.001 Å. However, these effects may be due to the complex non-bonding interactions affecting F(1), which will be discussed later in *Section 4.4*. The selected bond angles show very close agreement with the experimental results, and the largest deviation of 1.93° observed between C(1)−C(6)−C(18'). Table 4-1 highlights selected bond lengths and angles for both the calculated and experimental data.

*Table 4-1: Selected experimental and calculated bond lengths (Å) and bond angles (°) for **29**.*

	Experimental	**Calculated**	**Difference**
Cp*–Rh[a]	1.8093(2)	1.8550	0.045
Rh–C(11)	2.063(3)	2.036	0.027
Rh–Cl(1)	2.4012(6)	2.414	0.012
Rh–Cl(2)	2.4129(6)	2.430	0.017
C(6)–C(18')	1.518(3)	1.512	0.006
C(17)–C(18)	1.386(3)	1.390	0.004
C(20)–C(21)	1.384(4)	1.392	0.008
C(17)–F(1)	1.349(3)	1.333	0.016
C(19)–F(2)	1.341(3)	1.333	0.008
C(20)–F(3)	1.353(3)	1.328	0.025
C(21)–F(4)	1.345(3)	1.344	0.001
Cp*–Rh–C(11)[a]	130.982(8)	132.34	1.36
Cp*–Rh–Cl(1)[a]	120.930(5)	121.35	0.42
C(1)–C(6)–C(18')	111.3(2)	113.23	1.93
C(1')–C(6')–C(18)	113.3(2)	113.33	0.03
C(17)–C(18)–C(19)	115.39(2)	115.61	0.22
C(16)–C(17)–C(18)	126.1(2)	125.17	0.93
Cl(1)–Rh–Cl(2)	86.60(2)	87.73	1.13
N(2)–C(15)–C(16)	111.0(2)	112.26	1.26

[a]Cp* represents the centroid of the η^5-pentamethylcyclopentadienyl ring

The fluorine substituents have a noteworthy influence on the structure of the phenyl ring. The bond angles of the fluorine substituted ring show a non-ideal or distorted orientation (Figure 4-5). The presence of the fluorine atom (F(1)), results in a relatively large angle contortion from the ideal 120° for C(16)–C(17)–C(18) of +5.52°, resulting in puckering of the adjacent carbon centres C(17)–C(18)–C(19) and C(17)–C(16)–C(21) angles by -4.61° and -4.12° respectively. This is a known phenomenon, where substituent effects result in the distortion the phenyl ring,[310] however this effect can similarly be observed in strained systems.[311] The observed bond angles are consistent with the calculated bond angles and this observed distortion in bond angle from ideal (120° for benzene) is consistent with other 2,4,5,6-tetrafluorophenyl groups, although with a more pronounced deviation from ideal.[312, 313]
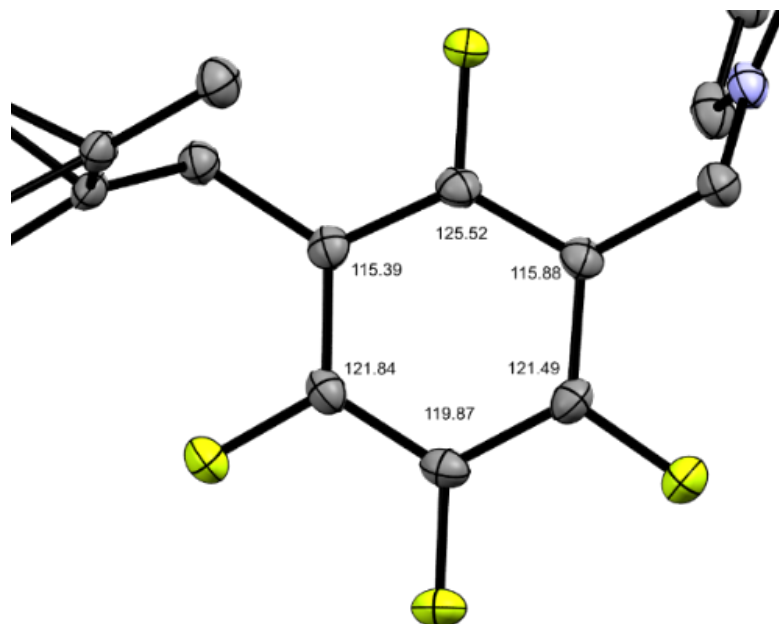
*Figure 4-5: Partial molecular structure view of **29** with bond angles labelled, showing 50 % thermal ellipsoid probabilities. The labelled angles highlight the distortion of the ring system, highlighting the puckering observed between adjacent carbon atoms.*

Analysis of the molecular structure of **29** also suggested the presence of non-covalent interactions between F(1) and F(1)' with an interatomic distance of 2.59(2) Å. This is significant as the interatomic distance is less than the sum of their two van der Waals radii.[314] The interatomic distance (2.59(2) Å) and torsion angle of ∠ C−F ⋯ F-C = 136.64(1)° is consistent with other fluorine (halogen) bonding systems.[315] These so called closed shell weak interactions for F⋯F bonding occur with an interatomic distance of between 2.3 and 2.8 Å, and can result in up to 14 kcal/mol of local stability.[316] However, the *trans* arrangement of the C(17)-F(1)⋯F(1)'-C(17)' contact, with bond angles of 143.09(2)° and 138.57(2)° respectively (Figure 4-6), is characteristic of a type I halogen bonds, which provides very low stabilization of crystal packing.[317, 318] These type I electrostatic interactions between the fluorine atoms occur due to the geometry constraints of the metallocycle.[319] The formation of a halogen bond between F(1) and F(1)' could be responsible for the deshielding effect observed for this fluorine atom within ^{19}F NMR, as electron density moves towards the central cavity of the metallocycle, in the form of non-covalent interactions. With a chemical shift of -117.4 ppm this fluorine resonance displays a downfield shift with respect to the other fluorine atoms within the phenyl ring consistent with a change in electron environment. Additionally, the observed lengthening of the C(17)–F(1) bond, coupled with the bond angle distortion centred at C(17) corroborate the presence of halogen bonding between these two fluorine atoms.
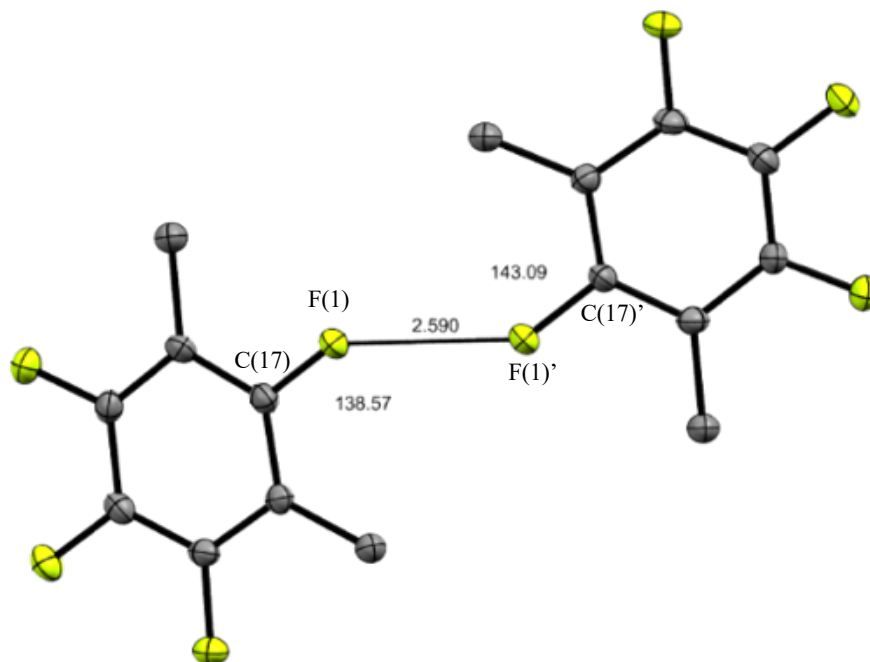
*Figure 4-6: Partial molecular structure of **29** highlighting interatomic distance between F(1) and F(1)'and the C(17)-F(1)···F(1)' and C(17)'-F(1)'···F bond angles highlighting the type 1 halogen bond trans-arrangement. The two fluorine atoms F(1) and F(1)' have an interatomic distance less than the sum of their two van der Waals radii*

Unlike other halogen bonding systems which can develop type II halogen bonding, which have a greater stabilization effect, the low polarizability of fluorine often restricts the formation of the σ-holes necessary for this type II interaction to occur. Therefore very few F···F type II interactions are found in the literature.[320] However, type I F···F interactions can be strengthened through the presence of cooperative noncovalent forces, such as hydrogen bonding.[321] It is these cooperative non-covalent interactions, which could be instrumental in providing localized stabilizing effect, enabling the selective recrystallisation of **29** observed.

Further computational analysis of the structure of **29**, gave insights into the observed halogen bonding effects observed from the experimentally determined molecular structure. The presence of type I fluorine interactions within the system was confirmed using the atoms in molecules (AIM) analysis of the electron density. AIM analysis indicates the presence of a roughly tetrahedral arrangement of bonds forming in the central cavity of **29** comprised of the F···H, H···H, and F···F interactions, as indicated by the bond paths and bond critical points (BCP) shown in Figure 4-7 and Table 4-2. This provides further evidence of cooperative noncovalent effects, with the F···F interaction being the strongest of these interactions.
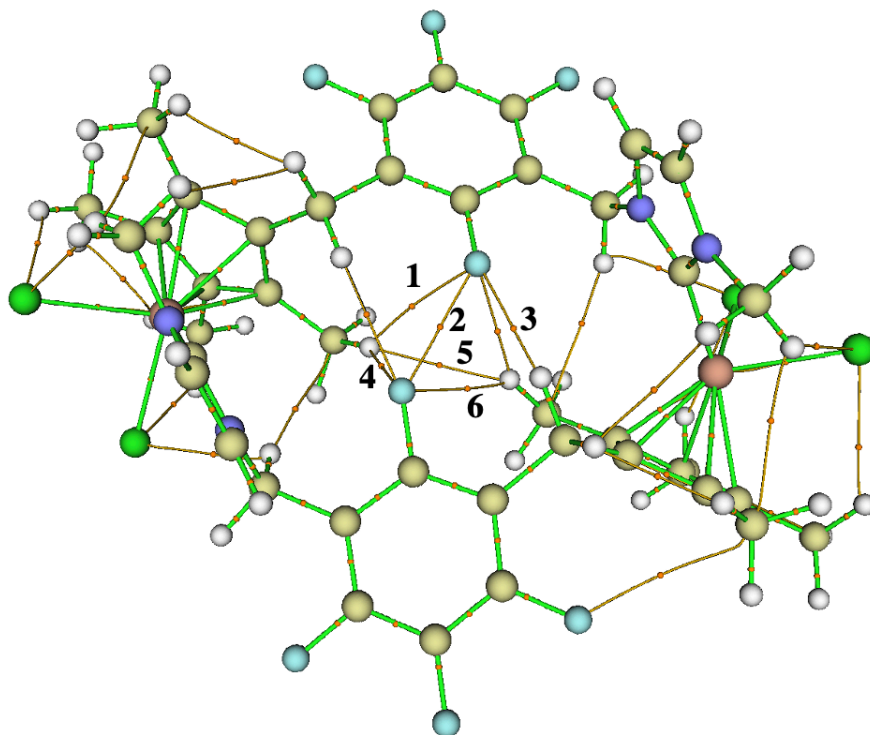
*Figure 4-7: Bond critical points (orange dots) and pathways (orange lines) calculated for **29** using QTAIM. A tetrahedron of interatomic interactions is located within the cavity of the rhodacycle. Numbering indicates the bond critical paths highlighted in Table 4-2.*

*Table 4-2: Interatomic distances, electron densities and laplacians of the electron density associated with the bond critical points (BCP) in the central cavity of **29**.*

BCP	Character	R (Å)	$\rho_{BCP} \times 10^{-2}$ (a.u.)	$\nabla^2 \rho_{BCP} \times 10^{-2}$ (a.u.)
1	F···H	2.798	0.36	1.94
2	F···F	2.576	1.21	5.99
3	F···H	2.442	0.80	3.54
4	F···H	2.430	0.82	3.61
5	H···H	2.552	0.33	1.19
6	F···H	2.749	0.40	2.13

4.5 Investigating rhodacycle transfer fluorination

To investigate the applicability of transfer fluorination and the formation of **29** the fluorination of additional substrates and functional groups was carried out (Table 4-3). This transfer fluorination system was not limited to the use of toluoyl chloride as a substrate, with transfer fluorination occurring more rapidly upon treatment of **22** with anhydrides, resulting in up to *ca*. 50 % contained yield of the resultant acyl fluoride product. Unlike in the case of toluoyl chloride, the acyl fluoride product formed upon fluorination with acetic anhydride was detected in as little as 10 minutes after addition.

Acetic anhydride rapidly underwent fluorination resulting in 11 % yield of acetyl fluoride over 10 minutes, with 12.5 % conversion to **29** (Table 4-3; entry 1). Similarly, rapid transfer fluorination was observed upon reaction with benzoic anhydride, resulting in 48 % formation of benzoyl fluoride and 50 % conversion from **22** to **29** (Table 4-3; entry 2) over the course of 30 minutes. Reduced activity was observed for butyric anhydride, resulting in 28 % conversion to butyryl fluoride and **29** over 20 hours (Table 4-3; entry 3). For each of the anhydrides tested, the acyl fluoride products were detected after 10 minutes highlighting the speed at which this spontaneous reaction can occur.

The reactivity observed for anhydrides is in contrast to that observed for acyl chlorides, where the fluorinated product was first identified following 4 hours. While initial results on transfer fluorination with toluoyl chloride found 13 % conversion to the analogous fluoride over 1 week, this was improved upon during development of the system used within this substrate scope, to give 18 % conversion of toluoyl fluoride after 72 hours (Table 4-3; entry 4). Similar lower activity was also observed in the case of benzoyl chloride (Table 4-3; entry 5).
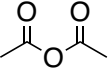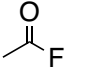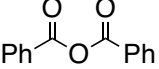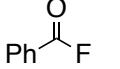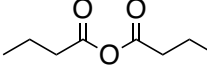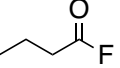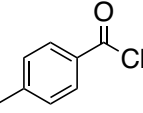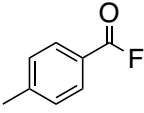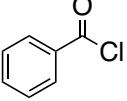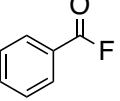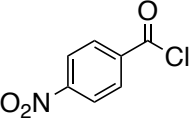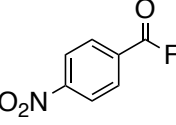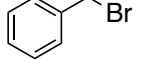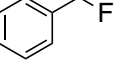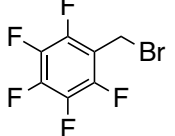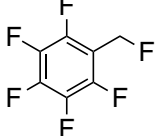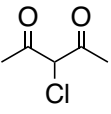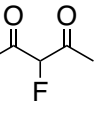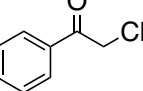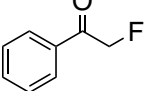
Transfer fluorination attempts with additional substrates proved less successful. Surprisingly, 4-nitrobenzoyl chloride was found to have low activity towards fluorination under these stoichiometric transfer fluorination conditions (Table 4-3; entry 6), unlike the relatively high rate of fluorination observed for the catalytic methodology described in *Section 3.5*. The reaction of **22** with both benzyl bromide and the more electron deficient fluoroalkyl substrate 2,3,4,5,6-pentafluorobenzyl bromide also resulted in reduced fluorination, over the course of one week (Table 4-3; entry 7 & 8 respectively). However, these results do show that transfer fluorination reactions using acyl chlorides, anhydrides and alkyl halides are feasible. Finally, 3-fluorohexa-2,4-dione and 2-fluoroacetaphenone were detected in trace quantities by ^{19}F NMR upon treatment with **22** over the course of 7 days (Table 4-3; entry 9 & 10 respectively). No further reaction was observed over timescales up to 1 month. Due to the reduced degree

of fluorination for these less electrophilic substrates further substrate scope and functional group tolerance were not conducted.

The rate of fluorination of toluoyl chloride under these transfer fluorination conditions was then examined (Figure 4-8). As noted earlier, toluoyl fluoride was first identified after 4 hours, leading to 13 % contained yield of the fluorinated product after 20 hours. The rate of formation of toluoyl fluoride reduced significantly as the reaction progressed, with a 23 % contained yield of toluoyl fluoride observed after 5 days. At this point no **22** remains in solution, with only toluoyl fluoride, **29** and **6** detected by ^{19}F NMR. As the concentration of **22** decreases in solution over time, so does the rate of fluorine transfer between **22** and toluoyl chloride. This is consistent with the rate of dimer formation becoming increasingly limited by the reducing concentration of **22** in solution.

Table 4-3: Summary of the transfer fluorination reaction scope including substrate, product, time and ^{19}F NMR conversion.

Entry	Substrate	Product	t	^{19}F NMR yield of fluorinated product (%)[a]	Conversion to *29* (%)
1			10 min	11.2	12.5
2			30 mins	47.7	49.7
3			20 h	28.3	28.5
4			72 h	18.0	20.8
5			72 h	15.9	16.1
6			1 week	7.7	ND
7[c]			1 week	7.5	11.6
8[c]			1 week	9.9	12.5
9[c]			1 week	trace	ND
10[c]			1 week	trace	4.2
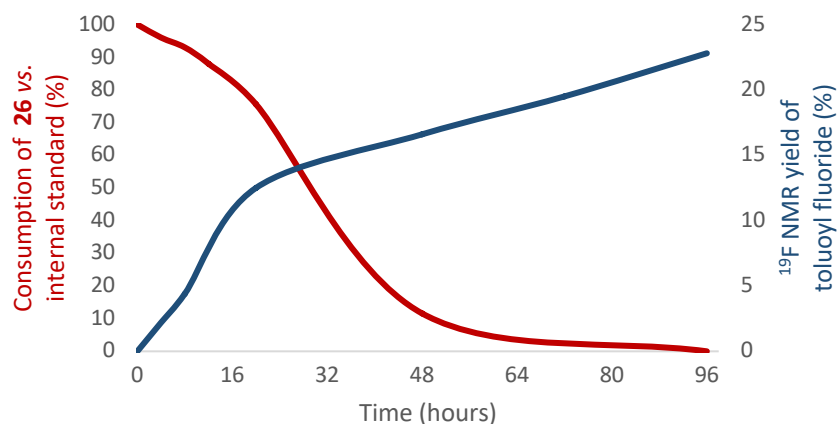
*Figure 4-8: Plot of the rate of formation of toluoyl fluoride (dark blue; ascending left to right) and consumption of **22** (red; descending left to right) over 96 hours, monitored over time via ^{19}F NMR.*

After investigating the formation of the fluorinated products under stoichiometric conditions and examining the brief reaction scope for this newly developed transfer fluorination protocol, further studies to determine the mechanism of fluorination were required. This would allow for a greater understanding of how nucleophilic fluorine was generated within this system, and whether "simple" transfer of fluorine from the perfluorinated ligand to the acyl chloride substrate was occurring. A multi-spectral approach was applied, where appropriate data collected from NMR, MS, FTIR and UV/Vis, in conjunction with computational calculations, to provide a comprehensive understanding of how the environment of **29** promotes transfer fluorination.

Acetic anhydride was found to be the best substrate tested for *in-situ* FTIR monitoring due to the shorter timeframes required for the experiment, as opposed to acyl chlorides, in which the time scale of reactivity were too long for this technique to be accessible. The IR probe was added to a Schlenk tube containing acetic acid and **22** in dry, degassed acetonitrile, following modified conditions (*Section 4.6.3*) and the reaction was monitored over time. During the course of the experiment, the C-O band at 1268 cm^{-1}, corresponding to the acetic anhydride substrate, and a C−F band of **22** at 1386 cm^{-1} reduced in intensity, alongside the formation of a new band at 1346 cm^{-1} consistent with the new acyl fluoride species (Figure 4-9). The formation of the acetic acid by-product was also identified through the growth in intensity of a C-O(H) band at 1130 cm^{-1}, consistent with the dissociation of the $[CH_3C(O)O]^-$ moiety alongside acetyl fluoride formation. Both of these substituents were identified by MS.
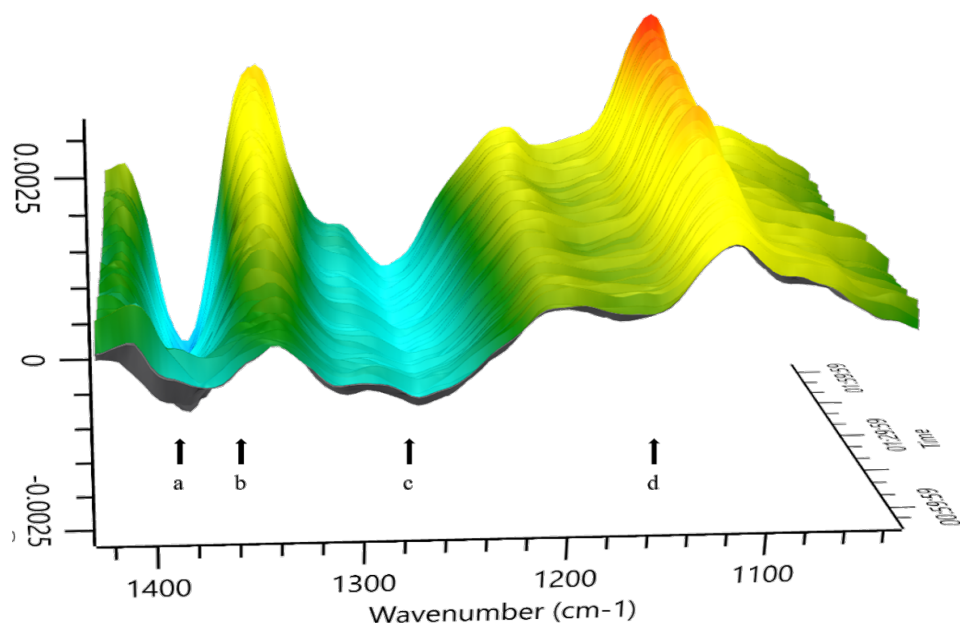
Figure 4-9: 3D surface plot for reaction of 1 (20 mg) with acetic anhydride (35 μL) in acetonitrile (5 mL). The peaks associated with the solvent, acetic anhydride, and 1 have been subtracted from the plot to allow for changes over time to be observed. The changes that occur over time include (from left to right) (a) the cleavage of a C−F bond of 1 at 1386 cm−1, (b) formation of a new C−F (COF) bond at 1346 cm−1, (c) cleavage of a C−O bond from acetic anhydride at 1268 cm−1, and (d) formation of a new C−O(H) group as by-product at 1130 cm−1.

Plotting the rate of formation of acetyl fluoride against the rate of consumption of the C−F bond associated with the perfluorinated ligand of **22** results in a linear regression plot (Figure 4-10). This shows that the rate of formation of acetyl fluoride is directly proportional to the rate of C−F bond activation. This correlation signifies that the fluorine incorporated in the acyl fluoride product comes directly from the perfluorinated ligand of **22**, confirming that the transfer of fluorine between a perfluorinated moiety and organic substrate is occurring and providing first evidence of a methodology of fluorine tracking. This confirms the applicability of ReactIR as an *in-situ* monitoring technique for transfer fluorination systems is appropriate, as the transfer of fluorine between substrates is observed.
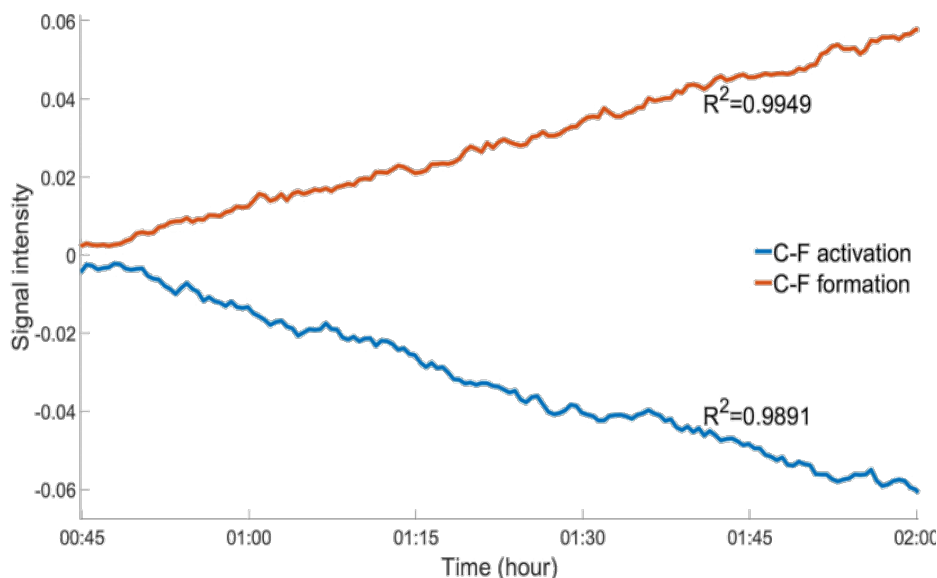
Figure 4-10: Plot of the rate of change of C−F bond fission (1386 cm−1) and C−F bond formation (1346 cm−1) over the course of the reaction highlighting the correlation between the two linear regression plots. The rate of C−F activation is proportional to the rate of C−F bond activation.

The evidence gathered from ^{19}F NMR, XRD and FTIR confirms that this reaction occurs through the activation of the perfluorinated ring of **22**, liberating nucleophilic fluorine, which undergoes nucleophilic attack of the organic electrophiles. We can also see from the molecular structure of **29** that intermolecular defluorinative coupling results in the formation of the rhodacycle. However, the spectroscopic methods described above provide insufficient data to conclude how this intermolecular defluorinative coupling occurs, post-fluorine transfer.

The re-aromatisation of the polyfluorocyclohexa-1,4-diene substituent from **22** to **29** results in a conformational change, caused by cyclic ring conversion from boat to planar geometry, resulting in concurrent ligand dissociation. Dissociation of either the Cp* or NHC ligand from the metal could be envisioned to alleviate conformational strain within the system, which could be a vital requirement for the formation of **29**. The formation of **29** is therefore proposed to occur following one of two pathways following acyl fluoride formation *via* fluorine transfer (Scheme 4-5);

i)   fission of the Rh-Cp* bond in **22** leading to the formation of a zwitterionic fragment, which rapidly undergoes intermolecular homo-dimerization with a second fragment

ii)   dissociation of the Rh-NHC bond forming a 16-electron neutral intermediate, which then undergoes recombination

i)

ii)
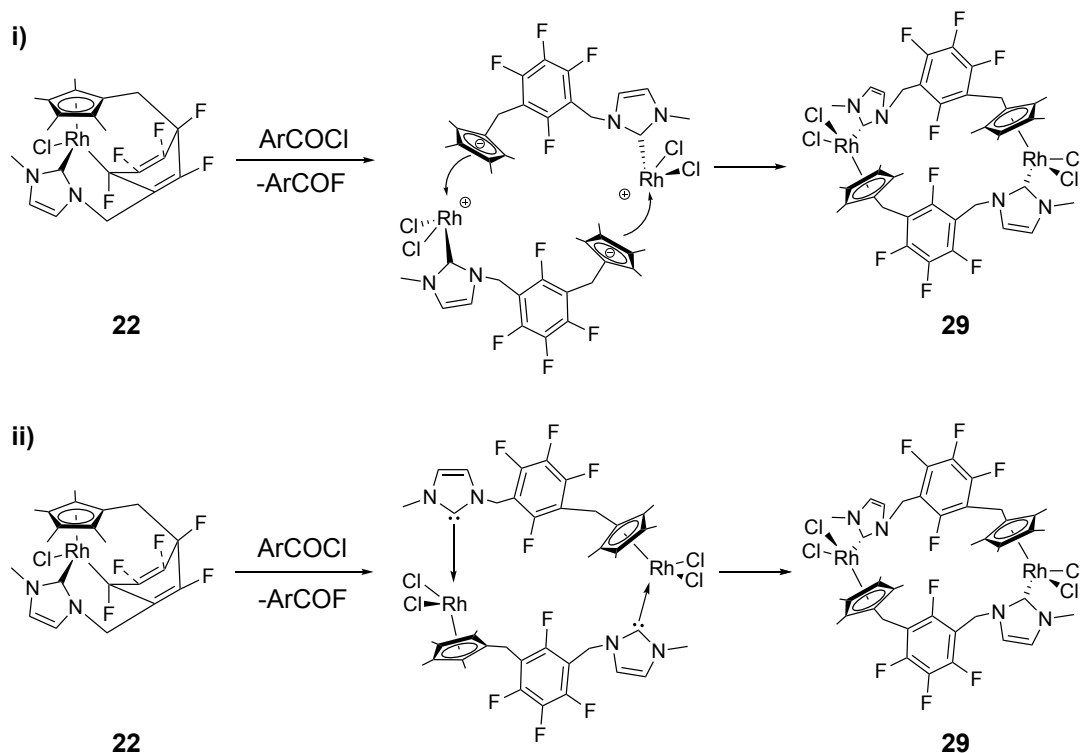
Scheme 4-5: Reaction of 22 with toluoyl chloride (i) showing dimerization of zwitterion following fission of the Rh−Cp* bond or (ii) showing recombination of free NHC to the neutral 16-electron Rh complex, resulting in the formation of 29. Further development lead to the discovery of photo-initiated activation of this reaction, which led to pathway i being the most favoured route.

From initial observation of these two pathways, pathway (ii) appears to be the most likely to occur, as it could be thought of qualitatively as a lower energy pathway than the fission of a η^5-metal-Cp* bond, leading to a charged zwitterionic species. Further experiments were required to gather quantitative data to differentiate which mechanism is the most likely to occur.

The photolysis of metal-Cp* bonds is a known process.[322-324] Brubaker and Lee reported in 1976 evidence of metal−Cp* bond migration and exchange promoted *via* photoexitation, resulting in the formation of a dimeric complex. It was found that metal−Cp* migration occurred slowly under thermal exchange conditions, resulting in roughly 10 % formation of the exchange products over 1 week, compared to 50 % over 24 hours *via* photoexcitation.[323] If the major reaction pathway described in Scheme 4-5 proceeds *via* pathway (i), through the fission of the metal−Cp* bond, it could be envisioned that photolysis with high intensity UV light would promote this transformation, and thus the reaction would occur more readily. Alternatively, if similar reactivity to the standard thermal route was observed following photolysis, this may provide evidence that pathway (ii) may be favoured.

To investigate whether photoinitiated Rh−Cp* bond migration was occurring the reaction mixture was exposed to high intensity UV light. UV photolysis experiments was carried out using a high intensity mercury arc lamp, which was filtered using Pyrex and Newport FSQ-BG40 glass bandpass filters to limit irradiation of the sample to 308 and 360 nm wavelengths. Photolysis was achieved by exposing a mixture of toluoyl chloride and **22**, in dry, degassed acetonitrile within an inert quartz reactor to UV light.

Sampling this reaction over time, under a dynamic flow of argon, showed the rapid formation of both toluoyl fluoride and **29** over the course of thirty minutes. After this time had elapsed the formation of toluoyl fluoride plateaued. ^{19}F NMR analysis of the reaction mixture after 30 minutes of irradiation gave a conversion of 40 % formation of toluoyl chloride, calculated against the internal standard, trifluorotoluene. UV irradiation resulted in a higher overall yield of the fluorinated product under reduced time. The formation of toluoyl fluoride and **29** were formed in a 1:1 ratio, consistent with the results observed *via* the thermal route. During the course of the reaction, an orange precipitate was found to form on the surface of the walls of the quartz reactor, following exposure to UV light. Analysis of this orange powder following isolation confirmed the formation of **29**.

Similarly, UV/Vis analysis of samples taken during the course of exposure displayed distinct changes occurring to the absorption spectra over the course of the reaction (Figure 4-11). The absorbance bands maximum associated with **22** at 259 nm was found to undergo blueshift, to 252 nm, coupled with the decrease in intensity of the absorption band at 328 nm, while a new absorption band at 408 nm, associated with **29**, grew in intensity. These results highlight the rapid transformation that occurs within this system upon exposure to UV irradiation, which is not observed when this reaction is carried out in darkness.

These results confirm that photoexitation of **22**, in the presence of toluoyl chloride, causes the rapid formation of **29** and results in photoinitiated transfer fluorination. Interestingly, these result show noticeable comparisons to the work conducted by Brubaker and Lee, particularly with regards to the observed differences in reactivity between the standard thermal route and photoactivation. Given that photoexcitation of toluoyl chloride and **22** result in a 40% conversion to toluoyl fluoride over 30 minutes compared to the thermal route, which initially gave 13% conversion to toluoyl fluoride over 1 week (Table 4-4), a similar process of metal-Cp* bond activation and migration is proposed to occur.
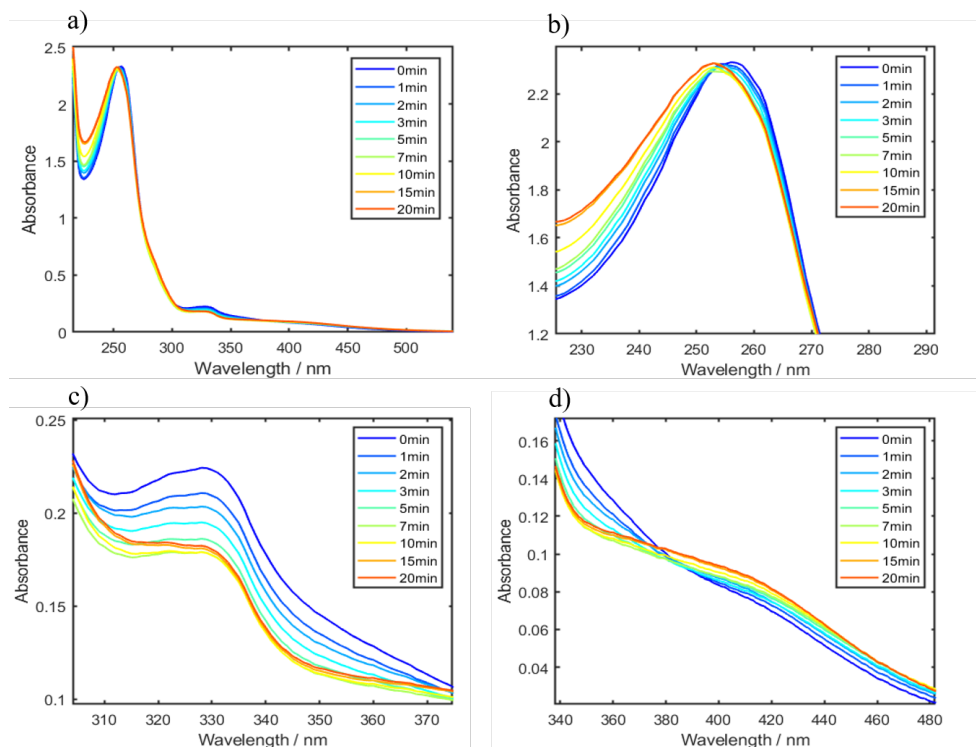
*Figure 4-11: (a) UV/vis plot of the photolysis of **22** with toluoyl chloride over time. (b) Shift of maximum peak to 252 nm. (c) Reduction in intensity of 330 nm band. (d) Appearance of a new band at 395 nm.*

*Table 4-4: Observed differences in the contained yield of toluoyl fluoride upon treatment with **22** under thermal and photoactivation routes for the reaction described above and the similarities compared to that proposed by Brubaker.[324]*

	Thermal		Photoactivation	
	Conversion (%)	Time	Conversion (%)	Time
Our method	13	1 week	40	0.5 hours
Brubaker method	10	1 week	50	24 hours

These experiments act to highlight the promotion of reactivity *via* Rh−Cp* fission and exchange under photoexcitation conditions. However, while photoactivation of this reaction was confirmed, this cannot rule out photoactivation of the Rh−NHC bond, although literature precedent suggests otherwise. Indeed, under standard thermal conditions either pathway may contribute to the observed reactivity.

Finally, DFT calculations contributed towards an understanding of the environment required to generate nucleophilic fluorine within **22**. Fluorine interaction energies, indicating the strength of the C−F bond, were calculated for the C−F bonds of the polyfluorocyclohexa-1,4-diene ring in **22**, indicated that the fluorine atoms that are displaced away from the plane of the ring (bonds 1 and 4) have interaction energies *ca.* 50 kJ/mol lower than the co-planar C−F

bonds of 2, 3 and 5 (Table 4-5). The C−F bond bound to the tethered Cp* ring (bond 1) was calculated to have the weakest overall fluorine interaction energy, at 6 kJ/mol lower than the fluorine atom attached to the metal bound carbon (bond 4). These results are in close approximation to the experimentally determined results, showing that the longest C−F bond length (1.394(7) Å), with the weakest interaction energy is the same bond that is observed to undergo C−F bond activation and dissociation resulting in fluorine transfer.

*Table 4-5: Calculated fluorine atom interaction energies and natural population analysis for **22**. Associated bonds are given in Figure 4-12.*

Bond	Fluorine Interaction Energy (kJ/mol)	Natural Population Analysis
1	446	0.372
2	498	0.333
3	501	0.305
4	452	0.373
5	502	0.349

These computational results also showed a weaker bonding interaction for the C−F bond closest to the metal centre (bond 4) compared to the co-planar fluorine atoms. Due to the similarity in the calculated fluorine bond dissociation energy between bond 1 and 4, it could be envisioned that bond 4 may also undergo C−F bond activation. While this has not been observed experimentally, buried volume calculations showed that activation at the site of fluorine atom (bond 4) was disfavoured, underscoring the importance of steric effects on this fluorine atom within the coordination sphere of the complex, in addition to proximity to the metal centre.

Natural population analysis, a measure of electron density found on an atom, were also calculated for the fluorine atoms on the ring. The fluorine atoms displaced away from the plane of the ring, bond 1 and 4, were found to have the most negative overall atom charges at 0.372 and 0.373 respectively (

Figure 4-12). This means that greater electron density is located on these fluorine atoms, compared to the planar fluorine atoms, rendering the fluorine atoms 1 and 4, more nucleophilic.
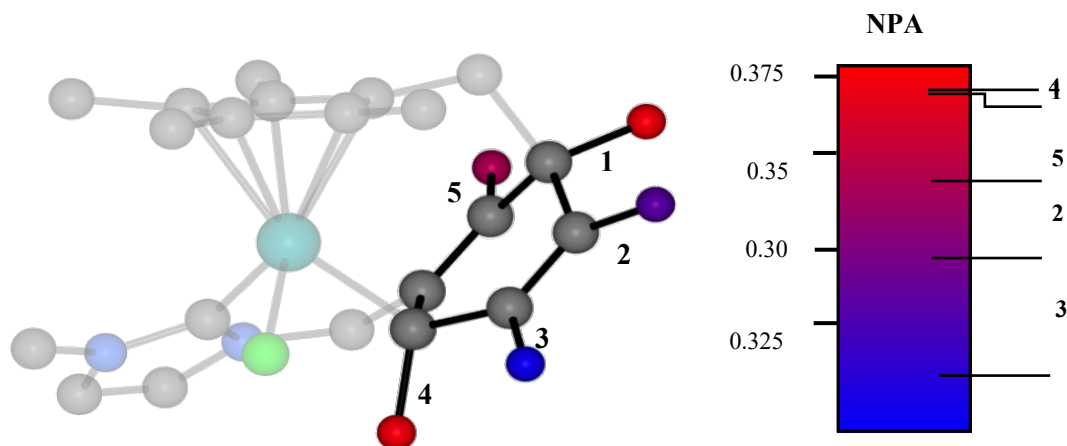
*Figure 4-12: Optimized geometry of **22** with the polyfluorocyclohexa-1,4-diene region highlighted (left). The colour of the fluorine atoms has been changed to correspond with their natural population analysis (NPA) as given in the gradient scale (right). The calculated fluorine atom interaction energies and the relative charge from natural population analysis for bonds 1−5 are given in Table 4-5.*

In conjunction, the results gathered from the different spectroscopic techniques suggest that the greater electron density located on fluorine atoms 1 and 4, renders these fluorine atoms more nucleophilic, which when coupled with the weaker C−F bond strength calculated *via* fluorine interaction energies give an environment in which C−F bond activation occurs spontaneously resulting in the formation of nucleophilic fluorine. This transfer fluorination system is a good example where computational calculations can be use in concert with experimental observations to give a better understanding of the physical phenomena occurring.

4.4 Summary

The work carried out as part of this chapter describes one of the first examples of transfer fluorination between a perfluorinated group and an organic electrophile. This methodology results in the selective defluorination of a non-innocent perfluorinated ligand resulting in the formation of a monodefluorinated bimetallic rhodacycle. The concerted C−F bond activation and formation reaction, in which nucleophilic fluorine is generated following C−F bond activation, results in the fluorination of an external organic electrophile, without the formation of deactivated fluorine bonds such as H−F, Si−F or B−F and without producing fluorine containing waste.

Multi-spectral analysis has been used to confirm fluorine transfer from the perfluorinated ligand of **22** to the electrophile is occurring, resulting in the formation of the fluorinated product and **29**. The data gathered from *in-situ* analysis, including FTIR, UV/Vis and ^{19}F NMR, in addition to the observations gathered from the crystal structure of **29** and computational theory provides an understanding of the environment required to initiate nucleophilic transfer fluorination. All these methodologies in cooperation were essential to understand the chemical nature required to generate nucleophilic fluorine within a perfluorinated group.

The structural environment of **22** renders the reactive C−F bond unusually electron rich, corresponding to the lowest fluorine interaction energy, one of the highest fluorine atom charges coupled with the most up-field chemical shift in ^{19}F NMR. Additionally, photoexcitation of **22** with toluoyl chloride gave the rapid formation of toluoyl fluoride and **29**, providing evidence towards the proposal of a reaction mechanism proceeding *via* Cp* migration.

4.6   Experimental

4.6.1   Instrumentation

NMR spectral analysis was carried out using a Bruker Ascend 400 spectrometer (400 MHz) and Bruker Ascend 500 spectrometer (500 MHz) at room temperature ($\approx$ 300 K). ^{1}H and ^{13}C NMR spectra were referenced to the corresponding residual solvent signals (CDCl$_3$: 7.26 ppm for ^{1}H, 77.16 ppm for ^{13}C). The ^{19}F NMR spectra were referenced by an internal method of the NMR. The chemical shifts are reported in ppm and coupling constants are given in Hz. NMR data was processed using MestReNova software. Multiplicity assignments in NMR spectra are labelled as follows: "s" = singlet, "d"= doublet, "t"= triplet, "q" = quartet, "p" = pentet, "m" = multiplet. NMR assignments for all synthesised complexes are given; ^{1}H NMR (green), ^{19}F NMR (red) and ^{13}C NMR (blue). Due to the 10 equivalents of substrate added during substrate scope investigation ^{1}H NMR analysis of products proved difficult in some cases due to overlapping signals. Electrospray mass spectra were recorded on a Bruker micrOTOF II with Agilent technologies 1200 Infinity Series mass spectrometer. *In-situ* ReactIR measurements conducted using Mettler Toledo ReactIR 15, collecting a spectral average of 256 scans at a scan rate of 256 scans per minute. Experiment set up and analysed using Mettler Toledo iC IR software. UV photolysis carried out using a high intensity mercury arc lamp, which was filtered using Pyrex and Newport FSQ-BG40 glass bandpass filter to limit irradiation of the sample by 308 and 360 nm wavelength. UV/Vis spectra were collected using an Agilent Cary 60 UV/Vis spectrophotometer, scanning from 800 nm to 200 nm at a scan rate of 600 nm/min. Glassware was oven-dried, evacuated and backfilled with argon before use.

4.6.2   Synthesis of **29**

Dichloromethane (5 mL) was added to a flask containing **22** (25 mg, 0.046 mmol). Once dissolved, toluoyl chloride (0.10 mmol, 2 equivalents) was added and the stirring (600 rpm) continued for 1 week. The reaction mixture was removed from the glovebox, and the solvent removed *in vacuo* resulting in an orange crystalline powder and an orange oil. CDCl$_3$ (0.5 mL) was added and the solution transferred to a Young's valve NMR tube under argon. Analysis of the ^{19}F NMR showed up to 30 % conversion of **22** to **29**. Toluoyl fluoride was extracted with ether and **29** was recrystallized from a saturated solution of dichloromethane.

Isolated yield of orange crystalline solid: 3.5 mg (13.7 % yield). **^{1}H NMR** (400 MHz, *d-chloroform*): δ 7.71 (d, $^3J_{HH}$ = 3.3 Hz, *H*CCH, 1H), 7.70 (d, $^3J_{HH}$ = 3.3 Hz, *H*CCH', 1H), 7.54 (d, $^3J_{HH}$ = 3.3 Hz, HCC*H*, 1H), 7.53 (d, $^3J_{HH}$ = 3.3 Hz, HCC*H'*, 1H), 5.82 (d, $^2J_{HH}$ = 16.5 Hz, C*H$_2$*, 2H), 5.56 (d, $^2J_{HH}$ = 16.2 Hz, C*H$_2$*, 2H), 4.05 (s, C*H$_3$*, 6H), 1.87 (s, C$_5$-C*H$_2$*, 4H), 1.77 (s, C$_5$-C*H$_3$*, 6H), 1.40 (s, C$_5$-C*H$_3$*, 6H), 1.25 (s, C$_5$-C*H$_3$*, 6H), 0.92 (s, C$_5$-C*H$_3$*, 6H). **^{19}F NMR** (376 MHz, *d-chloroform*): δ -117.43 (s, C$_6$-*F*, 1F), -131.12 (d, J_{FF} = 19.9 Hz, C$_6$-*F*, 1F), -135.12 (d, J_{FF} = 20.9 Hz, C$_6$-*F*, 1F), -160.86 (t, J_{FF} = 22.8 Hz, C$_6$-*F*, 1F). **^{13}C NMR** not as required. **MS** (ESI) of **29**: Theoretical for C$_{21}$H$_{21}$Cl$_1$F$_4$N$_2$Rh [M/2-Cl]$^+$ 515.0384; found [M/2-Cl]$^+$ 515.0389. Theoretical for C$_{42}$H$_{42}$Cl$_3$F$_8$N$_4$Rh$_2$ [M-Cl]$^+$ 1065.0457; found [M-Cl]$^+$ 1065.0445.
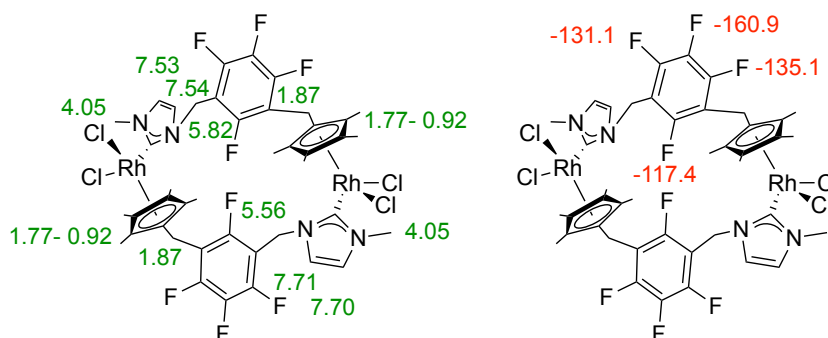
The formation of toluoyl fluoride was also identified by ^{19}F NMR: 1 mg (13.3 % yield; 97 % conversion vs 0.003 mmol of **29** formed.

^{1}H NMR (400 MHz, *d-chloroform*): δ 7.99 (d, $^2J_{HH}$ = 8.1 Hz, C$_6$-*H*, 2H), δ 7.27 (d, $^2J_{HH}$ = 8.1 Hz, C$_6$-*H*, 2H), 2.43 (s, Me, 3H). **^{19}F NMR** (376 MHz, *d-chloroform*): δ 17.30 (s, 1F, CO*F*). **MS** (ESI) of toluoyl fluoride: Theoretical [M-F]$^+$ [C$_8$H$_7$O]$^+$ 119.0497; found [C$_8$H$_7$O]$^+$ 119.0498.

4.6.3 ReactIR measurements

Dry, degassed MeCN (5 mL) was added to a Schlenk flask under argon. The IR probe was inserted under a positive pressure of argon and a background taken using Mettler Toledo iC IR software. The IR probe was lowered into acetonitrile and the experiment started. **22** (20 mg, 0.037 mmol) was added after five minutes, followed by acetic anhydride (35 µL, 0.37 mmol) after a further 20 minutes, once the IR signal of **22** plateaued. Changes that occurred were monitored over time *via* the "solvent abstraction" feature of the iC IR software showed a clear reduction in signal intensity at 1386 cm^{-1} (corresponding to **22**) and an increase in

signal intensity at 1346 cm^{-1} (corresponding to acyl fluoride), which became apparent at the 40 minute mark of the experiment. The reaction was monitored for 1 hour 30 minutes.

4.6.4   UV Photolysis

Toluoyl chloride (40 µL, 0.30 mmol) was added to a solution of **22** (27 mg, 0.05 mmol) in dry, degassed deuterated acetonitrile (5 mL) in an inert quartz reaction flask, fitted with a cuvette side arm (1 cm path length) under argon. The solution was transferred to the cuvette side arm, which was placed 5 cm in-front of a high intensity UV source from a mercury arc lamp. UV/Vis analysis was carried out by sampling the reaction mixture (0.1 mL reaction mixture made up to 10 mL with acetonitrile in volumetric flask) over time, under argon. During the course of the reaction an orange sediment formed on the walls of the cuvette facing the UV source, which was found to be **29** following ^{19}F NMR analysis and ESI-MS. The reaction mixture (0.5 mL) was transferred to Young's tap NMR tube under argon, with trifluorotoluene (2 µL) for NMR analysis after 30 minutes. ^{19}F NMR yield of toluoyl fluoride *vs* trifluorotoluene: 40 % yield.

4.6.5   DFT Studies

DFT geometry optimizations, transition state searches, NMR shifts, buried volume, energy and electron density calculations were performed with a developmental version of the Q-Chem software package.[325] Geometry optimization steps were carried out using the PBE0 exchange-correlation functional with the Los Alamos National Laboratory 2 double-ζ (LANL2DZ) pseudopotential and basis set used for the Rh atom and 6-31G(d) basis set for the lighter atoms.[326, 327] Geometries were confirmed as minima by the absence of imaginary harmonic vibrational frequencies present for these structures.

Energies and electron densities were then evaluated at these geometries using the 6-311++G(d,p) basis set for the light atoms and the Stuttgart Relativistic Small Core (SRSC) pseudopotential and basis set for rhodium.[328] Interaction energies for the fluorine atoms were calculated from the difference between the complex energy and the sum of the isolated F atom and remaining fragment energies using the counterpoise correction method to account for basis set superposition error with all the associated fragment calculations performed using the same basis set as the complete complex.[329] The interaction energies are given by Equation 1:

$$E_{int} = - [E(AB) - E(A) - E(B)] \qquad\qquad \mathbf{1}$$

where E(AB) is the energy of the whole molecule, E(A) is the energy of the molecule with the fluorine atom removed and E(B) is the energy of the isolated fluorine atom, and natural population analysis (NPA) was then used to determine the charge on each fluorine atom.[330]

^{19}F NMR chemical shifts were evaluated at the minima energy geometries using the gauge-invariant atomic orbital (GIAO) method with the B3LYP functional and a combination of the 6-31+G(d,p) basis for the atoms of the ring system, 6-31G(d,p) for all other non-metal atoms, and the all-electron 3-21G basis set for Rh.[331, 332] This level of theory was chosen to increase the applicability of established NMR scaling factors,[333] while avoiding issues with linear dependence in the basis set and convergence during the GIAO NMR calculation. The scaled chemical shifts were calculated using the formula given in Equation 2:

$$\sigma_{scaled} = \frac{\theta_{isotropic} - C}{M}$$

2

where $\theta_{isotropic}$ is the unscaled isotropic chemical shift, while M and C are the gradient and the y-intercept of the fitting data, with values of -0.9652 and 194.71, respectively.

4.6.5.1   Calculated ^{19}F NMR chemical shift of **6**.
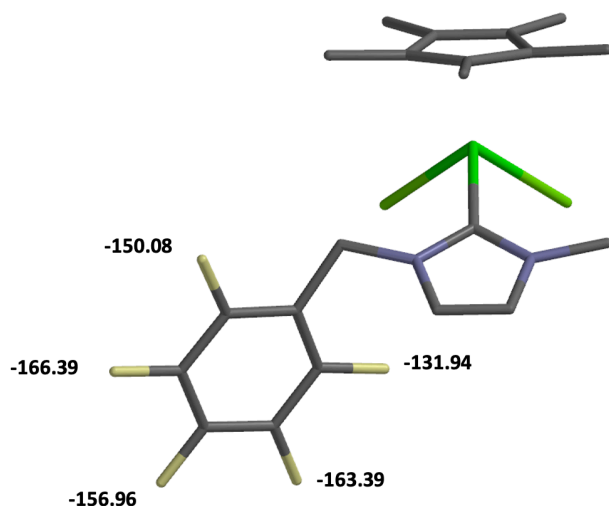
4.6.5.2 Calculated ^{19}F NMR chemical shift of **22**.
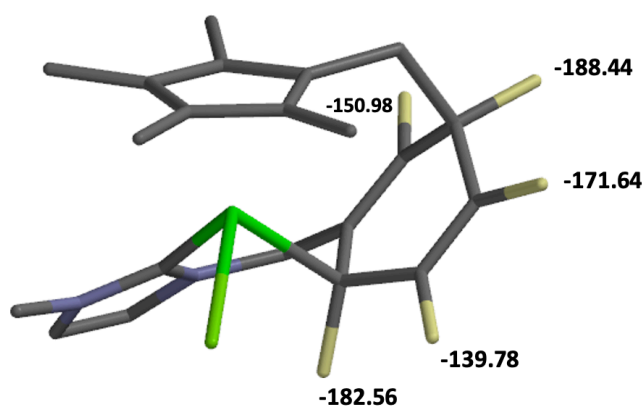
4.6.6 Transfer fluorination reactions

Due to substrate excess, ^{1}H NMR analysis prove difficult for some substrates. All product characterisation is consistent with previously reported literature.

4.6.6.1 Transfer fluorination reaction with acetic anhydride

Acetic anhydride (6 mg, 0.056 mmol) was added to a Young's tap NMR tube containing **22** (3 mg, 0.0056 mmol) in dry, degassed CD$_3$CN (0.5 mL), with trifluorotoluene (1 µL) under argon. The contents of the tube were shaken and NMR spectrum was recorded immediately. ^{19}F NMR yield *vs*. the internal standard after 10 minutes: 11.2 %.

^{19}F NMR (376 MHz, d_3-MeCN): δ 48.91 (q, J_{HF} = 7.3 Hz, CO*F*, 1F).[334]
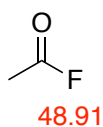
4.6.6.2 Transfer fluorination reaction with benzoic anhydride

Benzoic anhydride (13 mg, 0.056 mmol) was added to a Young's tap NMR tube containing **22** (3 mg, 0.0056 mmol) in dry, degassed CD$_3$CN (0.5 mL), with trifluorotoluene (1 µL) under argon. The contents of the tube were shaken and the reaction monitored *via* ^{19}F NMR over time. ^{19}F NMR yield *vs*. the internal standard after 30 minutes: 47.7 %.

^{1}H NMR (400 MHz, d_3-MeCN): δ 8.01 (d, $^2J_{HH}$ = 7.5 Hz, C$_6$-*H*, 2H), δ 7.56 (t, $^2J_{HH}$ = 8.1 Hz, C$_6$-*H*, 1H), 7.46 (t, $^2J_{HH}$ = 7.7 Hz, C$_6$-*H*, 2H). **^{19}F NMR** (376 MHz, d_3-MeCN): δ 16.57 (s,

CO*F*, 1F). **MS** (ESI): Theoretical [2M+K] [C₇H₅O]⁺ 249.0312; found for [C₇H₅O]⁺ 249.0523.
IR(*CO*F): 1812 (s) cm⁻¹.[250]
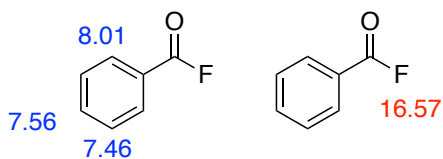
4.6.6.3 Transfer fluorination reaction with butyric anhydride

Butyric anhydride (12 mg, 0.056 mmol) was added to a Young's tap NMR tube containing **22**
(3 mg, 0.0056 mmol) in dry, degassed CD₃CN (0.5 mL), with trifluorotoluene (1 µL) under
argon. The contents of the tube were shaken and the reaction monitored *via* ¹⁹F NMR over
time. ¹⁹F NMR yield *vs*. the internal standard after 20 hours: 28.3 %.

¹⁹F NMR (376 MHz, *d₃*-MeCN): δ 43.10 (s, CO*F*, 1F).[334]
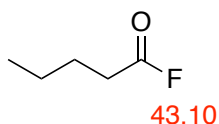
4.6.6.4   Transfer fluorination reaction with toluoyl chloride

Toluoyl chloride (9 mg, 0.056 mmol) was added to a Young's tap NMR tube containing **22** (3
mg, 0.0056 mmol) in dry, degassed CD₃CN (0.5 mL), with trifluorotoluene (1 µL) under
argon. The contents of the tube were shaken and the reaction monitored *via* ¹⁹F NMR over
time. ¹⁹F NMR yield *vs*. the internal standard after 72 hours: 18.0 %.

¹H NMR (400 MHz, *d₃*-MeCN): δ 7.92 (dt, $^2J_{HH}$ = 1.9, 8.2 Hz, C₆-*H*, 2H), δ 7.33 – 7.30 (m,
C₆-*H*, 2H), 2.42 (s, Me, 3H). **¹⁹F NMR** (376 MHz, *d₃*-MeCN): δ 15.85 (s, CO*F*, 1F). **MS**
(ESI): Theoretical [M]⁺ [C₈H₈O]⁺120.0569; found for [C₈H₈O]⁺120.0556. **IR**(*CO*F): 1805 (s)
cm⁻¹.[253]
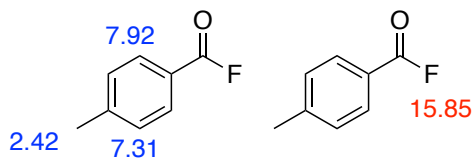
4.6.6.5 Transfer fluorination reaction with benzoyl chloride

Benzoyl chloride (8 mg, 0.056 mmol) was added to a Young's tap NMR tube containing **22** (3 mg, 0.0056 mmol) in dry, degassed CD_3CN (0.5 mL), with trifluorotoluene (1 μL) under argon. The contents of the tube were shaken and the reaction monitored *via* ^{19}F NMR over time. ^{19}F NMR yield *vs*. the internal standard after 72 hours: 15.9 %.

^{1}H NMR (400 MHz, *d-chloroform*): δ 7.96 (d, $^2J_{HH}$ = 7.5 Hz, C_6-*H*, 2H), δ 7.56 (t, $^2J_{HH}$ = 8.1 Hz, C_6-*H*, 1H), 7.43 (t, $^2J_{HH}$ = 7.7 Hz, C_6-*H*, 2H).**^{19}F NMR** (376 MHz, d_3-MeCN): δ 16.55 (s, CO*F*, 1F). **MS** (ESI): Theoretical [2M+K] $[C_7H_5O]^+$ 249.0312; found for $[C_7H_5O]^+$ 249.0523. **IR**(*CO*F): 1812 (s) cm^{-1}.[250]
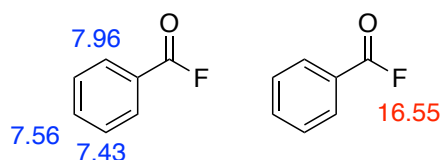
4.6.6.6 Transfer fluorination reaction with 4-Nitrobenzoyl chloride

4-nitrobenzoyl chloride (11 mg, 0.056 mmol) was added to a Young's tap NMR tube containing **22** (3 mg, 0.0056 mmol) in dry, degassed CD_3CN (0.5 mL), with trifluorotoluene (1 μL) under argon. The contents of the tube were shaken and the reaction monitored *via* ^{19}F NMR over time. ^{19}F NMR yield *vs*. the internal standard after 1 week: 7.7 %.

^{19}F NMR (376 MHz, d_3-MeCN): δ 19.69 (s, CO*F*, 1F).[7] **MS** (ESI): Theoretical [M+MeCN] $[C_7H_4NO_3]^+$ 191.0451 ; found for $[C_7H_4NO_3]^+$. 191.0931. [249]
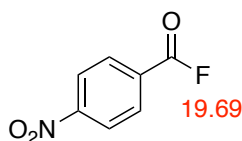
4.6.6.7 Transfer fluorination reaction with benzyl bromide

Benzyl bromide (10 mg, 0.056 mmol) was added to a Young's tap NMR tube containing **22** (3 mg, 0.0056 mmol) in dry, degassed CD_3CN (0.5 mL), with trifluorotoluene (1 μL) under argon. The contents of the tube were shaken and the reaction monitored *via* ^{19}F NMR over time. ^{19}F NMR yield *vs*. the internal standard after 1 week: 7.5 %.

^{19}F NMR (376 MHz, d_3-MeCN): δ -205.91 ppm (*t*, J_{FF} = 48.2 Hz, 1F).[335]

-205.91
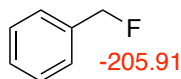
4.6.6.8 Transfer fluorination reaction with 2,3,4,5,6-(Pentafluorobenzyl) bromide

2,3,4,5,6-pentafluorobenzyl bromide (15 mg, 0.056 mmol) was added to a Young's tap NMR tube containing **22** (3 mg, 0.0056 mmol) in dry, degassed CD_3CN (0.5 mL), with trifluorotoluene (1 µL) under argon. The contents of the tube were shaken and the reaction monitored *via* ^{19}F NMR over time. ^{19}F NMR yield *vs*. the internal standard after 1 week: 9.9 %.

^{19}F NMR (376 MHz, d_3-MeCN): δ -211.79 (t, J_{HF} = 46 Hz, CO*F*, 1F) -144.51 (dd, J_{FF} = 14.0, 31.4 Hz, $C_3F_3C_2F_2C$), -155.77 (dt, J_{FF} = 14.2, 20.8 Hz, C_5F_4CF), -163.93 (m, $C_3F_2C_2F_2CF$).[336]

-163.93   -211.79   -155.77   -144.51
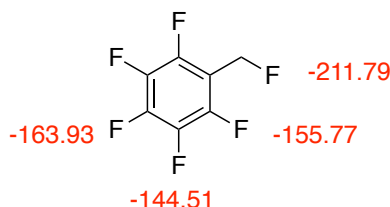
4.6.6.9 Transfer fluorination reaction with 3-Chloropenta-2,4-Dione

3-chloropenta-2,4-dione (14 mg, 0.056 mmol) was added to a Young's tap NMR tube containing **22** (3 mg, 0.0056 mmol) in dry, degassed CD_3CN (0.5 mL), with trifluorotoluene (1 µL) under argon. The contents of the tube were shaken and the reaction monitored *via* ^{19}F NMR over time. ^{19}F NMR yield *vs*. the internal standard after 1 week: trace.

^{19}F NMR (376 MHz, d_3-MeCN): δ -231.98 (s, CO*F*, 1F).[337]

-231.98
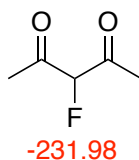
4.6.6.10 Transfer fluorination reaction with 2-Chloroacetaphenone

2-chloroacetaphenone (9 mg, 0.056 mmol) was added to a Young's tap NMR tube containing **22** (3 mg, 0.0056 mmol) in dry, degassed CD_3CN (0.5 mL), with trifluorotoluene (1 µL) under argon. The contents of the tube were shaken and the reaction monitored *via* ^{19}F NMR over time. ^{19}F NMR yield *vs*. the internal standard after 1 week: trace.

¹⁹F NMR (376 MHz, d_3-MeCN): δ -234.13 (t, J_{HF} = 45 Hz, CO*F*, 1F).[338]
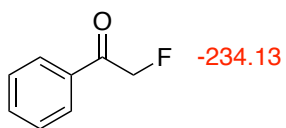
5 Chapter 5: Defluorination of heteroarenes

5.1 Overview

The defluorination of polyfluoroarenes is extremely important, especially when attempting to introduce new functionality at the site of C−F bonds *via* C−F bond activation. This can be carried out by introducing a proton at the site of C−F bond activation in a hydrodefluorination reaction, or through defluorinative substitution of polyfluoroarenes with other functional groups in order to access valuble partially fluorinated molecules.

This defluorinative process can be advantageous on an industrial level, as the synthesis of perfluorinated compounds is well established. The fluorine in these poly- or per-fluorinated compounds, which can readily be synthesised through the Halex, Balz-Schiemann or Fowler processes (as described in *Section 1.1*), can be utilised in the controlled cleavage of the C−F bond, giving access to valuble partially fluorinated compounds that can be difficult to synthesised from a "bottom up" approach.[339, 340] Accessing partially fluorinated fine chemicals often relies on the selective cleavage of C−F bonds, however the selective defluorination of perfluorinated organics still represents a significant challenge.[32, 341] Understanding the reaction chemistry of organo- and organometallo-fluorines is still at an early stage,[341, 342] and the reality is that useful fluorinations in industry are still dominated by expensive and wasteful stoichiometric reagents that contain highly activated fluorine atoms, resulting in unselective fluorination which creates fluorine and/or metal containing waste (*Section 1.1)*.

In recent years, the hydrodefluorination of polyfluoroarenes has been found to be a powerful methodology to access partially fluorinated molecules,[343-346] since first reported in 1994.[347] This process results in the formation of a C−H bond at the site of C−F bond activation, through treatment with a proton source, resulting in the partial defluorination of the substrate, forming fluorine containing waste. Traditionally, strong reducing agents such as silanes and boranes have been required to promote hydrodefluorination, due to the formation of strong Si−F and B−F bonds, which act as thermodynamic sinks for the reaction.

Utilising silanes as proton sources for the hydrodefluorination of fluorinated molecules has proved to be a very successful area of research, in part due to the thermodynamically favourable formation of the Si−F bond (> 190 kJ/mol).[348] Hydrodefluorination methodologies using silanes have been able to access a range of partially defluorinated molecules from aromatic and aliphatic fluoroorganics including fluorobenzenes,[349-355] fluoropyridines,[350] polyfluorocyclohexane,[356] and perfluoroalkyl groups.[348, 357, 358] Hydrodefluorination

methodologies with boron containing scavengers follow similar reactivities to those described with silanes.[286, 359, 360]

However, the use of these traditional fluorine scavengers in hydrodefluorination reactions results in the formation of large quantities of fluorine containing waste that cannot be reused. More recent developments have focussed around the discovery of alternative proton sources viable for hydrodefluorination reactions to proceed. These include using an alcohol as the proton source for the hydrodefluorination of polyfluoroarenes in a hydrogen transfer type reaction, under basic conditions, resulting in the formation of ketones and fluorinated salts as by-products, or through the direct addition of hydrogen gas.

In 2013, Peris *et al.*, reported one of the first homogeneous catalysed methodologies for the hydrodefluorination of polyfluoro- and trifluoromethyl-arenes, utilising an alcohol as a proton source *via* a hydrogen transfer methodology, with a heterobimetallic catalyst, **30** (Scheme 5-1).[361] This procedure demonstrates the cooperative effect of heterobimetallic complexes on challenging reactions, whereby the palladium centre activated the polyfluoroarene *via* C−F bond activation forming a new metal-fluorine and metal-carbon bond, while the ruthenium centre hydrogenates the substrate *via* transfer hydrogenation from the alcohol. This cooperative mechanism afforded the near complete defluorination of a range of fluoroarenes and trifluoromethylarenes.
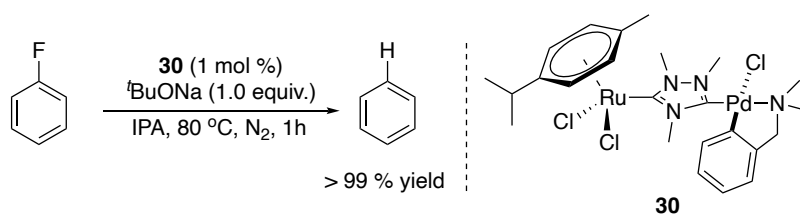
Scheme 5-1: Heterobimetallic catalysed hydrodefluorination of fluoroarenes utilising isopropanol as the proton source. This represented one of the first homogeneous catalysed hydrodefluorination reactions using isopropanol as the proton source. Scheme adapted from literature. [361]

Similarly, more recently Lu *et al.*, utilized a heterobimetallic rhodium-indium complex, **31**, to carry out the mono- and di-hydrodefluorination of polyfluorobenzenes, utilising hydrogen gas as the proton source (Scheme 5-2).[362] Once again, the cooperative nature of the heterometallic catalyst enabled both the activation of the fluorinated substrate and the proton source, to give access to partially fluorinated arenes.
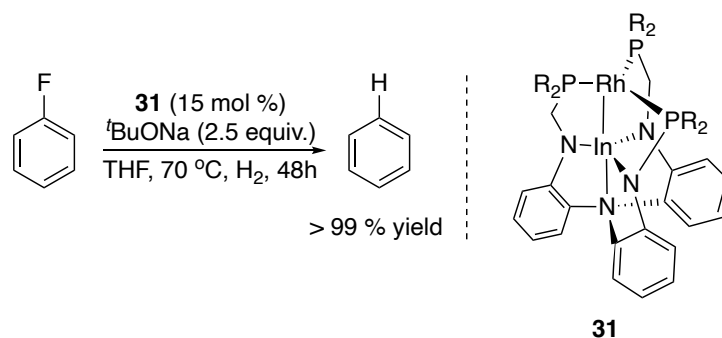
Scheme 5-2: Heterobimetallic catalysed hydrodefluorination of fluoroarenes utilising hydrogen gas as the proton source. The reactivity of each metal in the heterobimetallic catalyst was key in activating the fluoroarene and hydrogen gas towards hydrodefluorination. Scheme adapted from literature. [362]

Kayaki *et al.*, demonstrated the potential of an iridium hydrogen transfer catalyst, **32**, for the hydrodefluorination of polyfluoroarenes, utilising potassium formate as the proton source (Scheme 5-3).[363] A relativley high selectivity of *para*-monohydrodefluorination was observed across substrates investigated, producing CO_2 and potassium fluoride as waste. This is intriguing as it opens up the possibility of recovering the fluoride waste from this reaction and utilising it as a fluorine source downstream. Similarly, a cobalt catalysed hydrogen transfer methodology for the mono-hydrodefluorination of polyfluoroarenes was reported in 2013,[364] in which sodium formate was used as the proton source. However, 10 – 20 mol % of the catalyst was required with low TON recorded.
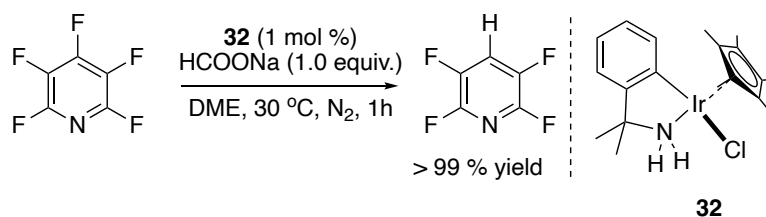
Scheme 5-3: Hydrodefluorination of pentafluoropyridine utilising sodium formate as the base and proton source. Utilisation of a hydrogen transfer catalyst enabled the hydrodefluorination of pentafluoropyridine utilising a formate salt. Scheme adapted from literature. [363]

Alternatively, instead of using a proton source to carry out hydrodefluorination reactions, other functional groups can undergo defluorinative substitution with polyfluoroarenes resulting in the formation of new partially fluorinated functionalised molecules. Of note is

defluorinative substitution of pentafluoropyridine with nucleophiles such as alkoxides, alcohols, sulfides and amines are known,[365-367] which facilitates the formation of new C-O, C-S and C-N bonds within partially fluorinated molecules. These partially fluorinated molecules can then be further utilised as building blocks in the design of new scaffolds, undergoing selective substitution and further derivatisation by organic moieties.[33, 368-372] This is of particular interest within pharmameutical development and drug design where the sequential selective formation of new functionallity at the site of partially fluorinated scaffolds is desirable.[59, 370, 373-376]

5.2 Research Aims

Using the knowledge and expertise gained from *Chapter 3* (catalytic fluorination) and *Chapter 4* (transfer fluorination) the defluorination of pentafluoropyridine was targeted. Accessing the fluorine within pentafluoropyridine towards the development of a catalytic transfer fluorination methodology was desirable and initial work focussed on the activation of pentafluoropyridine towards fluorine transfer proved successful, albeit with low levels of conversion. Further development and adaption of literature procedures enabled the successful catalytic transfer of fluorine between pentafluoropyridine and an organic electrophile, in moderate yields, resulting in the desired formation of the fluorinated product and a functionalised polyfluoroarene.

Further methodologies for the selective defluorination of pentafluoropyridine were developed enabling the synthesis of functionalised 4-substituted-2,3,5,6-tetrafluoropyridines *via* a defluorinative substitution route and through development of a hydrodefluorination protocol for the hydrodefluorination of pentafluoropyridine using group 8 and 9 hydrogen transfer catalysts.

All experiments described in *Section 5.4* were carried out with Hannah Brown, an undergraduate MSci project student.

5.3   Catalytic transfer fluorination

With the aim of developing a catalytic transfer fluorination methodology, following the work described in *Chapter 4*, the treatment of an external perfluorinated compound with benzoyl chloride was attempted. Pentafluoropyridine was chosen as a suitable perfluorinated compound, as it has been found to undergo C−F bond activation upon treatment with transition metal complexes.[377-382] To test the hypothesis where a nucleophilic TMF is formed through treatment with pentafluoropyridine, leading to the fluorination of an organic electrophile, pentafluoropyridine was treated with [RhCl(CO)(PPh₃)₂] (1 mol %) in the presence of benzoyl chloride and silver carbonate (Scheme 5-4). This resulted in limited success, with the observation of peaks within ¹⁹F NMR consistent with the formation of benzoyl fluoride and 2,3,5,6-tetrafluoro-4-chloropyridine. Unfortunately, the conversion from pentafluoropyridine under these initial conditions was low, resulting in the formation of benzoyl fluoride with a contained yield of 6 %.
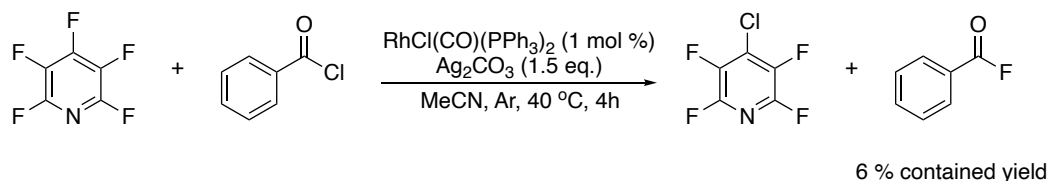
Scheme 5-4: Proposed fluorine transfer reaction between pentafluoropyridine and benzoyl chloride upon treatment with [RhCl(CO)(PPh₃)₂] (1 mol %) and silver carbonate. Reaction is proposed to proceed via the in-situ formation of silver fluoride, resulting in fluorination of organic electrophile, or via the activation of pentafluoropyridine by [RhCl(CO)(PPh₃)₂], leading to the formation of a TMF in-situ.

Further optimisation studies for this reaction were halted as shortly after the initial development of this catalytic transfer fluorination system, Crimmin *et al.*, published a transfer fluorination system utilising pentafluoropyridine as the fluoride source for the fluorination of benzoyl chloride and benzoic anhydride.[307] The reaction proceeds through the activation of the fluoroarenes with DMAP, forming a fluoroarene salt, containing a nucleophilic fluoride,

which undergoes nucleophilic attack with carbonyl electrophiles, to give the acyl fluoride and a new substituted mono-defluorinated arene.

Following our previous experience with catalytic and transfer fluorination reactions, the direction of our attention was altered to adapt the catalytic transfer fluorination route developed above with the successful developments made by Crimmin and co-workers, in an attempt to improve the efficacy of the system. Introducing a transition metal complex to the reaction described in Scheme 5-5, may result in the formation of a TMF upon reaction with the perfluoroarene salt, which may enhance the reactivity of the fluoride, increasing the rate and conversion of the transfer fluorination reaction (Scheme 5-5), similar to the stoichiometric fluorination reaction with $[RhF(CO)(PPh_3)_2]$ described in *Section 3.2*.
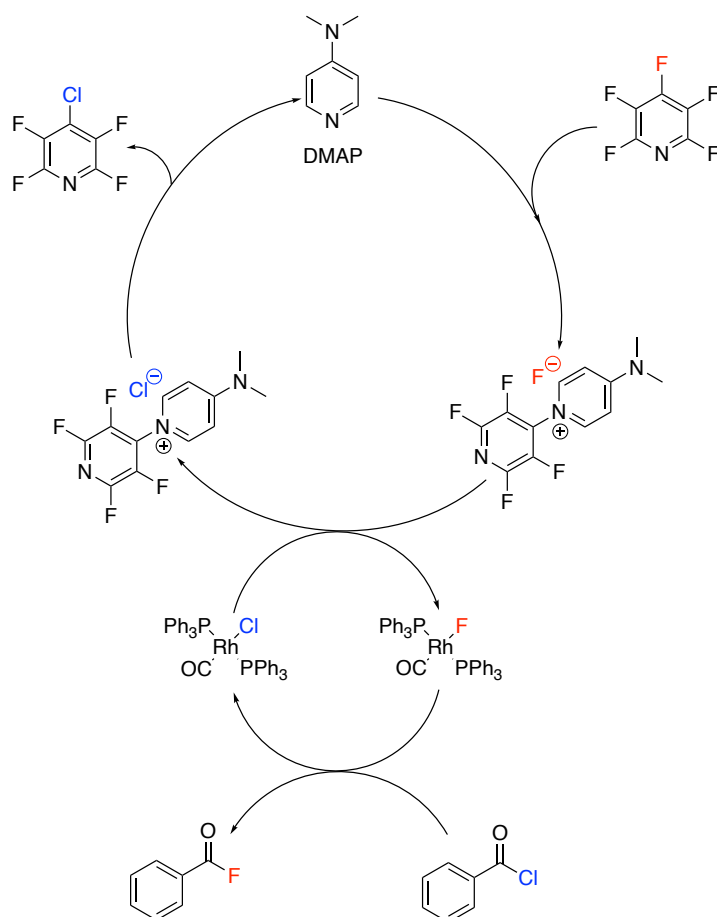
Scheme 5-5: Proposed adaption of Crimmin transfer fluorination reaction, resulting in the formation of a TMF, in an attempt to improve the efficacy of this reaction. Activation of pentafluoropyridine by DMAP leads to the formation of the fluoroarene salt. This fluoroarene salt then reacts with [RhCl(CO)(PPh3)2] giving the TMF, which then undergoes fluorination of the acyl chloride substrate.

Initially, control reactions were carried out, repeating the conditions developed by Crimmin and co-workers. Pentafluoropyridine (0.2 mmol) was added to a J. Young's tap NMR tube alongside benzoic anhydride (2.0 mmol), and trifluorotoluene (20 μL) as the internal standard, in a glovebox. The NMR tube was sealed and transferred to an inert NMR tube filler on a Schlenk line, evacuated and backfilled with argon, where a stock solution of DMAP (0.01 mmol) in C_6D_6 (0.1 mL) and dry, degassed acetonitrile (0.4 mL) were added *via* syringe. The sealed NMR tube was then heated in an oil bath at 100 °C for 17 hours (Scheme 5-6). The reaction was removed from the heat and allowed to cool. ^{19}F NMR analysis identified the formation of the desired benzoyl fluoride product (17.1 ppm), alongside 4-benzoic-2,3,5,6-Tetrafluoropyridine (-90.3, -152.8 ppm). Under these reaction conditions, Crimmin *et. al.*, reported the formation of benzoyl fluoride with a contained yield of 81 %, with a 73 % isolated yield. However, in our hands the maximum contained yield obtained for benzoyl fluoride was 39 % (37±2 % across 5 repeats). Similar reduction in contained yield were observed using 1,8-Diazabicyclo[5.4.0]undec-7-ene (DBU) (42 % *vs* 77 %) and 1,4-Diazabicyclo[2.2.2]octane (DABCO) (31 % *vs* 61 %) as the base.
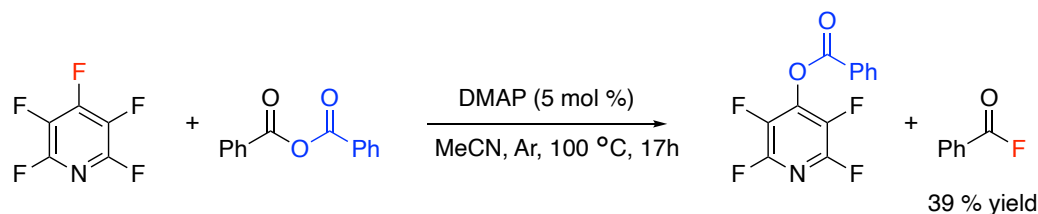
Scheme 5-6: Transfer fluorination protocol for the fluorination of benzoic anhydride. Pentafluoropyridine is activated by DMAP, resulting in the formation of a fluoroarene salt. The nucleophilic fluoride anion then reacts with benzoic anhydride resulting in the formation of the fluorinated product.

While the cause behind the reduction in the effectiveness of this reaction in our hands was not immediately determined, it was nonetheless used as a starting point to investigate the effect of addition of catalytic quantities of metal on the system. A range of commercially available metal complexes were added to reaction. Stock solutions of these complexes were made by dissolving the complex in dry, degassed acetonitrile or dimethylformamide to give a

concentration of 0.5 mM. These metal catalysts experiments follow the experimental details described in *Section 5.6.3*.

As shown in Table 5-1 the addition of metal complexes had a negligible effect on the yield of the fluorinated product over the time course of the reaction, giving a 37±1 % contained yield of benzoyl fluoride for [RhCp*Cl$_2$]$_2$, [IrCp*Cl$_2$]$_2$ and [Ru(p-Cy)Cl$_2$]$_2$ in acetonitrile (Table 5-1; entry 5, 6 and 7 respectively). The cobalt catalysts [Co$_2$(CO$_8$)], [CoCp*I$_2$(CO)] and [CoCp*I$_2$]$_2$ were incompatible with this procedure and underwent decomposition upon addition to NMR tube (Table 5-1; only entry 8 shown). Due to solubility issues [RhCl(CO)(PPh$_3$)$_2$] and [IrCl(CO)(PPh$_3$)$_2$] were tested in dimethylformamide giving the highest contained yield of benzoyl chloride with 42 and 45 % respectively (Table 5-1; entry 9 and 10 respectively). Interestingly, while no significant enhancement in overall yield was observed for these reactions, the rate of reaction was found to increase upon addition of metal. Over the course of 6 hours treatment of 1 mol % [RhCl(CO)(PPh$_3$)$_2$]and [IrCl(CO)(PPh$_3$)$_2$] in dimethylformamide resulted in the formation of benzoyl fluoride in 34 and 36 % contained yield respectively (Table 5-1; entry 11 and 12 respectively), compared to 24 % yield for the non-metal catalysed route (Table 5-1; entry 4). During these experiments the formation of a metal-fluorine bond was not determined. This indicated that the metal does have an effect on the system, most likely through some form of interaction to activate a component within the system resulting in faster reaction times, however overall conversion was not found to increase. Further work to conclude the effect of the metal on this system could be conducted in the future.

Table 5-1: Catalyst scope for the transfer fluorination between pentafluoropyridine and benzoic anhydride.[a]
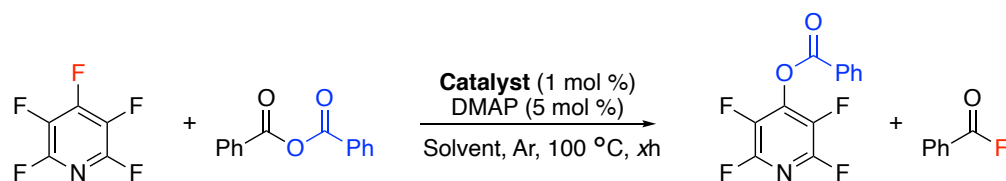
Entry	Catalyst (1 mol %)	Solvent	Time (h)	^{19}F NMR yield benzoyl fluoride (%)[b]
1	None	MeCN	17	38
2	None	MeCN	6	20
3	None	DMF	17	37
4	None	DMF	6	24
5	[RhCp*Cl$_2$]$_2$	MeCN	17	37
6	[IrCp*Cl$_2$]$_2$	MeCN	17	38
7	[Ru(*p*-Cy)Cl$_2$]$_2$	MeCN	17	37
8	[CoCp*I$_2$]$_2$	MeCN	17	Trace
9	RhCl(CO)(PPh$_3$)$_2$	DMF	17	42
10	IrCl(CO)(PPh$_3$)$_2$	DMF	17	45
11	RhCl(CO)(PPh$_3$)$_2$	DMF	6	34
12	IrCl(CO)(PPh$_3$)$_2$	DMF	6	36

[a] Pentafluoropyrydine (0.2 mmol), benzoic anhydride (2.0 mmol), acetonitrile (4.0 mL), catalyst (1.0 mol %), DMAP (5.0 mol %), C$_6$D$_6$ (50 µL), trifluorotoluene (20 µL), 100 °C, argon. [b] Contained yield of benzoyl fluoride determined by ^{19}F NMR against internal standard, trifluorotoluene (20 µL).

The consistent reduction in yield observed for benzoyl fluoride under these conditions, compared to that reported by Crimmin and co-workers, lead us to look more closely at the reported experimental conditions,[307] to understand if any deviation in synthetic methodology lead to the lessening of activity. While the reported synthesis was carried out under standard inert and anhydrous conditions, including the use of a Schlenk line and glovebox, using dry and degassed solvents, it was noted that the solvent was added by opening the NMR tube under ambient conditions. Therefore, a subsequent experiment was conducted opening the NMR tube to ambient conditions during addition of the solvent, instead of adding the solvent under inert conditions, to investigate whether the addition of air resulted in an increase in the activity of fluorine transfer. The presence of air did not result in any increase in the yield of benzoyl fluoride.

Next the effect of solvent was examined. A reaction was carried out using degassed acetonitrile, which had not previously been dried. This resulted in the highest yield of benzoyl

fluoride, giving a 76 % contained yield by ^{19}F NMR analysis, much closer to the 81 % contained yield of benzoyl fluoride reported by Crimmin and co-workers. This indicates that the presence of water is required to promote this transfer fluorination reaction. Water has previously been shown to facilitate the "shuttling" of fluoride in appropriate concentrations,[383, 384] however this activity is shut down at higher concentrations as water forms a solvation shell around the fluoride anion.[385] This may occur within this system, but further work investigating the effect of water doping within anhydrous systems would be required.

5.4 Defluorinative substitution of pentafluoropyridine

As mentioned in *Section 4.1* and *5.1*, the synthesis of fluorinated molecules from a "bottom up" approach can be challenging. In recent years new methods of synthesising substituted polyfluorinated compounds *via* C−F bond activation have been developed, however in most cases the fluorine displaced is lost from the system.[33] With our recent developments of transfer fluorination and catalytic fluorination reactions, a fluoroarene defluorination procedure was targeted, in which the fluoroarene underwent defluorinative substitution at the site of C−F bond activation, resulting in the formation of a metal fluoride salt as a by-product, which could then potentially be used as the fluorine source for further catalytic fluorination reactions, in one pot.

Using an adapted procedure developed by Peris group,[361] the hydrodefluorination of pentafluoropyridine was targeted, resulting in the formation of 2,3,5,6-Tetrafluoropyridine and potassium fluoride. This metal fluoride salt could then be used for the catalytic fluorination of acyl chlorides with **22**, analogous to the catalytic procedure developed in *Chapter 3*. Treatment of pentafluoropyridine with 1 mol % **22**, 2.5 equivalents of potassium carbonate, using isopropanol as the solvent and proton source at 80 °C, resulted in the successful defluorination of pentafluoropyridine, with a conversion of 90 % over two hours.

Although this system showed sufficient selectivity towards the monodefluorination of pentafluoropyridine, successful fluorine transfer forming acyl fluoride upon addition of the acyl chloride substrate was not observed. Additionally, due to the activated nature of the polyfluorocyclohexa-1,4-diene ring of **22**, the catalyst underwent decomposition under the reaction conditions and could not be recovered.

In addition to observing the complete decomposition of the catalyst by ^{19}F NMR analysis, the monodefluorinated product formed under the reaction conditions did not correspond to the expected ^{19}F NMR signature of the desired product 2,3,5,6-Tetrafluoropyridine (-92.1 and -142.6 ppm). This suggested that hydrodefluorination was not occurring for this reaction and a different 4-substituted-2,3,5,6-Tetrafluoropyidine product was being formed.

The substituted fluoroarene product was isolated as a colourless oil following column chromatography (1:10 ethyl acetate:*n*-heptane). Characterisation of this product by multi-nuclear NMR, MS and FTIR identified this substituted fluoroarene as 4-[i]Propoxy-2,3,5,6-Tetrafluoropyridine, **34**, corresponding to literature values,[365] with an isolated yield of 76 % (Scheme 5-7). ^{19}F NMR indicated the formation of a two fluorine environment species, with a chemical shift of -91.2 and -158.6 ppm, corresponding to the two equivalent fluorine environments within **34** (Figure 5-1). ^{1}H NMR was consistent with an [i]propoxy group shifted downfield due to the influence of the electron withdrawing fluoropyridine. MS also corresponded to the formation of 4-[i]Propoxy-2,3,5,6-Tetrafluoropyridine (*Section 5.6.3.1)*, with FTIR correlating to literature values.[365] A minor product, 4,6-di[i]propoxy-2,3,5-trifluoropyridine, **35**, was also identified in the later fractions obtained following column chromatography (Figure 5-2), showing the potential of pentafluoropyridine to undergo di-defluorination.
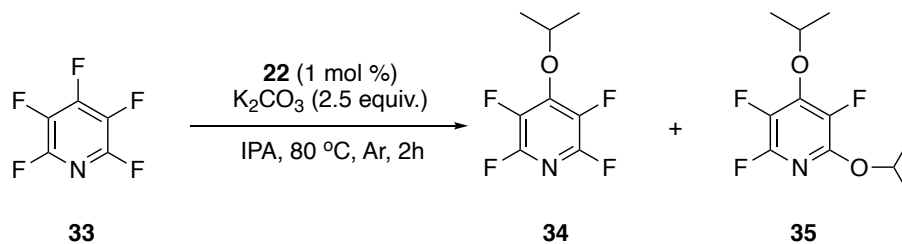
Scheme 5-7: *Formation of major product 4-ⁱPropoxy-2,3,5,6-Tetrafluoropyridine,* **34**, *and minor product 4,6-diⁱpropoxy-2,3,5-trifluoropyridine,* **35**, *from the defluorinative substitution of pentafluoropyridine catalysed by* **22**.
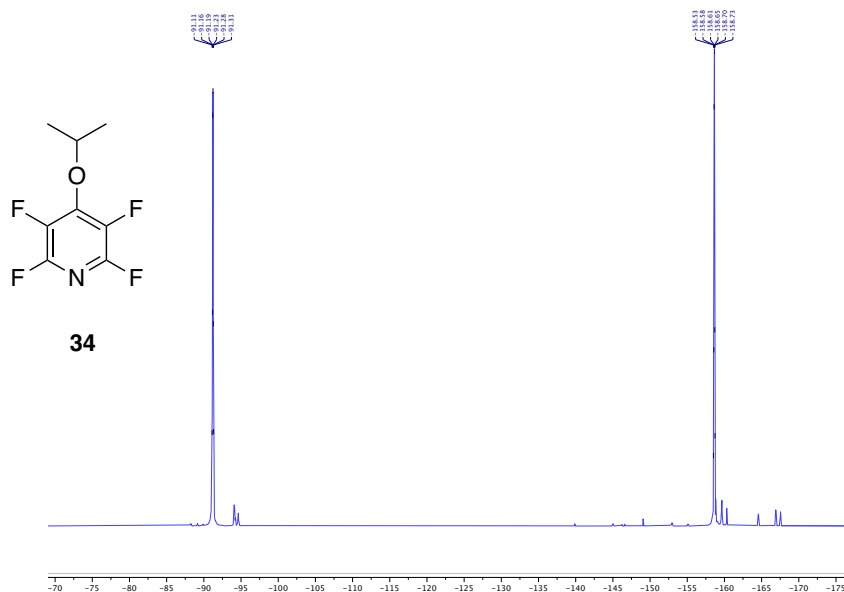
Figure 5-1: *¹⁹F NMR spectrum of 4-ⁱPropoxy-2,3,5,6-Tetrafluoropyridine,* **34**, *with a chemical shift of -91.2 and -158.6 ppm, collected following column chromatography containing some minor impurities. NMR carried out in deuterated chloroform.*
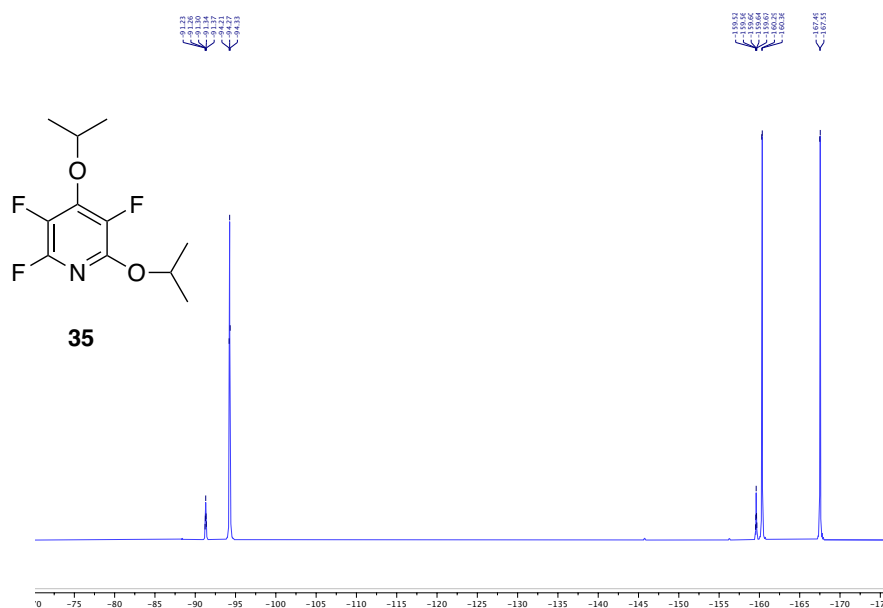
Figure 5-2: *¹⁹F NMR spectrum of 2,4-di-ⁱpropoxy-3,5,6-trifluoropyridine,* **35**, *(-93.9, -158.6 and -166.7 ppm) following column chromatography, with a small quantity of 4-ⁱPropoxy-2,3,5,6-Tetrafluoropyridine,* **34**, *(-91.2 and -158.6 ppm) impurity, which could not be separated. NMR carried out in deuterated chloroform.*

5.4.1 Catalytic defluorinative alkoxylation of pentafluoropyridine

Alkoxy substituted fluoropyridine compounds have previously been reported in the literature.[365, 386-388] They are found to form upon treatment of pentafluoropyridine, with an alcohol in the presence of base (Scheme 5-8). However, these procedures often result in low selectivity and conversion, resulting in the formation of a mixture of products, with various distributions of mono-, di- or tri-substituted fluoropyridines. Catalytic studies were continued (Table 5-2; entry 9). As **22** was found to decompose under the reaction conditions, observed through loss of the fluorine on the polyfluorocyclohexadiene ring by ^{19}F NMR, alternative catalytic targets were required. Therefore, the efficacy of a range of commercially available group 8 and 9 catalysts were investigated for base assisted defluorinative substitution of pentafluoropyridine.
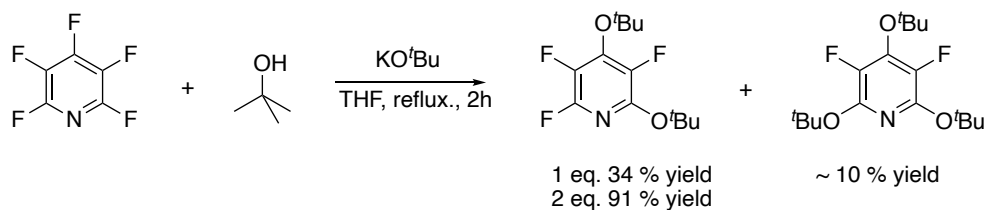
Wakefield, B. *J. Chem. Soc. Perkin Trans.,* **1988**, 3301 - 3305.
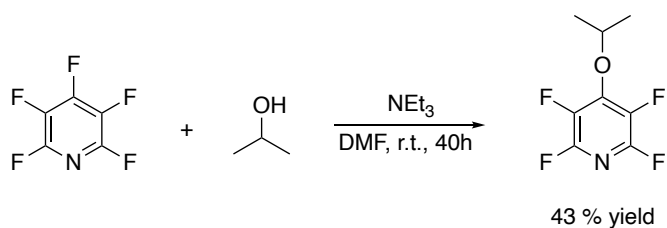
Litvak, M. *Russian Journal of Bioorganic Chemistry,* **2004**, 30, 47 - 52.
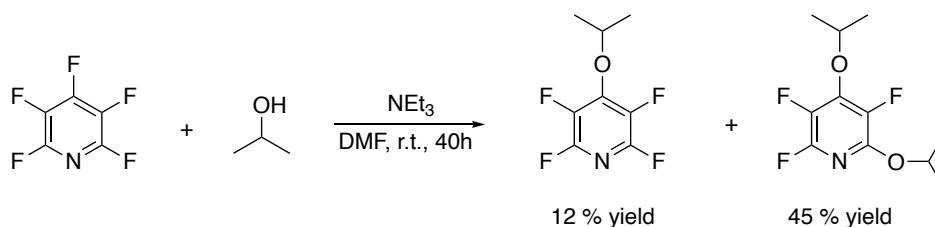
Schmidt, A. *Journal of Heterocyclic Chemistry,* **2007**, 44, 679 - 684.
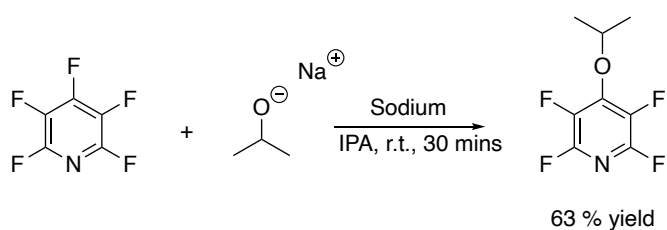
Chambers, R. *J. Chem. Soc. C.,* **1968**, 625 - 629.

Scheme 5-8: Literature examples for the base promoted defluorinated substitution of pentafluoropyridine with alcohol. Current techniques are characterised by poor selectivity and low to moderate yields of the substitution product.

All catalytic targets tested, exhibited enhanced conversion and selectivity towards mono-defluorinative substitution of pentafluoropyridine compared to the non-metal catalysed reaction (Table 5-2; entry 1). Treatment of 1 mol % catalyst with pentafluoropyridine (1 mmol) , in the presence of 2.5 equivalents of potassium carbonate, in isopropanol (5 mL) under argon at 80 °C afforded the selective formation of 4-*i*Propoxy-2,3,5,6-

Tetrafluoropyridine, **34**. Treatment with 1 mol % [RhCl(PPh$_3$)$_3$] resulted in quantitative conversion from pentafluoropyridine, giving a 98% contained ^{19}F NMR yield of the major product, **34** (Table 5-2; entry 2,). The cobalt analogue, [CoCl(PPh$_3$)$_3$], was found to result in similarly high activity with one of the highest yields and conversions of the complexes tested (Table 5-2; entry 3). Unlike other dehalogenation reactions which have been reported in the literature,[389] in which [CoCl(PPh$_3$)$_3$] has shown very low activity, the defluorination of pentafluoropyridine by [CoCl(PPh$_3$)$_3$]was found to occur readily. [RhCl(CO)(PPh$_3$)$_2$] was found to exhibit the lowest conversion of pentafluoropyridine of the catalysts tested (Table 5-2; entry 4), whereas the iridium analogue, [IrCl(CO)(PPh$_3$)$_2$], demonstrated high conversion from pentafluoropyridine (96 %) with excellent selectivity towards **34** (Table 5-2; entry 5). The group 8 ruthenium catalysts [RuCp*Cl(PPh$_3$)$_2$] and [*(S,S)*-Teth-TsDpen RuCl] gave near quantitative conversion of pentafluoropyridine with the highest selectivity towards **34** observed (Table 5-2; entry 6 and 8 respectively), while [Ru(*p*-Cy)Cl$_2$]$_2$ resulted in 93 % conversion of pentafluoropyridine, retaining high selectivity towards **34** (Table 5-2; entry 7). When [IrCp*Cl$_2$]$_2$ was used as the catalyst (Table 5-2; entry10), full conversion from pentafluoropyridine was observed, with a 90 % contained yield of **34**. This reduction in yield of the major product is due to a secondary side reaction occurring, resulting in the observed formation of 2,3,5,6-Tetrafluoropyridine *via* hydrodefluorination.

All of the catalysts tested showed a high level of selectivity towards mono-defluorination of pentafluoropyridine unlike that observed for the non-metal catalysed control reaction, with the exception of [IrCp*Cl$_2$]$_2$ in which 2,3,5,6-Tetrafluoropyridine (6 % contained yield) and 4,6-Di^{i}propoxy-2,3,5-Trifluoropyridine, **35** (3 % contained yield), were observed. With these results it was decided to take [CoCl(PPh$_3$)$_3$], [IrCl(CO)(PPh$_3$)$_2$] and [RuCp*Cl(PPh$_3$)$_2$] on for further investigation. While [*(S,S)*-Teth-TsDpen RuCl] displayed one of the best results of the complexes tested, showing high conversion from pentafluoropyridine with excellent selectivity towards **34**, further testing was not conducted at this time due as limited supplies

of the complex that were on hand at the time these experiments were conducted and as other catalytic targets showed similar activity.

*Table 5-2: Catalyst Screen for the base assisted defluorination of pentafluoropyridine resulting in the formation of 4-^{i}Propoxy-2,3,5,6-Tetrafluoropyridine, **34** and 4,6-di^{i}propoxy-2,3,5-trifluoropyridine, **35**.^{a}*
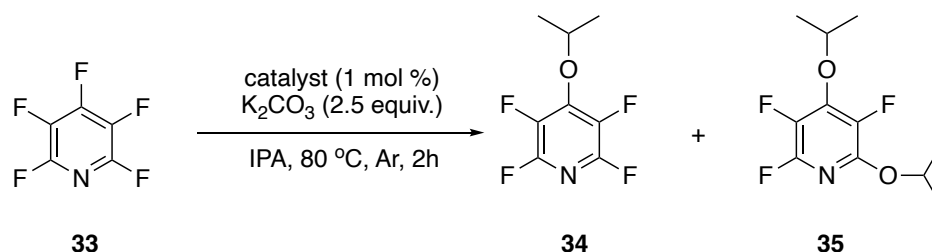
Entry	Catalyst	Conversion from 33 (%)[b]	Yield of 34 (%)[c]	Yield of 35 (%)[c]	TON	TOF (h^{-1})
1	None	70	55	14	-	-
2	RhCl(PPh$_3$)$_3$	>99	98	1	98	49
3	CoCl(PPh$_3$)$_3$	98	94	2	94	47
4	RhCl(CO)(PPh$_3$)$_2$	83	82	1	82	41
5	IrCl(CO)(PPh$_3$)$_2$	96	95	1	95	47.5
6	RuCp*Cl(PPh$_3$)$_2$	99	99	1	99	49.5
7	[Ru(*p*-Cy)Cl$_2$]$_2$	94	93	1	93	46.5
8	[(*S,S*)-Teth-TsDpen RuCl]	>99	99	1	99	49.5
9	**22**	99	96	3	96	48
10[d]	[IrCp*Cl$_2$]$_2$	>99	90	3	90	45

[a] Pentafluoropyridine (1.0 mmol), IPA (5.0 mL), K$_2$CO$_3$ (2.5 mmol), catalyst (1.0 mol %), 80 °C, argon, 2 hours. [b] Conversion calculated as loss of pentafluoropyridine determined by ^{19}F NMR against internal standard, trifluorotoluene (20 μL). [c] Contained yields calculated as formation of product determined by ^{19}F NMR against internal standard, trifluorotoluene (20 μL). [d] ^{19}F NMR analysis identified the formation of 6 % 2,3,5,6-Tetrafluoropyridine.

Following the results obtained for the catalyst screen above, the effects of metal loading on the mono-defluorination of pentafluoropyridine was investigated. Excellent conversion and selectivity towards the formation of **34** were retained for each metal tested when dropping the metal loading by half to 0.5 mol %. [RuCp*Cl(PPh$_3$)$_2$] retained activity over two hours (Table 5-3; entry 3), similar to that for observed at 1 mol % loading. While dropping metal loading 10-fold to 0.1 mol % [RuCp*Cl(PPh$_3$)$_2$] resulting in a drop in conversion from pentafluoropyridine (80 % conversion) over the course of two hours (Table 5-3; entry 4), while excellent selectivity was retained, with TON in excess of 780 and TOF of 390 h^{-1}. Similarly, Vaska's complex, [IrCl(CO)(PPh$_3$)$_2$], maintained excellent yield and selectivity as metal loading was reduced by half (Table 5-3; entry 6), resulting in 86 % contained yield of **34**, over the course of two hours at 0.1 mol % [IrCl(CO)(PPh$_3$)$_2$] (Table 5-3; entry 7). Excellent

conversions from pentafluoropyridine were retained upon treatment with 0.1 mol % [CoCl(PPh$_3$)$_3$], demonstrating remarkable activity for this first row transition metal complex, with a TON of 900 and TOF of 450 h^{-1} (Table 5-3; entry 10), exhibiting the highest conversion and yield of complexes investigated at this reduced metal loading of 0.1 mol %.

*Table 5-3: Investigation into the effect of catalyst loading for the base assisted defluorination of pentafluoropyridine resulting in the formation of 4-^{i}Propoxy-2,3,5,6-Tetrafluoropyridine, **34**.^{a}*
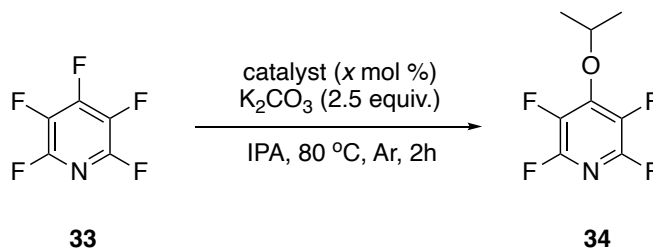
Entry	Catalyst	Catalyst loading (mol %)	Conversion from 35 (%)^b	Yield of 34 (%)^c	TON	TOF (h^{-1})
1	RhCl(PPh$_3$)$_3$	1.0	>99	98	98	49
2	RuCp*Cl(PPh$_3$)$_2$	1.0	>99	99	99	49.5
3	RuCp*Cl(PPh$_3$)$_2$	0.5	98	97	194	97
4	RuCp*Cl(PPh$_3$)$_2$	0.1	80	78	780	390
5	IrCl(CO)(PPh$_3$)$_2$	1.0	96	95	95	47.5
6	IrCl(CO)(PPh$_3$)$_2$	0.5	92	90	180	90
7	IrCl(CO)(PPh$_3$)$_2$	0.1	87	86	860	430
8	CoCl(PPh$_3$)$_3$	1.0	98	94	94	47
9	CoCl(PPh$_3$)$_3$	0.5	95	93	186	93
10	CoCl(PPh$_3$)$_3$	0.1	92	90	900	450

^{a} Pentafluoropyridine (1.0 mmol), IPA (5.0 mL), K$_2$CO$_3$ (2.5 mmol), catalyst (*x* mol %), 80 °C, argon, 2 hours. ^{b} Conversion calculated as loss of pentafluoropyridine determined by ^{19}F NMR against internal standard, trifluorotoluene (20 μL). ^{c} Contained yields calculated as formation of product determined by ^{19}F NMR against internal standard, trifluorotoluene (20 μL).

As high selectivity towards **34** were retained for each of the metals tested at 0.1 mol % catalyst loading, while conversion from pentafluoropyridine reduced over the two hour time scale of the reaction as catalyst loading was also reduced, the effect of time on the reaction was investigated to determine whether higher conversions could be achieved at 0.1 mol % catalyst loading at longer reaction times. When the reaction time was increased to 4 hours near quantitative conversion from pentafluoropyridine was observed for both [RuCp*Cl(PPh$_3$)$_2$] and [CoCl(PPh$_3$)$_3$] (Table 5-4; entry 2 and 5 respectively) with [IrCl(CO)(PPh$_3$)$_2$] giving 97 % conversion over 4 hours (Table 5-4; entry 9). This confirmed that for a catalyst loading of 0.1 mol % the reaction had not gone to completion over the initial timescale of two hours. Due to the high activity of these catalysts towards selective mono-defluorinative substitution of

pentafluoropyridine, relatively high conversions were retained over the course of one hour with 55 % conversion observed for [RuCp*Cl(PPh$_3$)$_2$] (Table 5-4; entry 4), while [CoCl(PPh$_3$)$_3$] exhibited 66 % conversion from pentafluoropyridine, demonstrating the highest TOF determined for this system at 650 h^{-1} (Table 5-4; entry 7). These results are illustrated in Figure 5-3. Excellent selectivity towards **34** was retained throughout.

Table 5-4: Investigation of time for the base assisted defluorination of pentafluoropyridine at 0.1 mol % catalyst loading.[a]
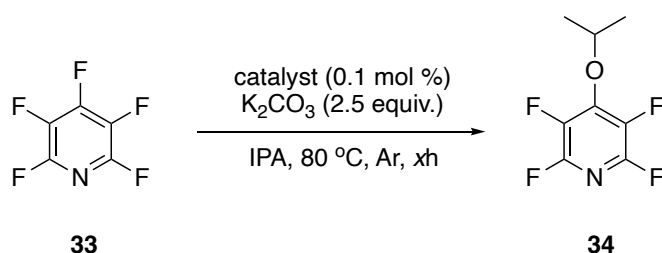
	33				**34**	
Entry	**Catalyst**	**Time (h)**	**Conversion from 33 (%)[b]**	**Yield of 34 (%)[c]**	**TON**	**TOF (h^{-1})**
1[d]	RhCl(PPh$_3$)$_3$	2	>99	98	98	49
2	RuCp*Cl(PPh$_3$)$_2$	4	98	97	970	243
3	RuCp*Cl(PPh$_3$)$_2$	2	80	78	780	390
4	RuCp*Cl(PPh$_3$)$_2$	1	55	53	530	530
5	CoCl(PPh$_3$)$_3$	4	99	98	980	245
6	CoCl(PPh$_3$)$_3$	2	92	90	900	450
7	CoCl(PPh$_3$)$_3$	1	66	65	650	650
8	IrCl(CO)(PPh$_3$)$_2$	4	97	96	960	240
9	IrCl(CO)(PPh$_3$)$_2$	2	87	86	860	430

[a] Pentafluoropyridine (1.0 mmol), IPA (5.0 mL), K$_2$CO$_3$ (2.5 mmol), catalyst (0.1 mol %), 80 °C, argon, x hours. [b] Conversion calculated as loss of pentafluoropyridine determined by ^{19}F NMR against internal standard, trifluorotoluene (20 μL). [c] Contained yields calculated as formation of product determined by ^{19}F NMR against internal standard, trifluorotoluene (20 μL). [d] 1 mol % [RhCl(PPh$_3$)$_3$] result from Table 5-2 for reference.

In the future *in-situ* measurements or frequent sampling of this reaction could be conducted to calculate initial rates of reaction and determine kinetic properties to help elucidate the possible reaction mechanism for this system and to help give insight to further optimise this reaction to maximise catalyst activity. Further work in this area could look into the effect of temperature on the system, to investigate whether increased conversion of pentafluoropyridine can be achieved over shorter timeframes.
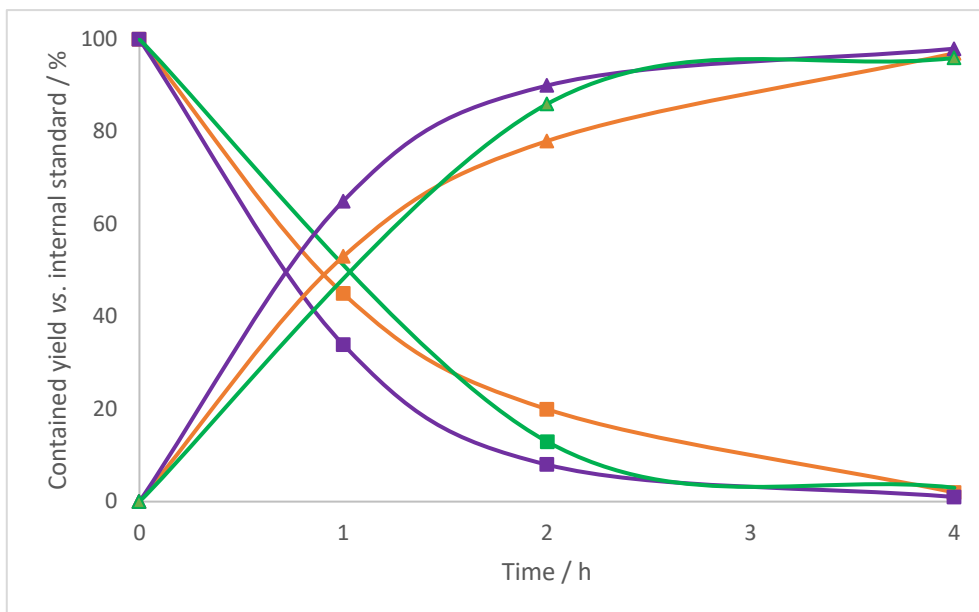
Figure 5-3: Plot showing the contained yield of pentafluoropyridine (square) decreasing and 4-ipropoxy-2,3,5,6-Tetrafluoropyridine, 34 (triangle) increasing over time, corresponding to the results recorded in Table 5-4. The data shown was collected by running the reactions for one, two and four hours (two and four hours for [IrCl(CO)(PPh₃)₂)] prior to full work-up and analysis. Direct sampling of the reaction mixtures over the time course of the reaction was not conducted.

Within this system, isopropanol is utilised as both the solvent and the substrate, resulting in the formation of the isopropoxide product. Due to the success of this system other alcohol based solvents were utilised to investigate whether other alcohol substituents could be incorporated into the structure of the polyfluoroarene. Catalytic activity was retained for the selective mono-defluorination of pentafluoropyridine in the presence of both 2-butanol and ethanol for 0.1 mol % [RuCp*Cl(PPh₃)₂] (Table 5-5; entry 2 and 3 respectively) resulting in 98 % and 97 % contained yield of 4-ᵗButoxy-2,3,5,6-Tetrafluoropyridine and 4-Ethoxy-2,3,5,6-Tetrafluoro pyridine respectively, showing excellent yield and selectivity could be maintained, resulting in higher conversion of pentafluoropyridine over two hours compared with the standard isopropanol experiment (Table 5-5; entry 1). This result was intriguing as it shows potential for this reaction to be utilised in the synthesis of alcohol functionalised polyfluorinated molecules, which could undergo further sequential derivatisation, giving access to fluorine functionalised heterocycles commonly found in pharmaceuticals.[15] The scope of alcohol substitution requires further investigation.

Table 5-5: Investigation of alcohol substrate on the base assisted defluorination of pentafluoropyridine.[a]
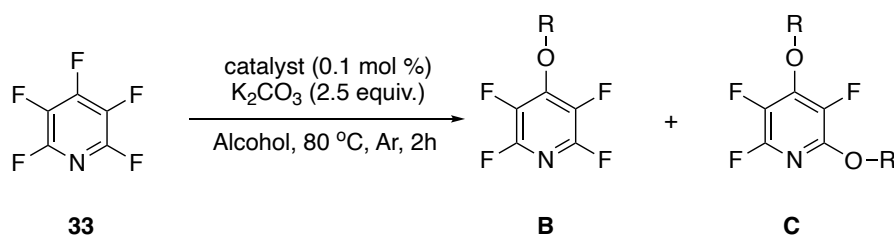
Entry	Catalyst	Solvent	Conversion from 33 (%)[b]	Yield of B (%)[c]	Yield of C (%)[c]	TON	TOF (h^{-1})
1	RuCp*Cl(PPh$_3$)$_2$	^{i}propanol	80	78	2	780	390
2	RuCp*Cl(PPh$_3$)$_2$	2-butanol	99	98	1	980	490
3	RuCp*Cl(PPh$_3$)$_2$	ethanol	98	97	1	970	485

[a] Pentafluoropyridine (1.0 mmol), solvent (5.0 mL), K$_2$CO$_3$ (2.5 mmol), catalyst (0.1 mol %), 80 °C, argon, 2 hours. [b] Conversion calculated as loss of pentafluoropyridine determined by ^{19}F NMR against internal standard, trifluorotoluene (20 µL). [c] Contained yields calculated as formation of product determined by ^{19}F NMR against internal standard, trifluorotoluene (20 µL).

The effect of base on the system was investigated prior to the optimisation studies described above (Table 5.2 – 5.5). Potassium carbonate was found to be the most suitable base to promote this reaction resulting in >99 % conversion of pentafluoropyridine and a 98 % contained yield of **34**, when using 1 mol % [RhCl(PPh$_3$)$_3$] over four hours (Table 5-6; entry 2), similar to the results obtained during the catalyst screening above (Table 5-2; entry 1). Potassium carbonate gave the greatest selectivity towards the mono-defluorinated product, exemplifying the importance in the choice of base and catalyst on the selective formation of the mono-defluorinated product. Unlike potassium carbonate, silver carbonate showed no activity towards defluorinative substitution (Table 5-6; entry 3), with no formation of **34** detected. Silver carbonate was observed to decompose when stirred (500 rpm) in darkness upon heating above 40 °C. Sodium *tert*-butoxide and potassium *tert*-butoxide both gave quantitative conversion of pentafluoropyridine (Table 5-6; entry 4 and 5 respectively) similar to that observed with potassium carbonate. However, the selectivity towards mono-defluorination was not observed with a mixture of the mono-defluorinated product **34** and the di-defluorinated product **C**. 4-^{i}Propoxy-2,3,5,6-Tetrafluoropyridine, **34**, was still observed as the major product in both cases with 53 % and 75 % contained yield of **34** in the case of sodium *tert*-butoxide and potassium *tert*-butoxide respectively. Treatment with sodium *tert*-butoxide gave the highest contained yield of the di-defluorinated product, 4,6-di^{i}propoxy-2,3,5-trifluoropyridine, **35**, at 47 %, close to a 1:1 ratio with the mono-defluorinated product, while a 3:1 mono-:di-fluorinated product ratio was observed for potassium *tert*-butoxide. When potassium bis(trimethylsilyl)amide was tested as the base, multiple unidentified minor products were observed by ^{19}F NMR, in addition to the major product **34**, at 80 % contained

yield (Table 5-6; entry 6). Due to the unselective nature of this base, further testing was discontinued.

The final base tested as part of this investigation was potassium formate (Table 5-6; entry 7). Treatment of potassium formate with 1 mol % [RhCl(PPh$_3$)$_3$], in the presence of isopropanol resulted in 95 % conversion from pentafluoropyridine with the formation of a mixture of products identified by ^{19}F NMR including **34** in 33 % contained yield. However, the major product identified within this reaction was found to be 2,3,5,6-Tetrafluoropyridine in a 43 % contained yield. Potassium formate has previously been shown to promote the hydrodefluorination of pentafluoropyridine in the presence of isopropanol as a proton source, as discussed in *Section 5.1*.

Table 5-6: Effect of base on the defluorinative substitution of pentafluoropyridine.^{a}
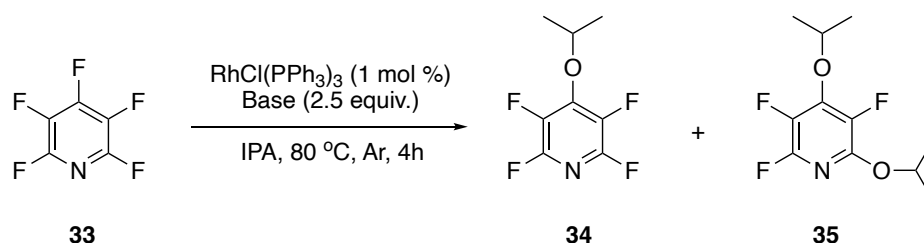
Entry	Base	Conversion from 33 (%)^b	Yield of 34 (%)^c	Yield of 35 (%)^c
1	None	0	0	0
2	K$_2$CO$_3$	>99	98	1
3	Ag$_2$CO$_3$	0	0	0
4	Na^{t}OBu	>99	53	47
5	K^{t}OBu	>99	75	25
6^d	KHMDS	89	80	4
7^{d,e}	HCOOK	95	33	1

^{a} Pentafluoropyridine (1.0 mmol), IPA (5.0 mL), base (2.5 mmol), RhCl(PPh$_3$)$_3$ (1.0 mol %), 80 °C, argon, 4 hours. ^{b} Conversion calculated as loss of pentafluoropyridine determined by ^{19}F NMR against internal standard, trifluorotoluene (20 µL). ^{c} Contained yields calculated as formation of product determined by ^{19}F NMR against internal standard, trifluorotoluene (20 µL). ^{d} Unidentified peaks present in the baseline of ^{19}F NMR. ^{e} 43 % 2,3,5,6-Tetrafluoropyridine determined by ^{19}F NMR against internal standard, trifluorotoluene (20 µL).

5.4.2 Catalytic hydrodefluorination of pentafluoropyridine

The observed changes in reactivity describe in Table 5-6 highlighted the importance of the choice of base on accessing the hydrodefluorination product 2,3,5,6-Tetrafluoropyridine over **34**. Additionally, in order to promote the formation of 2,3,5,6-Tetrafluoropyridine, potential side reaction must be limited. Therefore, to limit the formation of **34** in the reaction the solvent

was changed from isopropanol, with potassium formate acting as the proton source for hydrodefluorination.

Different solvent systems were investigated including acetonitrile, dimethylformamide, toluene and dimethyl sulfoxide, however this either resulted in no observed reactivity, in the case of toluene, or the formation of currently unidentified two fluorine environment products, in the case of acetonitrile, dimethylformamide and dimethyl sulfoxide, with no formation of 2,3,5,6-Tetrafluoropyridine observed. Tetrahydrofuran was found to be the best solvent tested for the hydrodefluorination of pentafluoropyridine, affording 2,3,5,6-Tetrafluoropyridine upon treatment with the catalyst (1 mol %) and pentafluoropyridine (1 mmol), in the presence of potassium formate (2.5 mmol) in tetrahydrofuran (5 mL), under argon at 80 °C for four hours. Quantitative ^{19}F NMR analysis of the reaction mixture, with trifluorotoluene (20 μL) as the internal standard, following work-up enabled the contained yield of the product to be determined.

With the reaction conditions for hydrodefluorination determined, a number of catalysts were tested to probe their hydrodefluorination potential, including [RuCp*Cl(PPh$_3$)$_2$] and [CoCl(PPh$_3$)$_3$], the best catalysts tested for defluorinative substitution of pentafluoropyridine above (Table 5-4), and two known hydrogen transfer catalysts, IrCp*Cl$_2$(Bzmim), **15**,[180] and [*(S,S)*-Teth-TsDpen RuCl],[390] to investigate whether this hydrogen transfer ability could be exploited in hydrodefluorination reactions. The results of this investigation are summarised in Table 5-7.

Unlike the high activities observed for defluorinative substitution with alcohols, treatment with [RuCp*Cl(PPh$_3$)$_2$] and [CoCl(PPh$_3$)$_3$] (Table 5-7; entry 1 and 2 respectively) resulted in the formation of only trace quantity of 2,3,5,6-Tetrafluoropyridine, **36**, detected by ^{19}F NMR (-92.1 and -142.6 ppm). The hydrogen transfer catalysts **15** and [*(S,S)*-Teth-TsDpen RuCl] proved more active resulting in 32 and 54 % contained yield of 2,3,5,6-Tetrafluoropyridine, **36**, respectively (Table 5-7;entry 3 and 4 respectively). While [*(S,S)*-Teth-TsDpen RuCl] gave the best hydrodefluorination activity of the catalysts tested the formation of 2,3,5,6-Tetrafluoropyridine could not be improved upon further testing. [*(S,S)*-Teth-TsDpen RuCl] was observed to undergo deactivation after three hours, as illustrated through the change in colour of solution from royal purple to orange (Figure 5-4). Sampling of the reaction at this point and after 24 hours showed no increase in the yield of 2,3,5,6-Tetrafluoropyridine, **36**, after the colour change had occurred. Further optimisation studies could be conducted in the future.

Table 5-7: Investigation of catalysts on the hydrodefluorination of pentafluoropyridine with potassium formate.[a]
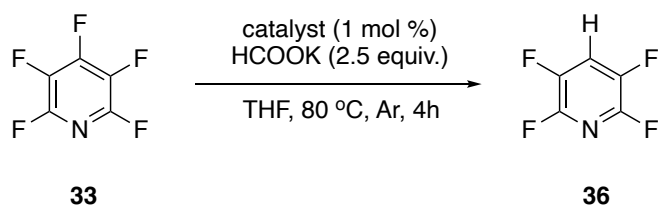
Entry	Catalyst	Conversion from 33 (%)[b]	Yield of 36 (%)[c]	TON	TOF (h⁻¹)
1	CoCl(PPh₃)₃	2	1	-	-
2	RuCp*Cl(PPh₃)₂	2	1	-	-
3[c]	**15**	35	32	32	8
4	[(S,S)-Teth-TsDpen RuCl]	54	54	54	13.5

[a] Pentafluoropyridine (1.0 mmol), THF (5.0 mL), HCOOK (2.5 mmol), catalyst (1.0 mol %), 80 °C, argon, 4 hours. [b] Conversion calculated as loss of pentafluoropyridine determined by ¹⁹F NMR against internal standard, trifluorotoluene (20 μL). [c] Contained yields calculated as formation of 2,3,5,6-Tetrafluoropyridine determined by ¹⁹F NMR against internal standard, trifluorotoluene (20 μL). [c] Minor unidentified product on ¹⁹F NMR spectra baseline.
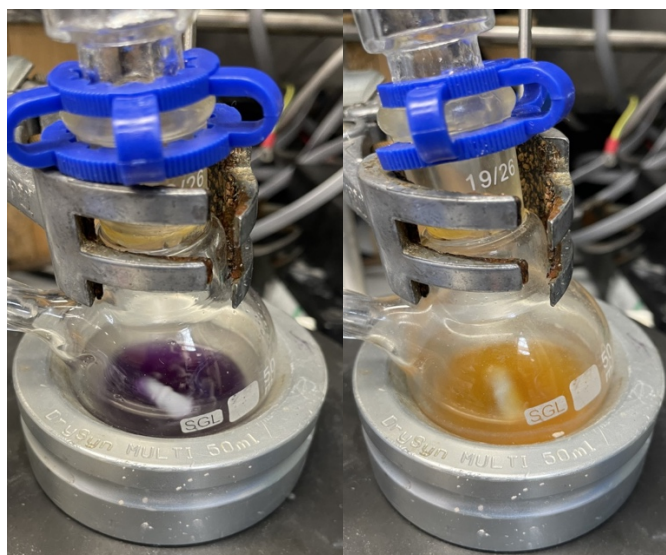
Figure 5-4: The colour of solution containing [(S,S)-Teth-TsDpen RuCl] (1 mol %) and potassium formation after addition of pentafluoropyridine upon heating to 80 °C for 10 minutes (left); for 3 hours (right). After 3 hours no increase in the contained yield of 2,3,5,6-Tetrafluoropyridine was observed, indicating catalyst deactivation.

5.5 Summary

Adapted methodologies for the defluorination of pentafluoropyridine have been described. A catalytic transfer fluorination methodology was attempted, using pentafluoropyridine as the fluorine source for the fluorination of acyl chlorides in the presence of 1 mol % [RhCl(CO)(PPh$_3$)$_2$]. This resulted in the formation of the acyl fluoride product and the mono-defluorinated 2,3,5,6-pentafluoropyridine by ^{19}F NMR analysis, however only small quantities of the fluorinated product (*ca*. 6 %) were formed for this protocol. During the development of this system a catalytic fluorine transfer methodology was described, utilising DMAP as the organocatalyst, for the successful transfer fluorination reaction between pentafluoropyridine and acyl chlorides.[307] This methodology was adapted through the inclusion of a metal catalyst. Inclusion of metal was found to have a minimal impact on the overall yield of the acyl fluoride products, however it was found that transfer fluorination occurred more rapidly, occurring over the course of 6 hours, *vs*. 17 hours for the published system. This represents a methodology for the synthesis of a range of acyl fluoride and acyl-substituted tetrafluoropyridine products.

In an attempt to develop an efficient hydrodefluorination procedure, a base assisted defluorinative substitution of pentafluoropyridine was developed. Treatment of a metal catalyst, with low metal loading of 0.1 mol %, afforded the selective mono-defluorination of pentafluoropyridine, resulting in up to 73 % isolated yield of the 4-alkoxy-2,3,5,6-Tetrafluoropyridine products. The cobalt catalyst, [CoCl(PPh$_3$)$_3$], was found to be particularly active towards the selective mono-defluorination of pentafluoropyridine, affording the highest TOF for this reaction at 650 h^{-1}. The choice of base was found to be significant in achieving selective mono-defluorination, with di-defluorination of pentafluoropyridine observed upon use of sodium and potassium *tert*-butoxide. Potassium formate was found to promote the formation of 2,3,5,6-Tetrafluoropyridine *via* a hydrodefluorination route, which was further developed to limit defluorinative substitution of pentafluoropyridine and resulted in good contained yields of the hydrodefluorination product upon treatment with hydrogen transfer catalysts.

5.6   Experimental

5.6.1   Instrumentation

NMR spectral analysis was carried out using a Bruker Ascend 400 spectrometer (400 MHz) and Bruker Ascend 500 spectrometer (500 MHz) at room temperature ($\approx$ 300 K). ^{1}H and ^{13}C NMR spectra were referenced to the corresponding residual solvent signals (CDCl$_3$: 7.26 ppm for ^{1}H, 77.16 ppm for ^{13}C). The ^{19}F NMR spectra were referenced by an internal method of the NMR. The chemical shifts are reported in ppm and coupling constants are given in Hz. NMR data was processed using MestReNova software. Multiplicity assignments in NMR spectra are labelled as follows: "s" = singlet, "d"= doublet, "t"= triplet, "q" = quartet, "p" = pentet, "h" = heptet, "m" = multiplet. NMR assignments for all synthesised complexes are given; ^{1}H NMR (green), ^{19}F NMR (red) and ^{13}C NMR (blue). Due to the 10 equivalents of substrate added during substrate scope investigation ^{1}H NMR analysis of products proved difficult in some cases due to overlapping signals. Electrospray mass spectra were recorded on a Bruker micrOTOF II with Agilent technologies 1200 Infinity Series mass spectrometer. All experiments were carried out under an inert gas atmosphere using standard Schleck techniques and/or a glove box (MBraun MG-200-B Eco), using oven and flame-dried glassware that had been put under vacuum and back-filled with argon three consecutive times, unless otherwise noted.

5.6.2   Materials

[IrCl(CO)(PPh$_3$)$_2$] and [RhCl(CO)(PPh$_3$)$_2$] were synthesized as previously described.[34] Wilkinson's catalyst, [*(S,S)*-Teth-TsDpen RuCl], 4-N,N-dimethylaminopyridine, DABCO, DBU, trifluorotoluene, potassium carbonate, sodium carbonate, silver carbonate, potassium *tert*-butoxide, sodium *tert*-butoxide and potassium hexamethyldisilylamide were purchased from Sigma Aldrich (Merck). [RhCp*Cl$_2$]$_2$, [IrCp*Cl$_2$]$_2$, CoCl(PPh$_3$)$_3$, [Ru(*p*-Cy)Cl$_2$]$_2$ were purchased from Alfa Aesar. RuCp*Cl(PPh$_3$)$_3$ and benzoic anhydride were purchased from Strem Chemicals. All solvents, with the exception of isopropanol, 2-butanol and ethanol were dried over 3Å molecular sieves for 24 hours followed by degasification *via* standard freeze-thaw-degas techniques prior to use. Benzoyl chloride and pentafluoropyridine were dried over 3Å molecular sieves for 24 hours followed by degasification *via* standard freeze-thaw-degas techniques prior to use.

5.6.3 Catalytic transfer fluorination

5.6.3.1 Procedure for the transfer fluorination between pentafluoropyridine and benzoyl chloride

[RhCl(CO)(PPh$_3$)$_2$] (6.90 mg, 0.01 mmol) and silver carbonate (0.41 g, 1.50 mmol) was added to a side-arm round bottomed flask, containing a magnetic stir bar and evacuated and backfilled with argon three times. Acetonitrile (5 mL) was added *via* syringe, followed by pentafluoropyridine (110 µL, 1.0 mmol) and benzoyl chloride (116 µL, 1.0 mmol). The reaction mixture was heated to 40 °C and allowed to stir (400 rpm) in darkness for four hours. After the reaction time had elapsed the reaction mixture was filtered through a plug of celite, washed with acetonitrile (3 x 5 mL) and the solvent was removed under reduced pressure (150 mbar). The resulting pale yellow oily residue was transferred to an NMR tube, with the aid of deuterated chloroform (0.5 mL) alongside trifluorotoluene (20 µL). Internal contained yield of the benzoyl fluoride product was determined against trifluorotoluene as the internal standard. ^{19}F NMR yield *vs.* the internal standard: 6 %.

Benzoyl fluoride: **^{19}F NMR:** (376 MHz, *d-chloroform*): δ 17.10 (s, CO*F*, 1F).[242]

4-Chloro-2,3,5,6-Tetrafluoropyridine: **^{19}F NMR:** (376 MHz, *d-chloroform*): δ -88.23 (m, C*F*, 2F), -141.21 (m, C*F*, 2F).[391]
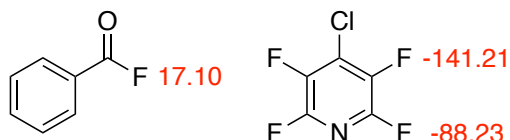
5.6.3.2 General procedure for the transfer fluorinated protocol adapted from work by Crimmin and co-workers.[307]

In a glovebox, pentafluoropyridine (0.2 mmol), benzoic anhydride (2.0 mmol) and trifluorotoluene (20 µL) were added to an empty J. Young's NMR tube. The NMR tube was sealed and then removed from the glovebox and placed in an inert NMR tube filler, which was evacuated and backfilled with argon three times. For catalytic testing stock solutions were made by dissolving 0.01 mmol of the metal complex in 20 mL of acetonitrile or dimethylformamide. A stock solution of 4-N,N-dimethylaminopyridine (DMAP) was also prepared by dissolving DMAP (43 mg, 0.35 mmol) in deuterated benzene (4 mL). Under a dynamic pressure of argon the NMR tube was unsealed and the catalyst / acetonitrile or

dimethylformamide stock solution (1.0 mol %, 0.002 mmol / 0.4 mL), followed by the DMAP / deuterated benzene stock solution (5.0 mol %, 0.01 mmol / 50 μL) were added *via* syringe. The NMR tube was sealed under a dynamic pressure of argon and heated at 100 °C in an oil bath for 17 hours. The reaction mixture was allowed to cool and contained yields were calculated *via* quantitative ^{19}F NMR analysis against the internal standard, trifluorotoluene (20 μL).

Benzoyl fluoride: ^{19}**F NMR** (376 MHz, d_6-benzene): δ 17.40 (s, CO*F*, 1F).[242]

4-Benzoic-2,3,5,6-Tetrafluoropyridine: ^{19}**F NMR** (376 MHz, d_6-benzene): δ -90.33 (m, 2F), -152.82 (m, 2F).
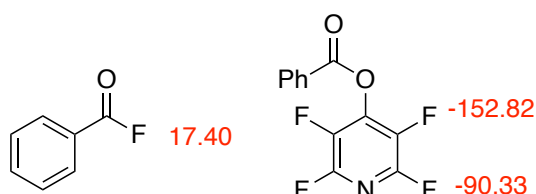
Characterisation is consistent with previously reported literature.[307]

5.6.4   Base assisted defluorination of pentafluoropyridine

5.6.4.1   Synthesis of 4-*i*Propoxy-2,3,5,6-Tetrafluoropyridine, **34**.

RuCp*Cl(PPh$_3$)$_2$ (8.0 mg, 0.01 mmol) and potassium carbonate (346 mg, 2.5 mmol) were added to a Schlenk flask alongside a magnetic stirrer bar. The flask was evacuated and backfilled with argon three times, taking care not to disturb the solids. Isopropanol (5 mL) was added under a dynamic pressure of argon, before pentafluoropyridine (110 μL, 1.0 mmol) was added *via* pipette and the reaction was stirred at 500 rpm. The flask was then sealed and heated to 80°C for 2 hours. The reaction mixture was filtered through a plug of celite while hot and the solvent was removed under reduced pressure, to give a pale orange oil. Product isolation was achieved by column chromatography using n-heptane (R$_f$ 0.73, *n*-heptane).

4-*i*Propoxy-2,3,5,6-Tetrafluoropyridine, **34**; colourless oil. Isolated yield: 153 mg (73 %). ^{1}**H NMR** (400 MHz, *d-chloroform*): δ 5.01 (h, $^3J_{HH}$ = 6.1 Hz, C*H*, 1H), 1.43 (d, $^3J_{HH}$ = 6.0 Hz, C*H*$_3$, 6H). ^{19}**F NMR** (376 MHz, *d-chloroform*): δ -91.2 (m, C*F*, 2F), -158.63 (m, C*F*, 2F). ^{13}**C NMR** (101 MHz, *d-chloroform*): δ 145.6 (d, J_{CF} = 12.4 Hz, *Ar*F), 143.1 (d, J_{CF} = 15.0 Hz,

*Ar*F), 134.4 (d, J_{CF} = 31.9 Hz, *Ar*F), 78.4 (q, J_{CH} = 5.0 Hz, CH_3), 22.6 (d, J_{CH} = 1.7 Hz, *C*H). **MS** (ESI): Theoretical [M+MeCN+H]$^+$ [$C_{12}H_9F_8N_2O$]$^+$ 391.2342; found for [$C_{12}H_9F_8N_2O$]$^+$ 391.2840. **IR**: 2937, 2843, 1732, 1596, 1505, 1460, 1422, 1264, 1159, 1023, 869, 777,606, 407.
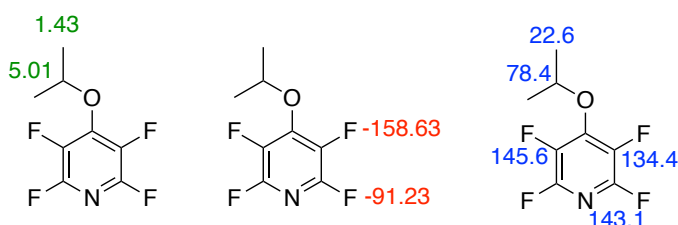
Characterisation is consistent with previously reported literature. [365]

5.6.4.2   Synthesis of 2,4-di-*i*propoxy-3,5,6-trifluoropyridine, **35**.

RuCp*Cl(PPh$_3$)$_2$ (8.0 mg, 0.01 mmol) and potassium carbonate (346 mg, 2.5 mmol) were added to a Schlenk flask alongside a magnetic stirrer bar. The flask was evacuated and backfilled with argon three times, taking care not to disturb the solids. Isopropanol (5 mL) was added under a dynamic pressure of argon, before pentafluoropyridine (110 µL, 1.0 mmol) was added *via* pipette and the reaction was stirred at 500 rpm. The flask was then sealed and heated to 80°C for 2 hours. The reaction mixture was filtered through a plug of celite while hot and the solvent was removed under reduced pressure, to give a pale orange oil. Product isolation was achieved by column chromatography using 10:1 *n*-heptane:ethyl acetate as a mixture with 4-*i*Propoxy-2,3,5,6-Tetrafluoropyridine, **34** (R_f 0.74, 10:1 ethyl acetate: *n*-heptane).

2,4-di*i*propoxy-3,5,6-trifluoropyridine, **35**; colourless solid. Isolated yield: trace. **^{1}H NMR** (400 MHz, *d-chloroform*): δ 5.19 (h, $^3J_{HH}$ = 6.1 Hz, C*H,* 1H), 4.85 (h, $^3J_{HH}$ = 6.1 Hz, C*H,* 1H). Other protons difficult to assign due to overlap with 4-*i*Propoxy-2,3,5,6-Tetrafluoropyridine, **34**. **^{19}F NMR** (376 MHz, *d-chloroform*): δ -93.94 (t, J_{FF} = 24.1 Hz, C*F*, 1F), -158.66 (d, J_{FF} = 25.4 Hz, C*F*, 1F), -166.69 (d, J_{FF} = 23.1 Hz, C*F*, 1F). **^{13}C NMR** (101 MHz, *d-chloroform*): δ 145.6 (m, *C*O), 143.8(m, N*C*O), 143.4 (dd, J_{CF} = 10.6, 4.6 Hz, N*C*F), 137.2 (d, J_{CF} = 30.4 Hz, *Ar*F), 131.5 (d, J_{CF} = 30.8 Hz, *Ar*F), 77.7 (m, *C*H), 70.5 (m, *C*H), 22.7 (m, *C*H$_3$), 22.0 (m, *C*H$_3$).
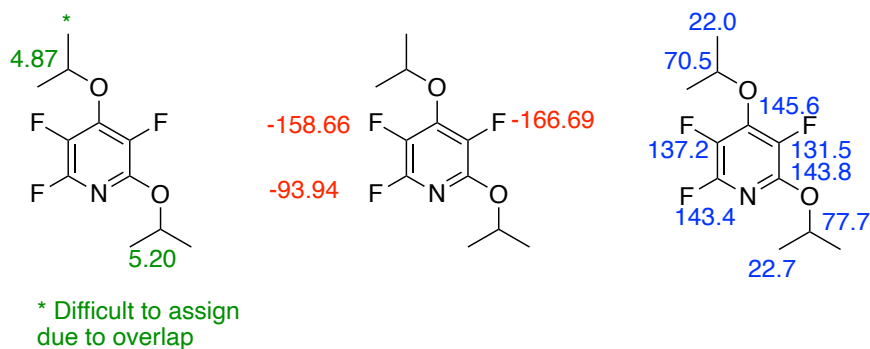
Characterisation is consistent with previously reported literature. [365]

5.6.4.3 General procedure for the development of base assisted defluorination of pentafluoropyridine.

5.6.4.3.1 General procedure for catalyst screen

The catalyst (0.01 mmol) and potassium carbonate (346 mg, 2.5 mmol) were added to a Schlenk flask alongside a magnetic stirrer bar. The flask was evacuated and backfilled with argon three times. Isopropanol (5 mL) was added under a dynamic pressure of argon, before pentafluoropyridine (110 μL, 1.0 mmol) was added *via* pipette. The flask was then sealed and heated to 80°C for 2 hours. The reaction mixture was then filtered through a plug of celite while hot. A sample of the filtrate (0.5 mL) was taken for NMR analysis.

5.6.4.3.2 General procedure for catalyst loading

The catalyst (0.001 - 0.01 mmol) and potassium carbonate (346 mg, 2.5 mmol) were added to a Schlenk flask alongside a magnetic stirrer bar. The flask was evacuated and backfilled with argon three times. Isopropanol (5 mL) was added under a dynamic pressure of argon, before pentafluoropyridine (110 μL, 1.0 mmol) was added *via* pipette. The flask was then sealed and heated to 80°C for 1 - 4 hours. The reaction mixture was then filtered through a plug of celite while hot. A sample of the filtrate (0.5 mL) was taken for NMR analysis.

5.6.4.3.3 General procedure for solvent screening

RuCp*Cl(PPh$_3$)$_2$ (0.8 mg, 0.001 mmol) and potassium carbonate (346 mg, 2.5 mmol) were added to a Schlenk flask alongside a magnetic stirrer bar. The flask was evacuated and backfilled with argon three times. Solvent (5 mL) was added under a dynamic pressure of

argon, before pentafluoropyridine (110 μL, 1.0 mmol) was added *via* pipette. The flask was then sealed and heated to 80°C for 2 hours. The reaction mixture was then filtered through a plug of celite while hot. A sample of the filtrate (0.5 mL) was taken for NMR analysis.

5.6.4.3.4 General procedure for base screening

RhCl(PPh$_3$)$_3$ (9.3 mg, 0.01 mmol) and base (2.5 mmol) were added to a Schlenk flask alongside a magnetic stirrer bar. The flask was evacuated and backfilled with argon three times. Isopropanol (5 mL) was added under a dynamic pressure of argon, before pentafluoropyridine (110 μL, 1.0 mmol) was added *via* pipette. The flask was then sealed and heated to 80°C for 4 hours. The reaction mixture was then filtered through a plug of celite while hot. A sample of the filtrate (0.5 mL) was taken for NMR analysis.

5.6.5 Hydrodefluorination of pentafluoropyridine

5.6.5.1 General procedure for catalyst screen

The catalyst (0.01 mmol) and potassium formate (210 mg, 2.5 mmol) were added to a Schlenk flask alongside a magnetic stirrer bar. The flask was evacuated and backfilled with argon three times. Tetrahydrofuran (5 mL) was added under a dynamic pressure of argon, before pentafluoropyridine (110 μL, 1.0 mmol) was added *via* pipette. The flask was then sealed and heated to 80°C for 2 hours. The reaction mixture was then filtered through a plug of celite while hot. A sample of the filtrate (0.5 mL) was taken for NMR analysis.

Contained yield of 2,3,5,6-Tetrafluoropyridine, **36**, *vs* internal standard: up to 54 %. **^{1}H NMR** (400 MHz, *d-chloroform*): δ 7.55 (m, C$_5$*H,* 1H). **^{19}F NMR** (376 MHz, *d-chloroform*): δ -91.88 (m, C*F*, 2F), -141.24 (m, C*F*, 2F). **MS** (ESI): Theoretical for [C$_5$F$_4$N] [M+Na$_2$-H]$^+$ 194.9683; found for [M+Na$_2$-H]$^+$ 194.9677.
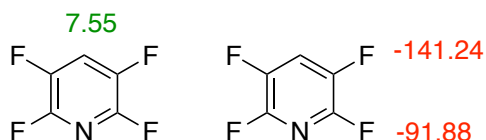
Characterisation is consistent with previously reported literature.[392]

6 Chapter 6: Conclusions and Future Work

This thesis has demonstrated the development of more sustainable fluorination practices to control the generation and reactivity of nucleophilic fluorine through the activation of inorganic and organic fluorine sources. The fluorination of organic electrophiles from a TMF has been demonstrated, exhibiting improved control of fluorine, leading to enhanced reactivity compared to the metal fluoride salt precursors. This led to the development of a catalytic methodology for the synthesis of fluorinated compounds, proposed to proceed through the generation of a reactive TMF *in-situ*. Spectroscopic analysis assisted in understanding how the reactivity of fluorine was improved, which can be used to inform future research. One of the first transfer fluorination methodologies, resulting in the fluorination of an organic electrophile from a perfluorinated moiety has been demonstrated. The environment required to activate organic fluorine towards nucleophilic fluorination was investigated, giving an understanding of how nucleophilic fluorine was generated. Coupled with the development of a catalytic protocol for the defluorination of pentafluoropyridine this work has explored how different fluorine methodologies can be used to synthesise desirable fluorinated compounds from more sustainable or potential waste sources of fluorine, presenting an intriguing possibility of realising a circular fluorine economy in the future.

To achieve these outcomes, the synthesis of a range of group 9 organometallic complexes bearing NHC ligands were targeted. The complexes were synthesised *via* a two-step process involving formation of an imidazolium silver adduct with silver oxide prior to *trans*metallation with a metal precursor to give the desired complex. Tuning the NHC ligands through the altering the fluorine content of the benzylic side chain was conducted, to investigate whether increasing the electron withdrawing nature of the imidazolium side arm had an impact on the fluorination potential of the complexes.

While the synthesis of the catalytic targets described above, is efficient, resulting in up to 93 % overall yield of the metal complexes in one pot over 3 steps, one of the major drawbacks of this procedure is the large quantity of silver waste produced as a by-product. The only sources of waste across the synthesis, not considering benign waste or solvent, is silver bromide and unreacted silver oxide, representing an atom economy of 0.59, for the synthesis of $IrCp^*Cl_2(F_5Bzmim)$, **11** (Scheme 6-1). Therefore, if an alternative route to activate the NHC precursor prior to complexation could be designed, avoiding the *trans*metallation step with silver, the synthesis of these complexes could become more sustainable without generating expensive silver containing waste.

One alternative methodology which has briefly been explored is the synthesis of an imidazolium carboxylate species. These carboxylates are bench stable zwitterionic compounds which can act as NHC precursors upon treatment with an appropriate metal compound, under thermal decarboxylation to give the desired metal-NHC complex.[393, 394] Attempts to make the imidazolium carbonate from treatment of dimethyl carbonate with (2,3,4,5,6-pentafluorobenzyl)imidazolium bromide, **1**, proved unsuccessful, resulting in the formation of a brown sludge, which could not be purified further. Limited success was found when bubbling CO_2 through a solution of 3-methyl-1-pentafluorobenzylimidazolium bromide in the presence of potassium carbonate, resulting in the formation of the imidazolium carboxylate detected by ^{13}C NMR and FTIR, in low yields. Initial attempts to form **11**, *via* thermal decarboxylation proved inconclusive. If the appropriate imidazolium carboxylate compound could be prepared, in comparable yields and purity to the current silver oxide route, for the synthesis of **11**, it would drastically reduce the quantity of waste produced, compared to the current procedure, giving an atom economy of 0.95. The limited success of this project highlights the potential feasibility of developing the synthesis of these NHC piano stool complexes towards a more sustainable procedure, utilising CO_2 as a benign transfer agent. Future work could include using high purity CO_2 from a gas cylinder, as opposed to dry ice sublimation, in addition to optimising the reaction conditions focussing on solvent and base selection using a high pressure setup or the targeted synthesis of imidazolium hydrogen carbonates.[395] Decarboxylative addition to the metal precursor can then be conducted, looking at the effect of temperature and reduced pressures on the decarboxylation of the NHC precursor, followed by isolation and characterisation of the resultant metal NHC complex.

Atom economy = 0.59

11

Atom economy = 0.95

11
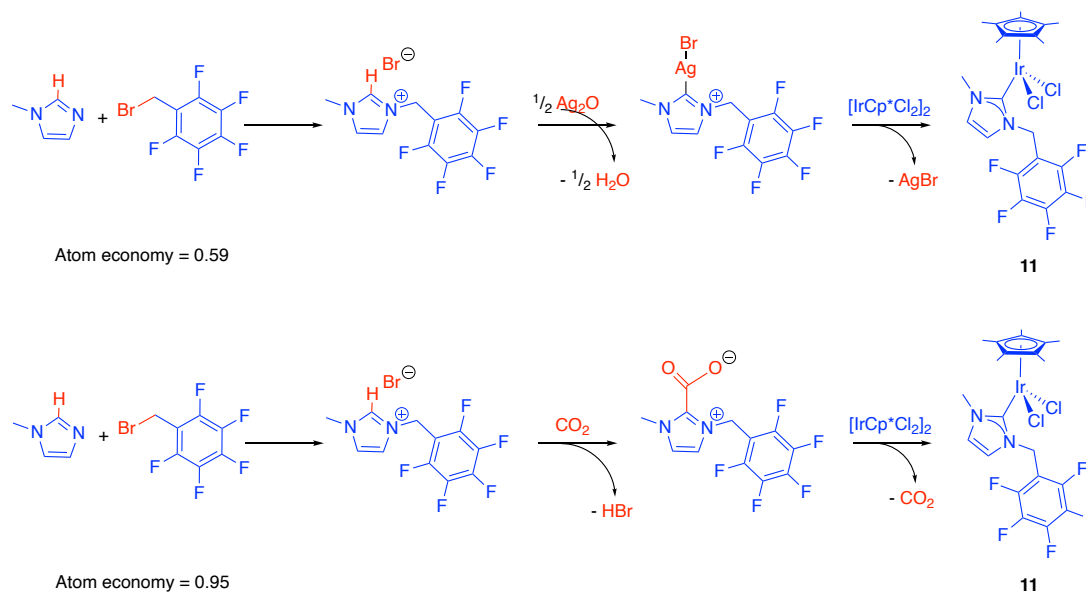
*Scheme 6-1: Synthetic steps towards the synthesis of IrCp*Cl₂(F₅Bzmim), **11**, highlighting the components incorporated into the final product (blue) and those contributing to waste (red) to give an overall atom economy of 0.59 for the silver mediated route and 0.95 for the carboxylate route.*

The formation of *ortho*metallated and *cyclo*metallated complexes of rhodium and iridium, formed through the addition of excess silver oxide was investigated and the development of practical synthetic routes towards there synthesis were explored. Outputs from early computational calculations, conducted by Professor Stuart Macgregor, of Heriott-Watt University, Edinburgh, indicate that fluorination from analogous *cyclo*metallated complexes containing less fluorinated ligands may result in the generation of more nucleophilic fluorine. Therefore, the development of a second generation of *cyclo*metallated complexes, bearing less fluorinated NHC ligands should be targeted in the future. Initial work attempting to form the *cyclo*metallated analogues of pentamethylcyclopentadienylrhodium-(-3-methyl-1-benzylimidazolium) chloride, **10**, pentamethylcyclopentadienyl rhodium(-3-methyl-1-(2,4,6-trifluoro)benzylimidazolium)chloride, **8** and pentamethylcyclopentadienyl rhodium-(-3-methyl-1-(4-trifluoromethyl)benzylimidazolium) chloride through the addition of silver oxide proved unsuccessful, but further studies examining the effect of base, solvent and temperature are warranted.

The synthesis of cobalt piano-stool complexes bearing NHC ligands was developed, where the cobalt precursor, $[CoCp*I_2]_2$, was targeted to allow for the synthesis of pentamethylcyclopentadienyl cobalt(-3-methyl-1-(2,3,4,5,6-pentafluoro)benzylimidazolium) chloride, **26**, complex following an analogous route to that developed previously for rhodium and iridium. Addition of silver oxide to pentamethylcyclopentadienylcobalt(-3-methyl-1-(2,3,4,5,6-pentafluoro)benzylimidazolium)chloride, **26**, in an attempt to form the *ortho*metallated or *cyclo*metallated complexes, analogous to that observed with pentamethylcyclopentadienyl rhodium(-3-methyl-1-(2,3,4,5,6-pentafluoro)benzylimidazolium) chloride, **6**, and pentamethylcyclopentadienyliridium(-3-methyl-1-(2,3,4,5,6-pentafluoro)benzylimidazolium)chloride, **11**, proved inconclusive. Therefore, additional method development will be required to achieve the clean formation of the *ortho*metallated and *cyclo*metallated cobalt complexes for further catalytic testing.

TMF complexes, based on Vaska's complex, $[MCl(CO)(PPh_3)_2]$, have been successfully synthesised and characterised. Treatment of $[IrF(CO)(PPh_3)_2]$ or $[RhF(CO)(PPh_3)_2]$ with the organic electrophile, toluoyl chloride, was found to result in the rapid fluorination of the substrate and the reformation of $[MCl(CO)(PPh_3)_2]$. $[MF(CO)(PR_3)_2]$ complexes were targeted due to their straightforward synthesis, crystallisation and spectroscopic handles (FTIR/^{19}F & ^{31}P NMR). A limited number of publications on the fluorination of organic substrates by TMF have been reported, therefore understanding the environment required to generate nucleophilic fluorine from a TMF complex is important. To our knowledge this

represents the first account of the fluorination of an organic electrophile using these complexes.

Due to the success of this stoichiometric fluorination from $[MF(CO)(PPh_3)_2]$, further work investigating the effect of the coordination sphere on fluorination could be conducted to improve the limited catalytic fluorination observed upon treatment of $[MCl(CO)(PPh_3)_2]$ with silver fluoride. The phosphine ligand can be readily exchanged, enabling the modification of the coordination sphere of the complex, tuning its steric and electronic nature. Changing the electronic and steric properties of the coordination sphere result in changes to the strength of the M–F and carbonyl bonds which can be probed spectroscopically through FTIR (CO stretching frequency) ^{19}F NMR (chemical shift) and single crystal XRD. The addition of electron withdrawing ligands adjacent to the metal centre results in the strengthening of the M–F bond, due to the reduced electron density of the metal centre and increasing π-donation from the fluorine atom which could lead to the stabilisation of the TMF. Alternatively, electron donating ligands could be used to weaken the bond strength of the TMF and increase the reactivity and nucleophilicity of the fluoride. Altering the ligand environment around the complex will alter the fluorination ability of the TMF allowing the nature of the M−F bond to be probed. Future experiments could be designed were treatment of these TMF complexes with organic electrophiles investigate the reactivity of the TMFs towards nucleophilic fluorination. As these reactions can be monitored spectroscopically, an understanding of the ideal bonding environments could be examined, the insights of which could be used to further inform future catalytic development. Complementary computational studies of these TMF complexes can be designed to calculate the complex geometry, fluoride nucleophilicity, M–F bond strength and carbonyl stretching frequency of complexes with differing phosphine ligands. These theoretical calculations could be used to target ligands which have not been carried out experimentally, informing further experimental targets.

The catalytic fluorination of acyl chlorides has been reported, resulting in up to quantitative yields of the fluorinated products, under mild conditions in as little as one hour. An investigation of the fluorination potential of the complexes synthesised in *chapter 2* showed that $[(\eta^5,\kappa_2C\text{-}C_5Me_4CH_2C_6F_5CH_2NC_3H_2NMe)\text{-} RhCl]$, **22**, was the most active catalyst towards the fluorination of toluoyl chloride. Following reaction development, monitoring of the catalytic fluorination reaction by *in-situ* FTIR enabled the generation of progress reaction profiles. This allowed for more precise determination of reaction time, as the consumption of toluoyl chloride and formation of toluoyl fluoride could be monitored in real time. This showed quantitative conversion of toluoyl fluoride after 3 $^{1/2}$ hours. This real time monitoring allowed for substituent effects to be explored, through the calculation of initial rates of

reaction. Comparing this against the electrophilicity of the carbonyl region (taken from the FTIR carbonyl stretching frequency of the substrate) illustrated that substrate containing electron withdrawing aryl substituents underwent fluorination faster than substrates containing electron donating substituents, consistent with a rate determining step involving the nucleophilic attack of the electrophile by fluoride. Subsequent VTNA analysis probed the effect of catalyst activation and deactivation, aiding in the proposal of a catalytic fluorination reaction mechanism first order with respect to the acyl chloride substrate and catalyst. The development of a second generation catalyst, with the potential of generating more nucleophilic fluorine would be advantageous. The formation of more nucleophilic fluorine through the treatment of the catalyst with the metal fluoride salt could allow for the fluorination of less electrophilic substrates. Continued catalytic development could allow for the enhancement of fluorination using more abundant and sustainable fluorine sources such as potassium fluoride.

Observations of fluorination in the absence of an external fluorine source within these catalytic fluorination experiments lead to the discovery of one of the first examples of transfer fluorination between a perfluorinated group and an organic electrophile (Scheme 6-2). Single crystal XRD and ^{19}F NMR studies gave evidence of the formation of a new bimetallic rhodacycle, upon treatment of **22** with toluoyl chloride. Multi-spectral analysis provided an understanding of the environment required to generate nucleophilic fluorine, allowing the transfer of fluorine between the organometallic species and organic electrophile to be tracked in real time.
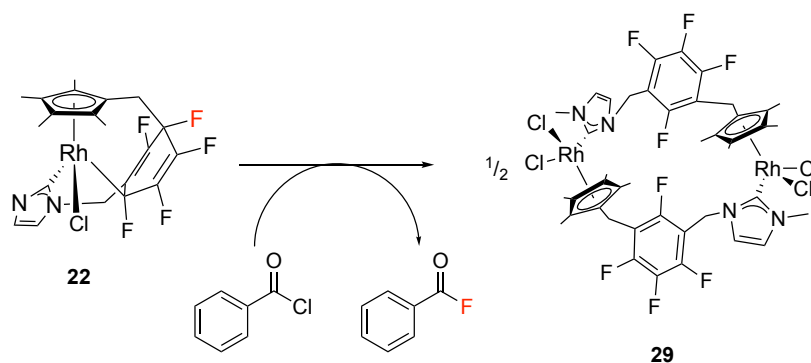
*Scheme 6-2: Transfer fluorination between **22** and benzoyl chloride resulting in formation of benzoyl fluoride product and bimetallic rhodacycle, **29**.*

After demonstrating the ability of **22** to undergo a transfer fluorination reaction upon treatment with organic electrophiles, the defluorination of perfluoroarenes was conducted. The use of organic fluorine as fluorine sources for the fluorination of acyl chlorides, towards the development of a catalytic transfer fluorination was attempted, with limited success.

Chapter 6: Conclusions and Future Work

Activation of pentafluoropyridine towards fluoride transfer was conducted using catalytic quantities of [MCl(CO)(PPh$_3$)$_2$] (M = Ir or Rh) and DMAP *via* an adapted literature methodology facilitating the transfer of fluorine from pentafluoropyridine resulting in the formation of 4-benzoic-2,3,5,6-Tetrafluoropyridine and benzoyl fluoride in moderate yields. Initial results highlight that adventitious water may enhance the transfer of fluorine in this system, leading to a higher yield of fluorinated product. Addition of water may result in the formation of a partial solvation shell around the fluoride anion, acting to "shuttle" the fluoride, enhancing its reactivity. [383, 384] Therefore, additional experiments exploring the effect of water doping on anhydrous systems could be conducted. These experiments may inform the fluoride environment required to ensure high levels of transfer fluorination activity and prove valuable in exploring further mechanistic studies.

Subsequently, a base assisted pentafluoropyridine defluorinative substitution protocol was developed, allowing for the selective alkoxylation of *para*-C−F bond by **22** and commercially available group 8 and 9 complexes, using low metal loading of 0.1 mol %, giving TONs up to 650 h^{-1} for [CoCl(PPh$_3$)$_3$]. Further work to explore the scope of alcohol addition to pentafluoropyridine could allow for this protocol to be useful in the synthesis of fluorinated scaffolds for the synthesis of functionalised fluorinated molecules of interest within drug discovery. The effect of base on this reaction was also found to be significant. Conducting a base screen led to the development of a hydrodefluorination reaction, with potassium formate, in the presence of hydrogen transfer catalysts. Solvent selection was important for the reduction of side-reactions, with tetrahydrofuran giving up to 64 % of the mono-hydrodefluorinated product without the formation of minor side-products observed by ^{19}F NMR. Future work could include the optimising the conditions for hydrogen transfer catalysed hydrodefluorination of pentafluoropyridine.

These results are significant as they explore a methodology to stimulate fluorine activation within a perfluorinated compound. This represents an opportunity to take these over fluorinated compounds, which are readily synthesised using established industrially processes, and access valuble partially fluorinated compounds *via* selective defluorination. These defluorination processes also produce metal fluoride salts as a by-product. Therefore, these salts could potentially be utilised as fluoride sources for selective catalytic fluorination, providing a methodology to transfer fluorine from where it is not wanted, to where it is desirable, resulting in the valorisation of both substituents. Alternatively, oxidative addition of perfluorinated compounds across low oxidation state, coordinatively unsaturated complexes could afford the formation of a metal–fluoride bond,[382] resulting in transfer fluorination upon addition of an electrophile. These represent two methodologies which have

to potential of achieving catalytic transfer fluorination utilising simple perfluorinated molecules as the fluorine source.

To our knowledge, **22** represents the first reported complex that has exhibited activity towards catalytic fluorination, defluorination and fluorine transfer methodologies.

7   References

1.   Banks, R. E., Isolation of flourine by Moissan: setting the scene. *J. Fluor. Chem.* **1986,** *33* (1), 3-26.

2.   Scheele, c., Fluorspar and its acid. *Akad. Stolkholm* **1771,** *33*, 120.

3.   Davy, H., Some experiments and observations on the substances produced in different chemical processes on fluor spar. *Phil. Trans. R. Soc.* **1813,** *103*, 263-279.

4.   Frémy, E., Fremy Fluorine attempt. *Ann. Chim. Phys.* **1856**, 5.

5.   Fremy, E., Decomposition des fluorines au moyen de la pile. *Compt. Rend. Chim.* **1855,** *40*, 966-968.

6.   Moissan, H., Action d'un couraut Gectrique sur l'acide fluorhydrique. *Compt. Rend. Chim.* **1886,** *102*, 1543-1544.

7.   Borodin, A., Preparation of benzoyl fluoride. *C. R. Acad. Sci.* **1862,** *55*, 553 - 556.

8.   Gottlieb, H. B., The Replacement of Chlorine by Fluorine in Organic Compounds. *J. Am. Chem. Soc.* **1936,** *58* (3), 532-533.

9.   Fowler, R.; Buford, W.; Hamilton, J. J., Synthesis of fluorocarbons. *Ind. Eng. Chem.* **1947,** *39* (3), 292-298.

10.   Buford Iii, W.; Fowler, R.; Hamilton, J. J.; Anderson, H.; Weber, C.; Sweet, R., Pilot Plant Syntheses - Perfluoro-n-heptane, perfluorodimethylcyclohexane, and high boiling fluorocarbon oils. *Ind. Eng. Chem.* **1947,** *39* (3), 319-329.

11.   W.E. Hanford; Joyce, R. M., Polytetrafluoroethylene. *J Am Chem Soc* **1946,** *68*, 2082.

12.   Renfrew, M. M.; Lewis, E. E., Polytetrafluoroethylene. Heat Resistant, Chemically Inert Plastic. *Ind. Eng. Chem.* **1946,** *38*, 870-877.

13.   Goldwhite, H., The Manhattan Project. *J. Fluor. Chem.* **1986,** *33*, 109 - 132.

14.   B, alTorre; Albericio, F., The Pharmaceutical Industry in 2018. An Analysis of FDA Drug Approvals from the Perspective of Molecules. *Molecules* **2019,** *24* (4) 745-758.

15.   Inoue, M.; Sumii, Y.; Shibata, N., Contribution of Organofluorine Compounds to Pharmaceuticals. *ACS Omega* **2020,** *5* (19), 10633-10640.

16.   Jacobson, O.; Kiesewetter, D. O.; Chen, X., Fluorine-18 radiochemistry, labeling strategies and synthetic routes. *Bioconjug. Chem.* **2015,** *26* (1), 1-18.

17.   Ragni, R.; Punzi, A.; Babudri, F.; Farinola, G. M., Organic and Organometallic Fluorinated Materials for Electronics and Optoelectronics: A Survey on Recent Research. *Eur. J. Org. Chem.* **2018,** *2018* (27-28), 3500-3519.

18.   Cardoso, V. F.; Correia, D. M.; Ribeiro, C.; Fernandes, M. M.; Lanceros-Mendez, S., Fluorinated Polymers as Smart Materials for Advanced Biomedical Applications. *Polymers* **2018,** *10* (2) 161-187.

19.   C.A. Moody; Field, J. A., Perfluorinated Surfactants and the Environmental Implications of Their Use in Fire-Fighting Foams. *Environ. Sci. Technol.* **2000,** *34* (18), 3864 - 3870.

20.   Gottlieb, H. B., The Replacement of Chlorine by Fluorine in Organic Compounds. *J. Am. Chem. Soc.* **1936,** *58* (3), 532-533.

21.   Schiemann, B. G., Über Aromatische Fluorverbindungen, I.: Ein Neues Verfahren Zu Ihrer Darstellung. *Berichte der Dtsch. Chem. Gesellschaft* **1927,** *60* (5), 1186.

22.   Swarts, F., Fluorination of organic polyhalides with antimony trifluoride (or zinc and mercury fluorides) in the presence of a trace of a pentavalent antimony salt. *Bull. Acad. Roy. Belg.* **1892,** *24*, 309.

23.   R. D. Fowler; W. B. Burford; J. M. Hamilton, J.; R. G. Sweet; C. E. Weber; J. S. Kasper; Litant, I., Synthesis of Fluorocarbons. *Ind. Eng. Chem.* **1947,** *39* (3), 292 - 298.

24.   Simons, J. H.; Harland, W. J., Production of Fluorocarbons from hydrogen fluoride soluble organic substances. *J. Electrochem. Soc* **1949,** *95*, 55 - 59.

25.   Pearlson, W. H., The Simons electrochemical fluorination process (commercial development at 3M). *J. Fluor. Chem.* **1986,** *32* (1), 29 - 40.

References

26.   Hu, J.; Zeng, Y., Recent advances in green fluorine chemistry. *Reports in Organic Chemistry* **2015**, *5*, 19-39.

27.   States), F. s. C. f. D. E. a. R. U. *Advancing Health Through Innovation: New Drug Therapy Approvals 2020*; Silver Springs, MD, **2021**.

28.   insightSlice *Fluorochemicals Market - Global Market Share, Trends, Analysis and Forcasts, 2021 - 2031*; **2020**.

29.   Mei, H.; Han, J.; Fustero, S.; Medio-Simon, M.; Sedgwick, D. M.; Santi, C.; Ruzziconi, R.; Soloshonok, V. A., Fluorine-Containing Drugs Approved by the FDA in 2018. *Chem. Eur. J.* **2019**, *25* (51), 11797-11819.

30.   Constable, D. J. C.; Dunn, P. J.; Hayler, J. D.; Humphrey, G. R.; Leazer, J. J. L.; Linderman, R. J.; Lorenz, K.; Manley, J.; Pearlman, B. A.; Wells, A.; Zaks, A.; Zhang, T. Y., Key green chemistry research areas—a perspective from pharmaceutical manufacturers. *Green Chem.* **2007,** *9* (5), 411-420.

31.   Szpera, R.; Moseley, D. F. J.; Smith, L. B.; Sterling, A. J.; Gouverneur, V., The Fluorination of C−H Bonds: Developments and Perspectives. *Angew. Chem. Int. Ed.* **2019,** *58* (42), 14824-14848.

32.   Kuehnel, M. F.; Lentz, D.; Braun, T., Synthesis of fluorinated building blocks by transition-metal-mediated hydrodefluorination reactions. *Angew. Chem. Int. Ed.* **2013,** *52* (12), 3328-48.

33.   Ahrens, T.; Kohlmann, J.; Ahrens, M.; Braun, T., Functionalization of fluorinated molecules by transition-metal-mediated C-F bond activation to access fluorinated building blocks. *Chem. Re.v* **2015,** *115* (2), 931-72.

34.   Belhomme, M.-C.; Besset, T.; Poisson, T.; Pannecoucke, X., Recent Progress toward the Introduction of Functionalized Difluoromethylated Building Blocks onto $C(sp^2)$ and $C(sp)$ Centers. *Chem. Eur. J.* **2015,** *21* (37), 12836-12865.

35.   Landelle, G.; Bergeron, M.; Turcotte-Savard, M. O.; Paquin, J. F., Synthetic approaches to monofluoroalkenes. *Chem. Soc. Rev.* **2011,** *40* (5), 2867-908.

36.   Ferguson, D. M.; Malapit, C. A.; Bour, J. R.; Sanford, M. S., Palladium-Catalyzed Difluoromethylation of Aryl Chlorides and Bromides with $TMSCF_2H$. *J. Org. Chem.* **2019,** *84* (6), 3735-3740.

37.   Cismesia, M. A.; Ryan, S. J.; Bland, D. C.; Sanford, M. S., Multiple Approaches to the In Situ Generation of Anhydrous Tetraalkylammonium Fluoride Salts for S_NAr Fluorination Reactions. *J. Org. Chem.* **2017,** *82* (10), 5020-5026.

38.   Schimler, S. D.; Cismesia, M. A.; Hanley, P. S.; Froese, R. D.; Jansma, M. J.; Bland, D. C.; Sanford, M. S., Nucleophilic Deoxyfluorination of Phenols via Aryl Fluorosulfonate Intermediates. *J. Am. Chem. Soc.* **2017,** *139* (4), 1452-1455.

39.   Neumann, C. N.; Ritter, T., Late-stage fluorination: Fancy novelty or useful tool? *Angew. Chem. Int. Ed.* **2015,** *54*, 3216-3221.

40.   Börgel, J.; Ritter, T., Late-Stage Functionalization. *Chem* **2020,** *6* (8), 1877-1887.

41.   Ogiwara, Y.; Sakai, N., Acyl Fluorides in Late-Transition-Metal Catalysis. *Angew. Chem. Int. Ed.* **2020,** *59* (2), 574-594.

42.   Remete, A. M.; Novák, T. T.; Nonn, M.; Haukka, M.; Fülöp, F.; Kiss, L., Synthesis of novel fluorinated building blocks via halofluorination and related reactions. *Beil. J. Org. Chem.* **2020,** *16*, 2562-2575.

43.   Bryan, M. C.; Dunn, P. J.; Entwistle, D.; Gallou, F.; Koenig, S. G.; Hayler, J. D.; Hickey, M. R.; Hughes, S.; Kopach, M. E.; Moine, G.; Richardson, P.; Roschangar, F.; Steven, A.; Weiberth, F. J., Key Green Chemistry research areas from a pharmaceutical manufacturers' perspective revisited. *Green Chem.* **2018,** *20* (22), 5082-5103.

44.   Caron, S., Where Does the Fluorine Come From? A Review on the Challenges Associated with the Synthesis of Organofluorine Compounds. *OPRD* **2020,** *24* (4), 470-480.

45.   Wang, J.; Sánchez-Roselló, M.; Aceña, J. L.; del Pozo, C.; Sorochinsky, A. E.; Fustero, S.; Soloshonok, V. A.; Liu, H., Fluorine in Pharmaceutical Industry: Fluorine-Containing Drugs Introduced to the Market in the Last Decade (2001–2011). *Chem. Rev.* **2014,** *114* (4), 2432-2506.

46.   Zhou, Y.; Wang, J.; Gu, Z.; Wang, S.; Zhu, W.; Aceña, J. L.; Soloshonok, V. A.; Izawa, K.; Liu, H., Next Generation of Fluorine-Containing Pharmaceuticals, Compounds Currently in Phase II–III Clinical Trials of Major Pharmaceutical Companies: New Structural Trends and Therapeutic Areas. *Chem. Rev.* **2016,** *116* (2), 422-518.

47.   Gillis, E. P.; Eastman, K. J.; Hill, M. D.; Donnelly, D. J.; Meanwell, N. A., Applications of Fluorine in Medicinal Chemistry. *J. Med. Chem.* **2015,** *58* (21), 8315-59.

48.   Han, J.; Remete, A. M.; Dobson, L. S.; Kiss, L.; Izawa, K.; Moriwaki, H.; Soloshonok, V. A.; O'Hagan, D., Next generation organofluorine containing blockbuster drugs. *J. Fluor. Chem.* **2020,** *239*, 109639.

49.   Zhou, J.; Jin, C.; Su, W., Improved Synthesis of Fluticasone Propionate. *OPRD* **2014,** *18* (8), 928-933.

50.   Barth, R.; Rose, C. A.; Schöne, O., Synthetic Routes to Sofosbuvir. In *Synthesis of Heterocycles in Contemporary Medicinal Chemistry*, Časar, Z., Ed. Springer International Publishing: Cham, **2016**, 51-88.

51.   Clark, J. H.; Wails, D.; Bastock, T. W., *Aromatic Fluorine Chemistry*. CRC: New York, **1997**.

52.   Szpera, R.; Moseley, D. F. J.; Smith, L. B.; Sterling, A. J.; Gouverneur, V., The Fluorination of C-H Bonds: Developments and Perspectives. *Angew. Chem. Int. Ed.* **2019,** *58* (42), 14824-14848.

53.   Kohlhepp, S. V.; Gulder, T., Hypervalent iodine(iii) fluorinations of alkenes and diazo compounds: new opportunities in fluorination chemistry. *Chem. Soc. Rev.*, **2016**, *45*, 6270-6288.

54.   Furuya, T.; Kuttruff, C. A.; Ritter, T., Carbon-fluorine bond formation. *Curr. Op. Drug Dis. Develop.*, **2008**, *11*, 803-819.

55.   Furuya, T.; Kamlet, A. S.; Ritter, T., Catalysis for fluorination and trifluoromethylation. *Nature* **2011,** *473* (7348), 470-477.

56.   Kirk, K. L., Fluorination in Medicinal Chemistry: Methods, Strategies, and Recent Developments. *OPRD* **2008,** *12* (2), 305-321.

57.   Liang, T.; Neumann, C. N.; Ritter, T., Introduction of fluorine and fluorine-containing functional groups. *Angew. Chem. Int. Ed.* **2013,** *52*, 8214-8264.

58.   Champagne, P. A.; Desroches, J.; Hamel, J.-D.; Vandamme, M.; Paquin, J.-F., Monofluorination of Organic Compounds: 10 Years of Innovation. *Chem. Rev.* **2015,** *115* (17), 9073-9174.

59.   Yerien, D. E.; Bonesi, S.; Postigo, A., Fluorination methods in drug discovery. *Org. Biomol. Chem.* **2016,** *14* (36), 8398-8427.

60.   Szpera, R.; Moseley, D. F. J.; Smith, L. B.; Sterling, A. J.; Gouverneur, V., The Fluorination of C−H Bonds: Developments and Perspectives. *Angew. Chem. Int. Ed.* **2019**, *58*, 14824-14848.

61.   Hollingworth, C.; Gouverneur, V., Transition metal catalysis and nucleophilic fluorination. *Chem. Commun.* **2012,** *48* (24), 2929.

62.   Campbell, M. G.; Ritter, T., Late-Stage Fluorination: From Fundamentals to Application. *OPRD* **2014,** *18* (4), 474-480.

63.   Gouverneur, V.; Seppelt, K., Introduction: Fluorine Chemistry. **2015,** *115* (2), 563-565.

64.   Zupan, M.; Pollak, A., Fluorination with xenon difluoride. Fluorine addition to 1-phenylacetylenes. *J. Org. Chem.* **1974,** *39* (17), 2646-2647.

65.   Boris, Š.; Marko, Z., Fluorination with Xenon Difluoride. 23. Fluorination of Ortho Substituted Aromatic Molecules. *Bull. Chem. Soc. Japan* **1981,** *54* (1), 279-281.

66.   Shaw, M. J.; Hyman, H. H.; Filler, R., Reaction of xenon difluoride with benzene. *J. Am. Chem. Soc* **1969,** *91* (6), 1563-1565.

67.   Gibson, J. A.; Marat, R. K.; Janzen, A. F., Reaction of Xenon Difluoride. Part II. Oxidative-fluorination of Phosphorus and Iodine Compounds and Cleavage of Silicon–Sulfur and Silicon–Nitrogen Bonds. *Can. J. Chem.* **1975,** *53* (20), 3044-3052.

68.   Rozatian, N.; Hodgson, D. R. W., Reactivities of electrophilic N–F fluorinating reagents. *Chem. Commun.* **2021,** *57* (6), 683-712.

References

69.   Lal, G. S.; Pez, G. P.; Syvret, R. G., Electrophilic NF Fluorinating Agents. *Chem. Rev.* **1996,** *96* (5), 1737-1756.

70.   Ofner, H.; Differding, E., N-Fluorobenzenesulfonimide: A Practical Reagent For Electrophilic Fluorinations. *Synlett* **1991,** *1991*, 187 - 189.

71.   Banks, R. E.; Mohialdin-Khaffaf, S. N.; Lal, G. S.; Sharif, I.; Syvret, R. G., 1-Alkyl-4-fluoro-1,4-diazoniabicyclo[2.2.2] octane salts: a novel family of electrophilic fluorinating agents. *Chem. Commun.* **1992,** (8), 595-596.

72.   Hull, K. L.; Anani, W. Q.; Sanford, M. S., Palladium-Catalyzed Fluorination of Carbon−Hydrogen Bonds. *J. Am. Chem. Soc.* **2006,** *128* (22), 7134-7135.

73.   Wang, X.;   Mei, T.-S.; Yu, J.-Q., Versatile Pd(OTf)$_2$·2H2O-Catalyzed ortho-Fluorination Using NMP as a Promoter. *J. Am. Chem. Soc.* **2009,** *131* (22), 7520-7521.

74.   Ding, Q.; Ye, C.; Pu, S.; Cao, B., Pd(PPh$_3$)$_4$-catalyzed direct ortho-fluorination of 2-arylbenzothiazoles with an electrophilic fluoride N-fluorobenzenesulfonimide (NFSI). *Tetrahedron* **2014,** *70* (2), 409-416.

75.   Chan, K. S. L.; Wasa, M.; Wang, X.; Yu, J.-Q., Palladium(II)-Catalyzed Selective Monofluorination of Benzoic Acids Using a Practical Auxiliary: A Weak-Coordination Approach. *Angew. Chem. Int. Ed.* **2011,** *50* (39), 9081-9084.

76.   Lou, S.-J.; Xu, D.-Q.; Xu, Z.-Y., Mild and Versatile Nitrate-Promoted C-H Bond Fluorination. *Angew. Chem. Int. Ed.* **2014,** *53* (39), 10330-10335.

77.   Cheng, Q.; Ritter, T., New Directions in C–H Fluorination. *Trends in Chemistry* **2019,** *1* (5), 461-470.

78.   Li, M.;   Zheng, H.;   Xue, X.-s.; Cheng, J.-p., Ordering the relative power of electrophilic fluorinating, trifluoromethylating, and trifluoromethylthiolating reagents: A summary of recent efforts. *Tet. Lett.* **2018,** *59* (14), 1278-1285.

79.   Zhu, Y.; Han, J.; Wang, J.; Shibata, N.; Sodeoka, M.; Soloshonok, V. A.; Coelho, J. A. S.; Toste, F. D., Modern Approaches for Asymmetric Construction of Carbon-Fluorine Quaternary Stereogenic Centers: Synthetic Challenges and Pharmaceutical Needs. *Chem. Rev.* **2018,** *118* (7), 3887-3964.

80.   Anastas, P. T.; Warner, J. C., *Green chemistry : theory and practice*. Oxford University Press: Oxford [England]; New York, **1998**.

81.   Banks, E. Safer, cheaper fluorination – a boon for pharmaceutical manufacturing. https://www.chemistry.manchester.ac.uk/research/impact/safer-cheaper-fluorination/ (accessed 08/09/21).

82.   Lide, D. R., *Handbook of Chemistry and Physics, 85th Ed.* CRC: New York, **2004**.

83.   Takahashi, K.; Yokoo, A.; Kaneko, Y.; Abe, T.; Seki, S., Fluoride Ion Conductive Polymer Electrolytes for All-solid-state Fluoride Shuttle Batteries. *Electrochem.* **2020,** *88* (4), 310-313.

84.   Mascaretti, O. A., Modern methods for the monofluorination of aliphatic organic compounds. *Aldrichim. Acta* **1993,** *26*, 47-58.

85.   Gerstenberger, M. R. C.; Haas, A., Methods of Fluorination in Organic Chemistry. *Angew. Chem. International Ed.* **1981,** *20* (8), 647-667.

86.   Labban, A. K. S.; Marcus, Y., The Solubility and Solvation of Salts in Mixed Nonaqueous Solvents. 1. Potassium Halides in Mixed Aprotic Solvents. *J. Sol. Chem.* **1991,** *20*, 221 - 232.

87.   Li, H.; Liu, J.; Chen, X.; Ren, T., Solubility of KF in tributyl phosphate, dimethyl sulfoxide, N,N-dimethylacetamide and 1,4-dioxane from 300.87 to 359.50K. *J. Mol. Liq.* **2012,** *166*, 67-69.

88.   Liang, S.; Hammond, G. B.; Xu, B., Hydrogen Bonding: Regulator for Nucleophilic Fluorination. *Chem. Eur. J.* **2017,** *23* (71), 17850-17861.

89.   Liotta, C. L.; Harris, H. P., Chemistry of naked anions. I. Reactions of the 18-crown-6 complex of potassium fluoride with organic substrates in aprotic organic solvents. *J. Am. Chem. Soc.* **1974,** *96*, 2250-2252.

90.   Kim, D. W.; Song, C. E.; Chi, D. Y., New method of fluorination using potassium fluoride in ionic liquid: Significantly enhanced reactivity of fluoride and improved selectivity. *J. Am. Chem. Soc.* **2002,** *124*, 10278-10279.

91.   Shinde, S. S.; Patil, S. N.; Ghatge, A.; Kumar, P., Nucleophilic fluorination using imidazolium based ionic liquid bearing tert-alcohol moiety. *New J. Chem.* **2015,** *39* (6), 4368-4374.

92.   Jadhav, V. H.; Jeong, H.-J.; Lim, S. T.; Sohn, M.-H.; Kim, D. W., Tailor-Made Hexaethylene Glycolic Ionic Liquids as Organic Catalysts for Specific Chemical Reactions. *Org. Lett.* **2011,** *13* (9), 2502-2505.

93.   Jadhav, V. H.; Kim, J. G.; Park, S. H.; Kim, D. W., Task-specific hexaethylene glycol bridged di-cationic ionic liquids as catalysts for nucleophilic fluorination using potassium fluoride. *Chem. Eng. J.* **2017,** *308*, 664-668.

94.   Taher, A.; Lee, K. C.; Han, H. J.; Kim, D. W., Pyrene-Tagged Ionic Liquids: Separable Organic Catalysts for S$_N$2 Fluorination. *Org. Lett.* **2017,** *19* (13), 3342-3345.

95.   Jessop, P. G., Searching for green solvents. *Green Chem.* **2011,** *13* (6), 1391-1398.

96.   Oh, Y. H.; Choi, H.; Park, C.; Kim, D. W.; Lee, S., Harnessing Ionic Interactions and Hydrogen Bonding for Nucleophilic Fluorination. *Molecules* **2020,** *25* (3).

97.   Pupo, G.; Ibba, F.; Ascough, D. M. H.; Vicini, A. C.; Ricci, P.; Christensen, K. E.; Pfeifer, L.; Morphy, J. R.; Brown, J. M.; Paton, R. S.; Gouverneur, V., Asymmetric nucleophilic fluorination under hydrogen bonding phase-transfer catalysis. *Science* **2018,** *360*, 638-642.

98.   Pupo, G.; Vicini, A. C.; Ascough, D. M. H.; Ibba, F.; Christensen, K. E.; Thompson, A. L.; Brown, J. M.; Paton, R. S.; Gouverneur, V., Hydrogen Bonding Phase-Transfer Catalysis with Potassium Fluoride: Enantioselective Synthesis of β-Fluoroamines. *J. Am. Chem. Soc.* **2019,** *141* (7), 2878-2883.

99.   Morgenthaler, M.; Schweizer, E.; Hoffmann-Röder, A.; Benini, F.; Martin, R. E.; Jaeschke, G.; Wagner, B.; Fischer, H.; Bendels, S.; Zimmerli, D.; Schneider, J.; Diederich, F.; Kansy, M.; Müller, K., Predicting and Tuning Physicochemical Properties in Lead Optimization: Amine Basicities. *ChemMedChem* **2007,** *2* (8), 1100-1115.

100.   Briggs, C. R.; O'Hagan, D.; Howard, J. A.; Yufit, D. S., The C---F bond as a tool in the conformational control of amides. *J. Fluor. Chem.* **2003,** *119*, 9-13.

101.   Sofia, M. J.; Bao, D.; Chang, W.; Du, J.; Nagarathnam, D.; Rachakonda, S.; Reddy, P. G.; Ross, B. S.; Wang, P.; Zhang, H.-R.; Bansal, S.; Espiritu, C.; Keilman, M.; Lam, A. M.; Steuer, H. M. M.; Niu, C.; Otto, M. J.; Furman, P. A., Discovery of a β-d-2′-Deoxy-2′-α-fluoro-2′-β-C-methyluridine Nucleotide Prodrug (PSI-7977) for the Treatment of Hepatitis C Virus. *J. Med. Chem.* **2010,** *53* (19), 7202-7218.

102.   Roagna, G.; Ascough, D. M. H.; Ibba, F.; Vicini, A. C.; Fontana, A.; Christensen, K. E.; Peschiulli, A.; Oehlrich, D.; Misale, A.; Trabanco, A. A.; Paton, R. S.; Pupo, G.; Gouverneur, V., Hydrogen Bonding Phase-Transfer Catalysis with Ionic Reactants: Enantioselective Synthesis of γ-Fluoroamines. *J. Am. Chem. Soc.* **2020,** *142* (33), 14045-14051.

103.   Doherty, N. M.; Hoffmann, N. W., Transition-metal fluoro compounds containing carbonyl, phosphine, arsine, and stibine ligands. *Chem. Rev.* **1991,** *91* (4), 553-573.

104.   Hepworth, M. A.; Robinson, P. L.; Westland, G. J., Complex fluorides of iridium and osmium. *J. Chem. Soc.* **1954,** *1954*, 4269 - 4275.

105.   Hepworth, M. A.; Jack, K. H.; Peacock, R. D.; Westland, G. J., The Crystal Structures of the Trifluorides of Iron, Cobalt, Ruthenium, Rhodium, Palladium and Iridium. *Acta Cryst.* **1957,** *10*, 63 - 69.

106.   Bartlett, N.; Rao, P. R., Iridium Pentafluoridde. *Chem. Commun.* **1965,** *1965*, 252 - 253.

107.   Robinson, P. L.; Westland, G. J., The simple fluorides of iridium, including new trifluoride. *J. Chem. Soc.* **1956,** *1956*, 4481 - 4487.

108.   Bartlett, N.; Lohmann, D. H., 124. Fluorides of the noble metals. Part III. The fluorides of platinum. *Dalton Trans.* **1964,** (0), 619-626.

109.   Pearson, R. G., Hard and soft acids and bases. *J. American Chem. Soc.* **1963,** *85* (22), 3533-3539.

110.   Cairns, M. A.; Dixon, K. R.; McFarland, J. J., Fluoro-complexes of platinum metals, *Dalton Trans.* **1975,** (12), 1159-1164.

References

111.   Grinberg, A. A.; Singh, M. M.; Varshavskii, Y. S., *Russ. J. Inorg. Chem.* **1968,** *13*, 1399.

112.   Vaska, L.; J, P., Fluoro complexes of rhodium(I) and iridium(I). *Inorg. Syn.* **1974,** *15*, 64 - 68.

113.   Van Gall, H. L. M.; Van den Bekerom, F. L. A.; Verlaan, J. P. J., Fluorodicyclooctenerhodium(I): A Versitile Rhodium Complex. *J. Organometallic Chem.* **1976,** *114*, 35 - 37.

114.   Pfister, N.; Braun, T.; Wittwer, P.; Ahrens, M., Selective Formation and Characterization of a RhIII Difluorido λ4-Trifluorosulfanyl Complex. *J. Inorg. Gen. Chem.* **2018,** *644*, 1064-1070.

115.   Veltheer, J. E.; Burger, P.; Bergman, R. G., Synthesis and Chemistry of the Aryliridium(III) Fluorides Cp'Ir(PMe₃)(Aryl)F: High Reactivity due to Surprisingly Easy Ir-F Ionization. *J. Am. Chem. Soc.* **1995,** *117* (50), 12478-12488.

116.   Gorol, M.; Mösch-Zanetti, Nadia C.; Roesky, Herbert W.; Noltemeyer, M.; Schmidt, H.-G., Synthesis of a Novel Organoiridium(I) Fluoro Complex. *Eur. J. Inorg. Chem.* **2004,** *2004* (13), 2678-2682.

117.   Bourgeois, C.J.; Garratt, S. A.; Hughes, R. P.;Larichev, R. B.; Smith, J. M.; Ward, A. J.; Willemsen, S.; Zhang, D.; DiPasquale, A. G.; Zakharov, L. N.; Rheingold, Ar. L.; Synthesis and Structural Characterization of (Perfluoroalkyl)fluoroiridium(III) and (Perfluoroalkyl)methyliridium(III) Compounds. *Organometallics* **2006,** *25*, 3474-3480.

118.   Bourgeois, C. J.; Garratt, S. A.; Hughes, R. P.; Larichev, R. B.; Smith, J. M.; Ward, A. J.; Willemsen, S.; Zhang, D.; DiPasquale, A. G.; Zakharov, L. N.; Rheingold, A. L., Synthesis and Structural Characterization of (Perfluoroalkyl)fluoroiridium(III) and (Perfluoroalkyl)methyliridium(III) Compounds. *Organometallics* **2006,** *25* (14), 3474-3480.

119.   Maity, A.; Stanek, R. J.; Anderson, B. L.; Zeller, M.; Hunter, A. D.; Moore, C. E.; Rheingold, A. L.; Gray, T. G., Fluoride complexes of cyclometalated iridium(III). *Organometallics* **2015,** *34*, 109-120.

120.   Leclerc, M. C.; Bayne, J. M.; Lee, G. M.; Gorelsky, S. I.; Vasiliu, M.; Korobkov, I.; Harrison, D. J.; Dixon, D. A.; Baker, R. T., Perfluoroalkyl Cobalt(III) Fluoride and Bis(perfluoroalkyl) Complexes: Catalytic Fluorination and Selective Difluorocarbene Formation. *J. Am. Chem. Soc.* **2015,** *137*, 16064-16073.

121.   Maity, A.; Stanek, R. J.; Anderson, B. L.; Zeller, M.; Hunter, A. D.; Moore, C. E.; Rheingold, A. L.; Gray, T. G., Fluoride Complexes of Cyclometalated Iridium(III). *Organometallics* **2015,** *34* (1), 109-120.

122.   Ding, K.; Dugan, T. R.; Brennessel, W. W.; Bill, E.; Holland, P. L., Synthesis, Properties, and Reactivity of Diketiminate-Supported Cobalt Fluoride Complexes. *Organometallics* **2009,** *28* (23), 6650-6656.

123.   Dugan, T. R.; Goldberg, J. M.; Brennessel, W. W.; Holland, P. L., Low-Coordinate Cobalt Fluoride Complexes: Synthesis, Reactions, and Production from C–F Activation Reactions. *Organometallics* **2012,** *31* (4), 1349-1360.

124.   Campbell, M. G.; Ritter, T., Modern Carbon–Fluorine Bond Forming Reactions for Aryl Fluoride Synthesis. *Chem. Rev.* **2015,** *115* (2), 612-633.

125.   Grushin, V. V., The Organometallic Fluorine Chemistry of Palladium and Rhodium: Studies toward Aromatic Fluorination. *Acc. Chem. Res.* **2010,** *43* (1), 160-171.

126.   Lee, G. M.; Clément, R.; Tom Baker, R., High-throughput evaluation of in situ-generated cobalt(iii) catalysts for acyl fluoride synthesis. *Catal. Sci. Technol.* **2017,** *7* (21), 4996-5003.

127.   Liu, W.; Huang, X.; Cheng, M. J.; Nielsen, R. J.; Goddard III, W. A.; Groves, J. T., Oxidative Aliphatic C-H Fluorination with Fluoride Ion Catalyzed by a Manganese Porphyrin. *Science* **2012,** *337*, 1322 - 1325.

128.   Huang, X.; Liu, W.; Hooker, J. M.; Groves, J. T., Targeted Fluorination with the Fluoride Ion by Manganese-Catalyzed Decarboxylation. *Angew. Chem. Int. Ed.* **2015,** *54* (17), 5241-5245.

129.   Gamache, R. F.; Waldmann, C.; Murphy, J. M., Copper-Mediated Oxidative Fluorination of Aryl Stannanes with Fluoride. *Org. Lett.* **2016,** *18* (18), 4522-4525.

130.   Dorel, R.; Boehm, P.; Schwinger, D. P.; Hartwig, J. F., Copper-Mediated Fluorination of Aryl Trisiloxanes with Nucleophilic Fluoride. *Chem. Eur. J.* **2020,** *26* (8), 1759-1762.

131.   Casitas, A.; Canta, M.; Solà, M.; Costas, M.; Ribas, X., Nucleophilic Aryl Fluorination and Aryl Halide Exchange Mediated by a CuI/CuIII Catalytic Cycle. *J. Am. Chem. Soc.* **2011,** *133* (48), 19386-19392.

132.   Fier, P. S.; Hartwig, J. F., Copper-Mediated Fluorination of Aryl Iodides. *J. Am. Chem. Soc.* **2012,** *134* (26), 10795-10798.

133.   Ye, Y.; Schimler, S. D.; Hanley, P. S.; Sanford, M. S., Cu(OTf)₂-Mediated Fluorination of Aryltrifluoroborates with Potassium Fluoride. *J. Am. Chem. Soc.* **2013,** *135* (44), 16292-16295.

134.   Ichiishi, N.; Canty, A. J.; Yates, B. F.; Sanford, M. S., Mechanistic Investigations of Cu-Catalyzed Fluorination of Diaryliodonium Salts: Elaborating the CuI/CuIII Manifold in Copper Catalysis. *Organometallics* **2014,** *33* (19), 5525-5534.

135.   Truong, T.; Klimovica, K.; Daugulis, O., Copper-Catalyzed, Directing Group-Assisted Fluorination of Arene and Heteroarene C–H Bonds. *J. Am. Chem. Soc.* **2013,** *135* (25), 9342-9345.

136.   Sharninghausen, L. S.; Brooks, A. F.; Winton, W. P.; Makaravage, K. J.; Scott, P. J. H.; Sanford, M. S., NHC-Copper Mediated Ligand-Directed Radiofluorination of Aryl Halides. *J. Am. Chem. Soc.* **2020,** *142* (16), 7362-7367.

137.   McMurtrey, K. B.; Racowski, J. M.; Sanford, M. S., Pd-Catalyzed C–H Fluorination with Nucleophilic Fluoride. *Org. Lett.* **2012,** *14* (16), 4094-4097.

138.   Furuya, T.; Ritter, T., Carbon−Fluorine Reductive Elimination from a High-Valent Palladium Fluoride. *J. Am. Chem. Soc.* **2008,** *130* (31), 10060-10061.

139.   Furuya, T.; Benitez, D.; Tkatchouk, E.; Strom, A. E.; Tang, P.; Goddard, W. A.; Ritter, T., Mechanism of C−F Reductive Elimination from Palladium(IV) Fluorides. *J. Am. Chem. Soc.* **2010,** *132* (11), 3793-3807.

140.   Watson, D. A.; Su, M.; Teverovskiy, G.; Zhang, Y.; Garcia-Fortanet, J.; Kinzel, T.; Buchwald, S. L., Formation of ArF from LPdAr(F): Catalytic Conversion of Aryl Triflates to Aryl Fluorides. *Science* **2009,** *325*, 1661 - 1664.

141.   Maimone, T. J.; Milner, P. J.; Kinzel, T.; Zhang, Y.; Takase, M. K.; Buchwald, S. L., Evidence for in situ catalyst modification during the Pd-catalyzed conversion of aryl triflates to aryl fluorides. *J. Am. Chem. Soc.* **2011,** *133*, 18106-18109.

142.   Lee, H. G.; Milner, P. J.; Buchwald, S. L., An Improved Catalyst System for the Pd-Catalyzed Fluorination of (Hetero)Aryl Triflates. *Org. Lett.* **2013,** *15* (21), 5602-5605.

143.   Milner, P. J.; Kinzel, T.; Zhang, Y.; Buchwald, S. L., Studying regioisomer formation in the pd-catalyzed fluorination of aryl triflates by deuterium labeling. *J. Am. Chem. Soc.* **2014,** *136*, 15757-15766.

144.   Lee, H. G.; Milner, P. J.; Buchwald, S. L., Pd-catalyzed nucleophilic fluorination of aryl bromides. *J. Am. Chem. Soc.* **2014,** *136*, 3792-3795.

145.   Milner, P. J.; Yang, Y.; Buchwald, S. L., In-Depth Assessment of the Palladium-Catalyzed Fluorination of Five-Membered Heteroaryl Bromides. *Organometallics* **2015,** *34*, 4775-4780.

146.   Sather, A. C.; Lee, H. G.; De La Rosa, V. Y.; Yang, Y.; Müller, P.; Buchwald, S. L., A Fluorinated Ligand Enables Room-Temperature and Regioselective Pd-Catalyzed Fluorination of Aryl Triflates and Bromides. *J. Am. Chem. Soc.* **2015,** *137* (41), 13433-13438.

147.   Sather, A. C.; Buchwald, S. L., The Evolution of Pd0/PdII-Catalyzed Aromatic Fluorination. *Acc. Chem. Res.* **2016,** *49* (10), 2146-2157.

148.   Lee, H.; Borgel, J.; Ritter, T., Carbon-Fluorine Reductive Elimination from Nickel(III) Complexes. *Angew. Chem. Int. Ed.* **2017,** *56* (24), 6966-6969.

149.   Katcher, M. H.; Doyle, A. G., Palladium-Catalyzed Asymmetric Synthesis of Allylic Fluorides. *J. Am. Chem. Soc.* **2010,** *132* (49), 17402-17404.

150.   Katcher, M. H.; Sha, A.; Doyle, A. G., Palladium-Catalyzed Regio- and Enantioselective Fluorination of Acyclic Allylic Halides. *J. Am. Chem. Soc.* **2011,** *133* (40), 15902-15905.

References

151.   Cheng, L.-J.; Cordier, C. J., Catalytic Nucleophilic Fluorination of Secondary and Tertiary Propargylic Electrophiles with a Copper-N-Heterocyclic Carbene Complex. *Angew. Chem. Int. Ed.* **2015,** *54* (46), 13734-13738.

152.   Sorlin, A. M.; Mixdorf, J. C.; Rotella, M. E.; Martin, R. T.; Gutierrez, O.; Nguyen, H. M., The Role of Trichloroacetimidate To Enable Iridium-Catalyzed Regio- and Enantioselective Allylic Fluorination: A Combined Experimental and Computational Study. *J. Am. Chem. Soc.* **2019**.

153.   Zhang, Q.; Mixdorf, J. C.; Reynders, G. J.; Nguyen, H. M., Rhodium-catalyzed benzylic fluorination of trichloroacetimidates. *Tetrahedron* **2015,** *71* (35), 5932-5938.

154.   Zhang, Q.; Stockdale, D. P.; Mixdorf, J. C.; Topczewski, J. J.; Nguyen, H. M., Iridium-Catalyzed Enantioselective Fluorination of Racemic, Secondary Allylic Trichloroacetimidates. *J. Am. Chem. Soc.* **2015,** *137* (37), 11912-11915.

155.   Mixdorf, J. C.; Sorlin, A. M.; Zhang, Q.; Nguyen, H. M., Asymmetric Synthesis of Allylic Fluorides via Fluorination of Racemic Allylic Trichloroacetimidates Catalyzed by a Chiral Diene-Iridium Complex. *ACS Catal.* **2018,** *8* (2), 790-801.

156.   Sorlin, A. M.; Usman, F. O.; English, C. K.; Nguyen, H. M., Advances in Nucleophilic Allylic Fluorination. *ACS Catal.* **2020,** *10* (20), 11980-12010.

157.   Zhu, J.; Tsui, G. C.; Lautens, M., Rhodium-Catalyzed Enantioselective Nucleophilic Fluorination: Ring Opening of Oxabicyclic Alkenes. *Angew. Chem. Int. Ed.* **2012,** *51* (49), 12353-12356.

158.   Konovalov, A. I.; Gorbacheva, E. O.; Miloserdov, F. M.; Grushin, V. V., Ruthenium-catalyzed nucleophilic fluorination of halobenzenes. *Chem. Commun.* **2015,** *51* (70), 13527-30.

159.   Medici, S.; Peana, M.; Pelucelli, A.; Zoroddu, M. A., Rh(I) Complexes in Catalysis: A Five-Year Trend. *Molecules* **2021,** *26* (9).

160.   Forster, J., On the mechanism of a rhodium complex catalysed carbonylation of methanol to acetic acid. *J. Am. Chem. Soc.* **1976,** *98*, 846 - 848.

161.   Eby, R. T.; Singleton, T. C., Academic Press: London, **1983**, 1, 275.

162.   Jones, J. H., The Cativa Process for the Manufacture of Acetic Acid. *Platinum Met. Rev.* **2000,** *44* (44), 94 - 105.

163.   N. von Kutepow; W. Himmele; Hohenschutz, H., The synthesis of acetic acid from methanol and carbon dioxide. *Chem. Eng. Technol.* **1965,** *37*, 297 - 303.

164.   Roelen, O. Production of oxygenated carbon compounds. **1938**, US2327066A.

165.   Adkins, H.; Krsek, G., Preparation of Aldehydes from Alkenes by the Addition of Carbon Monoxide and Hydrogen with Cobalt Carbonyls as Intermediates. *J. Am. Chem. Soc.* **1948,** *70* (1), 383 - 386.

166.   Tudor, R.; Ashley, M., Enhancement of Industrial Hydroformylation Processes by the Adoption of Rhodium-Based Catalyst: Part I. *Platinum Met. Rev.* **2007,** *51* (3), 116-126.

167.   Partenheimer, W., A Chemical Model for the Amoco "MC" Oxygenation Process to Produce Terphthalic Acid. CRC Press: **1990**, 1, 26.

168.   Leclerc, M. C.; Bayne, J. M.; Lee, G. M.; Gorelsky, S. I.; Vasiliu, M.; Korobkov, I.; Harrison, D. J.; Dixon, D. A.; Baker, R. T., Perfluoroalkyl Cobalt(III) Fluoride and Bis(perfluoroalkyl) Complexes: Catalytic Fluorination and Selective Difluorocarbene Formation. *J. Am. Chem. Soc.* **2015,** *137* (51), 16064-73.

169.   Mixdorf, J. C.; Sorlin, A. M.; Zhang, Q.; Nguyen, H. M., Asymmetric Synthesis of Allylic Fluorides via Fluorination of Racemic Allylic Trichloroacetimidates Catalyzed by a Chiral Diene-Iridium Complex. *ACS Catal.* **2017,** *8* (2), 790-801.

170.   Zhang, Q.; Mixdorf, J. C.; Reynders, G. J.; H.M, N., Rhodium-catalyzed benzylic fluorination of trichloroacetimidates. *Tetrahedron* **2015,** *71* (35), 5932 - 5938.

171.   Arisawa, M.; Tanii, S.; Tazawa, T.; Yamaguchi, M., Rhodium-catalyzed transformation of heteroaryl aryl ethers into heteroaryl fluorides. *Chem. Commun.* **2016,** *52* (76), 11390-11393.

172.   Gillespie, J. A.; Zuidema, E.; van Leeuwen, P. W. N. M.; Kamer, P. C. J., Phosphorus Ligand Effects in Homogeneous Catalysis and Rational Catalyst Design. *Phosphorus(III) Ligands in Homogeneous Catalysis: Design and Synthesis*, **2012**, Wiley, 1-26.

173.   Wilson, D. J.; Couchman, S. A.; Dutton, J. L., Are N-heterocyclic carbenes "better" ligands than phosphines in main group chemistry? A theoretical case study of ligand-stabilized E2 molecules, L-E-E-L (L = NHC, phosphine; E = C, Si, Ge, Sn, Pb, N, P, As, Sb, Bi). *Inorg. Chem.* **2012,** *51* (14), 7657-68.

174.   Hopkinson, M. N.; Richter, C.; Schedler, M.; Glorius, F., An overview of N-heterocyclic carbenes. *Nature* **2014,** *510* (7506), 485-96.

175.   Nahra, F.; Cazin, C. S. J., Sustainability in Ru- and Pd-based catalytic systems using N-heterocyclic carbenes as ligands. *Chem. Soc. Rev.* **2021,** *50* (5), 3094-3142.

176.   Arduengo, A. J.; Harlow, R. L.; Kline, M., A Stable Crystalline Carbene. *J. Am. Chem. Soc.* **1991,** *113*, 361 - 363.

177.   Dzieszkowski, K.; Rafiński, Z., N-Heterocyclic Carbene Catalysis under Oxidizing Conditions. *Catalysts* **2018,** *8* (11).

178.   Wang, N.; Xu, J.; Lee, J. K., The importance of N-heterocyclic carbene basicity in organocatalysis. *Org. Biomol. Chem.* **2018,** *16* (37), 8230-8244.

179.   Song, Q.-W.; Zhou, Z.-H.; He, L.-N., Efficient, selective and sustainable catalysis of carbon dioxide. *Green Chem.* **2017,** *19* (16), 3707-3728.

180.   Ma, Y.; Wang, Y. M.; Morgan, P. J.; Jackson, R. E.; Liu, X. H.; Saunders, G. C.; Lorenzini, F.; Marr, A. C., Designing effective homogeneous catalysis for glycerol valorisation: selective synthesis of a value-added aldehyde from 1,3-propanediol via hydrogen transfer catalysed by a highly recyclable, fluorinated Cp*Ir(NHC) catalyst. *Catal. Today* **2018,** *307*, 248-259.

181.   Marr, A. C.; Nieuwenhuyzen, M.; Pollock, C. L.; Saunders, G. C., Synthesis of piano stool complexes employing the pentafluorophenyl- substituted diphosphine $(C_6F_5)_2PCH_2P(C_6F_5)_2$ and the effect of phosphine modifiers on hydrogen transfer catalysis. *Organometallics* **2007,** *26* (10), 2659-2671.

182.   Kaufhold, S.; Petermann, L.; Staehle, R.; Rau, S., Transition metal complexes with N-heterocyclic carbene ligands: From organometallic hydrogenation reactions toward water splitting. *Coord. Chem. Rev.* **2015,** *304-305*, 73-87.

183.   Danopoulos, A. A.; Simler, T.; Braunstein, P., N-Heterocyclic Carbene Complexes of Copper, Nickel, and Cobalt. *Chem. Rev.* **2019,** *119* (6), 3730-3961.

184.   Ezugwu, C. I.; Kabir, N. A.; Yusubov, M.; Verpoort, F., Metal–organic frameworks containing N-heterocyclic carbenes and their precursors. *Coord. Chem. Rev.* **2016,** *307*, 188-210.

185.   Pan, Y.; Jiang, X.; So, Y.-M.; To, C. T.; He, G., Recent Advances in Rare Earth Complexes Containing N-Heterocyclic Carbenes: Synthesis, Reactivity, and Applications in Polymerization. *Catalysts* **2020,** *10* (1).

186.   Jain, I.; Malik, P., N-heterocyclic carbene complexes in ring opening polymerization. *Eur. Pol. J.* **2021,** *150*.

187.   Smith, C. A.; Narouz, M. R.; Lummis, P. A.; Singh, I.; Nazemi, A.; Li, C. H.; Crudden, C. M., N-Heterocyclic Carbenes in Materials Chemistry. *Chem. Rev.* **2019,** *119* (8), 4986-5056.

188.   Briel, O.; Cazin, C. S. J., N-Heterocyclic Carbene Complexes in Industrial Processes. In *N-Heterocyclic Carbenes in Transition Metal Catalysis and Organocatalysis*, Cazin, C. S. J., Ed. Springer Netherlands: Dordrecht, **2011**, 315-324.

189.   Cheng, L. J.; Cordier, C. J., Catalytic Nucleophilic Fluorination of Secondary and Tertiary Propargylic Electrophiles with a Copper-N-Heterocyclic Carbene Complex. *Angew. Chem. Int. Ed.* **2015,** *54* (46), 13734-8.

190.   Ryan, S. J.; Schimler, S. D.; Bland, D. C.; Sanford, M. S., Acyl azolium fluorides for room temperature nucleophilic aromatic fluorination of chloro- and nitroarenes. *Org. Lett.* **2015,** *17* (8), 1866-9.

191.   McGrandle, S.; Saunders, G. C., Group 9 complexes of an N-heterocycle carbene bearing a pentafluorobenzyl substituent: attempted dehydrofluorinative coupling of cyclopentadienyl and N-heterocycle carbene ligands. *J. Fluor. Chem.* **2005,** *126*, 449-453.

References

192.   Codola, Z.; Cardoso, J. M.; Royo, B.; Costas, M.; Lloret-Fillol, J., Highly effective water oxidation catalysis with iridium complexes through the use of NaIO₄. *Chemistry* **2013,** *19* (22), 7203-13.
193.   Hetterscheid, D. G.; Reek, J. N., Me₂-NHC based robust Ir catalyst for efficient water oxidation. *Chem. Commun.* **2011,** *47* (9), 2712-4.
194.   Corberan, R.; Sanau, M.; Peris, E., "Cp*Ir(III)" Complexes with Hemicleaveable Ligands of the Type N-Alkenyl Imidazolin-2-ylidene. Reactivity and Catalytic Properties. *Organometallics* **2007,** *26*, 3492 - 3498.
195.   Marr, A. C.; Pollock, C. L.; Saunders, G. C., Base-free dynamic kinetic resolution of secondary alcohols using "piano-stool" complexes of N-heterocyclic carbenes. *Organometallics* **2007,** *26* (14), 3283-3285.
196.   Fernandes, A.; Royo, B., Water-Soluble Iridium N-Heterocyclic Carbene Complexes for the Alkylation of Amines with Alcohols. *ChemCatChem* **2017,** *9* (20), 3912-3917.
197.   Gulcemal, S.; Gulcemal, D.; Whitehead, G. F.; Xiao, J., Acceptorless Dehydrogenative Oxidation of Secondary Alcohols Catalysed by Cp*Ir(III) -NHC Complexes. *Chemistry* **2016,** *22* (30), 10513-22.
198.   Prinz, M.; Grosche, M.; JHerdtweck, E.; Herrmann, W., A., Unsymmetrically Substituted Iridium(III)-Carbene Complexes by a CH-Activation Process. *Organometallics* **2000,** *19*, 1692 - 1694.
199.   Corberan, R.; Sanau, M.; Peris, E., Aliphatic and Aromatic Intramolecular C-H Activation on Cp*Ir(NHC) Complexes. *Organometallics* **2006,** *25*, 4002 - 4008.
200.   Thomas, H. P.; Wang, Y.-M.; Lorenzini, F.; Coles, S. J.; Horton, P. N.; Marr, A. C.; Saunders, G. C., Cyclometalation via Carbon–Fluorine Bond Activation Induced by Silver Particles. *Organometallics* **2017,** *36* (5), 960-963.
201.   S, M.; Graham, S., Group 9 complexes of an N-heterocycle carbene bearing a pentafluorobenzyl substituent: attempted dehydrofluorinative coupling of cyclopentadienyl and N-heterocycle carbene ligands. *J. Fluor. Chem.* **2005,** *126* (4), 449 - 453.
202.   Thomas, H. P.; Wang, Y. M.; Lorenzini, F.; Coles, S. J.; Horton, P. N.; Marr, A. C.; Saunders, G. C., Cyclometalation via Carbon-Fluorine Bond Activation Induced by Silver Particles. *Organometallics* **2017,** *36* (5), 960-963.
203.   Bellabarba, R. M.; Saunders, G. C., Carbon–fluorine bond cleavage as a route to hybrid ligands. *J. Fluor. Chem.* **2001,** *112* (1), 139-144.
204.   Thomas, H. P.; Marr, A. C.; Morgan, P. J.; Saunders, G. C., Tethering of Pentamethylcyclopentadienyl and N-Heterocycle Stabilized Carbene Ligands by Intramolecular 1,4-Addition to a Polyfluorophenyl Substituent. *Organometallics* **2018,** *37* (9), 1339-1341.
205.   Ralli, P.; Zhang, Y.; Lemal, D. M., Perfluorobarrelene. *Tet. Lett.* **2008,** *49* (52), 7349-7351.
206.   Morgan, P. J.; Hanson-Heine, M. W. D.; Thomas, H. P.; Saunders, G. C.; Marr, A. C.; Licence, P., C–F Bond Activation of a Perfluorinated Ligand Leading to Nucleophilic Fluorination of an Organic Electrophile. *Organometallics* **2020,** *39* (11), 2116-2124.
207.   Wu, J.-T.; Hsu, S. L.-C., Preparation of triethylamine stabilized silver nanoparticles for low-temperature sintering. *J. Nanopart. Res.* **2011,** *13* (9), 3877-3883.
208.   Fooladi, E.; Dalhus, B. R.; Tilset, M., Synthesis and characterization of half-sandwich N-heterocyclic carbene complexes of cobalt and rhodium. *Dalton Trans.* **2004,** (22), 3909-3917.
209.   Heck, R. F., π-Allyl-π-Cyclopentadienylcobalt Halides. *J. Org. Chem.* **1963,** *28* (2), 604-604.
210.   Byers, L. R.; Dahl, L. F., Structural Analysis of (Pentamethylcyclopentadienyl)cobalt(I) Dicarbonyl: Evidence for an Electronically Induced Distortion of the Cyclopentadienyl Ring due to Its Interaction with a Planar Co(CO)₂ Fragment. *Inorg. Chem.* **1980,** *19*, 277 - 284.
211.   Rausch, M. D.; R.A, G., The Chemistry of TT-Cyclopentadienyltetraphenylcyclobutadienecobalt and Related Compounds. *J. Org. Chem.* **1970,** *35*, 3888 - 3897.

212.   Roe, D. M.; Maitlis, P. M., Disproportionation of Dihalogenocyclopentadienylcobalt Complexes to Cobaltocenium Salts. *J. Chem. Soc. (A)* **1971**, 3173 - 3175.

213.   Hughes, R. P.; Lindner, D. C.; Rheingold, A. L.; Yap, G. P. A., Perfluorobenzyl Complexes of Cobalt and Rhodium. Unusual Coupling between Pentafluorophenyl and Pentamethylcyclopentadienyl Rings. *Organometallics* **1996,** *15* (26), 5678-5686.

214.   Kolle, U.; Fuss, B., (Pentamethylcyclopentadienyl) cobalt(III)-halogeno and amido-complexes. *Chem. Ber.* **1984,** *117*, 743 - 752.

215.   Sun, B.; Yoshino, T.; Matsunaga, S.; Kanai, M., A Cp*CoI$_2$-dimer as a precursor for cationic Co(III)-catalysis: application to C-H phosphoramidation of indoles. *Chem. Commun.* **2015,** *51* (22), 4659-61.

216.   Kölle, U.; Khouzami, F.; Fuss, B., Verbrückte C$_5$Me$_5$CoII-Komplexe - reaktive Zwischenstufen der Cyclopentadienylierung von Cobalt(II)-halogeniden. *Angew. Chem.* **2006,** *94* (2), 132-132.

217.   Pollock, C. L.; Fox, K. J.; Lacroix, S. D.; McDonagh, J.; Marr, P. C.; Nethercott, A. M.; Pennycook, A.; Qian, S.; Robinson, L.; Saunders, G. C.; Marr, A. C., Minimizing side reactions in chemoenzymatic dynamic kinetic resolution: Organometallic and material strategies. *Dalton Trans.* **2012,** *41* (43), 13423-13428.

218.   Heck, R. F., Dihalocarbonylcyclopentadienylcobalt Complexes. *Inorg. Chem.* **1965,** *4* (6), 855 - 857.

219.   Fagnou, K.; L'autens, M., A., Halide Effects in Transition Metal Catalysis. *Angew. Chem. Int. Ed.* **2002,** *41*, 26 - 47.

220.   Baumgarth, H.; Meier, G.; Braun, T.; Braun-Cula, B., Rhodium and Iridium Fluorido and Bifluorido Complexes Derived from Peroxido Precursors. *Eur. J. Inorg. Chem.* **2016,** *2016* (28), 4565-4572.

221.   Truscott, B. J.; Nahra, F.; Slawin, A. M. Z.; Cordes, D. B.; Nolan, S. P., Fluoride, bifluoride and trifluoromethyl complexes of iridium(i) and rhodium(i). *Chem. Commun.* **2015,** *51* (1), 62-65.

222.   Truscott, B. J.; Fortman, G. C.; Slawin, A. M. Z.; Nolan, S. P., Well-defined [Rh(NHC)(OH)] complexes enabling the conjugate addition of arylboronic acids to α,β-unsaturated ketones. *Org. Biomol. Chem.* **2011,** *9* (20), 7038-7041.

223.   Truscott, B. J.; Nelson, D. J.; Lujan, C.; Slawin, A. M. Z.; Nolan, S. P., Iridium(I) Hydroxides: Powerful Synthons for Bond Activation. *Chem. Eur. J.* **2013,** *19* (24), 7904-7916.

224.   Kluge, S.; Weston, J., Can a Hydroxide Ligand Trigger a Change in the Coordination Number of Magnesium Ions in Biological Systems? *Biochemistry* **2005,** *44* (12), 4877-4885.

225.   Bramananthan, N.; Carmona, M.; Lowe, J. P.; Mahon, M. F.; Poulten, R. C.; Whittlesey, M. K., Rh–FHF and Rh–F Complexes Containing Small N-Alkyl Substituted Six-Membered Ring N-Heterocyclic Carbenes. *Organometallics* **2014,** *33* (8), 1986-1995.

226.   Jasim, N. A.; Perutz, R. N., Hydrogen Bonding in Transition Metal Complexes: Synthesis, Dynamics, and Reactivity of Platinum Hydride Bifluoride Complexes. *J. Am. Chem. Soc.* **2000,** *122* (36), 8685-8693.

227.   Leclerc, M. C.; Bayne, J. M.; Lee, G. M.; Gorelsky, S. I.; Vasiliu, M.; Korobkov, I.; Harrison, D. J.; Dixon, D. A.; Baker, R. T., Perfluoroalkyl Cobalt(III) Fluoride and Bis(perfluoroalkyl) Complexes: Catalytic Fluorination and Selective Difluorocarbene Formation. *J. Am. Chem. Soc.* **2015,** *137* (51), 16064-16073.

228.   Ogiwara, Y.; Hosaka, S.; Sakai, N., Benzoyl Fluorides as Fluorination Reagents: Reconstruction of Acyl Fluorides via Reversible Acyl C–F Bond Cleavage/Formation in Palladium Catalysis. *Organometallics* **2020,** *39* (6), 856-861.

229.   Ogiwara, Y.; Maegawa, Y.; Sakino, D.; Sakai, N., Palladium-catalyzed Coupling of Benzoyl Halides with Aryltrifluorosilanes Leading to Diaryl Ketones. *Chem. Lett.* **2016,** *45* (7), 790-792.

230.   Ogiwara, Y.; Sakurai, Y.; Hattori, H.; Sakai, N., Palladium-Catalyzed Reductive Conversion of Acyl Fluorides via Ligand-Controlled Decarbonylation. *Org. Lett.* **2018,** *20* (14), 4204-4208.

References

231.   Sakurai, S.; Yoshida, T.; Tobisu, M., Iridium-catalyzed Decarbonylative Coupling of Acyl Fluorides with Arenes and Heteroarenes via C-H Activation. *Chem. Lett.* **2019,** *48* (2), 94-97.

232.   Malapit, C. A.; Bour, J. R.; Brigham, C. E.; Sanford, M. S., Base-free nickel-catalysed decarbonylative Suzuki–Miyaura coupling of acid fluorides. *Nature* **2018,** *563* (7729), 100-104.

233.   Ogiwara, Y.; Sakai, N., Acyl Fluorides in Late-Transition-Metal Catalysis. *Angew. Chem. Int. Ed.* **2020,** *59* (2), 574-594.

234.   Craig, R.; Litvajova, M.; Cronin, S. A.; Connon, S. J., Enantioselective acyl-transfer catalysis by fluoride ions. *Chem. Commun.* **2018,** *54* (72), 10108-10111.

235.   Gillard, R. M.; Fernando, J. E. M.; Lupton, D. W., Enantioselective N-Heterocyclic Carbene Catalysis via the Dienyl Acyl Azolium. *Angew. Chem. Int. Ed.* **2018,** *57* (17), 4712-4716.

236.   Ogiwara, Y.; Sakai, N., Acyl Fluorides in Late-Transition-Metal Catalysis. *Angew. Chem. Int. Ed.* **2019**, 574-594.

237.   Keaveney, S. T.; Schoenebeck, F., Palladium-Catalyzed Decarbonylative Trifluoromethylation of Acid Fluorides. *Angew. Chem. Int. Ed.* **2018,** *57* (15), 4073-4077.

238.   Olah, G. A.; Nojima, M.; Kerekes, I., Synthetic methods and reactions. I. Seleniuum tetrafluoride and its pyridine complex. Convenient fluorinating agents for fluorination of ketones, aldehydes, amides, alcohols, carboxylic acids, and anhydrides. *J. Am. Chem. Soc.* **1974,** *96* (3), 925-927.

239.   Olah, G. A.; Nojima, M.; Kerekes, I., Synthetic Methods and Reactions; IV. Fluorination of Carboxylic Acids with Cyanuric Fluoride. *Synthesis* **1973,** *8*, 487 - 488.

240.   Middleton, W. J., New Fluorinating Reagents. Dialkylaminosulfur fluorides. *J. Org. Chem.* **1975,** *40*, 574 - 578.

241.   L'Heureux, A.; Beaulieu, F.; Bennett, C.; Bill, D. R.; Clayton, S.; Laflamme, F.; Mirmehrabi, M.; Tadayon, S.; Tovell, D.; Couturier, M., Aminodifluorosulfinium salts: selective fluorination reagents with enhanced thermal stability and ease of handling. *J. Org. Chem.* **2010,** *75* (10), 3401-11.

242.   Munoz, S. B.; Dang, H.; Ispizua-Rodriguez, X.; Mathew, T.; Prakash, G. K. S., Direct Access to Acyl Fluorides from Carboxylic Acids Using a Phosphine/Fluoride Deoxyfluorination Reagent System. *Org. Lett.* **2019,** *21* (6), 1659-1663.

243.   Foth, P. J.; Malig, T. C.; Yu, H.; Bolduc, T. G.; Hein, J. E.; Sammis, G. M., Halide-Accelerated Acyl Fluoride Formation Using Sulfuryl Fluoride. *Org. Lett.* **2020,** *22* (16), 6682-6686.

244.   Song, H. X.; Tian, Z. Y.; Xiao, J. C.; Zhang, C. P., Tertiary-Amine-Initiated Synthesis of Acyl Fluorides from Carboxylic Acids and $CF_3SO_2OCF_3$. *Eur. Chem. J.* **2020**, 26 (69), 16261-16265.

245.   Liang, Y.; Zhao, Z.; Taya, A.; Shibata, N., Acyl Fluorides from Carboxylic Acids, Aldehydes, or Alcohols under Oxidative Fluorination. *Org. Lett.* **2021,** *23* (3), 847-852.

246.   Mao, S.; Kramer, J. H.; Sun, H., Deoxyfluorination of Carboxylic Acids with KF and Highly Electron-Deficient Fluoroarenes. *J. Org. Chem.* **2021,** *86* (9), 6066-6074.

247.   Scattolin, T.; Deckers, K.; Schoenebeck, F., Direct Synthesis of Acyl Fluorides from Carboxylic Acids with the Bench-Stable Solid Reagent (Me_4N)SCF_3. *Org. Lett.* **2017,** *19* (21), 5740-5743.

248.   Murali, N.; Srinivas, K.; Ahring, B. K., Biochemical Production and Separation of Carboxylic Acids for Biorefinery Applications. *Fermentation* **2017,** *3* (2).

249.   Scattolin, T.; Deckers, K.; Schoenebeck, F., Direct Synthesis of Acyl Fluorides from Carboxylic Acids with the Bench-Stable Solid Reagent (Me_4N)SCF_3. *Org. Lett.* **2017,** *19* (21), 5740-5743.

250.   Munoz, S. B.; Dang, H.; Ispizua-Rodriguez, X.; Mathew, T.; Prakash, G. K. S., Direct Access to Acyl Fluorides from Carboxylic Acids Using a Phosphine/Fluoride Deoxyfluorination Reagent System. *Org. Lett.* **2019,** *21* (6), 1659-1663.

251.   Grushin, V. V.; Marshall, W. J., The Fluoro Analogue of Wilkinson's Catalyst and Unexpected Ph−Cl Activation. *J. Am. Chem. Soc.* **2004,** *126* (10), 3068-3069.

252.   Kampmeier, J. A.; Mahalingam, S., Mechanistic and synthetic implications of the reactions of aroyl chlorides with chlorocarbonylbis(triphenylphosphine)rhodium(I). A catalytic procedure for the preparation of carbonyl-labeled aroyl chlorides. *Organometallics* **1984,** *3* (3), 489-491.

253.   Malapit, C. A.; Bour, J. R.; Brigham, C. E.; Sanford, M. S., Base-free nickel-catalysed decarbonylative Suzuki-Miyaura coupling of acid fluorides. *Nature* **2018,** *563* (7729), 100-104.

254.   See, Y. Y.; Morales-Colon, M. T.; Bland, D. C.; Sanford, M. S., Development of SNAr Nucleophilic Fluorination: A Fruitful Academia-Industry Collaboration. *Acc. Chem. Res.* **2020,** *53* (10), 2372-2383.

255.   Shende, V. S.; Saptal, V. B.; Bhanage, B. M., Recent Advances Utilized in the Recycling of Homogeneous Catalysis. *Chem. Rec.* **2019,** *19* (9), 2022-2043.

256.   Dreimanna, J.; Lutze, P.; Zagajewski, M.; Behr, A.; Andrzej; Górak; J.Vorholt, A., Highly integrated reactor–separator systems for the recycling of homogeneous catalysts. *Chem. Eng. Process. Process Inten.* **2016,** *99*, 124 - 131.

257.   Dreimann, J. M.; Skiborowski, M.; Behr, A.; Vorholt, A. J., Recycling Homogeneous Catalysts Simply by Organic Solvent Nanofiltration: New Ways to Efficient Catalysis. *ChemCatChem* **2016,** *8* (21), 3330-3333.

258.   Cole-Hamilton, D. J., Homogeneous catalysis: New Approaches to Catalyst Seperation, Recovery and Recycling. *Science* **2003,** *299*, 1702 - 1706.

259.   Bianga, J.; Kunnemann, K. U.; Gaide, T.; Vorholt, A. J.; Seidensticker, T.; Dreimann, J. M.; Vogt, D., Thermomorphic Multiphase Systems: Switchable Solvent Mixtures for the Recovery of Homogeneous Catalysts in Batch and Flow Processes. *Eur. Chem. J.* **2019,** *25* (50), 11586-11608.

260.   Hollingworth, C.; Gouverneur, V., Transition metal catalysis and nucleophilic fluorination. *Chem. Commun.* **2012,** *48* (24), 2929-42.

261.   Hutchinson, G.; Welsh, C. D. M.; Bures, J., Use of Standard Addition to Quantify In Situ FTIR Reaction Data. *J. Org. Chem.* **2021,** *86* (2), 2012-2016.

262.   Ogiwara, Y.; Iino, Y.; Sakai, N., Catalytic C−H/C−F Coupling of Azoles and Acyl Fluorides. *Chem. Eur. J.* **2019,** *25* (26), 6513-6516.

263.   Pan, F.-F.; Guo, P.; Li, C.-L.; Su, P.; Shu, X.-Z., Enones from Acid Fluorides and Vinyl Triflates by Reductive Nickel Catalysis. *Org. Lett.* **2019,** *21* (10), 3701-3705.

264.   Kayumov, M.; Zhao, J. N.; Mirzaakhmedov, S.; Wang, D. Y.; Zhang, A., Synthesis of Arylstannanes via Palladium-Catalyzed Decarbonylative Coupling of Aroyl Fluorides. *Adv. Syn. Catal.* **2020,** *362* (4), 776-781.

265.   Nielsen, C. D.; Bures, J., Visual kinetic analysis. *Chem Sci* **2019,** *10* (2), 348-353.

266.   C. White; A. Yates; Maitlis, P. M., Pentamethylcyclopentadienylrhodium and iridium compounds. *Inorg. Syn.* **1992,** *29*, 228 -234.

267.   McAuliff.Ca; Pollock, R., Relative Dioxygenation rates of some trans-Ir(CO)x(PR$_3$)$_2$ complexes - Effect of phosphine and halogen exchange. *J. Organometallic Chem.* **1974,** *77* (2), 265-268.

268.   Song, H. X.; Tian, Z. Y.; Xiao, J. C.; Zhang, C. P., Tertiary-Amine-Initiated Synthesis of Acyl Fluorides from Carboxylic Acids and CF$_3$SO$_2$OCF$_3$. *Chem. Eur. J.* **2020,** *26* (69), 16261-16265.

269.   A. I. Shipilov; Kolpashchikova, L. A.; Igumnov, S. M., Selective Hydrolysis of Pentafluorobenzotrichloride. *Russian J. Org. Chem.* **2003,** *39* (7), 975 - 978.

270.   Meanwell, M.; Lehmann, J.; Eichenberger, M.; Martin, R. E.; Britton, R., Synthesis of acyl fluorides via photocatalytic fluorination of aldehydic C-H bonds. *Chem. Commun.* **2018,** *54* (71), 9985-9988.

271.   O'Hagan, D., Understanding organofluorine chemistry. An introduction to the C-F bond. *Chem. Soc. Rev.* **2008,** *37* (2), 308-19.

272.   Adams, D. E. C.; Halden, R. U., Fluorinated Chemicals and the Impacts of Anthropogenic Use. Contaminants of Emerging Concern in the Environment: Ecological and Human Health Considerations, **2010**, 539-560.

References

273.   Harada, K. H.; Koizumi, A., Environmental and biological monitoring of persistent fluorinated compounds in Japan and their toxicities. *Environ. Health Prev. Med.* **2009,** *14* (1), 7-19.

274.   Lim, X. Z., Tainted Water: The Scientists Tracing Thousands of Fluorinated Chemicals in Our Environment. *Nature* **2019,** *566*, 26 -29.

275.   De Tonni, A.; Mudgal, S., Study on the Environmental Risks of Medicinal Products. *Exectutive Agency for Health and Consumers* **2013**.

276.   Kuster, A.; Adler, N., Pharmaceuticals in the environment: scientific evidence of risks and its regulation. *Philos. Trans. R. Soc. Lond. B Biol. Sci.* **2014,** *369* (1656).

277.   Martyn Kirk; Kayla Smurthwaite; Jennifer Bräunig; Susan Trevenar; Cate D'Este; Robyn Lucas; Aparna Lal; Rosemary Korda; Archie Clements; Jochen Mueller; Armstrong, B. *The PFAS Health Study: Systematic Literature Review*; The Australian National University: Canberra, **2018**.

278.   Landmarks, A. C. S. N. H. C. Chlorofluorocarbons and Ozone Depletion. http://www.acs.org/content/acs/en/education/whatischemistry/landmarks/cfcs-ozone.html (accessed 12/08/21).

279.   United Nations Environmental Programme. *Montreal Protocol on Substances that Deplete the Ozone Layer*; United Nations Environment Programme: **1987**.

280.   Blum, O.; Milstein, D., A Unique Process Involving P-C Bond Cleavage, P-F Bond Formation and Net Retention of Oxidation State. *J. Chem. Soc. Chem. Commun.* **1991**, 258 - 259.

281.   Belt, S. T.; Helliwell, M.; Jones, W. D.; Partridge, M. G.; Perutz, R. N., η^2 Coordination and carbon-fluorine activation of hexafluorobenzene by cyclopentadienylrhodium and -iridium complexes. *J. Am. Chem. Soc.* **1993,** *115* (4), 1429-1440.

282.   Klahn, A. H.; Moore, M. H.; Perutz, R. N., Intermolecular C-F and intramolecular C-H activation reaction of $[\text{Re}(\eta^5\text{-}C_5Me_5)(CO)_3]$ with hexafluorobenzene: Crystal and molecular structure of $[\text{Re}(\eta^6\text{-}C_5Me_4CH_2)(CO)_2(C_6F_5)]$. *Chem. Commun.* **1992,** *23*, 1699-1701.

283.   Aizenberg, M.; Milstein, D., Catalytic Activation of Carbon-Fluorine Bonds by a Soluble Transition Metal Complex. *Science* **1994,** *265* (5170), 359-361.

284.   Kiplinger, J. L.; Richmond, T. G.; Osterberg, C. E., Activation of Carbon-Fluorine Bonds by Metal Complexes. *Chem. Rev.* **1994,** *94*, 373-431.

285.   Fujita, T.; Fuchibe, K.; Ichikawa, J., Transition-Metal-Mediated and -Catalyzed C-F Bond Activation by Fluorine Elimination. *Angew. Chem. Int. Ed.* **2019,** *58* (2), 390-402.

286.   Stahl, T.; Klare, H. F. T.; Oestreich, M., Main-Group Lewis Acids for C–F Bond Activation. *ACS Catal.* **2013,** *3* (7), 1578-1587.

287.   Hamel, J.-D.; Paquin, J.-F., Activation of C–F bonds α to C–C multiple bonds. *Chem. Commun.* **2018,** *54* (73), 10224-10239.

288.   Weaver, J.; Senaweera, S., C-F activation and functionalization of perfluoro- and polyfluoroarenes. *Tetrahedron* **2018,** *70*, 7413 - 7428.

289.   Clot, E.; Eisenstein, O.; Jasim, N.; Macgregor, S. A.; McGrady, J. E.; Perutz, R. N., C−F and C−H Bond Activation of Fluorobenzenes and Fluoropyridines at Transition Metal Centers: How Fluorine Tips the Scales. *Acc. Chem. Res.* **2011,** *44*, 333 - 348.

290.   Eisenstein, O.; Milani, J.; Perutz, R. N., Selectivity of C-H Activation and Competition between C-H and C-F Bond Activation at Fluorocarbons. *Chem. Rev.* **2017,** *117* (13), 8710-8753.

291.   Unzner, T. A.; Magauer, T., Carbon–fluorine bond activation for the synthesis of functionalized molecules. *Tet. Lett.* **2015,** *56* (7), 877-883.

292.   Tan, D.-H.; Lin, E.; Ji, W.-W.; Zeng, Y.-F.; Fan, W.-X.; Li, Q.; Gao, H.; Wang, H., Copper-Catalyzed Stereoselective Defluorinative Borylation and Silylation of gem - Difluoroalkenes. *Adv. Syn. Catal.* **2018,** *360* (5), 1032-1037.

293.   Liu, X. W.; Echavarren, J.; Zarate, C.; Martin, R., Ni-Catalyzed Borylation of Aryl Fluorides via C-F Cleavage. *J. Am. Chem. Soc.* **2015,** *137* (39), 12470-3.

294. Lindup, R. J.; Marder, T. B.; Perutz, R. N.; Whitwood, A. C., Sequential C-F activation and borylation of fluoropyridines via intermediate Rh(I) fluoropyridyl complexes: a multinuclear NMR investigation. *Chem. Commun.* **2007,** (35), 3664-6.

295. Teltewskoi, M.; Panetier, J. A.; Macgregor, S. A.; Braun, T., A highly reactive rhodium(I)-boryl complex as a useful tool for C-H bond activation and catalytic C-F bond borylation. *Angew. Chem. Int. Ed.* **2010,** *49* (23), 3947-51.

296. Ishii, Y.; Chatani, N.; Yorimitsu, S.; Murai, S., Rhodium-Catalyzed Si-F Exchange Reaction between Fluorobenzenes and a Disilane. Catalytic Reaction Involving Cleavage of C-F Bonds. *Chem. Lett.* **2003,** *27*, 157 - 158.

297. Cui, B.; Jia, S.; Tokunaga, E.; Shibata, N., Defluorosilylation of fluoroarenes and fluoroalkanes. *Nature Commun.* **2018,** *9* (1).

298. Liu, X. W.; Zarate, C.; Martin, R., Base-Mediated Defluorosilylation of C(sp^2)−F and C(sp^3)−F Bonds. *Angew. Chem. Int. Ed.* **2019,** *58*, 2064-2068.

299. Harada, T.; Ueda, Y.; Iwai, T.; Sawamura, M., Nickel-catalyzed amination of aryl fluorides with primary amines. *Chem. Commun.* **2018,** *54* (14), 1718-1721.

300. Wang, Y.; Wei, C.; Tang, R.; Zhan, H.; Lin, J.; Liu, Z.; Tao, W.; Fang, Z., Silver-catalyzed intermolecular amination of fluoroarenes. *Org. Biomol. Chem.* **2018,** *16* (34), 6191-6194.

301. Tamoa, K.; Sumitani, K.; Kumada, M., Selective Carbon-Carbon Bond Formation by Cross-Coupling of Grignard Reagents with Organic Halides. Catalysis by Nickel-Phosphine Complexes. *J. Am. Chem. Soc.* **1972,** *94*, 4374 - 4376.

302. Schaub, T.; Backes, M.; Radius, U., Catalytic C-C Bond Formation Accomplished by Selective C-F Activation of Perfluorinated Arenes. *J. Am. Chem. Soc.* **2006,** *128*, 15964 - 15965.

303. Steffen, A.; Sladek, M. I.; Braun, T.; Neumann, B.; Stammler, H. G., Catalytic C-C Coupling Reactions at Nickel by C-F Activation of a Pyrimidine in the Presence of a C-Cl Bond: The Crucial Role of Highly Reactive Fluoro Complexes. *Organometallics* **2005,** *24*, 4057–4064.

304. Ogiwara, Y.; Sakino, D.; Sakurai, Y.; Sakai, N., Acid fluorides as acyl electrophiles in suzuki–miyaura coupling. *Eur. J. Org. Chem.* **2017,** *2017*, 4324-4327.

305. Yu, D.; Shen, Q.; Lu, L., Selective palladium-catalyzed C-F activation/carbon-carbon bond formation of polyfluoroaryl oxazolines. *J. Org. Chem.* **2012,** *77* (4), 1798-804.

306. Bennett, B. K.; Harrison, R. G.; Richmond, T. G., Cobaltocenium Fluoride: A Novel Source of "Naked" Fluoride Formed by Carbon-Fluorine Bond Activation in a Saturated Perfluorocarbon. *J. Am. Chem. Soc.* **1994,** *116* (24), 11165-11166.

307. Mulryan, D.; White, A. J. P.; Crimmin, M. R., Organocatalyzed Fluoride Metathesis. *Org. Lett.* **2020,** *22* (23), 9351-9355.

308. Brittain, W. D. G.; Cobb, S. L., Carboxylic Acid Deoxyfluorination and One-Pot Amide Bond Formation Using Pentafluoropyridine (PFP). *Org. Lett.* **2021,** *23* (15), 5793-5798.

309. Hashimoto, S.; Nakatsuka, S.; Nakamura, M.; Hatakeyama, T., Construction of a Highly Distorted Benzene Ring in a Double Helicene. *Angew. Chem. Int. Ed.* **2014,** *53* (51), 14074-14076.

310. Demaison, J.; Rudolph, H. D.; Császár, A. G., Deformation of the benzene ring upon fluorination: equilibrium structures of all fluorobenzenes. *Mol. Phys.* **2013,** *111* (9-11), 1539-1562.

311. Domenicano, A.; Vaciago, A., Molecular Geometry of Substituted Benzene Derivatives.
I. On the Nature of the Ring Deformations Induced by Substitution. *Acta Cryst. B.* **1975,** *31*, 221 - 233.

312. Ma, J.-x.; Yang, Z.; Zhou, T.; Guo, Q.; Yang, J.; Yang, T.; Yang, Q., Construction of structurally diverse luminescent lead(ii) fluorinated coordination polymers based on auxiliary ligands. *New J. Chem.* **2018,** *42* (18), 15413-15419.

References

313.   King, J. B.; Gabbai, F. P., Ortho-Bis(Cyanomercurio)Tetrafluorobenzene as a Bidentate Lewis Acid Co-Catalyst in the Cyanosilylation of Benzaldehyde. *Organometallics* **2003,** *22*, 1275 - 1280.

314.   Pauling, L., The Nature of the Chemical Bond. *J. Am. Chem. Soc.* **1931**, *53* (4), 1367-1400.

315.   Baker, R. J.; Colavita, P. E.; Murphy, D. M.; Platts, J. A.; Wallis, J. D., Fluorine-fluorine interactions in the solid state: an experimental and theoretical study. *J. Phys. Chem. A* **2012,** *116* (5), 1435-44.

316.   Matta, C. F.; Castillo, N.; Boyd, R. J., Characterization of a closed-shell fluorine-fluorine bonding interaction in aromatic compounds on the basis of the electron density. *J. Phys. Chem. A* **2005,** *109*, 3669-3681.

317.   Ramasubbu, N.; Parthasarathy, R.; Murray-Rust, P., Angular Preferences of Intermolecular Forces around Halogen Centers: Preferred Directions of Approach of Electrophiles and Nucleophiles around Carbon-Halogen Bond. *J. Am. Chem. Soc.* **1986,** *108*, 4308 - 4314.

318.   Panini, P.; Chopra, D., Understanding of Noncovalent Interactions Involving Organic Fluorine. Hydrogen Bonded Supramolecular Structures, Li, Z.-T.; Wu, L.-Z., Eds. Springer: Berlin, Heidelberg, **2015**, 37-67.

319.   Cavallo, G.; Metrangolo, P.; Milani, R.; Pilati, T.; Priimagi, A.; Resnati, G.; Terraneo, G., The Halogen Bond. *Chem. Rev.* **2016,** *116* (4), 2478-601.

320.   Siram, R. B. K.; Karothu, D. P.; Guru Row, T. N.; Patil, S., Unique Type II Halogen⋯Halogen Interactions in Pentafluorophenyl-Appended 2,2′-Bithiazoles. *Cryst. Growth Design* **2013,** *13* (3), 1045-1049.

321.   Bauza, A.; Frontera, A., Electrostatically enhanced FF interactions through hydrogen bonding, halogen bonding and metal coordination: an ab initio study. *Phys. Chem. Chem. Phys.* **2016,** *18* (30), 20381-8.

322.   Foust, D. F.; Rausch, M. D., Photodegredration Studies on Cp2TaMe3 and Some Deuterated Analogues. *J. Organometallic Chem.* **1982,** *226*, 47 - 55.

323.   J., G.-s.; Brubaker, C. H., Photolytic Cyclopentadienyl Ligand Exchange in Selected Systems. *Inorg. Chem. Acta* **1977,** *25*, 181 - 184.

324.   Vitz, E.; Brubaker, C. H., Photoexchange of η^5-Cyclo- pentadienide Ligands in Selected Systems. *J. Organometallic Chem.* **1976,** *104*, 33 - 35.

325.   Shao, Y.; Gan, Z.; Epifanovsky, E.; Gilbert, A. T. B.; Wormit, M.; Kussmann, J.; Lange, A. W.; Behn, A.; Deng, J.; Feng, X.; Ghosh, D.; Goldey, M.; Horn, P. R.; Jacobson, L. D.; Kaliman, I.; Khaliullin, R. Z.; Kuś, T.; Landau, A.; Liu, J.; Proynov, E. I.; Rhee, Y. M.; Richard, R. M.; Rohrdanz, M. A.; Steele, R. P.; Sundstrom, E. J.; Woodcock, H. L.; Zimmerman, P. M.; Zuev, D.; Albrecht, B.; Alguire, E.; Austin, B.; Beran, G. J. O.; Bernard, Y. A.; Berquist, E.; Brandhorst, K.; Bravaya, K. B.; Brown, S. T.; Casanova, D.; Chang, C.-M.; Chen, Y.; Chien, S. H.; Closser, K. D.; Crittenden, D. L.; Diedenhofen, M.; DiStasio, R. A.; Do, H.; Dutoi, A. D.; Edgar, R. G.; Fatehi, S.; Fusti-Molnar, L.; Ghysels, A.; Golubeva-Zadorozhnaya, A.; Gomes, J.; Hanson-Heine, M. W. D.; Harbach, P. H. P.; Hauser, A. W.; Hohenstein, E. G.; Holden, Z. C.; Jagau, T.-C.; Ji, H.; Kaduk, B.; Khistyaev, K.; Kim, J.; Kim, J.; King, R. A.; Klunzinger, P.; Kosenkov, D.; Kowalczyk, T.; Krauter, C. M.; Lao, K. U.; Laurent, A. D.; Lawler, K. V.; Levchenko, S. V.; Lin, C. Y.; Liu, F.; Livshits, E.; Lochan, R. C.; Luenser, A.; Manohar, P.; Manzer, S. F.; Mao, S.-P.; Mardirossian, N.; Marenich, A. V.; Maurer, S. A.; Mayhall, N. J.; Neuscamman, E.; Oana, C. M.; Olivares-Amaya, R.; O'Neill, D. P.; Parkhill, J. A.; Perrine, T. M.; Peverati, R.; Prociuk, A.; Rehn, D. R.; Rosta, E.; Russ, N. J.; Sharada, S. M.; Sharma, S.; Small, D. W.; Sodt, A.; Stein, T.; Stück, D.; Su, Y.-C.; Thom, A. J. W.; Tsuchimochi, T.; Vanovschi, V.; Vogt, L.; Vydrov, O.; Wang, T.; Watson, M. A.; Wenzel, J.; White, A.; Williams, C. F.; Yang, J.; Yeganeh, S.; Yost, S. R.; You, Z.-Q.; Zhang, I. Y.; Zhang, X.; Zhao, Y.; Brooks, B. R.; Chan, G. K. L.; Chipman, D. M.; Cramer, C. J.; Goddard, W. A.; Gordon, M. S.; Hehre, W. J.; Klamt, A.; Schaefer, H. F.; Schmidt, M. W.; Sherrill, C. D.; Truhlar, D. G.; Warshel, A.; Xu, X.; Aspuru-Guzik, A.; Baer, R.; Bell, A. T.; Besley, N. A.; Chai, J.-D.; Dreuw, A.; Dunietz, B. D.; Furlani, T. R.; Gwaltney, S. R.; Hsu, C.-P.; Jung, Y.; Kong, J.;

Lambrecht, D. S.; Liang, W.; Ochsenfeld, C.; Rassolov, V. A.; Slipchenko, L. V.; Subotnik, J. E.; Van Voorhis, T.; Herbert, J. M.; Krylov, A. I.; Gill, P. M. W.; Head-Gordon, M., Advances in molecular quantum chemistry contained in the Q-Chem 4 program package. *Mol. Phys.* **2014,** *113* (2), 184-215.

326.   Hay, P. J.; Wadt, W. R., Ab Initio Effective Core Potentials for Molecular Calculations. Potentials for K to Au Including the Outermost Core Orbitale. *J. Chem. Phys* **1985,** *82*, 299 - 310.

327.   Adamo, C.; Scuseria, G. E.; Barone, V., Accurate Excitation Energies from Time-Dependent Density Functional Theory: Assessing the PBE0 Model. *J. Chem. Phys.* **1999,** *111*, 2889 - 2899.

328.   Dolg, M.; Wedig, U.; Stoll, H.; Preuss, H., Energy-adjusted Ab Initio Pseudopotentials for the First Row Transition Elements. *J. Chem. Phys* **1987,** *86*, 866 - 872.

329.   Boys, S. F.; Bernardi, F., The Calculation of Small Molecular Interactions by the Differences of Separate Total Energies. Some Procedures with Reduced Errors. *Mol. Phys* **1970,** *19*, 533 - 566.

330.   Reed, A. E.; Curtiss, L. A.; Weinhold, F., Intermolecular Interactions from a Natural Bond Orbital, Donor—Acceptor Viewpoint. *Chem. Rev.* **1988,** *88*, 899 - 926.

331.   Becke, A. D., A New Mixing of Hartree-Fock and Local Density-Functional Theories. *J. Chem. Phys* **1993,** *98*, 1372 - 1377.

332.   Bader, R. F. W., A Quantum Theory of Molecular Structure and Its Applications. . *Chem. Rev.* **1991,** *91*, 983 - 928.

333.   Saunders, C.; Khaled, M. B.; Weaver, J. D.; Tantillo, D. J., Prediction of ^{19}F NMR Chemical Shifts for Fluorinated Aromatic Compounds. *J. Org. Chem.* **2018,** *83*, 3220 - 3225.

334.   Dmowski, W.; Kaminski, M., Dialkyl-∝,∝-Difluorobenzylamines and Dialkyl(Trifluoromethyl)-Amines - Novel Fluorinating Reagents. *J. Fluor. Chem.* **1983,** *23*, 219 - 228.

335.   Xiang, M.; Xin, Z. K.; Chen, B.; Tung, C. H.; Wu, L. Z., Exploring the Reducing Ability of Organic Dye (Acr(+)-Mes) for Fluorination and Oxidation of Benzylic C(sp[3])-H Bonds under Visible Light Irradiation. *Org. Lett.* **2017,** *19* (11), 3009-3012.

336.   Olah, G. A.; Comisarow, M. B., Stable Carbonium Ions. Alkyl(Aryl)Halocarbonium Ions and Haloarylcarbonium Ions. *J. Am. Chem. Soc.* **1969,** *91*, 2955 - 2961.

337.   Chambers, R. D.; Greenhall, M. P.; Hutchinson, J., Direct fluorination of 1,3-dicarbonyl compounds. *Tetrahedron* **1996,** *52* (1), 1-8.

338.   Wu, S. W.; Liu, F., Synthesis of alpha-Fluoroketones from Vinyl Azides and Mechanism Interrogation. *Org. Lett.* **2016,** *18* (15), 3642-5.

339.   Braun, T.; Wehmeier, F., C–F Bond Activation of Highly Fluorinated Molecules at Rhodium: From Model Reactions to Catalysis. *Eur. J. Inorg. Chem.* **2011,** *2011* (5), 613-625.

340.   Clot, E.; Eisenstein, O.; Jasim, N.; Macgregor, S. A.; McGrady, J. E.; Perutz, R. N., C−F and C−H Bond Activation of Fluorobenzenes and Fluoropyridines at Transition Metal Centers: How Fluorine Tips the Scales. *Acc. Chem. Res.* **2011,** *44* (5), 333-348.

341.   LaBerge, N. A.; Love, J. A., Activation and Formation of Aromatic C–F Bonds. *Organometallic Fluorine Chemistry*, **2015**, 55-111.

342.   Braun, T., *Organometallic Fluorine Chemistry*. **2015**.

343.   Wiesenfeldt, M., P; Nairoukh, Z.; Li, W.; Glorius, F., Hydrogenation of fluoroarenes: Direct access to all-cis- (multi)fluorinated cycloalkanes. *Science* **2017,** *357*, 908 - 912.

344.   Kojima, R.; Kubota, K.; Ito, H., Stereodivergent hydrodefluorination of gem-difluoroalkenes: selective synthesis of (Z)- and (E)-monofluoroalkenes. *Chem. Commun.* **2017,** *53* (77), 10688-10691.

345.   Kikushima, K.; Grellier, M.; Ohashi, M.; Ogoshi, S., Transition-Metal-Free Catalytic Hydrodefluorination of Polyfluoroarenes by Concerted Nucleophilic Aromatic Substitution with a Hydrosilicate. *Angew. Chem. Int. Ed.* **2017,** *56* (51), 16191-16196.

346.   Bakewell, C.; White, A. J. P.; Crimmin, M. R., Reactions of Fluoroalkenes with an Aluminium(I) Complex. *Angew. Chem. Int. Ed.* **2018,** *57* (22), 6638-6642.

347.   Aizenberg, M.; Milstein, D., Catalytic Activation of Carbon-Fluorine Bonds by a Soluble Transition Metal Complex. *Science* **1994,** *265*, 359 - 361.

References

348. Dourvis, C.; Ozerov, O., V., Hydrodefluorination of Perfluoroalkyl Groups Using Silylium-Carborane Catalysts. *Science* **2008,** *321*, 1188 - 1190.

349. Kugl, S.; Schneider, R.; Y, F., Catalytic Carbon-Fluorine Bond Activation with Monocoordinated Nickel-Carbene Complexes: Reduction of Fluoroarenes. *Adv. Synth. Catal.* **2003,** *345*, 341 - 345.

350. Reade, S. P.; Mahon, M. F.; Whittlesey, M. K., Catalytic Hydrodefluorination of Aromatic Fluorocarbons by Ruthenium N-Heterocyclic Carbene Complexes. *J. Am. Chem. Soc.* **2009,** *131*, 1847 - 1861.

351. Ekkert, O.; Strudley, S. D. A.; Rozenfeld, A.; White, A. J. P.; Crimmin, M. R., Rhodium Catalyzed, Carbon–Hydrogen Bond Directed Hydrodefluorination of Fluoroarenes. *Organometallics* **2014,** *33* (24), 7027-7030.

352. Vela, J.; Smith, J. M.; Yu, Y.; Ketterer, N. A.; Flaschenriem, C. J.; Lachicotte, R. J.; Holland, P. L., Synthesis and Reactivity of Low-Coordinate Iron(II) Fluoride Complexes and Their Use in the Catalytic Hydrodefluorination of Fluorocarbons. *J. Am. Chem. Soc.* **2005,** *127*, 7857 - 7870.

353. Macgregor, S. A.; McKay, D.; Panetier, J. A.; Whittlesey, M. K., Computational study of the hydrodefluorination of fluoroarenes at $[Ru(NHC)(PR_3)_2(CO)(H)_2]$: predicted scope and regioselectivities. *Dalton Trans.* **2013,** *42* (20), 7386-95.

354. Cybulski, M. K.; Nicholls, J. E.; Lowe, J. P.; Mahon, M. F.; Whittlesey, M. K., Catalytic Hydrodefluorination of Fluoroarenes Using $Ru(IMe_4)_2L_2H_2$ (IMe_4 = 1,3,4,5-Tetramethylimidazol-2-ylidene; L_2 = $(PPh_3)_2$, dppe, dppp, dppm) Complexes. *Organometallics* **2017,** *36* (12), 2308-2316.

355. Cybulski, M. K.; McKay, D.; Macgregor, S. A.; Mahon, M. F.; Whittlesey, M. K., Room Temperature Regioselective Catalytic Hydrodefluorination of Fluoroarenes with trans-$[Ru(NHC)4 H2]$ through a Concerted Nucleophilic Ru-H Attack Pathway. *Angew. Chem. Int. Ed.* **2017,** *56* (6), 1515-1519.

356. Scott, V. J.; Celenligil-Cetin, R.; Ozerov, O., V., Room-Temperature Catalytic Hydrodefluorination of $C(sp^3)$-F Bonds. *J. Am. Chem. Soc.* **2005,** *127* (2852 - 2853).

357. Talavera, M.; von Hahmann, C. N.; Muller, R.; Ahrens, M.; Kaupp, M.; Braun, T., C-H and C-F Bond Activation Reactions of Fluorinated Propenes at Rhodium: Distinctive Reactivity of the Refrigerant HFO-1234yf. *Angew. Chem. Int. Ed.* **2019,** *58* (31), 10688-10692.

358. Yao, C.; Wang, S.; Norton, J.; Hammond, M., Catalyzing the Hydrodefluorination of CF_3-Substituted Alkenes by $PhSiH_3$. H* Transfer from a Nickel Hydride. *J. Am. Chem. Soc.* **2020,** *142* (10), 4793-4799.

359. Phillips, N. A.; O'Hanlon, J.; Hooper, T. N.; White, A. J. P.; Crimmin, M. R., Dihydridoboranes: Selective Reagents for Hydroboration and Hydrodefluorination. *Org. Lett.* **2019,** *21* (18), 7289-7293.

360. Chen, J.; Huang, D.; Ding, Y.; Chen, J.; Huang, D.; Ding, Y., Rhodium-Catalyzed ortho -Selective C-F Activation and Hydrodefluorination of Heterocycle-Substituted Polyfluoroarenes: Dominated by Phosphine Ligands. *Chem. Select* **2017,** *2*, 1219 - 1224.

361. Sabater, S.; Mata, J. A.; Peris, E., Hydrodefluorination of carbon-fluorine bonds by the synergistic action of a ruthenium-palladium catalyst. *Nat. Commun.* **2013,** *4*, 2553.

362. Moore, J. T.; Lu, C. C., Catalytic Hydrogenolysis of Aryl C-F Bonds Using a Bimetallic Rhodium-Indium Complex. *J. Am. Chem. Soc.* **2020,** *142* (27), 11641-11646.

363. Matsunami, A.; Kuwata, S.; Kayaki, Y., Hydrodefluorination of Fluoroarenes Using Hydrogen Transfer Catalysts with a Bifunctional Iridium/NH Moiety. *ACS Catal.* **2016,** *6* (8), 5181-5185.

364. Li, J.; Zheng, T.; Sun, H.; Li, X., Selectively catalytic hydrodefluorination of perfluoroarenes by Co(PMe3)4 with sodium formate as reducing agent and mechanism study. *Dalton Trans.* **2013,** *42* (36), 13048-53.

365. Schmidt, A.; Mordhorst, T.; Namyslo, J. C.; Toelle, W., Hetarenium Salts from Pentafluoropyridine. Syntheses, Spectroscopic Properties, and Applications *J. Heterocyclic Chem.* **2009,** *44*, 679 - 684.

366.   Hargreaves, C. A.; Sandford, G.; Slater, R.; Yufit, D. S.; Howard, J. A. K.; Vong, A., Synthesis of tetrahydropyrido[2,3-b]pyrazine scaffolds from 2,3,5,6-tetrafluoropyridine derivatives. *Tetrahedron* **2007,** *63* (24), 5204-5211.

367.   Peloquin, A. J.; Houck, M. B.; McMillen, C. D.; Iacono, S. T.; Pennington, W. T., Perfluoropyridine as an Efficient, Tunable Scaffold for Bis(pyrazol-1-yl)pyridine Copper Complexes. *Eur. J. Inorg. Chem.* **2020,** *2020* (18), 1720-1727.

368.   Chambers, R. D.; Hoskin, P. R.; Sandford, G.; Yufit, D. S.; Howard, J. A. K., Polyhalogenated heterocyclic compounds. Part 47.1 Syntheses of multi-substituted pyridine derivatives from pentafluoropyridine. *J. Chem. Soc., Perkin Trans. 1* **2001,** (21), 2788-2795.

369.   Christopher, J. A.; Brophy, L.; Lynn, S. M.; Miller, D. D.; Sloan, L. A.; Sandford, G., Synthetic utility of 4-bromo-2,3,5,6-tetrafluoropyridine. *J. Fluor. Chem.* **2008,** *129* (5), 447-454.

370.   Pattison, G.; Sandford, G.; Wilson, I.; Yufit, D. S.; Howard, J. A. K.; Christopher, J. A.; Miller, D. D., Polysubstituted and ring-fused pyridazine systems from tetrafluoropyridazine. *Tetrahedron* **2017,** *73* (5), 437-454.

371.   Fox, M. A.; Sandford, G.; Slater, R.; Yufit, D. S.; Howard, J. A. K.; Vong, A., Reactions of 4-substituted tetrafluoropyridine derivatives with sulfur nucleophiles: SNAr and annelation processes. *J. Fluor. Chem.* **2012,** *143*, 148-154.

372.   Sandford, G.; Slater, R.; Yufit, D. S.; Howard, J. A. K.; Vong, A., Tetrahydropyrido[3,4-b]pyrazine Scaffolds from Pentafluoropyridine. *J. Org. Chem.* **2005,** *70* (18), 7208-7216.

373.   Zhou, Y.; Wang, J.; Gu, Z.; Wang, S.; Zhu, W.; Acena, J. L.; Soloshonok, V. A.; Izawa, K.; Liu, H., Next Generation of Fluorine-Containing Pharmaceuticals, Compounds Currently in Phase II-III Clinical Trials of Major Pharmaceutical Companies: New Structural Trends and Therapeutic Areas. *Chem. Rev.* **2016,** *116* (2), 422-518.

374.   Gimenez, D.; Mooney, C. A.; Dose, A.; Sandford, G.; Coxon, C. R.; Cobb, S. L., The application of perfluoroheteroaromatic reagents in the preparation of modified peptide systems. *Org. Biomol. Chem.* **2017,** *15* (19), 4086-4095.

375.   Baron, A.; Sandford, G.; Slater, R.; Yufit, D. S.; Howard, J. A. K.; Vong, A., Polyfunctional Tetrahydropyrido[2,3-b]pyrazine Scaffolds from 4-Phenylsulfonyl Tetrafluoropyridine. *J. Org. Chem.* **2005,** *70* (23), 9377-9381.

376.   Cartwright, M. W.; Sandford, G.; Bousbaa, J.; Yufit, D. S.; Howard, J. A. K.; Christopher, J. A.; Miller, D. D., Imidazopyridine and pyrimidinopyridine systems from perfluorinated pyridine derivatives. *Tetrahedron* **2007,** *63* (30), 7027-7035.

377.   Nova, A.; Reinhold, M.; Perutz, R. N.; Macgregor, S. A.; McGrady, J. E., Selective Activation of the ortho C−F Bond in Pentafluoropyridine by Zerovalent Nickel: Reaction via a Metallophosphorane Intermediate Stabilized by Neighboring Group Assistance from the Pyridyl Nitrogen. *Organometallics* **2010,** *29* (7), 1824-1831.

378.   Braun, T.; Perutz, R. N.; Sladek, M. I., Catalytic C–F activation of polyfluorinated pyridines by nickel-mediated cross-coupling reactions. *Chem. Commun.* **2001,** (21), 2254-2255.

379.   Braun, T.; Noveski, D.; Ahijado, M.; Wehmeier, F., Hydrodefluorination of pentafluoropyridine at rhodium using dihydrogen: detection of unusual rhodium hydrido complexes. *Dalton Trans.* **2007,** (34), 3820-5.

380.   Breyer, D.; Berger, J.; Braun, T.; Mebs, S., Nickel fluoro complexes as intermediates in catalytic cross-coupling reactions. *J. Fluor. Chem.* **2012,** *143*, 263-271.

381.   Samuel, P. P.; Singh, A. P.; Sarish, S. P.; Matussek, J.; Objartel, I.; Roesky, H. W.; Stalke, D., Oxidative Addition Versus Substitution Reactions of Group 14 Dialkylamino Metalylenes with Pentafluoropyridine. *Inorg. Chem.* **2013,** *52* (3), 1544-1549.

382.   Cronin, L.; Higgitt, C. L.; Karch, R.; Perutz, R. N., Rapid Intermolecular Carbon−Fluorine Bond Activation of Pentafluoropyridine at Nickel(0): Comparative Reactivity of Fluorinated Arene and Fluorinated Pyridine Derivatives. *Organometallics* **1997,** *16* (22), 4920-4928.

References

383.   Lee, J.-W.; Oliveira, M. T.; Jang, H. B.; Lee, S.; Chi, D. Y.; Kim, D. W.; Song, C. E., Hydrogen-bond promoted nucleophilic fluorination: concept, mechanism and applications in positron emission tomography. *Chem. Soc. Rev.* **2016,** *45* (17), 4638-4650.

384.   Kim, D. W.; Song, C. E.; Chi, D. Y., New Method of Fluorination Using Potassium Fluoride in Ionic Liquid: Significantly Enhanced Reactivity of Fluoride and Improved Selectivity. *J. Am. Chem. Soc.* **2002,** *124* (35), 10278-10279.

385.   Kim, D. W.; Jeong; Lim, S. T.; Sohn, M.-H.; Katzenellenbogen, J. A.; Chi, D. Y., Facile Nucleophilic Fluorination Reactions Using tert-Alcohols as a Reaction Medium: Significantly Enhanced Reactivity of Alkali Metal Fluorides and Improved Selectivity. *J. Org. Chem.* **2008,** *73* (3), 957-962.

386.   Litvak, V. V.; Mainagashev, L. Y.; Bukhanets, O. G., Polynucleotides and Their Components in the Processes of Aromatic Nucleophilic Substitution: I. Chemistry and Dynamics of Nucleotide Arylation with Pentafluoropyridine; Obtaining of Synthons for Molecular Design of Nucleic Acid Analogues. *Russ. J. Bioorg. Chem.* **2004,** *30*, 47 - 52.

387.   Hu, J. Y.; Zhang, J.; Wang, G. X.; Sun, H. L.; Zhang, J. L., Constructing a Catalytic Cycle for C-F to C-X (X = O, S, N) Bond Transformation Based on Gold-Mediated Ligand Nucleophilic Attack. *Inorg. Chem.* **2016,** *55* (5), 2274-83.

388.   Cheong, C. L.; Wakefield, B. J., Polyhalogenoaromatic Compounds. Part 53. Substitution in Polyfluoroaromatic Compounds by Bulky Nucleophiles. *Perkin Trans.* **1988,** *12*, 3301 - 3305.

389.   Diaz, J.; Esteruelas, M. A.; J, H.; J, M.; M, O., Simultaneous Dehalogenation of Polychloroarenes and Chlorination of HSiEt$_3$ Catalyzed by Complexes of the Groups 8 and 9. *J. Catal.* **2000,** *195*, 187 - 192.

390.   Fang, Z.; Wills, M., Asymmetric Transfer Hydrogenation of Functionalized Acetylenic Ketones. *J. Org. Chem.* **2013,** *78* (17), 8594-8605.

391.   Schwabedissen, J.; Trapp, P. C.; Stammler, H. G.; Neumann, B.; Lamm, J. H.; Vishnevskiy, Y. V.; Korte, L. A.; Mitzel, N. W., Halogen Bonds of Halotetrafluoropyridines in Crystals and Co-crystals with Benzene and Pyridine. *Eur. Chem. J.* **2019,** *25* (30), 7339-7350.

392.   Wiesemann, M.; Stammler, H.-G.; Neumann, B.; Hoge, B., Synthesis and Properties of Lewis Acidic Perfluoroorganotin Halides with 2,3,5,6-Tetrafluoropyridyl and Pentafluoroethyl Substituents. *Eur. J. Inorg. Chem.* **2017,** *2017* (40), 4733-4743.

393.   Voutchkova, A. M.; Feliz, M.; Clot, E.; Eisenstein, O.; Crabtree, R. H., Imidazolium Carboxylates as Versatile and Selective N-Heterocyclic Carbene Transfer Agents: Synthesis, Mechanism, and Applications. *J. Am. Chem. Soc.* **2007,** *129* (42), 12834-12846.

394.   Van Ausdall, B. R.; Glass, J. L.; Wiggins, K. M.; Aarif, A. M.; Louie, J., A Systematic Investigation of Factors Influencing the Decarboxylation of Imidazolium Carboxylates. *J. Org. Chem.* **2009,** *74* (20), 7935-7942.

395.   Fèvre, M.; Pinaud, J.; Leteneur, A.; Gnanou, Y.; Vignolle, J.; Taton, D.; Miqueu, K.; Sotiropoulos, J.-M., Imidazol(in)ium Hydrogen Carbonates as a Genuine Source of N-Heterocyclic Carbenes (NHCs): Applications to the Facile Preparation of NHC Metal Complexes and to NHC-Organocatalyzed Molecular and Macromolecular Syntheses. *J. Am. Chem. Soc.* **2012,** *134* (15), 6776-6784.